University of Cyprus

DEPARTMENT OF ELECTRICAL AND COMPUTER ENGINEERING

A REAL-TIME SOLUTION FOR INTENTIONAL CONTROLLED ISLANDING AND RESTORATION OF POWER SYSTEMS

PANAYIOTIS DEMETRIOU

A dissertation submitted to the University of Cyprus in partial fulfillment of the requirements for the degree of Doctor of Philosophy

DECEMBER 2017

VALIDATION PAGE

Doctoral Candidate: Panayiotis Demetriou

Doctoral Thesis Title: A Real-Time Solution for Intentional Controlled Islanding and Restoration of Power Systems

The present Doctoral Dissertation was submitted in partial fulfilment of the requirements for the degree of Doctor of Philosophy at the ***Department of Electrical and Computer Engineering*** *and was approved on the 6th of December 2017 by the members of the* ***Examination Committee.***

Examination Committee:

Research Supervisor: _____

(Dr. Elias Kyriakides, Associate Professor)

Committee Member: _____

(Dr. Marios Polycarpou, Professor)

Committee Member: _____

(Dr. Charalambos A. Charalambous, Associate Professor)

Committee Member: _____

(Dr. Vladimir Terzija, Professor)

Committee Member: _____

(Dr. Mihaela Albu, Professor)

DECLARATION OF DOCTORAL CANDIDATE

The present doctoral dissertation was submitted in partial fulfillment of the requirements for the degree of Doctor of Philosophy of the University of Cyprus. It is a product of original work of my own, unless otherwise mentioned through references, notes, or any other statements.

……...…….. **[**Full name of Doctoral candidate]

……...…….. **[**Signature]

ΠΕΡΙΛΗΨΗ

Παρά τις σημαντικές εξελίξεις στην τεχνολογία, τα σύγχρονα συστήματα ηλεκτρικής ενέργειας εξακολουθούν να αντιμετωπίζουν κλιμακωτές βλάβες που οδηγούν σε μεγάλης έκτασης συσκοτίσεις. Η ηθελημένη ελεγχόμενη νησιδοποίηση, ή αλλιώς διάσπαση συστήματος ή ελεγχόμενος διαχωρισμός συστήματος, έχει προταθεί ως ένα αποτελεσματικό διορθωτικό μέτρο ελέγχου για τον περιορισμό αυτών των καταστροφικών γεγονότων. Η ελεγχόμενη νησιδοποίηση αποσκοπεί στο να χρησιμοποιηθεί ως μια έσχατη λύση για να προσπαθήσει να σώσει το σύστημα από μια μερική ή πλήρη συσκότιση. Όταν το σύστημα υποστεί μια σοβαρή διαταραχή και τα συμβατικά συστήματα ελέγχου δεν είναι σε θέση να το διατηρήσουν σε ευστάθεια, η ελεγχόμενη νησιδοποίηση μπορεί να καθορίσει σε πραγματικό χρόνο (μέσα σε λίγα δευτερόλεπτα στην πράξη) ένα σύνολο γραμμών που θα αποσυνδεθούν από το σύστημα μεταφοράς ώστε να δημιουργηθούν βιώσιμα και ευσταθή υποσυστήματα, γνωστά και ως νησίδες.

Κατά την υιοθέτηση της ηθελημένης ελεγχόμενης νησιδοποίησης, πρέπει να εξεταστούν τρεις βασικές πτυχές: "*σε ποια σημεία να διαχωριστεί το σύστημα*", "*πότε να διαχωριστεί το σύστημα*" και "*τι πρέπει να γίνει μετά τον διαχωρισμό του συστήματος*". Σε αυτή τη διατριβή, προτείνονται αρκετές μέθοδοι ελεγχόμενης νησιδοποίησης για την επίλυση της πρώτης πτυχής. Οι προτεινόμενες μέθοδοι αποσκοπούν στη διάσπαση του συστήματος με ελάχιστη διαταραχή της ροής ισχύος ή ελάχιστη ανισορροπία της ισχύος στις νησίδες, για οποιοδήποτε δεδομένο αριθμό νησίδων, διατηρώντας παράλληλα τις συνοχές των γεννητριών και άλλους στατικούς και δυναμικούς περιορισμούς (π.χ. διαθεσιμότητα μιας γραμμής μεταφοράς, συνδεσιμότητα). Δεδομένου ότι η ευστάθεια των νησίδων που δημιουργούνται εξαρτάται κυρίως από τη συνοχή των γεννητριών εντός των νησίδων, προτείνεται επίσης μια εφαρμογή δύο σταδίων για τον καθορισμό συνεκτικών γεννητριών σε διαταραγμένα συστήματα ηλεκτρικής ενέργειας. Η εφαρμογή αυτή βασίζεται στην ομοιότητα μεταξύ των διασυνδετικών ταλαντώσεων και των καμπυλών ταλάντωσης των γεννητριών. Το ερώτημα για το πότε πρέπει να διαχωριστεί το σύστημα είναι κρίσιμο για την επιτυχία της μεθόδου ελεγχόμενης νησιδοποίησης, δεδομένου ότι πρέπει να αντιμετωπιστούν τα πιθανά προβλήματα λανθασμένου συναγερμού και λανθασμένης χρονικής εκτέλεσης. Μια ενοποιημένη μεθοδολογία που βασίζεται σε ένα area-based Center of Inertia (COI)-referred rotor angle δείκτη εισάγεται για να προσδιορίσει τον καταλληλότερο χρόνο διαχωρισμού του

συστήματος. Αυτός ο έγκαιρος καθορισμός του χρόνου για ελεγχόμενη νησιδοποίηση μπορεί να συνδυαστεί με εφαρμογές που καθορίζουν τα σημεία διαχωρισμού του συστήματος.

Επιπλέον, σε αυτή τη διατριβή, εξετάζεται η έννοια μιας στρατηγικής για ελεγχόμενη νησιδοποίηση συνδυασμένη με μια εφαρμογή για παράλληλη αποκατάσταση του συστήματος ηλεκτρικής ενέργειας. Για το λόγο αυτό, ένας αλγόριθμος ελεγχόμενης νησιδοποίησης εξελίσσεται λαμβάνοντας υπόψιν περιορισμούς αποκατάστασης του συστήματος ηλεκτρικής ενέργειας (π.χ. πλήρης παρατηρησιμότητα, επαρκής ικανότητα "blackstart" και επαρκής ικανότητα παραγωγής για να καλύπτει την ζήτηση φορτίου σε κάθε νησίδα). Αυτοί οι νέοι περιορισμοί μπορούν να θεωρηθούν ως ένα στάδιο προγραμματισμού της αποκατάστασης του συστήματος ηλεκτρικής ενέργειας. Στη συνέχεια, προτείνεται μια καινοτόμα μέθοδος για να παρέχει λύσεις σε πραγματικό χρόνο τόσο για ελεγχόμενη νησιδοποίηση όσο και για αποκατάσταση του συστήματος ηλεκτρικής ενέργειας βασιζόμενη σε εκτιμημένες καταστάσεις του συστήματος. Η συγκεκριμένη μέθοδος, που αποτελείται από τον προαναφερθέντα αλγόριθμο ελεγχόμενης νησιδοποίησης που εξελίχθηκε, έναν εκτιμητή κατάστασης πραγματικού χρόνου και μια διαδικασία αποκατάστασης του συστήματος ηλεκτρικής ενέργειας, δίνει στο χειριστή του συστήματος την ευελιξία να παρακολουθεί τις νησίδες μετά τη νησιδοποίηση και να τις επανασυνδέει σε σχεδόν πραγματικό χρόνο, μόλις ικανοποιηθούν οι συνθήκες συγχρονισμού τους. Επιπλέον, προτείνεται ένα ενοποιημένο πλαίσιο που αποτελείται από μια καινοτόμα μέθοδο ελεγχόμενης νησιδοποίησης και μια μεθοδολογία εκτίμησης κινδύνου για να αξιολογήσει τον κίνδυνο των μεθόδων ελεγχόμενης νησιδοποίησης στο σύστημα ηλεκτρικής ενέργειας. Το ενοποιημένο πλαίσιο παρέχει στατιστικά στοιχεία σχετικά με τα οφέλη και τους κινδύνους της εφαρμογής μιας ελεγχόμενης νησιδοποίησης, λαμβάνοντας υπόψη τις αβεβαιότητες και τις ανησυχίες που σχετίζονται με την αξιοπιστία της. Για την ολοκλήρωση αυτής της έρευνας, αναπτύχθηκαν δυναμικά δοκιμαστικά συστήματα κατάλληλα για μελέτες μεταβατικής ανάλυσης τα οποία παρέχονται σε ανοικτή πρόσβαση.

ABSTRACT

Despite major advances in technology, modern power systems still experience cascading outages leading to large-scale blackouts. Intentional controlled islanding (ICI), also called system splitting or controlled system separation, has been proposed as an effective corrective control action to mitigate these catastrophic events. ICI is aimed to be used as a final resort to attempt to save the system from a partial or a complete blackout. When the system is subject to a severe disturbance and the conventional control systems are unable to keep the system stable, ICI can determine in real-time (within a few seconds in practice) a set of lines to be disconnected across the transmission system to create sustainable and stable subsystems, also known as *islands*.

When adopting ICI, three key aspects must be addressed: "*where to island*", "*when to island*" and "*what to do after islanding*". In this thesis, several ICI schemes are proposed for addressing the first one. The proposed schemes aim to split the system with *minimal power-flow disruption* or *minimal power imbalance* within islands, for any given number of islands, while maintaining generator coherencies and other static and dynamic constraints (e.g., transmission line availability, connectivity). Since the stability of islands created is mainly dependent on the coherency of the generators inside the islands, a two-step approach for defining coherent generators in disturbed power systems based on the similarity among their inter-area oscillations and swing curves is also proposed. The question of when to island is critical for the success of the ICI scheme, since the possible issues of false alarm and false dismissal have to be handled. A unified methodology based on area-based Center of Inertia (COI)-referred rotor angle index is introduced to determine the most suitable time for splitting the system. This timely definition of the time for islanding can be combined with approaches to determine the points where to island the system.

Furthermore, in this thesis, the concept of a controlled islanding strategy combined with an approach of Parallel Power System Restoration (PPSR) is considered. A proposed ICI algorithm is extended to consider power system restoration constraints (e.g., complete observability, sufficient blackstart (BS) capability and sufficient generation capacity to match the load consumption within each island). These new constraints can be viewed as a power system restoration planning stage. Next, a novel scheme is proposed to provide real-time solutions for both ICI and power system restoration based on estimated states. The particular

scheme, which consists of the aforementioned extended ICI algorithm, a real-time state estimator and a power system restoration process, gives the system operator the flexibility to monitor the islands during the post-islanding stage and reconnect them in quasi real time, as soon as their synchronizing conditions are met. In addition, a unified framework that consists of a novel ICI scheme and a risk assessment methodology is proposed to assess the risk of ICI schemes on the electricity system. The unified framework provides insights on the benefits and risks of implementing ICI, considering the uncertainties and concerns related to its reliability. For the completion of this research, dynamic test bed systems suitable for transient analysis studies are developed and provided in open access.

I dedicate this thesis to my family, with my gratitude for their support, love and their dedicated partnership for success in my life

ACKNOWLEDGMENTS

Firstly, I would like to offer my gratitude to my supervisor Prof. Elias Kyriakides for providing me with the opportunity to conduct this research and for all his guidance, encouragement and invaluable advice throughout my PhD studies. His enthusiasm for scientific research and his vast knowledge have been inspiring.

Furthermore, I would like to thank my examination committee members, Prof. Marios Polycarpou and Assoc. Prof. Charalambos A. Charalambous of the University of Cyprus, Prof. Vladimir Terzija of University of Manchester and Prof. Mihaela Albu of Politehnica University of Bucharest for the time and effort that they have spent to review my dissertation. Their valuable comments and suggestion have been very helpful for improving the quality of this dissertation.

I would like to offer a special thank you to Dr. Jairo Quiros-Tortos for his sound advice and kind help, and for his dynamic input towards the completion of this research.

I acknowledge the financial support for my research of the European Commission. This research work has been funded by the European Commission 7th Framework Programme under grant FP7-ERC Advanced Grant -291508.

All my thanks go to my colleagues at the Power Team at the KIOS Research and Innovation Center of Excellence of the University of Cyprus for our effective collaboration and sharing of research experience during all these years. My thanks also go to all at the KIOS CoE for the pleasant and positive work environment.

As always, my greatest thanks go to my parents, Kyriako and Despoina Demetriou, and my brothers Demetri, Constantino and Theodoro for strongly believing in me. Their continuous support and love provided me with confidence and courage to complete my PhD studies.

Finally, to all my friends and family who I have not been able to mention above, thank you for your support, understanding and constant companionship throughout my dissertation writing.

TABLE OF CONTENTS

LIST OF TABLES

LIST OF FIGURES

LIST OF ABBREVIATIONS

ANN	Artificial Neural Network
ANOVA	Analysis of Variance
AVR	Automatic Voltage Regulator
BFS	Breadth First Search
BS	Blackstart
CB	Circuit Breaker
COI	Center of Inertia
CSC	Constrained Spectral Clustering
DFS	Depth First Search
EMS	Energy Management System
FTA	Fault Tree Analysis
GR	Generation Rescheduling
HVDC	High-Voltage Direct Current
Hz	Hertz
ICC	Intraclass Correlation Coefficient
ICI	Intentional Controlled Islanding
IEEE	Institute of Electrical and Electronic Engineers
LP	Linear Programming
MILP	Mixed Integer Linear Programming
MSE	Mean Square Error
MST	Minimum Spanning Tree
MTTF	Mean Time To Failure
MTTFS	Mean Time To Fail Spurious
MVAr	Mega Volt Amps
MW	Mega Watt
NERC	North American Electric Reliability Corporation
OBDD	Ordered Binary Decision Diagram
PC	Partitioning Cost
PES	Power Energy Society
PFD	Probability of Failure on Demand

PFS	Probability to Fail Spurious
PLC	Programmable Logic Controller
PMUs	Phasor Measurement Units
PPSR	Parallel Power System Restoration
RA	Remedial Action
RES	Renewable Energy Sources
RSCCI	Robust Spectral Clustering Controlled Islanding
SCADA	Supervisory Control and Data Acquisition
SC	Spectral Clustering
SCCI	Spectral Clustering Controlled Islanding
SIPS	System Integrity Protection Scheme
SPS	Special Protection System
SSC	Sum of Square between Columns
SSR	Search Space Reduction
SVC	Static Var Compensator
TSI	Transmission System Reconfiguration
TSO	Transmission System Operator
TSR	Transient Stability Index
UFLS	Under-Frequency Load Shedding
UVLS	Under-Voltage Load Shedding
VOLL	Value of Lost Load
WAMPAC	Wide Area Monitoring Protection and Control
WAMS	Wide Area Monitoring System
WLS	Weighted Least Squares

CHAPTER 1
INTRODUCTION

1.1 Research Background

1.1.1 Power system blackouts

With the increasing size and complexity of modern power systems, and despite major advances in technology, the instances of large-scale blackouts have increased in the last two decades. Along with growing demand in electricity, modern power systems experience unprecedented changes in structure and operation due to economic and environmental pressures. As electricity systems moved to market based structures, the demand for cheaper electricity has grown. This has led to major increases in cross-border trading where it is often cheaper to import power than invest in new power stations. For instance, Italy is normally importing about 5 GW (25% of the country's total load) from the interconnected European Power System to cover its large deficit in energy. This is typically supplied from the cheap nuclear generation in France. Germany is also facing major problems with energy deficits caused by the shutting down of its nuclear units. The result of this decision means importing power from neighboring countries. Therefore, the interconnectors which were originally designed for greater frequency stability are now becoming vital sources of power transfer.

However, this is not the only pressure that the modern power systems are facing. Attempts to avert climate change through the introduction of renewable energy policies are already forcing radical changes in power systems. The most significant of these changes is that a large percentage of electrical energy is expected to be generated using Renewable Energy Sources (RES) like wind, solar and tidal. Major targets have been set for renewable generation across the world. Many of these targets range from 20% [1] with a push to achieve 50% in the future. This means that the ageing power plants will be replaced with newer carbon friendly technologies. Even if this brings great benefits for carbon reduction, it will make the operation of future power systems more variable and unpredictable due to the high influence of RES generation by climatic conditions and the intermittent nature of RES. Another issue with these technologies is that they provide no inertia to the system. Traditional steam turbines have very

large rotors whose large rotating mass adds inertia to a system. However, the wind farms are connected through a series of power electronic converters which decouple them from the grid and thus offer no inertia. Therefore, in a system with 50% renewables, the system inertia will be greatly reduced. Hence, for any given disturbance in the system, frequency will change much faster. At the same time, the weaker coupling between the machines may lead to more unpredictable system dynamic behavior. In addition, since new technologies are being connected into an old grid design, major grid reinforcement will be required. For instance, renewable energy generation on the transmission level requires the support of power electronic technologies such as High-Voltage Direct Current (HVDC) lines and Static Var Compensators (SVC). The use of these electronic technologies will introduce further complexity and uncertainty into power systems [2].

It is rare for large-scale power system blackouts to be directly caused by a single large disturbance. However, a single large disturbance in a stressed system with increased variation, complexity and unpredictability, may cause a series of unplanned and unexpected sequential outages. These outages will incrementally increase the stress on the system and force it into a more vulnerable state of operation. If proper protection and control actions are not taken quickly and properly by the system operators (e.g., load shedding, reactive power support), then the system may experience further cascading outages and separate into undesirable islands, or even completely collapse [3], [4].

With the modern power systems being operated close to their physical limits, and being put under extra stress, severe blackouts have occurred in the last 15 years. The largest blackout in the history of power systems occurred in 2012 in India which affected 620 million people. In 2011, a blackout in Brazil affected 55 million people while in 2010, Chile lost 15 million customers. A catastrophic statewide blackout in South Australia in 2016 resulted in the loss of 2.5 GW that affected 1.7 million people. In 2003, three major blackouts occurred. The United States with 55 million people affected, Italy with 56 million people affected and finally, 5 million in Sweden. A Europe-wide blackout was narrowly avoided in 2006 but 15 million customers were still affected due to un-intentional islanding.

The Indian blackout was a prime example of a blackout caused by the high imports on the interconnectors. One of the difficulties power exporters face is with importers keeping to the contractual levels. Before this blackout, many of the interconnectors were severely overloaded as areas were importing more power than the agreed levels. The Italian blackout was caused

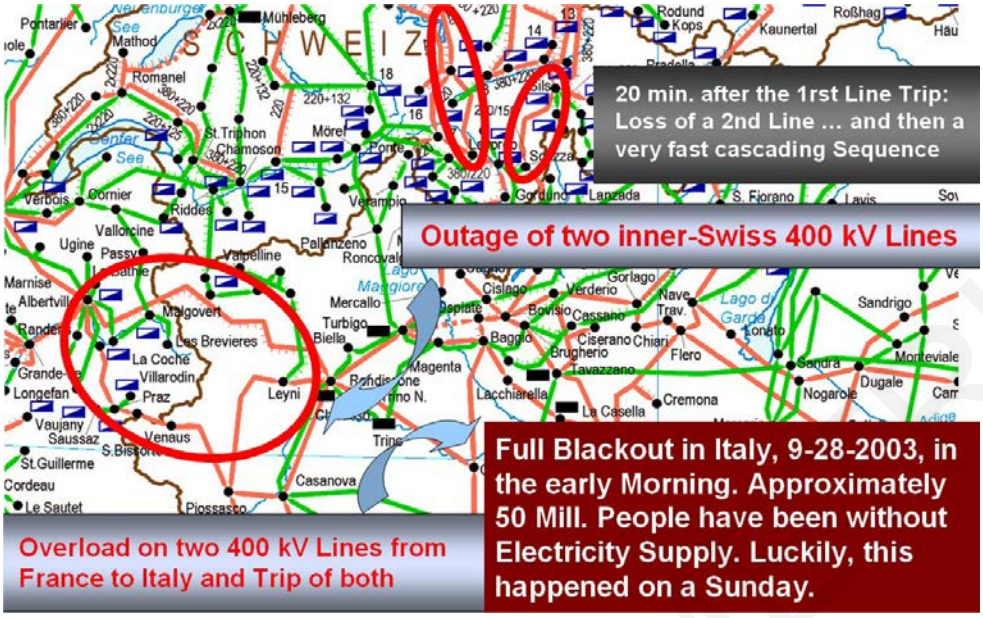

Figure 1.1: Blackout in Italy (2003)

by much the same reason. As mentioned above, the normal power import for Italy is about 5 GW. On September 28 2003, the demand was increased to 6.7 GW due to power station outages in combination with country-wide celebration activities for the festival “White Night”. 20 minutes after the first 400 kV inner-Swiss line trip, a second 400 kV line tripped in Switzerland, and immediately, a cascade of sequential line-trips occurred on all interconnections to Italy. As a result, the “White Night” turned into a “Black Night”. The 2006 European event was another example where a planned outage was not communicated properly to the neighboring operators. Therefore, it is obvious that the cause of many blackouts is often the lack of proper communication between neighboring system operators. The 2016 South Australian blackout was caused by an unexpected operation of the control settings of the wind farms in combination with the low inertia in the system at that moment. Immediately before the blackout, wind had been producing almost half of South Australia's power needs, with much of the remainder being imported from Victoria. South Australia's thermal generators (gas and diesel) had only been generating about 18 per cent of the state's power needs. When the protection feature of the wind farms kicked in, their output reduced by 456 MW over a period of less than seven seconds. This immediately led to the trip of the Heywood Interconnector from Victoria. The sudden loss of power flows across the interconnector sent the frequency in the South Australia grid plummeting. South Australia has an automatic load-shedding system designed to kick-in in just such an event. However, the rate of change of the frequency was so rapid (due to the low system inertia) that exceeded the ability of the under-

frequency load-shedding scheme to arrest the frequency fall before it dropped below 47 Hz. Without the automatic load-shedding scheme, the remaining generation was much less than the connected load, and as a result, the entire system collapsed. Finally, the events such as the Brazilian and Scandinavian blackouts were examples of hidden failures in the system which are often not highlighted until the critical moments. Scandinavia lost a major generator, which was then followed by a mechanical busbar fault which took out a key high-voltage corridor. In the case of the Brazilian blackout, it was found that in a severe storm the isolators were not adequate to cope with the high level of rainfall.

Undoubtedly, the introduction of further variation, complexity and unpredictability to modern power systems makes them more vulnerable and dramatically increases the likelihood of large scale power system blackouts. Whilst it is impossible to develop a solution that completely eliminates the possibility of a blackout, several measures can be implemented to minimize the probability of a blackout occurring. For many years, Energy Management Systems (EMS) have been used for the online monitoring of system conditions and assessment of system security. Traditional EMS use measurements with a low-refresh rate (i.e., several seconds to one minute), from a Supervisory Control and Data Acquisition (SCADA) system, to estimate the system operating condition and to perform offline system stability studies [5]. The EMS can provide sufficient information and support for normal steady-state system operation and to plan the system response to slow changes in the operating conditions. However, EMS is not capable of capturing system dynamics, particularly when the system is subjected to large disturbances. To overcome this issue, power system operators try to assess the stability condition of the power system through several offline studies. The transient analysis that is usually used in the control center enhances the situational awareness of the system operators by providing a visualization of the generator rotor angles, bus voltages, and system frequency for the assumed operational state of the system. Nonetheless, for running transient stability analysis both the type and the parameters of the dynamic model for the power system components should be available. In addition, the offline studies cannot be used to fully anticipate all the conditions faced by operators. Hence, any unplanned contingencies have the potential to initiate a cascade of events that will lead to a system blackout.

Apart from EMS, many power systems have the benefit of technological advances such as the System Integrity Protection Schemes (SIPSs). SIPSs are designed to preserve system integrity after a large disturbance, and restore the system to the normal state when the system

is in an emergency condition [3]. Traditionally, SIPSs use the results of offline studies to determine their actions [5]. These offline studies are based on the pre-calculated system behavior for the assumed operational state of the system. In addition, as SIPSs only use local or regional (within a power utility) measurements, they lack awareness of the operating conditions in the neighboring power systems [3]. Consequently, the traditional SIPS may not be sufficient to ensure proper control for any system instability that may occur. Finally, the conventional protection systems and controls (e.g., protective relays) have seen major development to add robustness to power systems. However, in some cases the protection systems themselves can be major contributors to blackouts such as the US blackout in 2003. As systems become increasingly complex it is much more difficult to rely on the old protection designs which are often fitted and forgotten about. On the other hand, when new protection systems are installed, conflicts can arise between the old protection settings. Thus, a proper co-ordination between the existing systems is required in order to provide the desired protection.

It is clear that new solutions should be developed and exploited to enhance future power system security. It is noted that a key contributor to this attempt could be the increased situational awareness within power systems through new measurement technologies, wide area measurement schemes, etc. In this sense, various task forces, advisory groups, research programs, and operating standards have been set-up for studying and designing a comprehensive system control strategy. A detailed report produced by an award winning task force (formed by the IEEE Power and Energy Society (PES)) [6] highlighted some important recommendations for improving system dynamic performance and thus minimizing the risk of wide spread disturbances and subsequent blackouts. Among these recommendations, Intentional Controlled Islanding (ICI) through special protection schemes (SPSs) is in prominent place.

1.1.2 Intentional Controlled Islanding

Intentional controlled islanding (ICI), also called system splitting or controlled system separation, has been proposed as an effective corrective control action for mitigating the consequences of large disturbances which might eventually lead to a partial or complete blackout [6], [7]. ICI is aimed to be used as the last resort to prevent blackouts, usually after severe disturbances and when conventional control systems have failed to keep the system

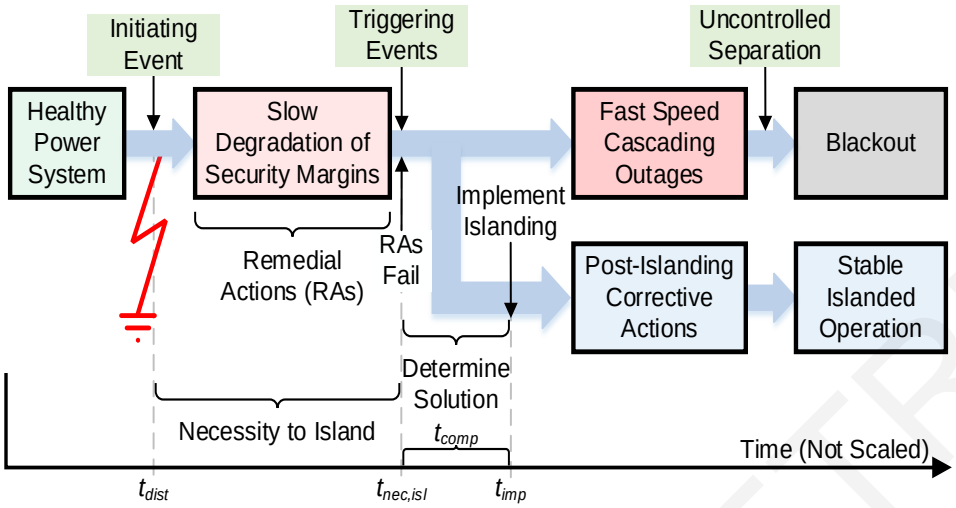

Figure 1.2: General framework of the intentional controlled islanding

within stability margins. In practice, ICI determines in real-time (within a few seconds in practice [7]) a set of lines to be disconnected across the transmission system to create sustainable and stable subsystems, also known as *islands* [8], [9].

Figure 1.2 illustrates the general concept of ICI, which is associated with the blackout progress [10]. Following a severe disturbance on a healthy system at $t = t_{dist}$ (known as initiating event), the slow degradation of the power system commonly takes place [11]. Although Remedial Actions (RAs) may be applied to avoid this degradation, they may fail, either because they are not sufficient or they may not be implemented on time by operators. This typically causes the system to enter the fast speed cascading outages, triggering the uncontrolled disconnection of components and causing large-scale blackouts.

In this context, ICI aims to limit these fast cascading outages, by splitting the power system into several stable islands [6], [7]. When the vulnerability analysis identifies the necessity to island the system, at $t = t_{nec,isl}$, (when RAs fail to minimize the impact of the initiating event), an optimal islanding solution must be determined, i.e., the lines to be disconnected in a controlled manner. To avoid any delay in the controlled islanding, it is crucial that the ICI algorithm is computationally efficient to reduce the computational time, denoted by t_{comp}. When the solution is determined, this will be implemented at time t_{imp}. Then, due to the inherent characteristics of the system, additional corrective measures (e.g., fast valving and load shedding) may be needed to ensure that each island retains its security margins during the post-islanding stage [12], [13]. Each island is then expected to reach a stable operation, and after a certain period, the whole system will be restored to the pre-disturbance healthy system by synchronizing the islands and connecting them into a unified system.

1.2 Research Objectives

A practical controlled islanding scheme needs to address three critical problems:

- *Where to island*? (i.e., the splitting points to form sustainable islands)
- *When to island*? (i.e., islanding timing)
- *What to do after islanding*? (i.e., post-splitting control actions in formed islands, e.g., generation rescheduling and load shedding)

In order to create stable islands, the islanding solution must satisfy a large number of constraints such as load-generation balance, generator coherency, transmission line availability, voltage stability, and transient stability [14], [15]. In general, it would be too complicated to find a real-time solution that satisfies all these constraints, or even confirm if such a solution exists. In addition, the combinatorial explosion of the solution space that occurs for large power systems increases the complexity of solving the problem [8]. However, considering only a sub-set of these constraints allows a set of feasible candidate islanding solutions to be produced. This set of candidates can be coordinated with other corrective measures (e.g., transmission system reconfiguration (TSR), generation rescheduling (GR), and load shedding (LS)) to find a final islanding solution that satisfies all the constraints (a solution which ensures that each island retains its stability and security margins in the post-islanding stage). This approximation reduces the complexity of the controlled islanding problem, especially when dealing with large-scale systems [8], [9], [14] - [16].

Among the aforementioned constraints, the generator coherency constraint is crucial for the success of the controlled separation, as it enhances the transient stability of the islands [8], [15]. Therefore, real-time knowledge of generator coherency will help plan the boundaries of these islands and avoid unnecessary tripping [17].

In this context, the ICI is usually modeled as a combinatorial optimization problem with constraints. The two main types of its objective function are the *minimal power-flow disruption* and the *minimal power imbalance* within islands, while the main constraints are the coherent generator groups. The *power-flow disruption* is expressed by the arithmetic sum of active power in each disconnected transmission line. Methods for minimal power-flow disruption minimize the change of the power flow pattern within the system following system splitting [18], also called absolute power exchange. On the other hand, the *power imbalance* is expressed by the algebraic sum of active power on each disconnected transmission line(considering the direction of power flow). Approaches for finding islanding solutions with

minimal power imbalance minimize the load-generation imbalance within the islands [14].

The question of when to island is critical for the success of the ICI scheme, since the possible issues of false alarm and false dismissal have to be handled. In the case of a false alarm, islanding is triggered too early, forcing a stable system to incorrectly be split into islands. In the case of false dismissal, islanding is triggered too late, allowing an unstable system to operate and to probably lead to an uncontrolled cascading blackout. Therefore, early recognition that could indicate if a disturbance will evolve into a blackout or not is important for mitigating the occurrence and cost of blackouts.

Another critical aspect regarding controlled islanding strategies is the lack of the Parallel Power System Restoration (PPSR) planning stage. Although the objective of controlled islanding schemes is to avoid a complete blackout, one or more islands might reach a local blackout after the splitting strategy is carried out. These undesirable events occur due to the lower stability margin in the created island compared to the one for the entire power system. When a local blackout occurs in an island, PPSR should be carried out in order to restore the island, and therefore, restore the power system. However, to properly run the PPSR process, a number of constraints, regarding the PPSR, should be considered when searching for proper islanding solutions [19]. The main ones are the complete observability, the sufficient blackstart capability and the sufficient generation capacity within the formed islands. On top of that, the concept of novel schemes that provide real-time solutions for both ICI and power system restoration is still an unexplored research area and a practical engineering challenge.

In conclusion, it is obvious that the ICI schemes are highly complex, composed of several components for gathering field data, detecting the triggering event and implementing the islanding solution. This might lead to reliability issues, i.e., inability of the ICI scheme to operate as designed, due to the numerous sources of possible malfunctions in the ICI components. The main failure modes of ICI schemes are (i) the failure to operate when needed and (ii) the incorrect (i.e., spurious) operation when there is no disturbance in the system. The impact of these failure modes varies and depends on the evolving system conditions. An example that shows the impact of the misoperation of such schemes is the Irish disturbance of August 2005 [20]. Due to false communication signaling, this country was incorrectly split into two areas, resulting in the disconnection of 326,000 customers in the Republic of Ireland and a further 74,000 customers in Northern Ireland. It is, therefore, critical to develop and apply risk assessment techniques to estimate and mitigate the risk introduced to the network

by such undesirable events.

Considering all the above key challenges/issues crucial for the success of an ICI scheme, the main objectives of this research can be summarized as follows:

1) Development of new real-time ICI algorithms and methods that find islanding solutions with minimal power flow disruption or minimal power imbalance which maintain the generator coherencies and other static and dynamic constraints.
2) Development of a methodology for defining in real-time coherent generators in disturbed power systems.
3) Proposing a methodology to address the "*when to island*" problem.
4) Development of real-time ICI algorithms that consider parallel power system restoration constraint. Consequently, proposing a novel scheme that provides real-time solutions for both ICI and power system restoration based on estimated states.
5) Assessing the risk of ICI schemes on the transmission system through a risk assessment methodology

The term "real-time" refers to methods and schemes that use Wide Area Monitoring Systems (WAMS) to gather synchronized measurements provided by strategically located PMUs (with a sampling rate between 30 to 60 samples per second). The utilization and analysis of such measurements allows system operators to gain real-time awareness of current power system operating conditions, and thus, to take real-time decisions and control actions. Any delays on taking these control actions are then solely based on how computationally efficient the proposed methods are.

Last but not the least, another objective of this research is the development of dynamic test bed systems for transient analysis studies. As mentioned in Section 1.1.1, the transient analysis can be used to assess the stability condition of the power system during large disturbances (through several offline studies). In general, for running transient stability analysis both the type and the parameters of the dynamic model for the power system components should be available. However, the several IEEE test bed systems available for steady state analysis, whose topology and power flow data can be found in [21], are lacking of dynamic models. Thus, although in the case of the steady state methodologies, the IEEE test bed systems provide a common background for the researchers to apply and test their methodologies, extracting results under the same conditions for the same test bed systems, this is not the case in the methodologies that are based on transient conditions where dynamic models and their

dynamic parameters are needed. In the literature, there are several cases where researchers are forced to choose dynamic models and their parameters for the IEEE systems in order to build their own dynamic systems [22], [23]. Hence, there is a lack of consistency and uniformity among the different dynamic test systems. Furthermore, there is a common desire among the research community for dynamic test bed systems that can be used for assessing methodologies based on dynamic simulations.

1.3 Thesis Structure

In Chapter 1, the need for systematic study and design of a comprehensive system control strategy is demonstrated based on the evaluation of existing solutions for power system monitoring, protection and control, and the anticipation of developments in modern power systems. Hence, Intentional Control Islanding is proposed as an efficient corrective measure for limiting system blackouts. Furthermore, the objectives of this research which were defined considering the key challenges/issues crucial for the success of ICI are also detailed in this chapter along with a list of the main contributions.

Chapter 2 presents the IEEE test bed systems (available in the literature for steady-state studies) that were extended and modified to consider dynamic data for time-domain simulations. Additionally, Chapter 2 further presents transient analysis results from the testing of two IEEE modified test systems (IEEE 14- and 39-bus modified test systems). These dynamic test systems are consequently used throughout the thesis for the validation of the proposed methodologies.

In Chapter 3, a two-step approach for defining coherent generators in disturbed power systems based on the similarity among their inter-area oscillations and swing curves is presented. The proposed methodology is applied to the 39-Bus New England System and coherent generators are obtained for different operating points to provide a more accurate and realistic grouping.

Chapter 4 introduces several ICI methods for addressing the "*where to island*" problem. The proposed methods aim to split the system with *minimal power-flow disruption* or *minimal power imbalance* within islands, for any given number of islands, while maintaining generator coherencies and other static and dynamic constraints (e.g., transmission line availability, connectivity). For completeness, the graph theory fundamentals applied in these methods are

first provided in this chapter. The proposed ICI methods are tested using the dynamic models of several IEEE test systems, as well as real large-scale power systems that are more representative of modern system operations footprints (e.g., actual power system of Cyprus, Polish Network). Multiple case studies are presented to demonstrate the effectiveness of the ICI methods to different system conditions.

In Chapter 5, a unified methodology based on the area-based Center of Inertia (COI)-referred rotor angle index is introduced to determine the most suitable time for splitting the system. The unified methodology is tested using the IEEE 39-bus test system. Different case studies are presented to demonstrate the adaptability and effectiveness of the proposed methodology in triggering promptly the ICI scheme and thus in minimizing the impact and cost of large-scale blackouts.

Chapter 6 investigates the concept of controlled islanding strategies combined with an approach of Parallel Power System Restoration planning stage. For this purpose, a proposed ICI algorithm is extended to consider power system restoration constraints (e.g., complete observability, sufficient blackstart capability and sufficient generation capacity to match the load consumption within each island). Simulation results on the IEEE 39- and 118-bus test systems are provided. To complete the investigation, this chapter also proposes a novel scheme that provides real-time solutions for both ICI and power system restoration based on estimated states. The proposed scheme consists of the aforementioned extended ICI algorithm, a real-time state estimator and a power system restoration process. Since system observability is guaranteed by the ICI algorithm used, the real-time state estimator can continuously provide to the system operator the operating conditions of the power system before and after its splitting. This gives the operator the flexibility to monitor the islands during the post-islanding stage and reconnect them in quasi real time, as soon as their synchronizing conditions are met. The ICI-restoration scheme is tested in this chapter using the dynamic models of the IEEE 39- and 118-bus test systems.

In Chapter 7, a unified framework that consists of a novel ICI scheme and a risk assessment methodology is proposed to assess the risk of ICI schemes on the transmission system. The unified framework provides insights on the benefits of implementing ICI, considering the uncertainties related to its reliability. The proposed framework is fully deployed on the actual power system of Cyprus, where multiple case studies are developed to demonstrate its adaptability to different system conditions.

Finally, Chapter 8 includes a general discussion about this research where all the important conclusions are summarized. A reference to future work related to the research is also performed.

1.4 Contribution to Knowledge

- ✓ Development of dynamic test bed systems for transient analysis studies (IEEE 14, 30, 39, 57, and 118 bus modified test systems)
- ✓ Development of a Robust Spectral Clustering Controlled Islanding (RSCCI) method for finding suitable islanding solutions with minimal power-flow disruption (for the bisection case) while maintaining generator coherency and transmission line availability constraints.
- ✓ Development of a novel ICI scheme based on graph theory (i.e., the cut-set matrix) for determining an islanding solution that creates islands with minimum power imbalance, while ensuring that each island contains only coherent generators and that the islanding solution excludes critical branches. The proposed ICI scheme is designed for the particular case of two electrical islands. More than two islands can be created by applying recursive bisection.
- ✓ Development of an ICI algorithm based on an exact Mixed Integer Linear Programming (MILP) Formulation that directly determines an optimal islanding solution with minimal power-flow disruption for any given number of islands, while ensuring that each island contains only coherent generators. In addition, the proposed algorithm enables operators to constrain any transmission line to be excluded from the solution, allows the control of the size of islands and ensures their connectivity.
- ✓ Development of a novel ICI algorithm based on a Linear Programming (LP) formulation that directly determines an optimal islanding solution with minimal power-flow disruption for large scale power systems, and for any given number of islands, in a timely manner. The proposed LP formulation is derived from the relaxation of the MILP formulation used in the above ICI algorithm.
- ✓ Development of a two-step methodology for defining in real-time coherent generators in disturbed power systems based on the similarity among their inter-area oscillations and swing curves

- ✓ Development of a unified methodology to address the "*when to island*" problem. The proposed methodology adopts the concept of area-based Center of Inertia-referred rotor angle index, widely used in transient stability analysis for tracking the stability of interconnected areas, to determine the actual time for islanding. The time at which a particular area is said to be unstable, is defined also as the moment where the ICI scheme should be triggered to split the unstable system into islands.
- ✓ Extension of the aforementioned MILP ICI algorithm to consider power system restoration constraints. Considering that data collection is essential to properly run a restoration process and assuming a completely observable power system at normal operating conditions, the extended ICI algorithm creates islands that are also completely observable, includes at least one blackstart unit within each island, and guarantees sufficient generation capacity to match the load consumption within each island. These new constraints can be viewed as a power system restoration planning stage.
- ✓ Development of a real-time ICI and restoration scheme based on estimated states. The proposed scheme consists of a sophisticated ICI algorithm (i.e., the extended MILP ICI algorithm), a real-time linear state estimator and a restoration process. Following the necessity to split the system, the MILP ICI algorithm firstly determines an exact islanding solution with minimal power-flow disruption while considering PPSR constraints. Since system observability is guaranteed, the real-time state estimator continuously provides to the system operator the operating conditions of the power system before and after its splitting. This gives the operator the flexibility to monitor the islands during the post-islanding stage. The reconnection of the islands is achieved in quasi real time, as soon as their synchronizing conditions are met.
- ✓ Development of a unified framework to assess the risk of ICI schemes on the transmission system. First, the aforementioned ICI scheme based on the graph theoretic cut-set matrix is used to create islands with minimum power imbalance. Then, a risk assessment methodology is applied to calculate the probability and impact of the main operational modes of the ICI scheme. The unified framework provides insights on the benefits of implementing ICI, considering the uncertainties related to its reliability.

CHAPTER 2

DEVELOPMENT OF DYNAMIC TEST BED SYSTEMS FOR TRANSIENT ANALYSIS STUDIES

2.1 Overview

The growing size of interconnected power systems intensifies the need for transient stability studies. The stability of the power system can be categorized into the angle and voltage stability [12]. In the case of the angle stability, the power system should be able to maintain synchronism between the generators and the rest of the system after a severe disturbance, while in the voltage stability the system voltage level after the disturbance should be preserved as in the steady state. In any of the two cases, the loss of stability could lead to devastating consequences.

In order to prevent such situations, power system operators assess the stability condition of the power system by examining several scenarios offline. The transient analysis that is usually used in the power system control center enhances the situational awareness of the power system operators by providing a visualization of the generator rotor angles, bus voltages, and system frequency during a large contingency based on the current operating condition of the power system. Therefore, operators can plan a set of remedial measures to maintain the stability of the system.

In general, for running transient stability analysis both the type and the parameters of the dynamic model for the power system components should be available. On one hand, each electric utility has its own dynamic parameters and models for its power system. On the other hand, the several IEEE test bed systems available for steady state analysis, whose topology and power flow data can be found in [21], are lacking of dynamic models. Thus, although in the case of the steady state methodologies, the IEEE test bed systems provide a common background for the researchers to apply and test their methodologies, extracting results under the same conditions for the same test bed systems, this is not the case in the methodologies that are based on transient conditions where dynamic models and their dynamic parameters are needed.

In the literature, a few test bed systems that can be used in transient analysis were proposed [24], [25], [26]. However, since the IEEE test bed systems are widely used by the research community, there are several cases where researchers are forced to choose dynamic models and their parameters for the IEEE systems in order to build their own dynamic systems [22], [23]. In this case, there is a lack of consistency and uniformity among the different dynamic test systems. Furthermore, there is a common desire among the research community for dynamic test bed systems that can be used for assessing methodologies based on dynamic simulations.

2.2 Dynamic IEEE Test Systems for Transient Analysis: Models and Parameters

The IEEE test bed systems available in the literature for steady-state studies (14, 30, 39, 57, and 118 bus systems) were extended and modified to consider dynamic data for time-domain simulations [27]. The dynamic parameters for a sixth order full machine model (i.e., machine, exciter, and governor) were defined for each generator in the IEEE test systems. Dynamic parameters were also determined for the condensers and motors. It is to be noted that the dynamic parameters are based on typical dynamic models provided in [28]. Particularly in [28], the dynamic parameters for fossil fuel generators are according to their rated power. For each generator the dynamic parameters for its exciter and governor are also available. Therefore, knowing the rated power of each generator in the IEEE test systems (available from their steady state data) the appropriate dynamic model from [28] was selected (including the exciter and the governor). The same procedure was followed for choosing dynamic parameters for the condensers and the motors in the IEEE test systems. The IEEE modified test systems were implemented in both the PowerWorld [29] and DIgSILENT PowerFactory [30] software and are available online in open access (www.kios.ucy.ac.cy/testsystems).

The dynamic models and parameters for each generator, condenser, and motor in the IEEE 14 bus system are provided here based on real data [28]. The full dynamic data for the IEEE 30, 39, 57, and 118 bus systems are provided in Appendix A and are also available online in open access. In the case of the generators, both the associated exciter and governor parameters are given, while in the case of the condensers and motors only exciter parameters are given. The excitation and governor system models used for the implementation of the IEEE dynamic test systems in the two software were the IEEE Type1 excitation model (exciter IEEET1) [31]

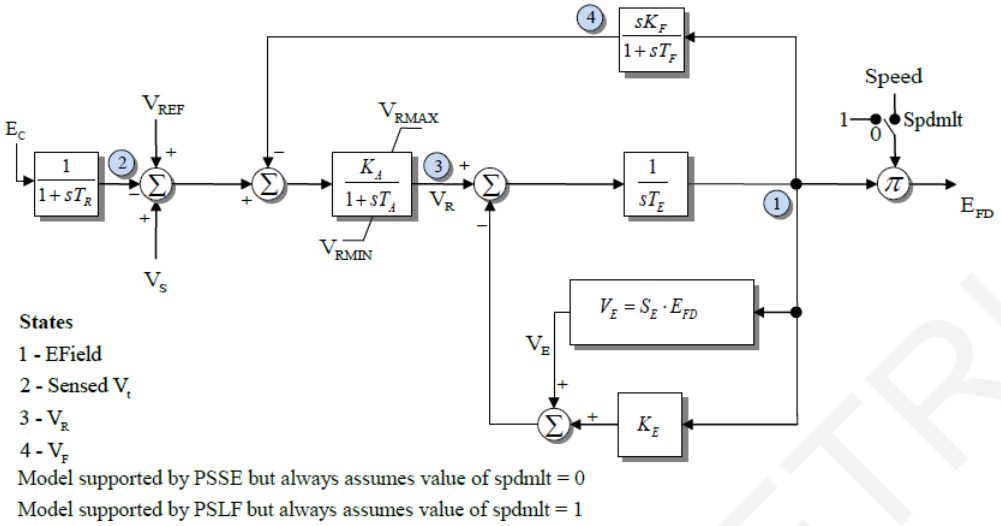

Figure 2.1: Block diagram of the IEEET1 excitation system model [31]

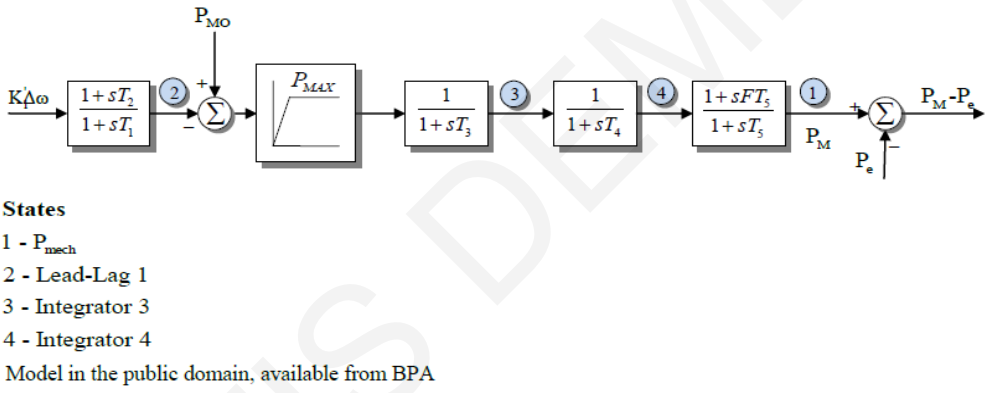

Figure 2.2: Block diagram of the WSCC Type G (BPA_GG) governor [31]

and WSCC Type G governor model (governor BPA_GG) [31] respectively. The block diagrams of both models are presented in Figure 2.1 and Figure 2.2. It is important to mention that the IEEE Type1 excitation model corresponds to the Type DC1A excitation system model of the IEEE Standard 421.5 (2005) [32], which is the currently accepted IEEE standard for excitation system models for power system stability studies. It is important to notice that the rated voltage of the machines (generators, motors, and condensers), as indicated in [28], is much smaller than the voltage levels of the IEEE test systems. To comply with the voltage levels of the generators as provided in [28], and thus build more realistic dynamic test bed systems, the machines were connected through an ideal transformer. Hence, it was necessary to add an additional bus having the same voltage level as the machine models in [28].

Performing this modification (Figure 2.3), the IEEE test systems topology was not changed, and at the same time, there was no change in the operating conditions of the systems since the power flows were not affected. This was confirmed by comparing the total power losses of the

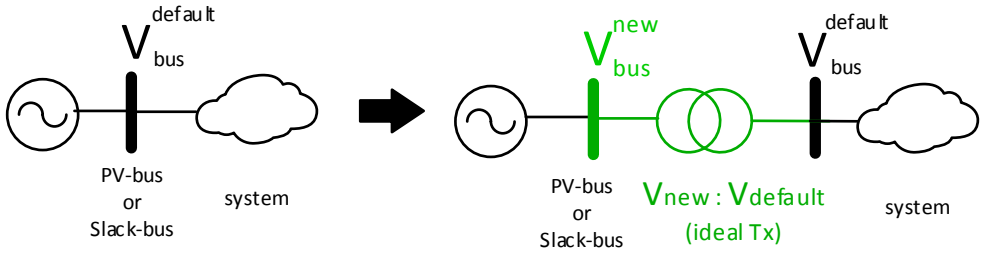

Figure 2.3: Extension and modification of an existing system

systems before and after the modification. The data of the transmission lines, existing transformers, voltage levels and other steady-state data were considered the same as those presented in [21]. Due to this modification, hereafter the IEEE test bed systems will be called as "modified IEEE systems". In order to better illustrate the modification to the IEEE dynamic test systems, the IEEE 14-bus test system before and after the modification is shown in Figure 2.4 and Figure 2.5 respectively.

The IEEE 14-bus modified test system consists of 5 synchronous machines with IEEE type-1 exciters, 3 of which are synchronous compensators used only for reactive power support. There are 19 buses, 17 transmission lines, 8 transformers and 11 constant impedance loads. The total load demand is 259 MW and 73.5 MVAr.

In the default topology of the IEEE 14-bus test system (Figure 2.4), the generators and the condensers are connected to high voltage buses (132 kV or 220 kV) [21]. In the case of the IEEE 14-bus modified test system (Figure 2.5), the generators and the condensers with their dynamic models are attached to the new buses added to the extended system, as explained

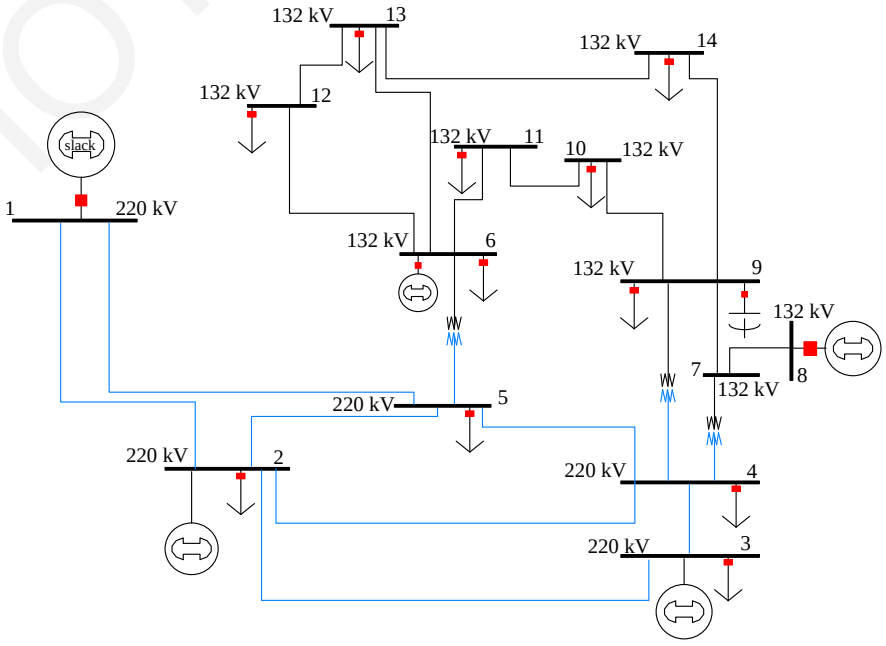

Figure 2.4: IEEE 14-bus test system: default topology

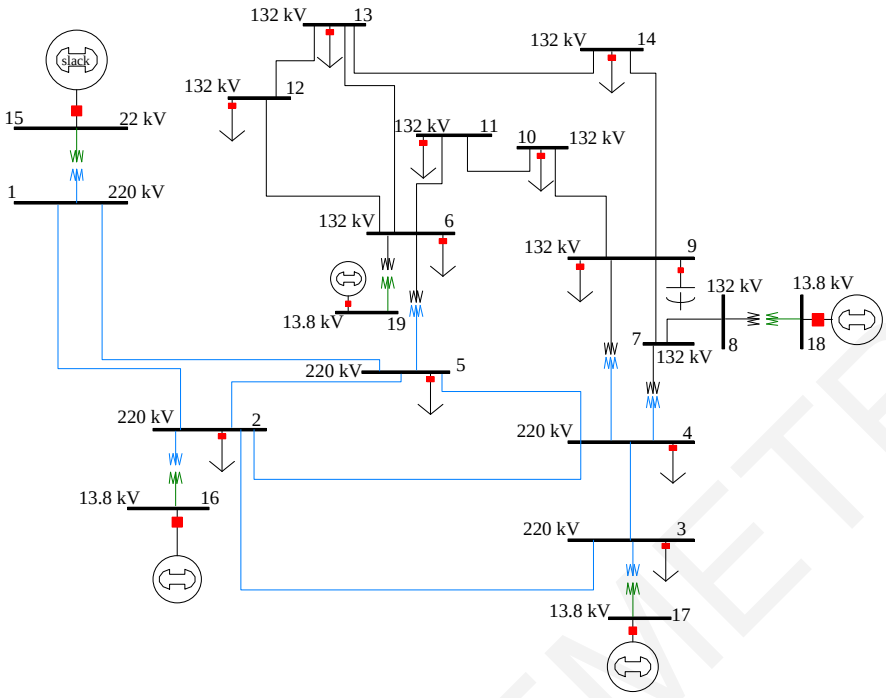

Figure 2.5: IEEE 14-bus modified test system

earlier. Table 2.1 to Table 2.3 provide the system data for the IEEE 14-bus modified test system. The numbers shown in the Tables for the bus numbers correspond to the default test system and the modified system (in parenthesis) respectively.

Table 2.1: IEEE 14-bus modified test system machine data

Type	GENROU	GENROU	GENROU	GENROU
Operation	Sync. Gen.	Sync. Gen.	Condenser	Condenser
Default Unit no. (New Unit no.)	1(15)	2(16)	3(17)	6(19), 8(18)
Rated power (MVA)	448	100	40	25
Rated voltage (kV)	22	13.8	13.8	13.8
H (s)	2.656	4.985	1.520	1.200
D	2.000	2.000	0.000	0.000
r_a (p.u)	0.0043	0.0035	0.000	0.0025
x_d (p.u)	1.670	1.180	2.373	1.769
x_q (p.u)	1.600	1.050	1.172	0.855
x'_d (p.u)	0.265	0.220	0.343	0.304
x'_q (p.u)	0.460	0.380	1.172	0.5795
x''_d (p.u)	0.205	0.145	0.231	0.2035
x''_q (p.u)	0.205	0.145	0.231	0.2035
x_l or x_p (p.u)	0.150	0.075	0.132	0.1045
T'_{d0} (s)	0.5871	1.100	11.600	8.000
T'_{q0} (s)	0.1351	0.1086	0.159	0.008
T''_{d0} (s)	0.0248	0.0277	0.058	0.0525
T''_{q0} (s)	0.0267	0.0351	0.201	0.0151
$S(1.0)$	0.091	0.0933	0.295	0.304
$S(1.2)$	0.400	0.4044	0.776	0.666

Table 2.2: IEEE 14-bus modified test system exciter data

Type	IEEET1	IEEET1	IEEET1	IEEET1
Default Unit no. (New Unit no.)	1(15)	2(16)	3(17)	6(19), 8(18)
Rated power (MVA)	448	100	40	25
Rated voltage (kV)	22	13.8	13.8	13.8
T_r (s)	0.000	0.060	0.000	0.000
K_a (p.u)	50	25	400	400
T_a (s)	0.060	0.200	0.050	0.050
V_{Rmax} (p.u)	1.000	1.000	6.630	4.407
V_{Rmin} (p.u)	-1.000	-1.000	-6.630	-4.407
K_e (p.u)	-0.0465	-0.0582	-0.170	-0.170
T_e (s)	0.520	0.6544	0.950	0.950
K_f (p.u)	0.0832	0.105	0.040	0.040
T_f (s)	1.000	0.350	1.000	1.000
E_1 (p.u)	3.240	2.5785	6.375	4.2375
$SE(E_1)$	0.072	0.0889	0.2174	0.2174
E_2 (p.u)	4.320	3.438	8.500	5.650
$SE(E_2)$	0.2821	0.3468	0.9388	0.9386

Table 2.3: IEEE 14-bus modified test system governor data

Type	BPA_GG	BPA_GG
Default Unit no. (New Unit no.)	1(15)	2(16)
Rated power (MVA)	448	100
Rated voltage (kV)	22	13.8
P_{max} (p.u)	0.870	1.050
R (p.u)	0.011	0.050
T_1 (s)	0.100	0.090
T_2 (s)	0.000	0.000
T_3 (s)	0.300	0.200
T_4 (s)	0.050	0.300
T_5 (s)	10.000	0.000
F	0.250	1.000

2.3 Dynamic IEEE Test Systems for Transient Analysis: Testing

The proposed dynamic test bed systems have been tested under transient conditions to demonstrate that their dynamic behavior conformed with the dynamic response of real systems. In this attempt, the proposed modified IEEE test systems were implemented in the PowerWorld and DIgSILENT PowerFactory software. The transient behavior of each dynamic system could be obtained with the use of the transient analysis of these software. For each case study, the angle, frequency and voltage stability were examined. Thus, a depiction of the generator rotor angle, bus voltage, and system frequency during transient conditions was

obtained. More specifically, for evaluating the proposed dynamic governor models and their parameters, the system frequency was obtained for two cases. In the first case, generators were equipped with governor models, while in the second case no governor models were considered (for both cases machine and exciter dynamic models were available). Moreover, to evaluate the proposed exciter models and their parameters, voltage magnitudes and angles for selected buses were presented for the case where system generators were equipped with and without exciter models (for both cases machine and governor dynamic models were available). Finally, the rotor angle for selected generators (with full machine models) was obtained to check their dynamic response during contingencies. It is important to mention that a comparison between the total power losses of each system before and after the modification (in steady state operation) was also performed to verify that the power flows were not affected. The transient analysis results for the IEEE 14- and 39-bus modified test systems are presented below. The results for the rest of the test systems can be found in [27].

2.3.1 IEEE 14-bus modified test system

In order to assess the stability condition of the IEEE 14-bus modified test system during transient analysis, a single load event was considered. At time $t = 1$ s, the value of loads at buses 3, 4 and 9 was increased by 20% (total step change of 34.3 MW). The IEEE 14-bus modified test system response under this event is given in Figures 2.6 - 2.11.

Table 2.4: Real power losses in IEEE 14-bus system

Losses in default topology (MW)	Modified topology (MW)
15.2	15.2

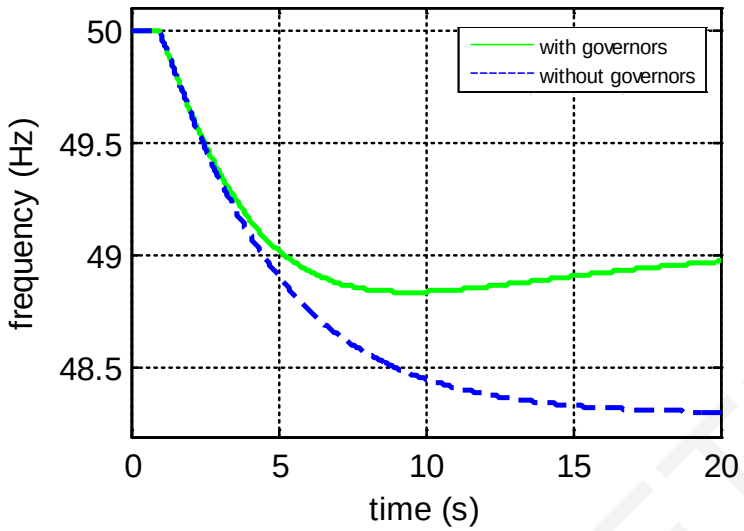

Figure 2.6: System frequency in the IEEE 14-bus modified test system with and without governor models

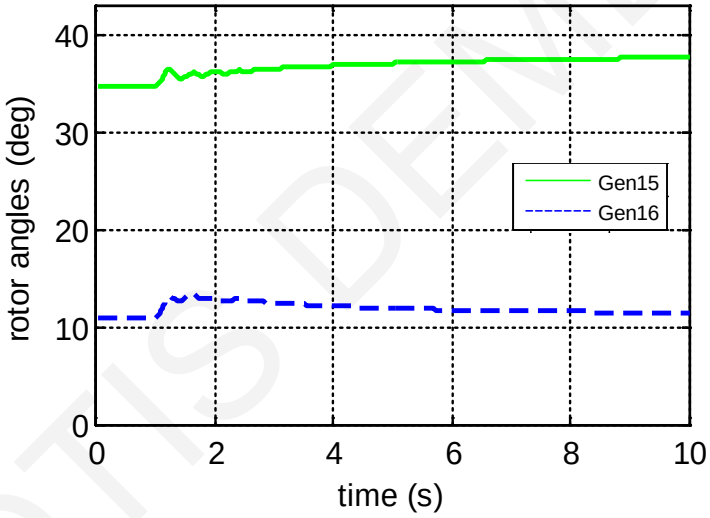

Figure 2.7: Generator rotor angle for the machines in the IEEE 14-bus modified test system

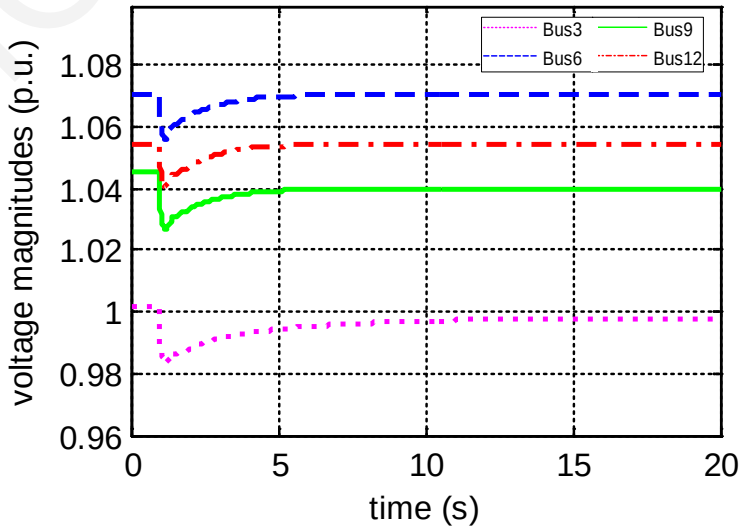

Figure 2.8: Voltage magnitudes for selected buses in the IEEE 14-bus modified test system with exciter models

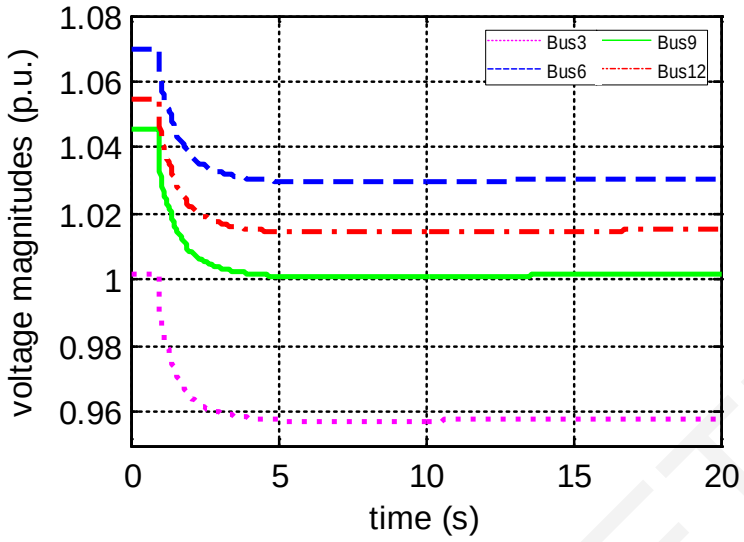

Figure 2.9: Voltage magnitudes for selected buses in the IEEE 14-bus modified system without exciter models

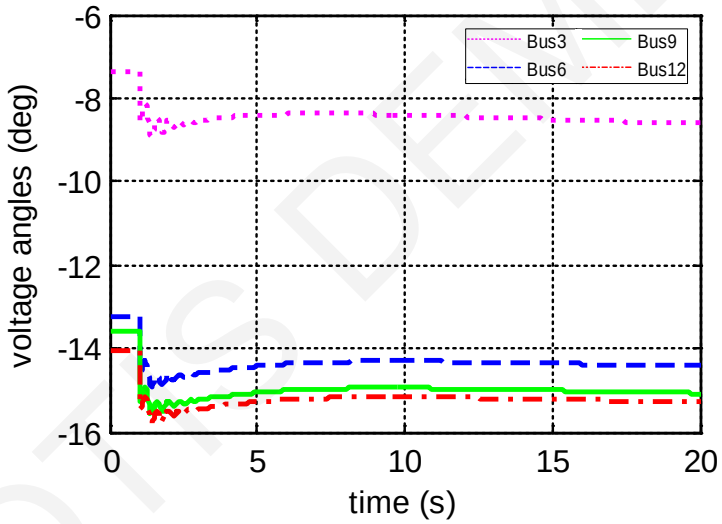

Figure 2.10: Voltage angles for selected buses in the IEEE 14-bus modified test system with exciter models

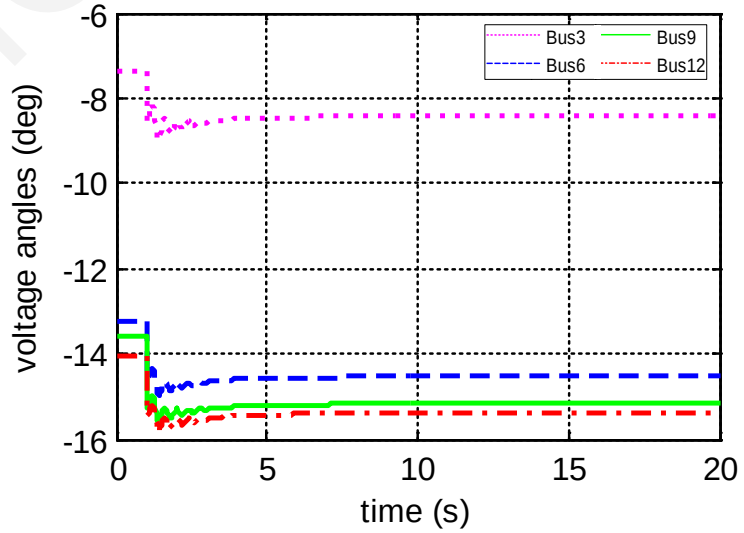

Figure 2.11: Voltage angles for selected buses in the IEEE 14-bus modified test system without exciter models

2.3.2 IEEE 39-bus modified test system

The IEEE 39-bus modified test system contains 49 buses, 32 transmission lines, 24 transformers and 10 generators. It has 19 constant impedance loads totaling 6097.1 MW and 1408.9 MVAr. All the generators are equipped with an IEEE type-1 exciter and a simple turbine governor, except generator 39 which is an aggregation of a large number of generators and is considered not to have a governor. The behavior of the IEEE 39-bus modified test system during transient analysis was evaluated by considering a single load event. At time $t = 1$ s, the value of loads at buses 3, 4, 7, 8, 25 and 39 was increased by 10% (total step change of 290.58 MW). Figures 2.12 – 2.17 show the response of the system during the event.

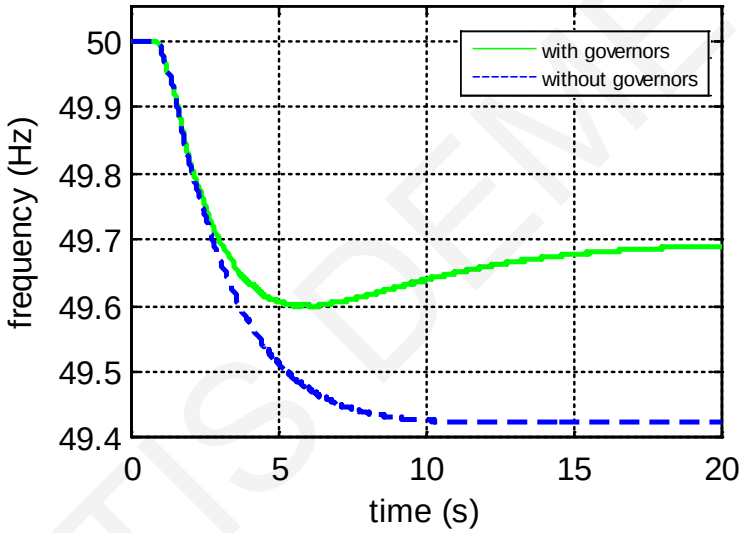

Figure 2.12: System frequency in the IEEE 39-bus modified test system with and without governor models

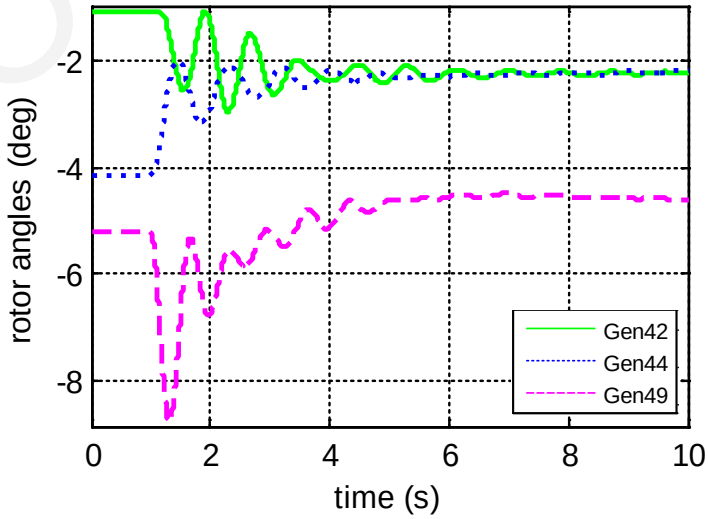

Figure 2.13: Generator rotor angle for selected machines in the IEEE 39-bus modified test system

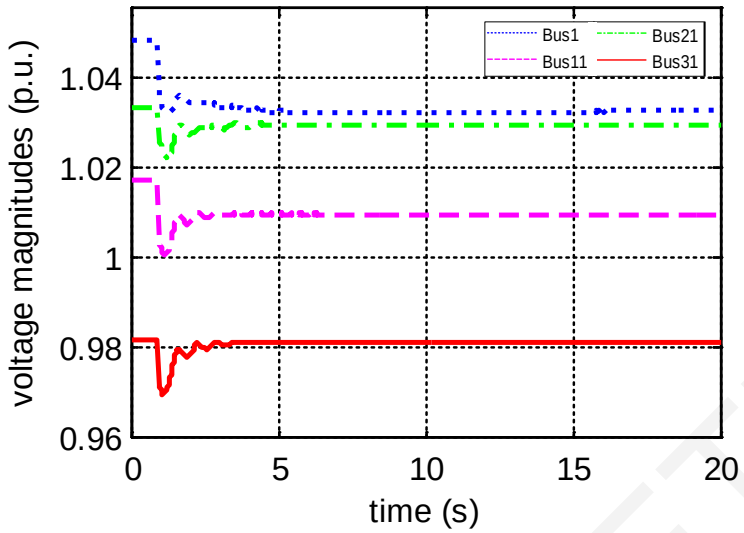

Figure 2.14: Voltage magnitudes for selected buses in the IEEE 39-bus modified test system with exciter models

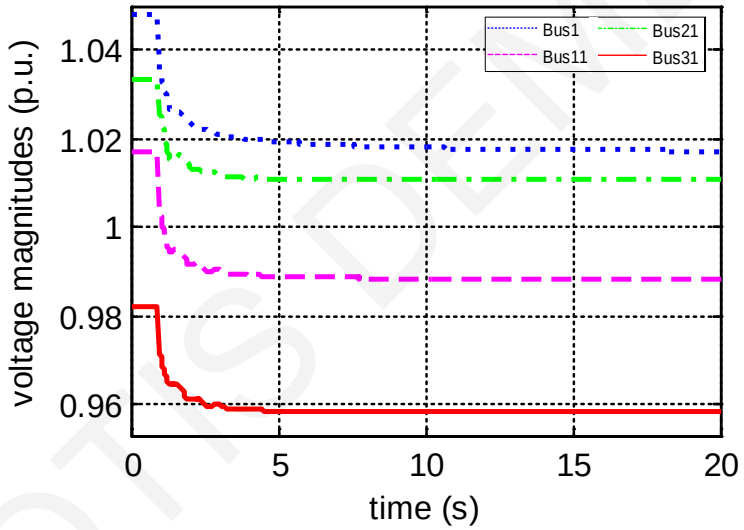

Figure 2.15: Voltage magnitudes for selected buses in the IEEE 39-bus modified system without exciter models

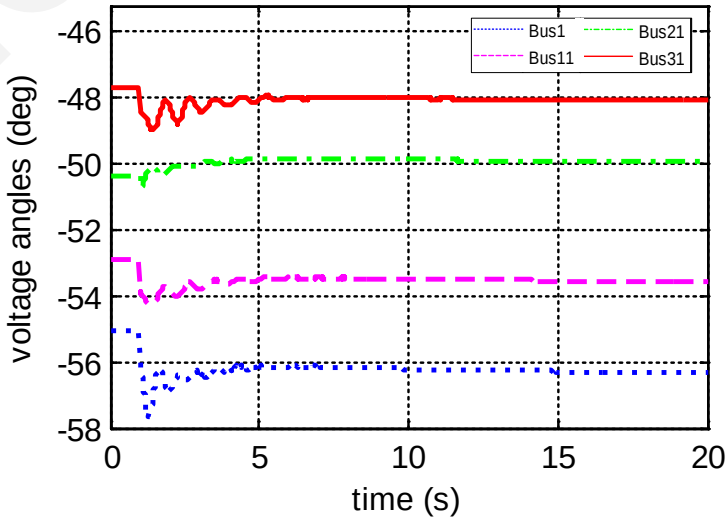

Figure 2.16: Voltage angles for selected buses in the IEEE 39-bus modified test system with exciter models

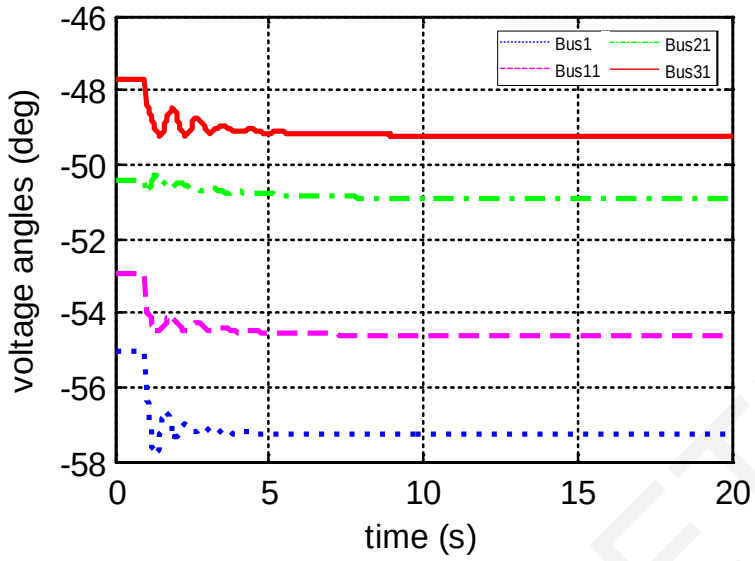

Figure 2.17: Voltage angles for selected buses in the IEEE 39-bus modified test system without exciter models

In addition, the stability condition of the IEEE 39-bus modified test system during transient analysis was further assessed by considering a worst case scenario. At time t = 1 s, a balanced three phase fault was applied at bus 39 and was cleared at t = 1.2 s. As shown in Figure 2.18, if the system generators were not equipped with governor models, then the system would collapse. In particular, when the speed limits of a generator are violated (in this case when the speed drops below 48 Hz or exceeds 52 Hz), auxiliary corrective measures are applied (e.g., under/over frequency control), and the corresponding generator is tripped. Consequently, since the system generators were not equipped with any governor models, a sequence of generator trips would ensued leading to system collapse. However, if the system generators were equipped with governor models, a generator trip through an under/over frequency control scheme would not lead to more generator trips, since the governors maintain the speed of each generator close to the nominal speed. As a result, the system could withstand the fault and it could maintain its synchronism, as shown in Figure 2.19.

Table 2.5: Real power losses in IEEE 39-bus system

Losses in default topology (MW)	Modified topology (MW)
42.8	42.8

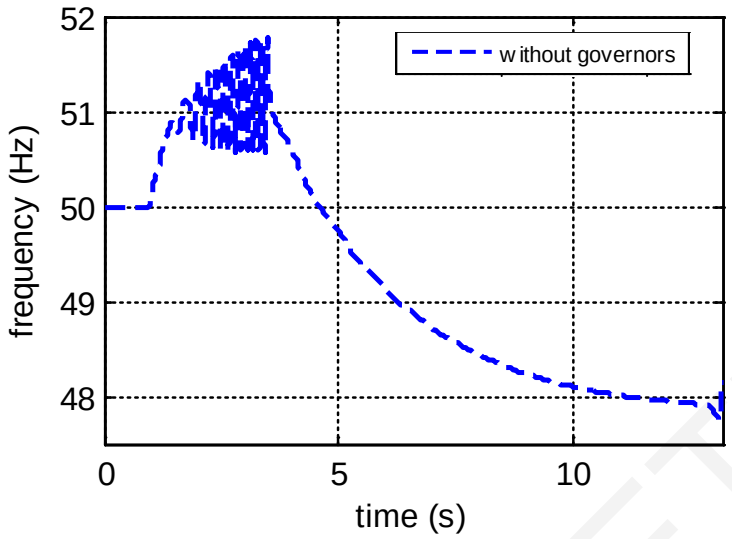

Figure 2.18: System frequency in the IEEE 39-bus modified test system without governor models

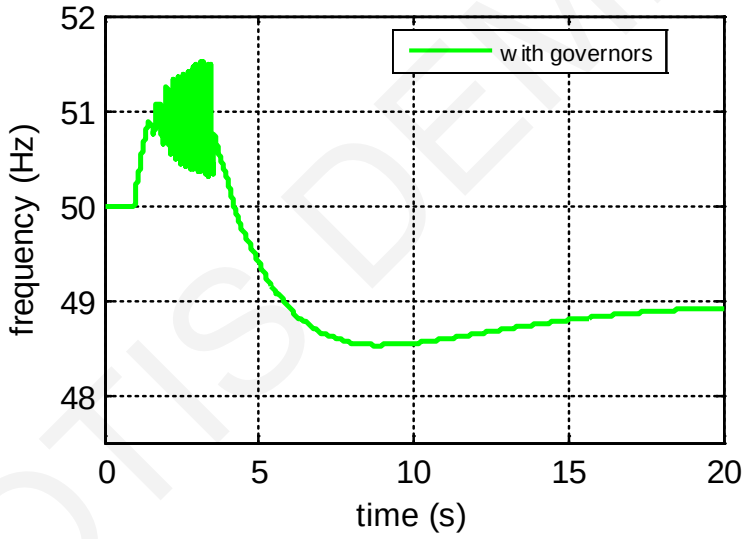

Figure 2.19: System frequency in the IEEE 39-bus modified test system with governor models

2.4 Conclusions

The dynamic models and the dynamic parameters for sixth order full machine models (i.e., machine, exciter, and governor) as well as for the condensers and motors contained in the IEEE 14, 30, 39, 57, and 118 bus systems were defined based on typical data provided in [28]. The topology of the proposed dynamic IEEE test bed systems was slightly altered from the default one by adding new buses with lower voltage level for the generators, condensers, and motors, in order to be compliant with the rated voltage level of the dynamic models provided in [28]. The procedure followed in this work for including dynamic models into a system can

be generalized for several systems, assuming that the rated power of the generators, motors, and condensers are known. The dynamic models allow researchers to test their methodologies on common test systems in order to compare results and performance. The dynamic test systems complement the existing steady state systems.

The behavior of the dynamic IEEE modified test systems has been examined under large disturbances. Based on the simulation results, it can be concluded that the dynamic models with the proposed typical parameters are reliable since the dynamic response of the IEEE modified test systems follow the expected behavior of actual systems under contingencies. It was shown that the proposed governor models play a crucial role in the maintenance of the system frequency, even under severe faults. Moreover, voltage magnitudes of the buses for all the test systems are preserved close to their pre-fault values in the presence of the proposed exciter models. In the case of the rotor angle stability, it is clear that the generators maintain the synchronism between them after the occurrence of a fault. Finally, it was shown that in steady state conditions the real power losses are the same in both the modified and the actual IEEE test systems. This indicates that the modifications of the default test systems topology do not influence the steady state conditions of the systems.

CHAPTER 3
GENERATOR COHERENCY

3.1 State-of-the-Art Overview

Transient stability or large disturbance rotor angle stability refers to the ability of the power system to maintain synchronism when subjected to a severe disturbance [12]. The instability that may result occurs in the form of increasing angular swings of some generators leading to their loss of synchronism with other generators. In steady state conditions, the rotor angles (swing curves) of all the generators swing together in a synchronous frame of reference. This means that the angular difference between any two generators is approximately constant over a period of time. However, in case of a disturbance in multi-machine power systems, a drift in the rotor angle of some generators is introduced, moving them away from the rest of the generators. Generators belonging to a certain coherent group are expected to exhibit similar responses to the disturbance. Hence, the difference between their swing curves is so small that they can be considered to be oscillating together and coherently. After the removal of the disturbance, the affected generators will again swing back to the rest of the generators. Power system coherency refers to the property of generators having similar time-domain responses during a system transient.

It is understood that the ICI scheme relies on generator coherency to decide when and where to inhibit/arm specialized relays. These specialized relays, when armed, will trip in response to local signals to create the isolated electrical islands. The stability is guaranteed by the fact that all the generators in these islands are coherent. In this context, real-time knowledge of generator coherency will help plan the boundaries of these islands and avoid unnecessary tripping [33].

In the literature, various methods for identifying coherent generators have been reported which can be categorized into three types. The first class identifies generator coherency by analyzing the empirical results of offline simulation (e.g., examine the similarity between the generator swing curves by comparing their trend visually) [34], [35]. Such approaches exhibit high accuracy but are inappropriate for addressing disturbances dynamically in real-time. The second type employs linearized power system models about the power flow equilibrium to

reduce complexity [36], but is often unsuitable to represent large or rapid deviations from the equilibrium. The third class introduces the notion of slow coherency arising from interarea oscillations [26], [37]. These methods use singular perturbation to assess time-scale separation of the interarea and local modes, and implement eigenvector-based methods to identify coherent generator groups. One disadvantage is the inefficiency of these methods when the interarea oscillation is not sufficiently reduced. Furthermore, all three classes require detailed power system topology data, which may not always be available when needed especially for emerging wide area smart grid systems.

To address this problem, measurement-based coherency identification employing Phasor Measurement Units (PMUs) has been proposed. PMUs provide real-time synchronized system measurements including voltage and current at generator buses and generator speeds [38]. The main advantage of direct PMU monitoring of generators is measurement accuracy resulting in enhanced transmission network reliability [39], [40]. Moreover, it is expected that PMU placement will include generator buses of interest in coherency identification applications due to the requirement of installing PMUs at new interconnections [41]. Under this assumption, the methodologies underlying measurement-based coherency identification approaches are diverse. In [42], a method based on measuring coherency in terms of frequency deviation and the application of an Artificial Neural Network (ANN) technique is proposed. Wide area generator speed measurements combined with Fourier analysis are used to determine coherent generator groups in [43]. The authors in [44] have presented the identification of coherent generators in power systems using Growing Self Organizing Feature Map. Coherency for power systems is obtained in [45] through principal component analysis. Researchers in [46] applied the Hilbert-Huang transform on generator phase angle data to identify coherency.

3.2 Two–Step Methodology for Real-Time Identification of Coherent Generator Groups

Generator coherency can be established by comparing synchronized data of generator rotor angle and frequency in real-time. A typical Wide Area Monitoring Protection and Control (WAMPAC) system consists of strategically located PMUs that provide synchronized system measurements [38]. The main contribution of this work [47] is to utilize such measurements to analyze the evolution of inherent system dynamic behavior. The generator speed, output power, voltage and current are measured continuously at all generator terminals and a

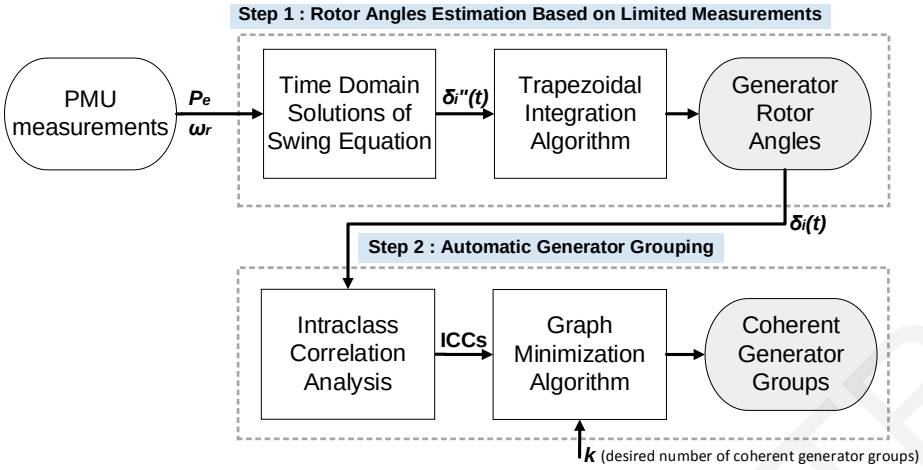

Figure 3.1: Identification of coherent generators in real-time

snapshot is utilized to find the coherent generator groups (Figure 3.1). The data are transmitted to the transmission control center in milliseconds time scale where a real-time estimation of the generator rotor angles is performed by extracting time domain solutions of the swing equation. The tool to identify similarity between each pair of the swing curves, which is based on an intraclass correlation analysis [48] (a well-established technique in statistics), has input data available in less than a second's time interval. The groups of the coherent generators are finally determined through a graph minimization algorithm. Therefore, the proposed two-step methodology for the real-time identification of coherent generator groups (Figure 3.1) might be a new WAMPAC application.

3.2.1 Step 1: Rotor angle estimation based on limited measurements

For an *n*-machine power system, the classical swing equation that describes the behavior of the rotor dynamics of a synchronous generator is [49]:

$$2H\frac{S_{rated}}{\omega_s^2}\omega_r\frac{d^2\delta}{dt^2} = P_m - P_e - K_D\Delta\omega_r = P_a \qquad (3.1)$$

where H is the inertia constant at the synchronous speed ω_s in seconds (ω_s in electrical radians/second), ω_r is the generator angular speed in radians/second, S_{rated} is the generator MVA rating, δ is the angle of the internal emf of the generator, P_m, P_e and P_a are the mechanical, electrical and accelerating power respectively in MW, K_D is the damping coefficient of the rotor and $\Delta\omega_r$ is the speed deviation in radians/second.

In nominal operating conditions, the machine angular speed is equal to the synchronous speed ($\omega_r = \omega_s$). Dividing both sides of (3.1) by S_{rated} and neglecting the damping constant

which does not significantly affect the more basic characteristics, such as the natural frequencies and mode shapes, (3.1) can be expressed as:

$$\frac{2H}{\omega_s}\frac{d^2\delta}{dt^2} = P_m - P_e = P_a \quad per\ unit \tag{3.2}$$

In non-nominal operating conditions, considering that an installed PMU at each generator terminal can provide synchronized measurements of the generator speed, output power, voltage and current with a rate up to 50 samples/s, a time domain solution of the swing equation can be obtained using an integration technique. In such a case, the mechanical power input to the machine (P_m) is assumed constant for a short duration of the fault (in this case for 1 s). In general, the assumption of constant P_m in a real power system is not far from reality.

$$2H\frac{\omega_r}{\omega_s^2}\frac{d^2\delta}{dt^2} = P_m - P_e = P_a \quad per\ unit \tag{3.3}$$

$$\frac{d^2\delta}{dt^2} = (P_m - P_e)\frac{\omega_s^2}{2H\omega_r} \tag{3.4}$$

Since (3.4) is linear (all the terms of the second part of (3.4) are known), a direct non-iterative solution can be obtained at each time step (defined in this work as Δt = 0.02 s) using the well-known trapezoidal integration algorithm [50]. It must be noted that since the trapezoidal integration algorithm is numerically stable [50] large step sizes can be used. The classical trapezoidal integration technique is described in (3.5).

$$\begin{gathered} f'(x) = \lim_{\Delta x \to 0}\frac{f(x+\Delta x) - f(x)}{\Delta x} \\ \Delta x \neq 0 \Rightarrow \frac{\Delta f(x)}{\Delta x} = \frac{f(x+\Delta x) - f(x)}{\Delta x} \\ f''(x) = \frac{\Delta^2 f(x)}{\Delta x^2} = \frac{f(x+2\Delta x) - 2f(x+\Delta x) + f(x)}{\Delta x^2} \end{gathered} \tag{3.5}$$

Applying the trapezoidal integration technique (3.5) to (3.4) yields the expressions (3.6)-(3.7).

$$\delta''(t) = \frac{\delta(t+2\Delta t) - 2\delta(t+\Delta t) + \delta(t)}{\Delta t^2} \tag{3.6}$$

At each time step $t + \Delta t$,

$$\begin{gathered} \delta''(k-1) = \frac{\delta(t+1) - 2\delta(k) + \delta(k-1)}{\Delta t^2} \\ \delta(k) = \delta''(k-2)\Delta t^2 + 2\delta(k-1) - \delta(k-2) \end{gathered} \tag{3.7}$$

with $\delta(-2) = 0$, $\delta(-1) = 0$ and $\delta''(k)$ known.

3.2.2 Step 2: Automatic generator grouping

A classical process for identifying the similarity between each pair of the generator swing curves, and thus forming the coherent generator groups, is to compare their trend visually. Typically, this procedure is executed by an experienced system operator. However, an estimation of the generator rotor angles in real-time followed by an evaluation of their similarity could help to automate this visual process and thus increase its flexibility. In this work, the similarity is evaluated based on an intraclass correlation analysis [48] and the coherent generator groups are identified through a graph minimization algorithm.

A) Intraclass Correlation Coefficient (ICC)

In statistics, the ICC is a general measurement of agreement or consensus [48]. The coefficient represents the agreement of two or more dependent variables (coders) by comparing the variability of different measurements (or ratings) within variables and between variables to the total variation across all measurements. There are numerous versions of the ICC that can give quite different results when applied to the same data. Each form is appropriate for specific situations defined by the experimental design and the conceptual intent of the study. There are six forms of ICC that are most common. However, the choice of the most appropriate form calls for three decisions: a) Is a one-way or two-way analysis of variance (ANOVA) appropriate for the analysis of the study? [51] b) Are differences between the means of the coders relevant to the study? and c) Is the unit of analysis an individual measurement or the mean of several measurements?

For this study, and to identify generator coherency through the assessment of the rotor angle samples, two dependent variables (coders) are necessary: the time-step of each sample and the identity of each generator. Therefore, a two-way ANOVA is suitable for this study and not the one-way ANOVA. The two-way ANOVA variables are presented in

Table 3.1. In this table, *SSC* is the Sum of Squares between Columns, *SSR* is the Sum of Squares between Rows and *MSE* is the Mean Square Error. The sets $\mathbf{J} = \{1,\ldots,j\}$ and $\mathbf{I} = \{1,\ldots,i\}$ denote the generators and the number of samples, respectively. Moreover, in this study, since the rotor angle samples of each generator are independent from the rotor angle samples of all the other generators, the differences between the means of the coders are relevant to the study. Finally, since a single rotor angle sample is obtained at each time-step, it is obvious that the unit of analysis is an individual measurement and not the mean of several

Table 3.1: Two-way ANOVA

Variation	***Sum of Square***	***Mean Squares***
Between Columns	$SSC = I\sum_{j=1}^{J}(\bar{X}_j - \bar{X})^2$	$MSC = \frac{SSC}{J-1}$
Between Rows	$SSR = J\sum_{i=1}^{I}(\bar{X}_i - \bar{X})^2$	$MSR = \frac{SSR}{I-1}$
Error	$SSE = \sum_{i=1}^{I}\sum_{j=1}^{J}(X_{ij} - \bar{X}_i - \bar{X}_j + \bar{X})^2$	$MSE = \frac{SSE}{(I-1)(J-1)}$

measurements. The variables $\overline{X}_i$, $\overline{X}_j$ and $\overline{X}$ in Table 3.1 are described by,

$$\overline{X}_i = \frac{\sum_{j=1}^{J} X_{i,j}}{J}, \qquad \overline{X}_j = \frac{\sum_{i=1}^{I} X_{i,j}}{I}, \qquad \overline{X} = \frac{\sum_{i=1}^{I}\sum_{j=1}^{J} X_{i,j}}{IJ} \tag{3.8}$$

According to the three decisions above, the appropriate ICC form for this study is given by the variance ratio:

$$\rho = \frac{\sigma_T^2}{\sigma_T^2 + \sigma_J^2 + \sigma_I^2 + \sigma_E^2} \tag{3.9}$$

where σ_J^2 is the variance of the deviation from the overall mean of each set of rotor angle samples, σ_I^2 is the variance of the difference of each time-step and each set of rotor angle samples from their mean, σ_T^2 is the variance of the difference from the overall mean of the j^{th} sample, and σ_E^2 is the variance of the sample error.

However, the true variance terms are rarely known due to the sampling variability of the PMUs and to the limited number of samples. Therefore, ICC can be estimated from the sample data as:

$$ICC(2,1) = r = \frac{MSR - MSE}{MSR + (n-1)MSE + n\frac{(MSC - MSE)}{I}}, r \in [-1,1] \tag{3.10}$$

where n refers to the number of data sets to be compared (n = 2 for the purpose of the identification of coherent generator groups). An *ICC(2,1)* equal to 1 denotes that the pair of generator swing curves is in perfect agreement, while an *ICC(2,1)* equal to 0 corresponds to random agreement.

B) Graph minimization algorithm for generator grouping

The generator coherency problem can be described using an undirected fully connected graph-model **G (V, E, W)**. In this graph-model, the node set **V**={v_1,…,v_n} denotes the machines while the edge weights set **W** with elements w_{ij} (i,j=1,…,n) denotes the calculated ICCs. The desired coherent groups (k=2,…,n) are represented by the subgraphs **Gm (Vm, Em, Wm)** where m=1,…,k.

For the case of two desired coherent groups (k = 2), the objective is to separate the positive and negative swing curves. Hence, the mean of the rotor angle samples of each generator is calculated and the separation of the two groups is performed based on the means sign. However, for k>2, the complexity of the problem is increased since additional features of the generator swing curves have to be considered. To solve this problem, the ICC between each pair of generators is firstly calculated separately at each subgraph (k=2). Then, for each subgraph a fully connected graph is formed using the calculated ICCs as its edge weights. Since the objective is to separate the generators into groups with the highest similarity, all but one negative ICC become zero. Furthermore, considering that the higher ICCs are of interest, a Minimum Spanning Tree (MST) with reversed edge weights (1/ w_{ij}) is suitable for this study. Therefore, two MSTs are derived that contain only the strongest relations. The formation of k>2 groups is achieved by selecting the k-2 globally smallest weight edges to be removed from the spanning trees.

3.2.3 Simulation results

The 39-bus New England System (Figure 3.2) was used to demonstrate the effectiveness of the proposed two-step methodology for the real-time identification of the coherent generator groups. The 39-bus New England System is a simplified model of the high voltage transmission system in the northeast of the U.S.A. (New England area). It consists of 39 buses (nodes), 10 generators, 19 loads, 34 lines and 12 transformers. The dynamic models and parameters for each generator have been taken from [52] and have been completed with data taken from [53], [54].

A) Case study 1

At time t = 1 s, both ends of transmission line 17-27 are opened. As a result, a transient instability is created into the system. Assuming that a PMU is installed at all generator

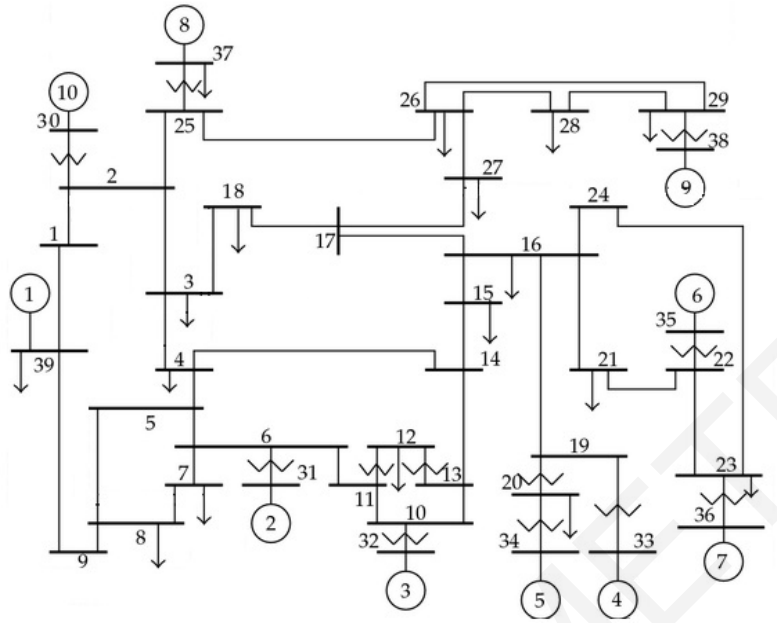

Figure 3.2: 39-Bus New England System

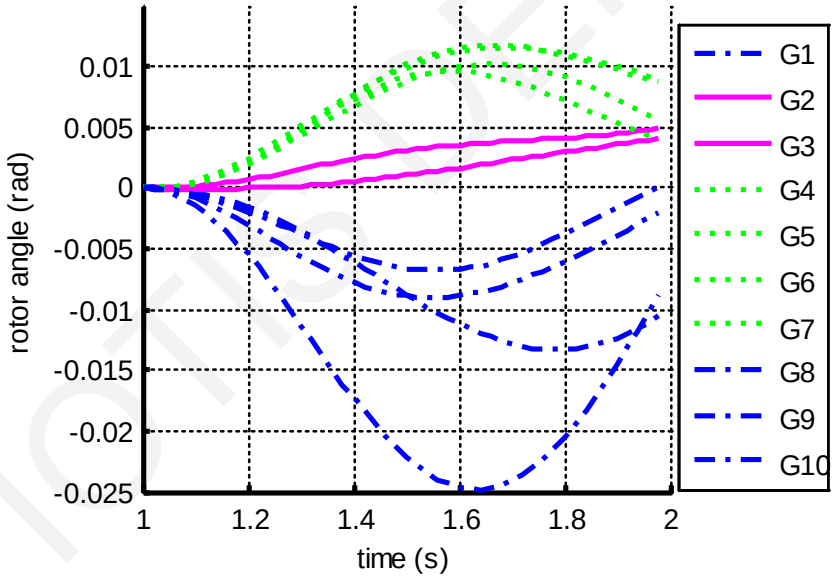

Figure 3.3: Generator swing curves of the 39-bus New England system obtained from the execution of Step 1

buses (10 PMUs in total), providing 50 synchronized measurements of the generator speed and output power per second, the swing curves obtained from the execution of Step 1 are shown in Figure 3.3.

After estimating the generator swing curves, the desired number of coherent generator groups (k) is formed based on the automatic generator grouping analysis of Section 3.2.2. For k=2, the positive and negative swings are directly separated and the coherent generator

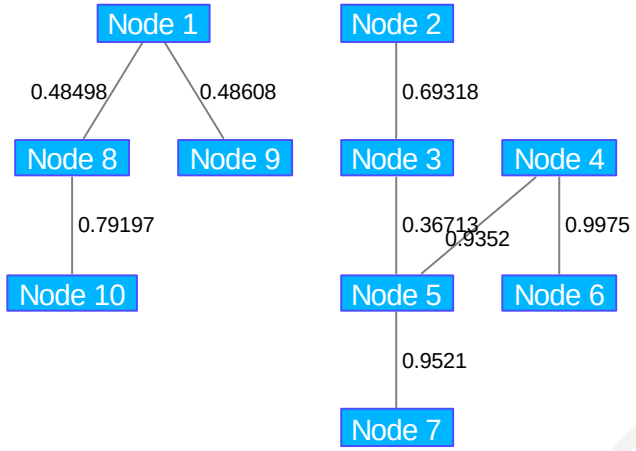

Figure 3.4: ICC between each pair of generators at each subgraph

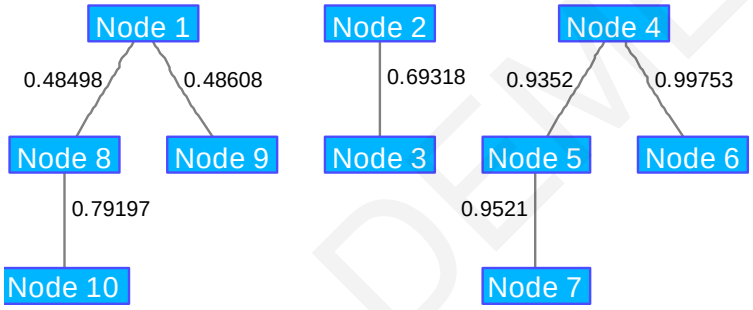

Figure 3.5: Coherent generator groups obtained from the execution of Step 2 for *k*=3

groups obtained are {G1, G8, G9, G10} and {G2, G3, G4, G5, G6, G7}. For *k*=3, the ICC between each pair of generators is firstly calculated separately at each subgraph (*k*=2) as shown in Figure 3.4. The coherent generator groups determined by the execution of Step 2 are {G1, G8, G9, G10}, {G2, G3} and {G4, G5, G6, G7} (Figure 3.5).

B) Case study 2

At time *t* = 1 s, both ends of transmission lines 3-18 and 4-14 are opened creating a transient instability into the system. Figure 3.6 shows the response of the generators during the event (Step 1). For *k*=2, the coherent generator groups obtained from the automatic generator grouping analysis are {G1, G8, G10} and {G2, G3, G4, G5, G6, G7, G9}. For *k*=3, the ICC between each pair of generators is firstly calculated separately at the two subgraph (*k*=2) and the resulted coherent generator groups are {G1}, {G8, G10} and {G2, G3, G4, G5, G6, G7, G9} (Figure 3.7).

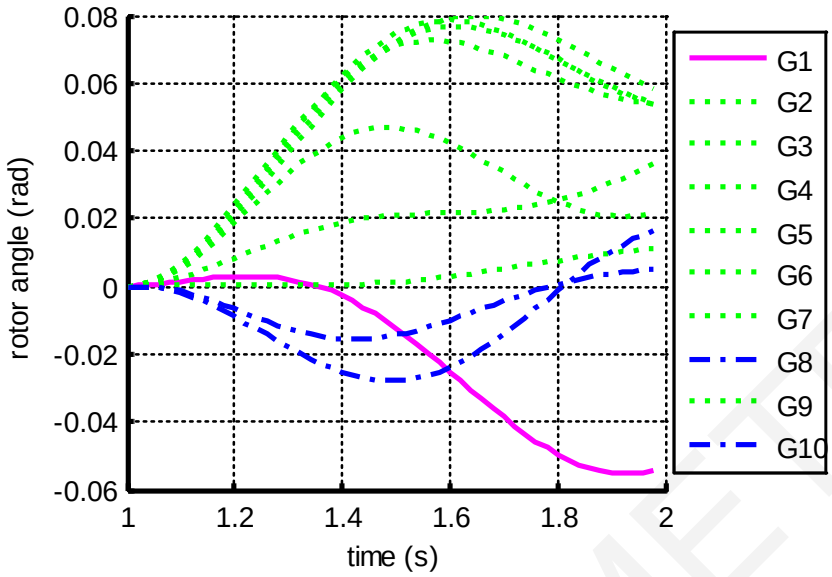

Figure 3.6: Generator swing curves of the 39-bus New England System obtained from the execution of Step 1

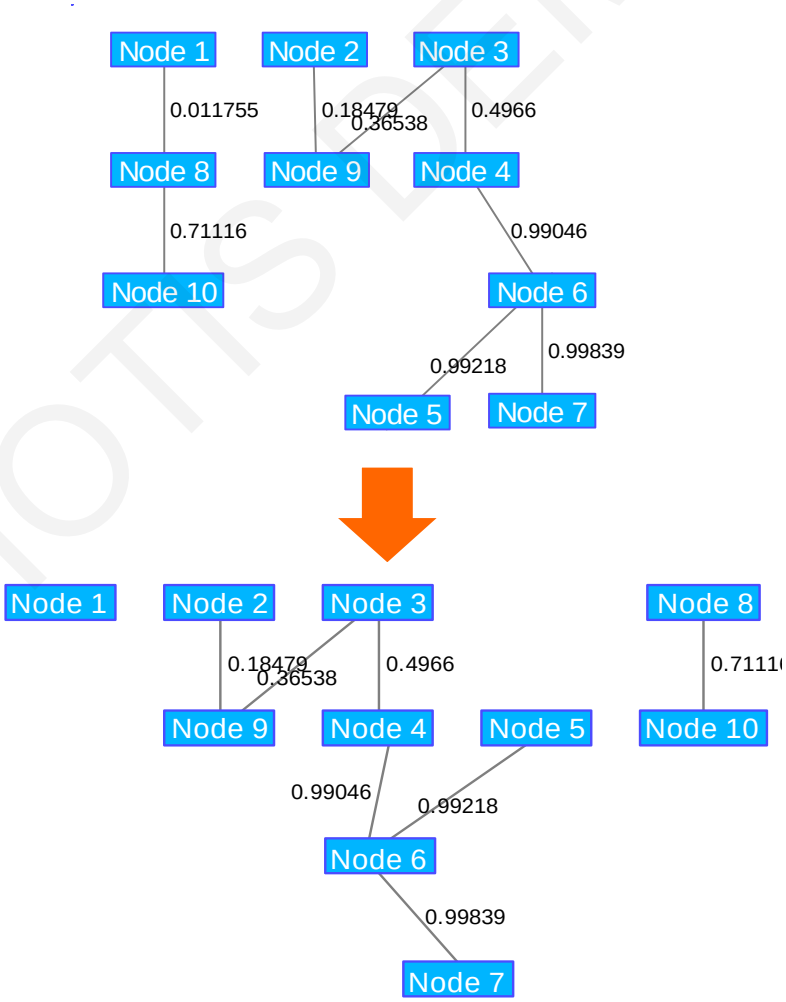

Figure 3.7: Coherent generator groups for *k*=3

3.3 Conclusions

In this Chapter, a two-step methodology for the real-time identification of coherent generator groups has been presented. During a disturbance, the inherent system dynamic behavior (rotor angle) is analyzed by utilizing synchronized PMU measurements (generator speed and output power at all generator terminals) and extracting time domain solutions of the swing equation. The generator swing curves obtained at Step 1 are served into Step 2, where the similarity between each pair of them is evaluated through an intraclass correlation analysis. The groups of the coherent generators are finally formed through a graph minimization algorithm. The effectiveness of the methodology was tested on the 39-bus New England System. In general, since the complexity of the methods involved is low, it can be deduced that the proposed methodology is suitable for real-time application.

CHAPTER 4

INTENTIONAL CONTROLLED ISLANDING – WHERE TO ISLAND

4.1 Graph Theory Fundamentals

In graph theory, an undirected graph-model $\mathcal{G} = (\mathcal{V}, \mathcal{E}, \mathcal{W})$ can be used to describe an *m*-generator and *n*-bus power system. In this graph model, the node set $\mathcal{V} = \{v_1, ..., v_n\}$ denotes the buses while the edge set $\mathcal{E}$ with elements $e_{ij}(i, j = 1, ..., n)$ denotes the transmission lines. The set $\mathcal{V}^{gen}$ is a subset of the node set $\mathcal{V}$ that contains only those buses with generators directly connected to them. The set $\mathcal{W}$, with elements $w_{ij}(i, j = 1, ..., n)$, is a set of edge weights representing the weight factors (power flows) associated with the transmission lines. To accommodate network losses, w_{ij} is calculated as follows:

$$w_{ij} = \begin{cases} \dfrac{|P_{ij}| + |P_{ji}|}{2} & \text{if } e_{ij} \in \mathcal{E}; \\ 0 & \text{otherwise.} \end{cases} \tag{4.1}$$

where P_{ij} and P_{ji} represent the active power flow in the line from bus *i* to *j*, and from *j* to *i*, respectively. Figure 4.1 shows as an example the graph representation of the IEEE 9-bus test system.

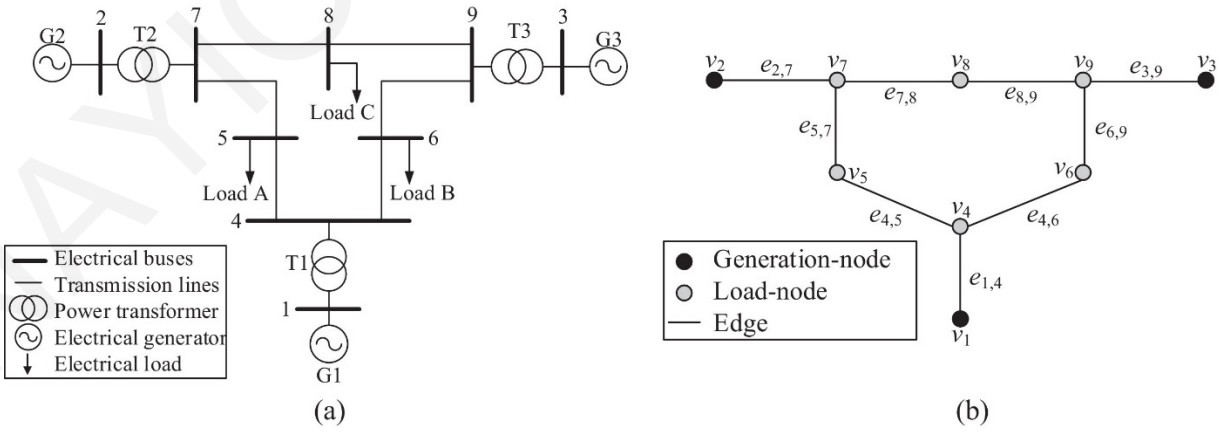

Figure 4.1: IEEE 9-bus test system (a) single line diagram. (b) simplified graph representation

The *cutset* $\mathcal{E}_S \subset \mathcal{E}$ [55] is the set of edges to be removed to split $\mathcal{G}$ into $K \in \mathbb{Z}^+$ subgraphs $\mathcal{G}_k = (\mathcal{V}_k, \mathcal{E}_k)$, where $k \in \mathcal{K}$, $\mathcal{K} = \{1, \ldots, K\}$. For K subgraphs, the sum of the weights of the edges within the cutset $\mathcal{E}_S$ is called the cut, which is defined as,

$$cut(\mathcal{V}_h, \mathcal{V}_k) = \sum_{i \in \mathcal{V}_h,\, j \in \mathcal{V}_k} w_{ij}, \quad h \neq k, \quad h, k \in \mathcal{K} \tag{4.2}$$

Bisection of the graph $\mathcal{G}$ means splitting the graph $\mathcal{G}$ into two subgraphs $\mathcal{G}_1 = (\mathcal{V}_1, \mathcal{E}_1)$ and $\mathcal{G}_2 = (\mathcal{V}_2, \mathcal{E}_2)$ by removing the edges connecting these two subgraphs [55]. Here, $\mathcal{V}_1$ and $\mathcal{V}_2$ are disjoint subsets of $\mathcal{V}$ ($\mathcal{V}_1 \cup \mathcal{V}_2 = \varnothing$ and $\mathcal{V}_1 \cap \mathcal{V}_2 = \mathcal{V}$). $\mathcal{V}_1^{gen}$ and $\mathcal{V}_2^{gen}$ are two disjoint subsets of $\mathcal{V}^{gen}$ which are also subsets of $\mathcal{V}_1$ and $\mathcal{V}_2$, respectively.

For a graph $\mathcal{G}$, the Laplacian matrix $\mathcal{L}$ [55] is defined as,

$$\mathcal{L} = \mathcal{D} - \mathcal{W} \tag{4.3}$$

where $\mathcal{D} = diag(d_i),\ i = 1, ..., n,$ is a diagonal degree matrix that contains the diagonal elements d_i which is equal to the total weight of the edges connected to node *i*.

The oriented incidence matrix $\mathcal{M}$ of $\mathcal{G}$ represents the incidence among nodes and edges, and is defined as follows [56]:

$$\mathcal{M} := [m_{ik}] = \begin{cases} 1 & \text{if arc } e_k = e_{ij} \text{ is incident from node } v_i; \\ -1 & \text{if arc } e_k = e_{ij} \text{ is incident to node } v_i; \\ 0 & \text{otherwise.} \end{cases} \tag{4.4}$$

4.2 State-of-the-Art Overview

Current approaches for ICI aim to split the system such that each island contains only coherent generators. In these approaches, the ICI is modeled as a combinatorial optimization problem, whose two main types of objective function are minimal power-flow disruption and minimal power imbalance within islands.

In [57], a two-phase Ordered Binary Decision Diagram (OBDD) method based on a simplified graph is presented to find the islanding solution that separated coherent generator groups with minimal power imbalance. In the first phase, the strategies that meet the conditions for the power balance of islands are identified by using the high-performance OBDD algorithm. In the second phase, power flow data are used to exclude strategies that

violate the transfer limits. The final results of this method represent the strategies that correspond to acceptable steady state operating points. In [58], the Breadth First Search (BFS)/Depth First Search (DFS) algorithms are used to find power-balanced islands containing coherent generator groups. BFS is a graph search algorithm which tries all one-step extensions of current paths before trying larger extensions. DFS is a graph search algorithm which extends the current path as far as possible before backtracking to the last choice point and trying the next alternative path. Even though these approaches ([57], [58]) result in different islanding solutions, they both can be described as searching problems on graphs, which are generally *NP-hard* [55]. In other words, there is no general polynomial time algorithm to find the optimal solution.

To overcome this problem, computationally more efficient algorithms that approximate the optimal solution must be used instead. In particular, the slow coherency theory (which can be used to find theoretically the weakest connection in a power network) is effectively used in [9], [15], [59] to split the system across weak connections (creating stable islands); however, this approach might not account for changes in the topology of the network, which can have an effect in the coherency results. Moreover, solutions with minimal power flow disruption can be achieved using efficient graph theoretic techniques such as spectral clustering. This technique uses the eigenvalues and eigenvectors of a matrix associated with a graph that represents the power system to determine splitting solutions within polynomial time. Spectral clustering is used in [60] to determine islanding solutions with minimal power flow disruption. Even though this method is computationally efficient, it does not include the generator coherency constraint in the ICI problem. Failure to consider this vital constraint restricts the use of this approach [8]. More recently, a Spectral Clustering Controlled Islanding (SCCI) algorithm has been proposed in [8]. The SCCI algorithm minimizes the power-flow disruption, while ensuring that each island contains only coherent generators. However, an islanding solution can only be directly determined when the number of islands is two, i.e., the SCCI algorithm only finds a solution for the bisection case. This issue is resolved by applying recursive bisection [8]. Nevertheless, recursive bisection is a computationally demanding technique that requires the repeated eigendecomposition of a matrix associated with the graph. Recursive bisection can also affect the quality of the islanding solution [61], [62]; better solutions may be missed. Efficient spectral clustering-based controlled islanding algorithms

are also presented in [63], [13], [64]. However, the unsupervised nature of these approaches makes difficult the introduction of ICI constraints in the problem.

4.3 Robust Spectral Clustering Controlled Islanding (RSCCI) Method

A novel two-step Spectral Clustering Controlled Islanding (SCCI) algorithm that minimizes the power-flow disruption, while ensuring that each island contains only coherent generators (dynamic constraint) has been proposed in [8]. The method was tested and validated using three different IEEE test systems. The results were promising and demonstrated the effectiveness of the SCCI method in networks with up to 118 buses. The method was later tested in various real networks, including small systems and very large-scale networks. The results achieved, when implementing the SCCI algorithm on real power systems, highlighted practical issues previously not considered that require to be addressed when using the existing SCCI method.

Therefore, the previously proposed SCCI algorithm is improved in this work and a Robust SCCI (RSCCI) is presented. In particular, the existing SCCI does not include constraints to unavailable transmission lines (static constraint). Thus, transformers and lines without synchro-check relays might eventually be included in the islanding solution. Synchro-check relays are essential during the synchronization of islands during the restoration process. Furthermore, the existing SCCI is also sensitive to outliers and computationally expensive for large scale (over 500 nodes) power systems. An *outlier* is an observation that is numerically distant from the rest of the data [65]. Therefore, this work presents possible solutions for when such problems occur. An outlier detection algorithm, to determine the optimal splitting strategy in strong connected networks and a constraint to exclude unavailable transmission lines from the splitting strategy are detailed in this work to determine the optimal splitting strategy in large scale power systems.

4.3.1 Outlier detection and robust clustering

After running the spectral analysis of the graph, a proper clustering algorithm should be selected to cluster the nodes of the graph based on the selected eigenvectors. There are many clustering algorithms that could be used. While *k-means*, the clustering algorithm used in the existing SCCI method, is the traditional and default algorithm in the literature as it is simple

and fast, it is very sensitive to outliers [66]. The *k-means* attempts to minimize a squared error function described as follows:

$$\mathrm{J} = \sum_{j=1}^{k} \sum_{i=1}^{n} \left\| x_i^{(j)} - c_j \right\|^2 \tag{4.5}$$

where $\left\| x_i^{(j)} - c_j \right\|^2$ is a chosen distance measure between a data-point $x_i^{(j)}$ and the cluster center (centroids) c_j, the mean value of the data-points in the cluster *j*.

When applying spectral analysis to solve the generalized eigenvalue problem, it is possible for graph nodes with very small weights and/or small degrees (e.g. a one-degree node with a very small weight) to produce eigenvectors that are outliers. Since the Spectral Clustering (SC) algorithm clusters nodes based on the eigenvectors of the graph, these outliers will affect the quality of the clustering.

There are two ways to handle this outlier problem. One is detecting the outliers through outlier detection algorithms and eliminating it before clustering. Another way is using a robust clustering algorithm which is not sensitive to outliers. In this work, a more robust clustering algorithm, *k-medoids*, to cluster the nodes in the solution subspace is implemented. Thus, a RSCCI method is obtained from the existing SCCI method. Instead of taking the mean value of data-points in a cluster as the cluster center, *k-medoids* chooses the most centrally located data-point in a cluster (medoids) as the cluster center. It is more robust to noise and outliers compared to *k*-means because it minimizes a sum of dissimilarities instead of a sum of squared distances between data-points [67].

4.3.2 Transmission line availability constraint

The RSCCI method applies constraints to unavailable transmission lines (e.g., transformers, critical lines). When a transmission line is unavailable to trip, the weight factor associated with the edge is changed as described in (4.6).

$$If\ e_{ij} \in \mathcal{E}_C,\ \ set\ w_{ij} = w_{ji} = max(\mathcal{W}) \tag{4.6}$$

where $\mathcal{E}_C \subset \mathcal{E}$ is an edge subset that contains all the branches that cannot be disconnected. The fact that the proposed RSCCI method considers both the dynamic (coherent groups of generators) and static (unavailable transmission lines) constraints, ensures the avoidance of the following two unacceptable solutions for system splitting: (i) a simple separation of one node from the rest of the graph and (ii) a solution where the stability of islands formed cannot be guaranteed.

4.3.3 Simulation results

The existing SCCI and the proposed RSCCI methods were tested on two large-scale networks, the simplified Cypriot Network [68] and the Polish Network available in MatPower [69]. The simplified Cypriot network resembles the actual Cypriot network [68]. The Polish Network available in MatPower represents the Polish 400, 220 and 110 kV networks during winter 2007-08 evening peak conditions and includes some equivalents of the German, Czech and Slovak networks.

A) Simplified Cypriot network

The simplified Cypriot network resembling the actual network was firstly used to demonstrate the problems caused by outliers. This test system was also used to constrain the solution when unavailable transmission lines are detected in the system. This equivalent system has 5 synchronous generators, 48 buses and 84 branches. The total system production during the off-peak winter load time is 544.32 MW while the total consumption 543 MW. It was assumed that this system would be split into two islands. Employing real-time solutions [43], the following two coherent groups of generators were assumed {1, 15, 48} and {25, 27}. It was also assumed that the following lines could not be included in the splitting strategy: {13-43, 42-43, and 22-24}. Thus, the weight factor associated with these edges was changed applying (4.6). Implementing the existing SCCI algorithm [8], the solution obtained does not satisfy the

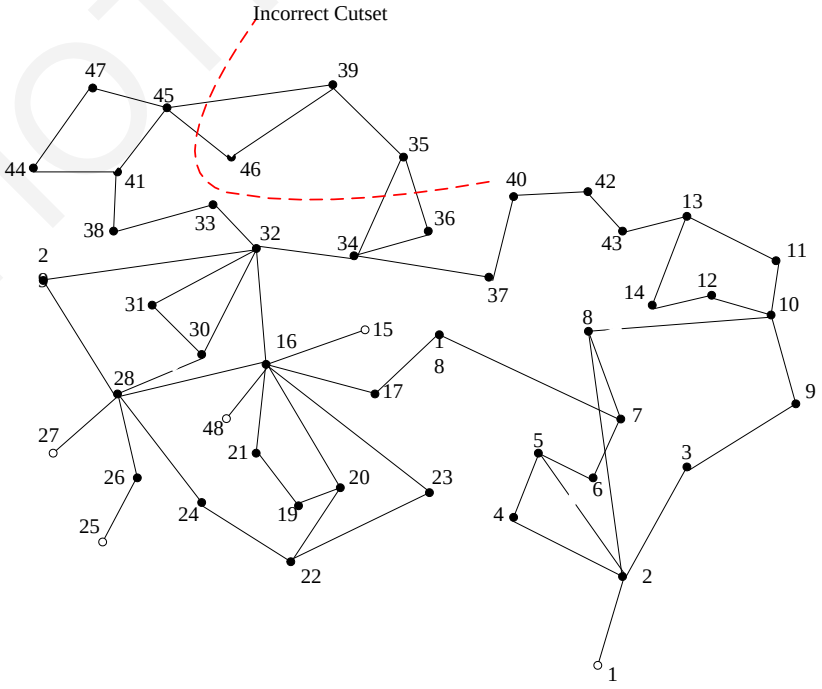

Figure 4.2: Cypriot network split into two islands - Incorrect solution determined by existing SCCI algorithm

coherency constraint. As shown in Figure 4.2, this solution does not separate the non-coherent groups of machines. Thus, transient instability within the islands might lead to a blackout. In addition, the solution obtained separates load nodes without a generator. An island without generation will unavoidably collapse.

The incorrect solution obtained by the existing SCCI is due to the presence of outliers. As shown in Figure 4.3, which plots the value of the eigenvector associated with the second smallest eigenvalue, there are four outliers (data-points 35, 39, 43, 46). As noticed, using the *k-means*, the solution obtained splits three of these outliers from the rest of the data. Thus, the existing SCCI incorrectly splits the power system. As previously mentioned, this incorrect

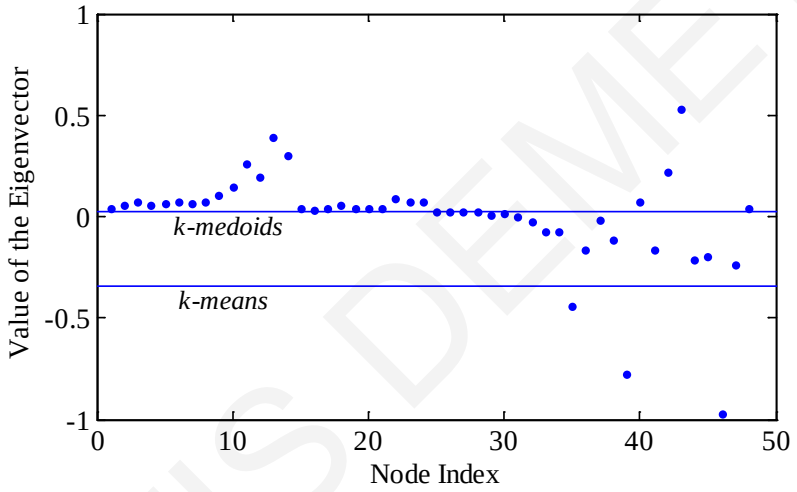

Figure 4.3: Value of the eigenvector associated with the second smallest eigenvalue

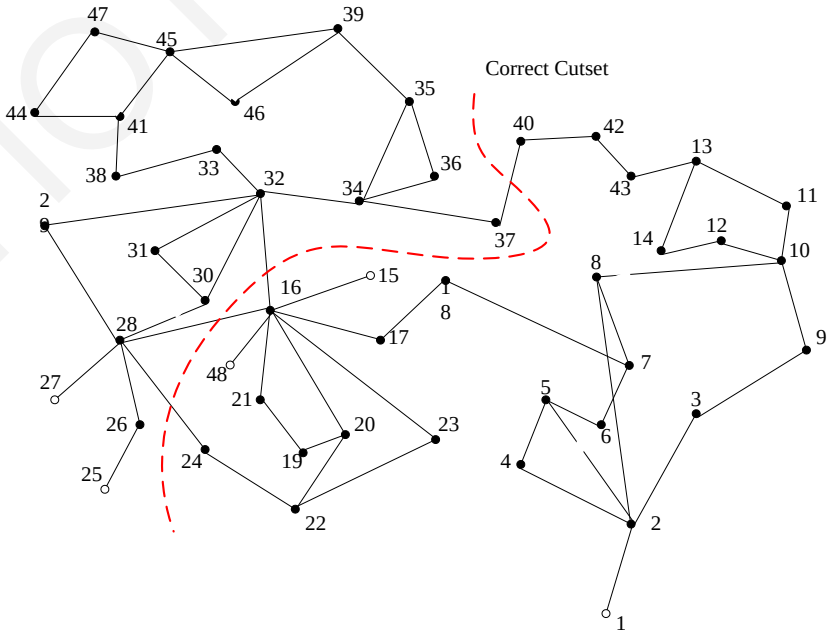

Figure 4.4: Cypriot network split into two islands - Correct solution using the RSCCI method

splitting might eventually lead to a complete blackout.

By implementing the *k-medoids* algorithm, the solution with the RSCCI solves the problem of outliers and detects the new solution. As it can be noticed in Figure 4.4, this new solution splits the power system into two islands. As expected, this solution minimizes the power-flow disruption, satisfying the constraint of grouping the coherent groups of generators. As the RSCCI method can also cope with unavailable lines in the system, the obtained solution excludes the lines 42-43 and 22-24 which would have been included in the optimal solution instead of lines 37-40 and 24-28, respectively.

B) Polish Network

The Polish Network, available in MatPower [69], was further used to test both the SCCI and the RSCCI methods. This test system contains 3375 buses. Application of the existing SCCI demonstrated that the methods require more than 45 s to determine the controlled islanding solution for minimal power-flow disruption. The complexity of the Spectral Clustering (SC) algorithm is due to the computation of the eigenvalues and eigenvectors associated with the graph employed to model the power system. The complexity is increased in Constrained Spectral Clustering (CSC) methods by introducing the dynamic constraint of the coherent generator groups and determining the constrained solution for the controlled islanding. Figure 4.5 shows a direct comparison of the time required by both the existing SCCI and the RSCCI methods.

As noticed in Figure 4.5, both methods have similar computation time. While the RSCCI is slightly slower (requires less than 5% of extra time respect to the existing SCCI in the analyzed cases), it will determine the optimal solution despite the presence of outliers. As it can be noticed, direct application of the existing SCCI, or the RSCCI, method in networks

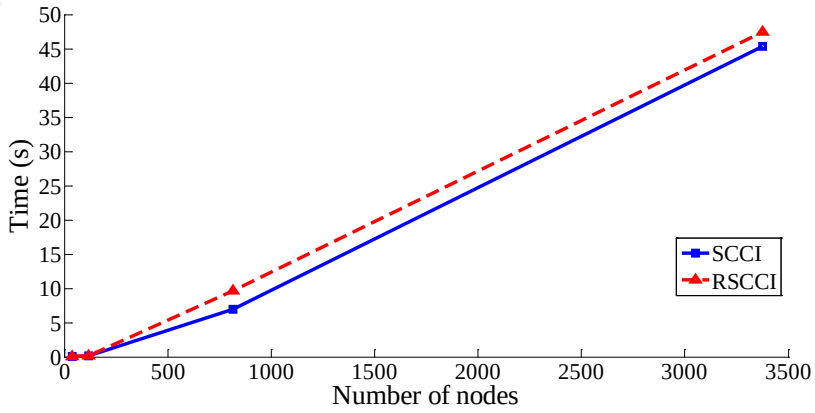

Figure 4.5: Performance of the SCCI and the RSCCI methods as a function of the number of nodes

with more than 500 nodes is not acceptable for real-time application. From Figure 4.5, it can be concluded that both the SCCI and the RSCCI are effective when the network, or a reduced set of nodes representing a reduced search space, is equal to 300 nodes, for which cases, both methods are expected to solve the problem in less than 2 seconds. However, as the RSCCI solves the problem of outliers and excludes certain branches from the splitting strategy, the RSCCI is better than the existing SCCI method.

4.4 ICI Algorithm Based on Graph Theoretic Cut-Set Matrix

This Section proposes a novel ICI scheme based on graph theory (i.e., the cut-set matrix) [70]. The proposed ICI scheme, which is designed here for the particular case of two electrical islands, determines an islanding solution that creates islands with minimal power imbalance, while ensuring that each island contains only coherent generators. Moreover, it enables the exclusion of critical branches (e.g., transformers) and explores the vast combinatorial space to find the optimal solution.

4.4.1 ICI problem for minimal power imbalance

The proposed ICI algorithm seeks to minimize the power imbalance (generation minus load) within each island, while ensuring that each one contains only coherent generators and that the islanding solution excludes critical branches. For the case of two islands (i.e., $\mathcal{G}_1$, $\mathcal{G}_2$ with node subsets $\mathcal{V}_1$, $\mathcal{V}_2$, respectively), the coherent groups of generators are denoted by $\mathcal{V}_1^{gen}$ and $\mathcal{V}_2^{gen}$. When determining a solution, each of these dynamic groups of generators must be separated into different islands to help the transient stability of the system. In addition, the system operators should be able to exclude any branch from the solution, particularly those that are deemed to be unfeasible for islanding, e.g., transformers or critical lines. For this, the subset $\mathcal{E}_C \subset \mathcal{E}$, which represents the branches that must not be disconnected, is defined.

The problem of minimizing the power imbalance within each island can then be formulated considering the power transfer between islands. Thus, the ICI problem for minimal imbalance to be solved here is defined as follows:

$$\min_{\mathcal{V}_1,\mathcal{V}_2}\left(\left|\sum_{v_i\in\mathcal{V}_1,v_j\in\mathcal{V}_2} w_{ij} - \sum_{v_j\in\mathcal{V}_1,v_i\in\mathcal{V}_2} w_{ji}\right|\right) \tag{4.7}$$

subject to

$$\mathcal{V}_k^{gen} \subset \mathcal{V}_k \text{ , and } \mathcal{E}_C \subset \mathcal{E} = \varnothing$$

The condition $\mathcal{V}_k^{gen} \subset \mathcal{V}_k$ constrains every island $\mathcal{G}_k$ to contain only coherent generators (denoted by the subset $\mathcal{V}_k^{gen}$). The second condition $\mathcal{E}_C \subset \mathcal{E} = \varnothing$ means that the ICI algorithm only considers partitions with cutsets $\mathcal{E}_S$ not containing any excluded edge from $\mathcal{E}_C$.

4.4.2 Methodology to solve the ICI problem

To solve the islanding problem formulated above (for two islands), the next steps are sequentially followed:

Step 1: Create the oriented incidence matrix **M** associated with $\mathcal{G}$ that represents the incidence among nodes and edges.

Step 2: Define the label of the generation-nodes. Generators in the same coherent group must have the same label to preserve their integrity (coherency constraint). Define the load-nodes as free-nodes. A free-node can be grouped into any island.

Step 3: Define the excluded edges $\mathcal{E}_C$ (unfeasible branches). To constrain these branches to be excluded from the solution, define both ends of each excluded edge with the same label.

Step 4: Build the indicator matrix, **X**, that contains combinations of node labels that would partition $\mathcal{G}$ [56]. The combinations in **X** label certain nodes to be in a given island and combine the free-node labels. This is a combinatorial problem that can be effectively solved by computing the permutations with repetitions of the free-node labels [71]. Each combination in **X** also includes the labels for the generation-nodes and any other constrained nodes so that each combination supplies a set of labels that defines the island each node will be clustered into.

Step 5: Compute the constrained cut-set matrix **C**, also known as the *cut-edge* incidence matrix, as follows [56]:

$$\mathbf{C} = \mathbf{X}^T\mathbf{M} \tag{4.8}$$

This matrix is used in graph theory to represent all the cutsets in a graph [56]. The *ik*-entry of

C is non-zero if the implementation of the i^{th} cutset requires the edge $e_k = e_{ij}$ to be removed to partition $\mathcal{G}$. Each cutset included in **C** represents the edges to be removed to separate the elements of $\mathcal{G}$ that have different labels in the corresponding combination in **X**. Use the concept of the rank of $\mathcal{G}$ to remove unfeasible cutsets (i.e., solutions that are not satisfying the generator coherency constraint or solutions that split the system into an incorrect number of islands).

Step 6: Compute the vector **w**, which is a column vector with the j^{th} row equal to the edge weight (power flow).

Step 7: Determine the power imbalance within each island induced by each of the cutsets included in **C** as follows:

$$cut(\mathcal{V}_1, \mathcal{V}_2) = \mathbf{C} \cdot \mathbf{w} \tag{4.9}$$

The islanding solution that results in the minimal power imbalance (i.e., the local optimal solution) is then found by finding the minimal entry of $cut(\mathcal{V}_1, \mathcal{V}_2)$, i.e., $\min(cut(\mathcal{V}_1, \mathcal{V}_2))$. It is noted that, more than two islands can be created by applying recursive bisection [56], [72].

4.4.3 Simulation results

To illustrate the ICI method, the dynamic model of the IEEE 9-bus test system was used [27]. Then, to demonstrate its effectiveness, two case studies were developed (i.e., two different faults leading to blackout) on the actual power system of Cyprus. The proposed ICI method was aimed to be used following the determination of the necessity to split the power system. All times quoted are based upon simulations performed on a PC with 2.33 GHz dual core CPU and 8 GB RAM.

A) IEEE 9-bus test system

Test case description: The base load defined in the IEEE 39-bus test system is increased by 25%, while maintaining the same power factor. This stresses the system and increases the likelihood of instability following a disturbance. The increment is equally distributed among the generators. It is considered that at time t = 0.1 s, a three phase to ground fault occurs near bus 7 at line 5–7, and it is cleared after local relays open the faulty line at t = 0.38 s (i.e., 0.28 s after the fault occurred). The swing trajectories obtained are shown in Figure 4.6. Given that no control actions are undertaken, two groups of generators are obtained after the fault, i.e.,

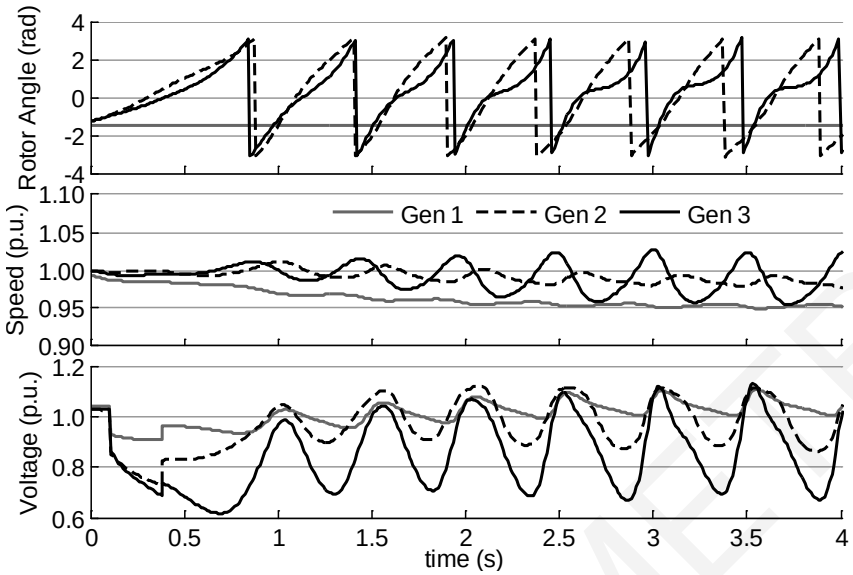

Figure 4.6: IEEE 9-bus test system - Electrical behavior without islanding

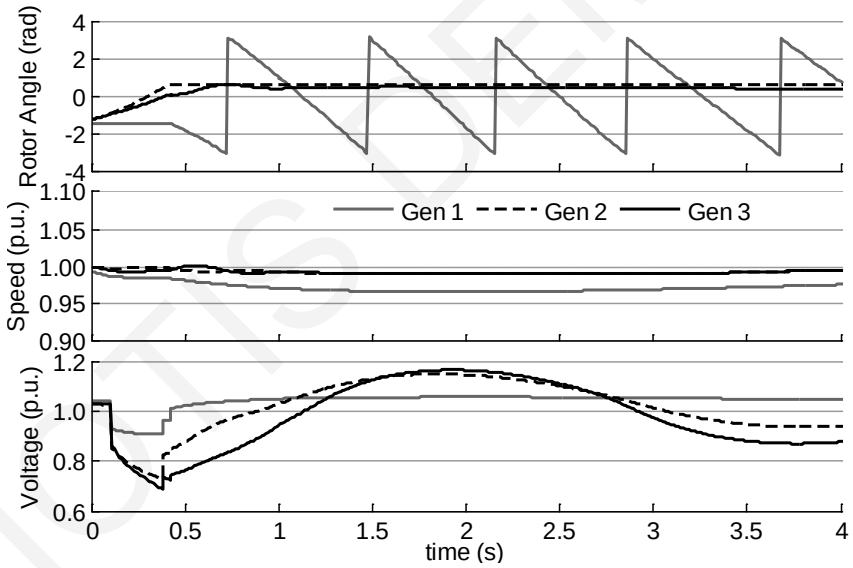

Figure 4.7: IEEE 9-bus test system - Electrical behavior with islanding

{1} and {2, 3}. More importantly, Figure 4.6 highlights that this disturbance results in a blackout quickly after the fault is cleared.

To avoid this blackout, the ICI method is used. The necessity to split the system is considered to be at t = 0.45 s (i.e., 0.07 s after the fault is cleared). As the scheme is adaptive and considers the actual topology and state of the system, the information (power flow and topology) at t = 0.45 s is used. To preserve the integrity of the coherent generators, v_1 is labeled '1' and v_2 and v_3 are labeled '2'. The load-buses 5, 6 and 8 are defined as free-nodes. The set of excluded arcs $E_C = \{e_{1,4}, e_{2,7}, e_{3,9}\}$ is defined as they represent transformers.

The implementation of the ICI method identifies the optimal solution (for minimum imbalance) across the lines 7-5 and 4-6. This solution was found in approximately 0.0014 s; islanding was undertaken at t = 0.4514 s. Figure 4.7 shows the dynamic trajectories after implementing the optimal solution. Two stable coherent groups are created. Moreover, the frequencies of Island 1 and Island 2 are 0.976 p.u. and 0.995 p.u., respectively. Voltages also reach values close to nominal values. The results highlight that the splitting strategy successfully retains the frequency of the islands and the corresponding voltages within the thresholds; thus preventing the blackout.

The ICI method can create more than two islands. To illustrate this, it is considered that three groups of generators are obtained after the fault: {1}, {2} and {3}. The method, in this case, will create two islands across lines 7-5 and 4-6 (like the case presented above), and will then split Island 2 into two more islands across line 9-8, for a total of three islands.

B) Power System of Cyprus

The power system in Cyprus consists of 151 buses, 344 branches and two power stations (i.e., Dhekelia, 460 MW, and Vasilikos, 867.5 MW) with eight and nine synchronous generators, respectively. The complete network parameters, protection settings, as well as the dynamic models and parameters of each generator (i.e., machine, exciter, and governor) have been provided by the Transmission System Operator (TSO) in Cyprus and the Electricity Authority of Cyprus [73]. It must be mentioned that loads are modeled as constant power as their dynamic characteristics are currently unavailable. Figure 4.8 shows the graph representation of the Cypriot network, which has been fully implemented in DigSilent PowerFactory [30].

Based on historical demand data, the winter and summer peak demand levels in Cyprus are 848.71 MW and 1187 MW, respectively. They represent the most stressed conditions that the Cypriot system experiences; thus, the analyses below focus on these demand levels ("*worst-case*" scenarios). To demonstrate the effectiveness of the proposed ICI method, feedback from the TSO was used to develop two case studies for each demand level (i.e., two different faults leading to blackout).

Case study 1 description: At t = 1 s, a three-phase to ground fault occurs near the largest power station (i.e., Vasilikos) at line 20-152 (lines shown in green in Figure 4.8). The fault is not cleared by local relays, and instead secondary protection schemes are triggered based on

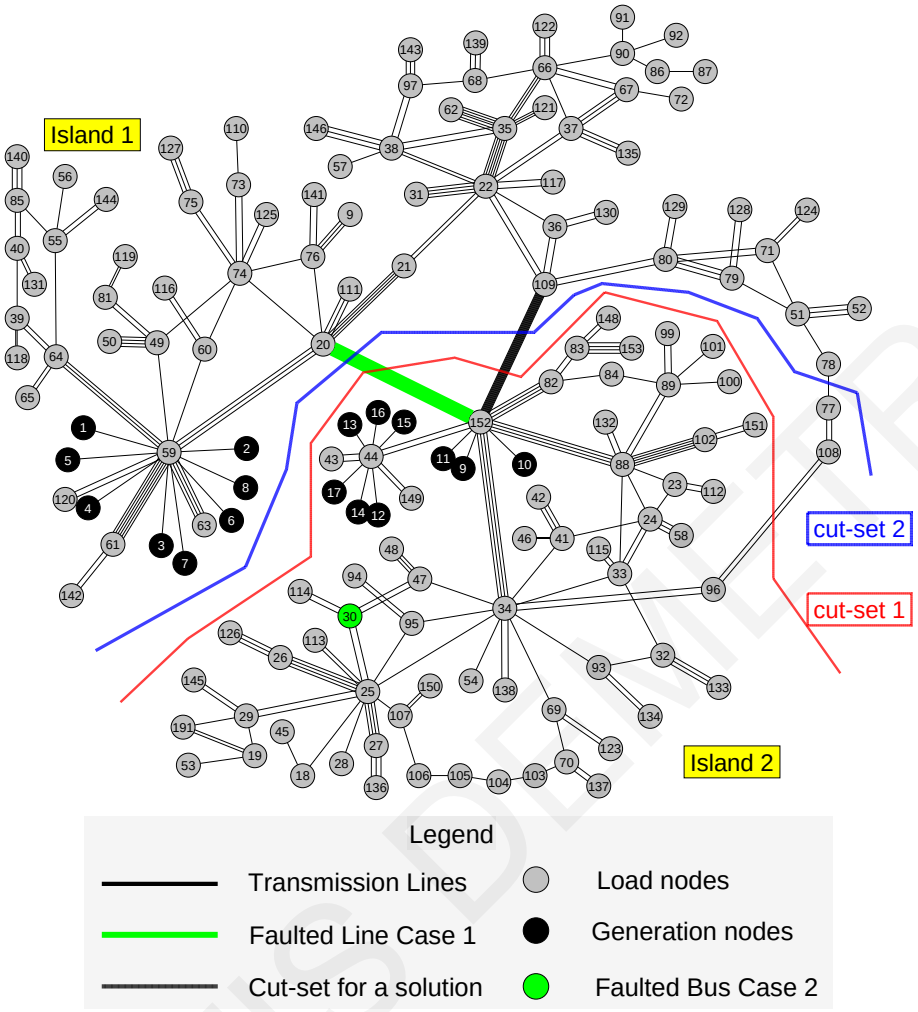

Figure 4.8: Graph of the Cypriot network (with optimal islanding solutions)

the actual settings of the real system. Indeed, it is important to mention that out-of-step relays disconnect several generators approximately after 1.5 s (see Figure 4.9 - Figure 4.11). In other words, the system response represents that of the real network given that protection settings have been set by the TSO. The generator rotor angles of the two stations without islanding are shown in Figure 4.9 and Figure 4.10. Shortly after the fault, the generators within each station swing together and those in different ones swing apart. Two groups are created: {1,2,3,4,5,6,7,8} and {9,10,11,12,13,14,15,16,17}. Although these groups can be created through visualization of the generator rotor angle trends, algorithms to automatically identify coherent groups of generators (e.g., [36], [43]) must be adopted in large-scale systems to ensure adequate generator grouping. In terms of the generators' speed, Figure 4.11 shows that they increase. It is noted that such increments cause the tripping of G8 and G7 at 1.798 s and 2.091 s respectively, due to the operation of overspeed protections (set to 1.115 p.u.). Finally,

Figure 4.12 highlights that the generator terminal voltages are significantly low. Thus, it can be concluded that the system needs to be split, if the blackout is to be avoided.

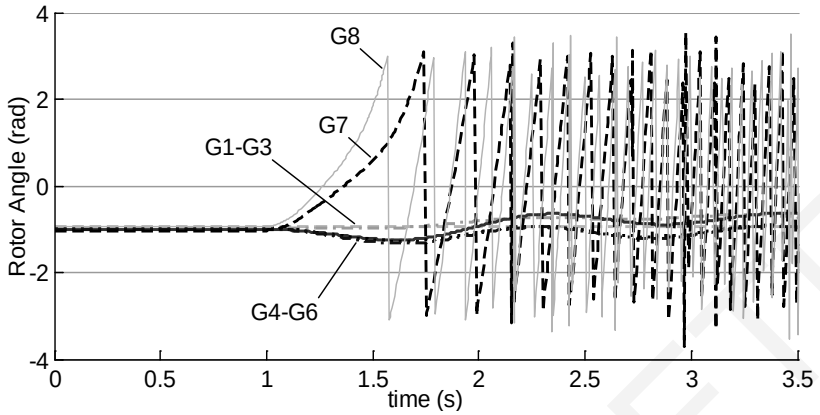

Figure 4.9: Generator rotor angles - Power station 1 in Cyprus without islanding

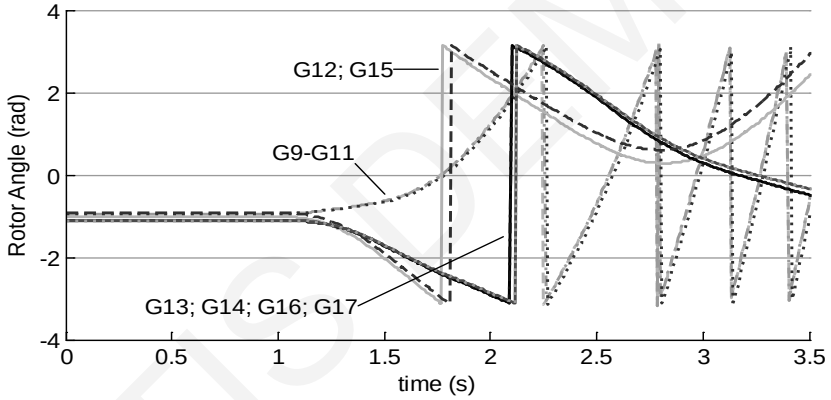

Figure 4.10: Generator rotor angles - Power station 2 in Cyprus without islanding

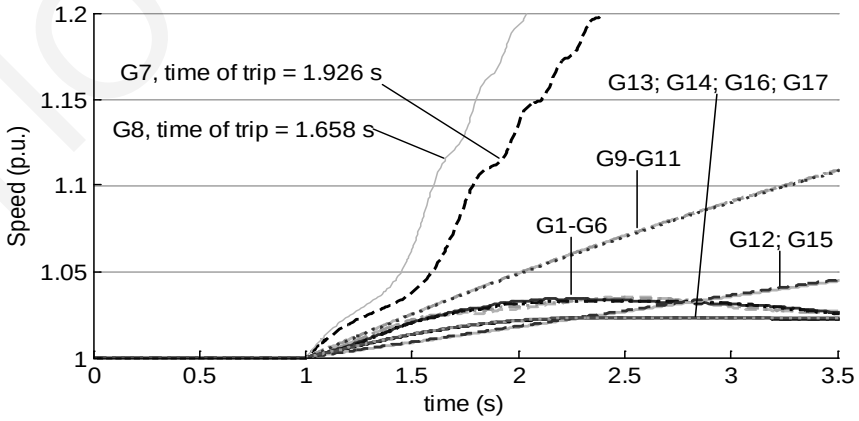

Figure 4.11: Generator speeds - Both power stations in Cyprus without islanding

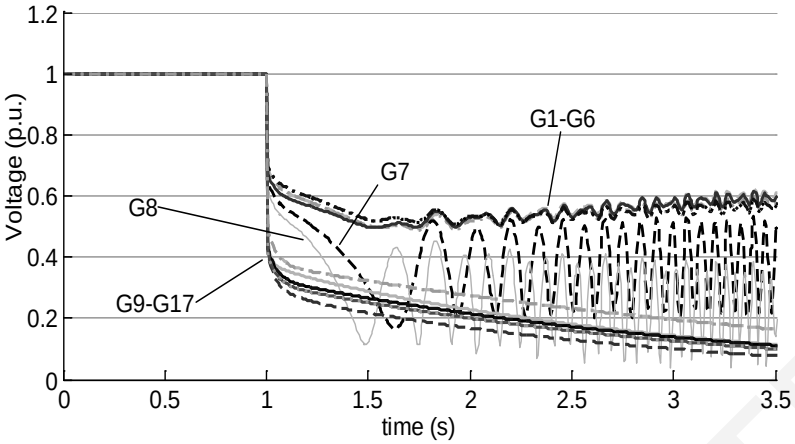

Figure 4.12: Generator voltages - Both power stations in Cyprus without islanding

Given that this is a very severe disturbance, feedback from the Cyprus TSO has been used to define the necessity to split the system 50 ms after the fault occurs, i.e., at t = 1.05 s. The ICI method is then implemented considering the power flows and system topology at t = 1.05 s. To accelerate the identification of the optimal solution, only twenty free-nodes were included in the combinatorial optimization. The free-nodes were defined considering the electrical distance between groups. Only load buses with similar distance from the coherent groups were included. Generators within each group were labelled accordingly. Transformers and critical lines, defined by the Cyprus TSO, were excluded from the solution space.

The optimal islanding solution is shown in Figure 4.8 (cut-set 1, red-dotted line). This solution was found in approximately 0.23 s. Hence, islanding was undertaken at t = 1.28 s (i.e., t_{imp} = 1.05 s + 0.23 s). It is important to mention that there are a few seconds for islanding after a severe disturbance. In practical implementations, it is expected to have high-performance computers, or even computer clusters, to carry out this critical task. For the purpose of this work, it can thus be seen that the proposed ICI method can meet the requirement of real-time controlled islanding in this real system.

The post-islanding behavior of the islands is shown in Figure 4.13 - Figure 4.15. Figure 4.13 shows the generators rotor angle in each island. It can be seen that two stable groups are created. Figure 4.14 further shows that the generator speeds (0.97 p.u. and 1.003 p.u. respectively) are within the limits which are defined by the Cyprus TSO as 0.95-1.04 p.u. It is important to mention that 99.57 MW and 208.11 MW of load for the winter and summer peak demand respectively was automatically shed by the protection relays in order to retain the frequency of the created islands within the thresholds. Figure 4.15 finally indicates that the generator terminal voltages are successfully kept within the desirable limits (which are defined

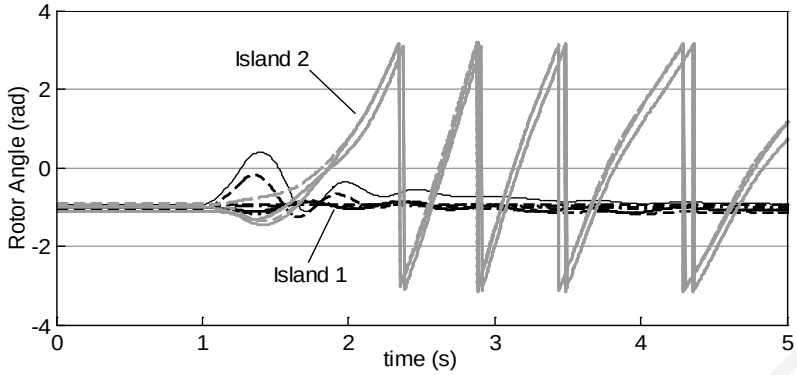

Figure 4.13: Generator rotor angles - Both power stations in Cyprus with islanding

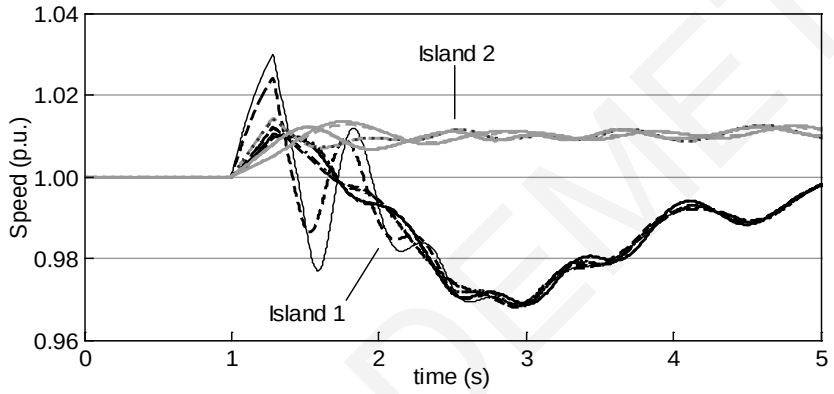

Figure 4.14: Generator speeds - Both power stations in Cyprus with islanding

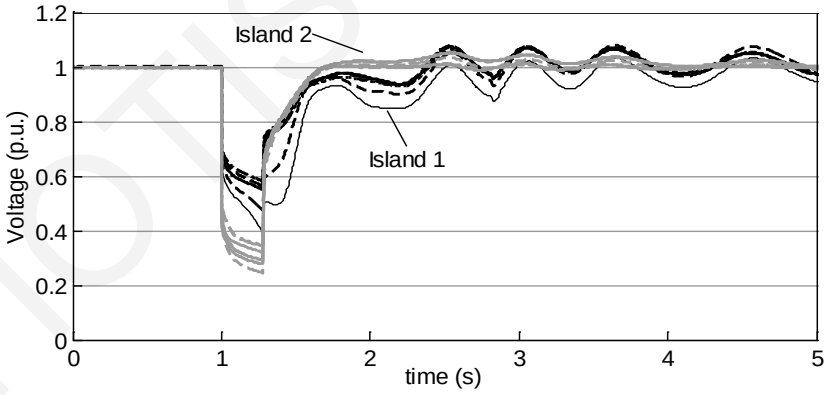

Figure 4.15: Generator voltages - Both power stations in Cyprus with islanding

as ±10% deviation of the nominal value). This result is important as it highlights that, although voltage constraints are not considered in the proposed ICI method, the solution found using this approach still retains voltages within the statutory thresholds. Consequently, it can be concluded that the proposed ICI method successfully prevents the power system blackout.

Case study 2 description: At t = 1 s, a three phase to ground fault occurs near bus 30 (132 kV substation, node shown in green in Figure 4.8), resulting again in the generators within

each station to swing together and those in different stations to swing apart. Although not shown here, two groups are created: {1,2,3,4,5,6,7,8} and {9,10,11,12,13,14,15,16,17}. The necessity to split the system is defined to be at 1.5 s. Hence, the ICI method is used to find the optimal islanding solution (considering 20 "free nodes" as well as power flows and topology at $t = 1.5$ s.). The disturbance analyzed in this case study is not as severe as the one investigated in case study 1. The islanding solution that produces the minimal power imbalance is illustrated in Figure 4.8 (cut-set 2, blue-dotted line). The optimal islanding solution was found in approximately 0.23 s and islanding was undertaken at $t = 1.73$ s. No further load shedding was undertaken by the protection relays into the two created islands. The behavior of the system without and with islanding is like the one given in Figure 4.9 - Figure 4.15 for case study 1.

4.5 ICI Algorithm Based on Exact Mixed Integer Linear Programming (MILP) Formulation

An exact Mixed Integer Linear Programming formulation (MILP) approach for the building partitioning problem has been proposed in [74]. The MILP formulation is based on graph decomposition approaches and partitions the building into smaller sections. The building is transformed into a graph which is partitioned into subgraphs, indicating the group of rooms in each section while ensuring (i) maximum decoupling between the various subgraphs, (ii) strong connectivity between the rooms of a subgraph, and (iii) control of the number of allocated rooms in each subgraph. Due to its easily adaptable constraints, the aforementioned algorithm can easily be applied to other applications. Consequently, an application of the exact MILP formulation on power systems for solving effectively the ICI problem is presented in this work.

More specifically, this work [75] proposes an exact ICI algorithm that directly determines an islanding solution with minimal power-flow disruption for any given number of islands, while ensuring that each island contains only coherent generators. Additionally, it enables operators to constrain any transmission line to be excluded from the solution (e.g., transformers), allows the control of the size of islands and ensures that each resulting island is connected. It is noted that, due to the high adaptability of the MILP formulation, more constraints can be easily incorporated.

Crucially, a preprocessing procedure which finds the trees that connect the generators of each coherent group with the minimum number of nodes (which should be connected in any case) is also proposed [75]. The nodes of these trees are assigned to specific islands through additional constraints to the MILP formulation for reducing its search space, and therefore, the overall complexity of the problem.

4.5.1 ICI problem for minimal power-flow disruption

The ICI problem for solving the minimal power-flow disruption can be represented as a constrained combinatorial optimization,

$$\min\left(\sum_{\substack{i\in\mathcal{V}_h,\ j\in\mathcal{V}_k \\ h\neq k,\ h,k\in\mathcal{K}}} \frac{\left|P_{ij}\right|+\left|P_{ji}\right|}{2}\right) \ s.t.\ \ \mathcal{V}_k^{gen}\subset\mathcal{V}_k\ ,\ \mathcal{E}_C\subset\mathcal{E} \tag{4.10}$$

where P_{ij} and P_{ji} represent the active power flow in the branch from bus *i* to *j*, and from *j* to *i*, respectively (to accommodate network losses). $\mathcal{V}_k^{gen}$ is a node subset that contains the coherent generator groups for each island $\mathcal{G}_k$. $\mathcal{E}_C$ is an edge subset that contains all the branches that cannot be disconnected (e.g., transformers, critical lines). The use of minimal power-flow disruption as the objective function minimizes the sum of the absolute values of the active power exchange between islands. This property improves the transient stability of the formed islands, reduces the possibility of overloading the transmission lines within the newly created islands and makes island resynchronization easier [14], [76]. The constraints applied when satisfying this objective function deal with coherent generator groups and line availability.

4.5.2 MILP formulation to solve the ICI problem

Consider an undirected, connected graph $\mathcal{G}=(\mathcal{V},\mathcal{E})$ and a matrix $\mathcal{W}\in\mathbb{R}^{|\mathcal{V}|\times|\mathcal{V}|}$ for the edge weights $w_{i,j},(i,j)\in\mathcal{E}$, with $w_{i,j}=w_{j,i}, i,j\in\mathcal{V}$. The objective is to partition the graph into *K* subgraphs indicating the islands while a) minimizing the weight of the edges that are not included in any subgraph which is defined as the partitioning cost and is described by the objective function:

$$\text{Partitioning Cost}=\min_{z}\sum_{(i,j)\in\mathcal{E}}\frac{1}{2}(1-z_{i,j})w_{i,j} \tag{4.11}$$

b) controlling the size of subgraphs and c) ensuring that each produced subgraph is connected. In addition, the resulting subgraphs $\mathcal{G}_k = (\mathcal{V}_k, \mathcal{E}_k)$ where $\bigcup_k \mathcal{V}_k = \mathcal{V}, k \in \mathcal{K}$ must follow a minimum cardinality restriction as $|\mathcal{V}_k| \geq M$, $k \in \mathcal{K}$, where $M \in \mathbb{N}^+$. Variables $z_{i,j}, (i,j) \in \mathcal{E}$ are defined as the decision variables where $z_{i,j} = 1$ if the edge is included in any subgraph and $z_{i,j} = 0$ otherwise. It is noted that a detailed description of the aforementioned MILP formulation can be found in [74].

4.5.3 Preprocessing procedure

Since the MILP formulation allows the easy manipulation of its existing constraints, a preprocessing procedure is developed for reducing the search space of the MILP and the overall complexity of the problem. The preprocessing procedure has as inputs i) the graph $\mathcal{G} = (\mathcal{V}, \mathcal{E})$ of the power system with all weights equal to one and ii) a set $\mathcal{V}_k^{gen}, k \in \mathcal{K}$, with $\bigcup_k \mathcal{V}_k^{gen} = \mathcal{V}^{gen}$, which holds the coherent generator groups for each island $\mathcal{G}_k$ to be formed. The objective of the preprocessing procedure is to find a tree $\mathcal{T}_k = (\mathcal{V}_k^T, \mathcal{E}_k^T), \quad k \in \mathcal{K}$ in $\mathcal{G}$ for each island with minimum number of nodes, spanning to all generator nodes in each $\mathcal{V}_k^{gen}$. Therefore, the nodes that are included in $\mathcal{T}_k$ will be directly assigned to their resulting island in the MILP formulation, ensuring the generator coherency. It is noted that in the case where a tree $\mathcal{T}_k = (\mathcal{V}_k^T, \mathcal{E}_k^T)$ does not contain any load-bus (e.g., a coherent group that consists of only one generator), then the particular tree is expanded to include one through finding the minimum path between them. This adjustment avoids the production of isolated generator nodes, and consequently, more reliable islands are formed.

The problem of connecting a set of nodes in a graph with the minimum tree is the minimum Steiner problem in graphs which is a well-known $\mathcal{NP}$ - *complete* problem [55]. Therefore, in time depended applications, approximation algorithms are more suitable. The proposed preprocessing procedure consists of a simple approximation of the Steiner problem in graphs that utilizes the shortest path algorithm, Dijkstra. Note that, providing an approximation for the Steiner problem in graphs is not the main objective of this work. The preprocessing procedure is as described in Table 4.1.

The preprocessing procedure addresses each generator group individually and can be separated in two sections. In the first section (lines 1-8 of preprocessing procedure), the objective is to form trees that include at least two generator vertices from set $\mathcal{V}_h^{gen}$. At the end of the first section, the generated unconnected trees $\mathcal{T}_h^{(m)} = (\mathcal{V}_h^{(m)}, \mathcal{E}_h^{(m)}), m \in \mathbb{Z}^+$, $\mathcal{M} = \{1, \ldots, m\}$ include all the generator nodes. However, the final solution should be a unified tree that consists of all the smaller trees. Therefore, in the second section (lines 9-18), all the individual trees are connected together using the smallest paths between them to form the final tree $\mathcal{T}_h \supseteq \bigcup_m \mathcal{T}_h^{(m)}$ that connects all the generator vertices $\mathcal{V}_h^{gen}$. Note that the preprocessing procedure can be executed simultaneously for all the generator groups.

Table 4.1: Preprocessing procedure

	$h \in \mathcal{K}$, $\mathcal{V}_h = \varnothing$
1:	**While** $\mathcal{V}_h^{gen} \subsetneq \mathcal{V}_h$ **do**
2:	**For all** $i \in \mathcal{V}_h^{gen}$
3:	Find the minimum path $\mathcal{P}_{i,j} = (\mathcal{V}_{i,j}, \mathcal{E}_{i,j}), \forall j \in \mathcal{V}_h^{gen}, j \notin \mathcal{V}_h$ in $\mathcal{G}$ using Dijkstra
4:	$\mathcal{P}_i^{\min} = \min_j \{\mathcal{P}_{i,j}\}$
5:	**End For**
6:	$\mathcal{P}^* = \min_{i \in \mathcal{V}_h^{gen}} \{\mathcal{P}_i^{\min}\}$
7:	$\mathcal{V}_h = \mathcal{V}_h \cup \mathcal{V}^*, \mathcal{E}_h = \mathcal{E}_h \cup \mathcal{E}^*$, where $\mathcal{V}^*$ and $\mathcal{E}^*$ correspond to the vertices and edges of $\mathcal{P}^*$ respectively
8:	**End While**
	At this point, $\mathcal{T}_h$ may not be connected. In such a case, $\mathcal{T}_h$ consists of $m \in \mathbb{Z}^+, \mathcal{M} = \{1, \ldots, m\}$ individual trees $\mathcal{T}_h^{(m)} = (\mathcal{V}_h^{(m)}, \mathcal{E}_h^{(m)})$.
9:	$\mathcal{G}' = (\mathcal{V}', \mathcal{E}') = \mathcal{G}$
10:	**While** $\mathcal{T}_h$ **is not connected do**
11:	$\mathcal{E}' = \mathcal{E}' \setminus \mathcal{E}_h$
12:	**For all** $i \in \mathcal{V}_h^{(m)}, m \in \mathcal{M}$
13:	Find the minimum path $\mathcal{P}_{i,j} = (\mathcal{V}_{i,j}, \mathcal{E}_{i,j}), \forall j \in \mathcal{V}_h^{(q)}, q \in \mathcal{M}, q \neq m$ in $\mathcal{G}'$ using Dijkstra

14: $\mathcal{P}_i^{\min} = \min_j \{\mathcal{P}_{i,j}\}$

15: **End For**

16: $\mathcal{P}^* = \min_{i \in \mathcal{V}_h^{(m)}} \{\mathcal{P}_i^{\min}\}$

17: $\mathcal{V}_h = \mathcal{V}_h \cup \mathcal{V}^*, \mathcal{E}_h = \mathcal{E}_h \cup \mathcal{E}^*$, where $\mathcal{V}^*$ and $\mathcal{E}^*$ correspond to the vertices and edges of $\mathcal{P}^*$ respectively

18: **End While**

4.5.4 Simulation results

To demonstrate the effectiveness of the proposed MILP ICI algorithm, the IEEE 39- and 118-bus test systems were used. The dynamic data of the generators and the details of the controllers (i.e., Automatic Voltage Regulators (AVR) and governors) can be found in [27]. The algorithm was aimed to be used following the determination of the necessity to split the power system. All times quoted are based upon simulations performed in Matlab (a PC with 3.10 GHz dual core CPU and 4 GB RAM).

A) IEEE 39-bus test system

Case study 1 description: At time t = 1 s, both ends of transmission line 17-27 are opened. As a result, a transient instability is created into the system. Based on a two-step methodology proposed in [47] for real-time identification of coherent generator groups, for the case of two islands (K=2), the coherent generator groups are {G30, G37, G38, G39} and {G31, G32, G33,

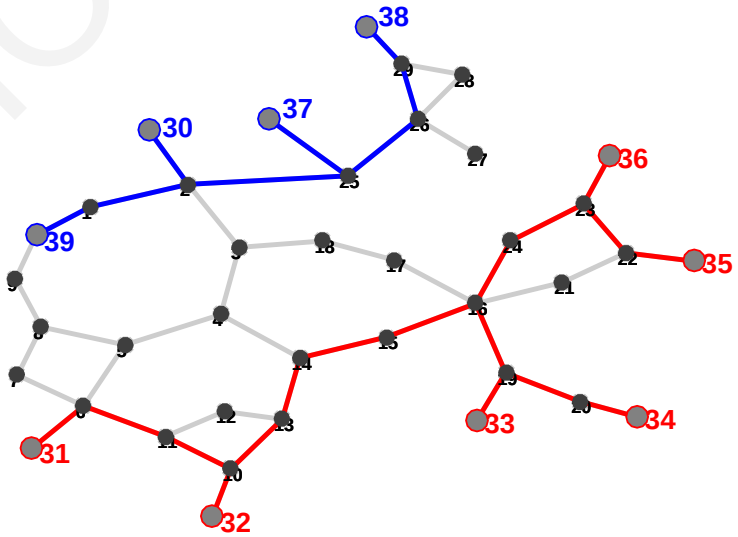

Figure 4.16: Case Study 1: Preprocessing procedure on IEEE 39-bus test system for K=2

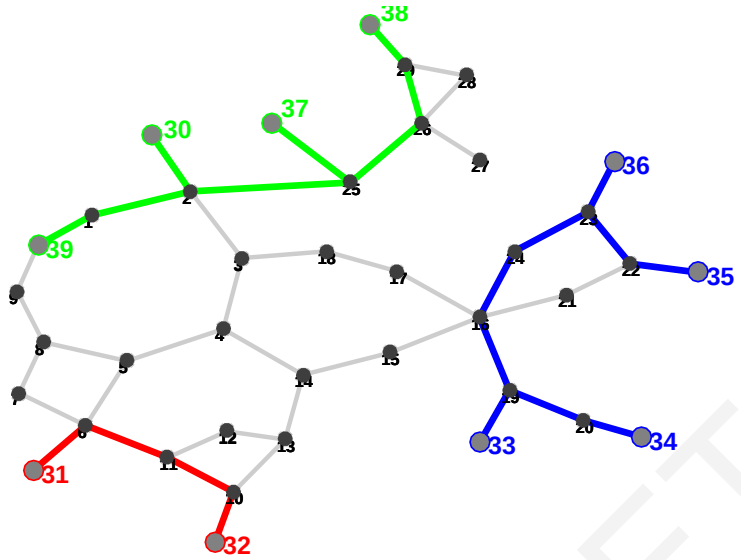

Figure 4.17: Case Study 1: Preprocessing procedure on IEEE 39-bus test system for *K*=3

Table 4.2: Exact islanding solutions for the IEEE 39-bus test system (Case study 1)

No. of Islands (k)	***Cutset***	***Cut (MW)***	***Time (s)***
2	8-9, 3-4, 3-18	173.078	0.043
3	8-9, 3-4, 3-18, 14-15	173.932	0.041

G34, G35, G36}. The necessity to split the system is considered to be at t = 2 s. Hence, considering the power flow and actual topology of the system at t = 2 s, the proposed exact ICI algorithm is used to find the optimal islanding solution. As mentioned in Section 4.5.3, the preprocessing procedure finds first the trees that connect all the generators of each coherent group with the minimum number of nodes (Figure 4.16). The nodes of these trees are then served as an additional constraint to the MILP formulation. The implementation of the ICI algorithm identifies the optimal solution (for minimal power-flow disruption) across the lines 8-9, 3-4 and 3-18 (red dashed line in Figure 4.18). The solution was found in approximately 0.043 s. Hence, islanding was undertaken at t = 2.043 s.

For *K*=3, the coherent generator groups obtained are {G30, G37, G38, G39}, {G31, G32} and {G33, G34, G35, G36} [47]. Figure 4.17 shows the trees found by the preprocessing procedure. The islanding solution determined by the execution of the exact ICI algorithm is marked in Figure 4.18 (blue dotted line). This solution was obtained in approximately 0.041 s and thus the corresponding corrective controlled strategy was undertaken at t = 2.041 s. Table 4.2 summarizes the islanding solution and the value of the cut for each case. It is important to note that there are a few seconds for controlled islanding after the system suffers a severe fault

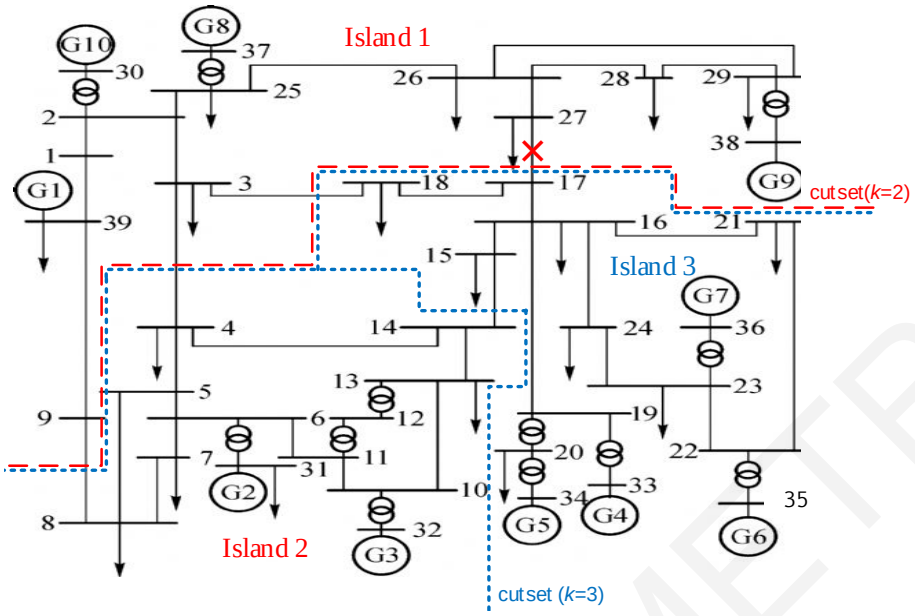

Figure 4.18: Case Study 1: Single-line diagram of IEEE 39-bus test system with optimal islanding solution for *K*=2 and *K*=3

[77]. Consequently, it can be seen that the proposed ICI algorithm can meet the requirement of real-time controlled islanding.

Case study 2 description: At time *t* = 1 s, the value of loads at buses 3, 4, 7, and 8 is increased by 10% (total step change of 157.78 MW). As a result, a transient instability is created into the system. For *K*=2, the coherent generator groups obtained are {G31, G32} and {G30, G33, G34, G35, G36, G37, G38, G39} while for *K*=3 the {G39}, {G31, G32} and {G30, G33, G34, G35, G36, G37, G38} [47]. The necessity to split the system is considered

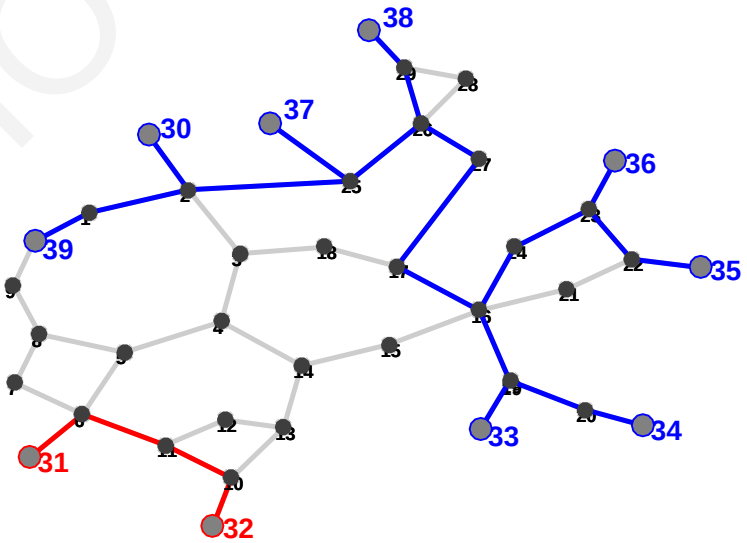

Figure 4.19: Case Study 2: Preprocessing procedure on IEEE 39-bus test system for *K*=2

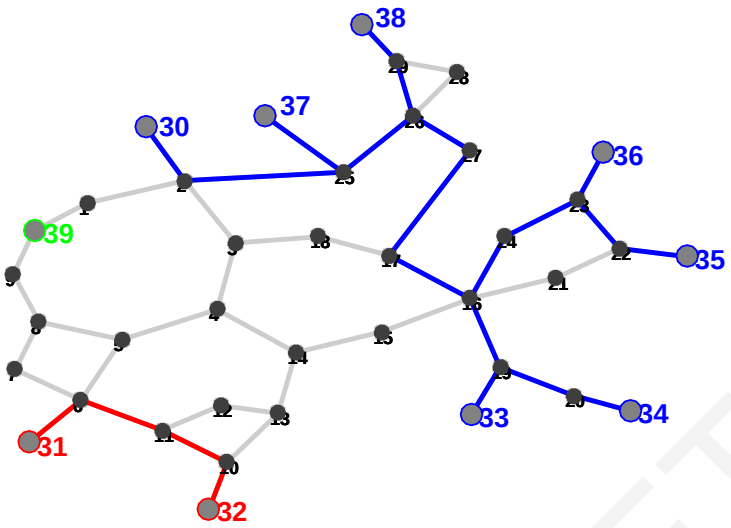

Figure 4.20: Case Study 2: Preprocessing procedure on IEEE 39-bus test system for K=3

Table 4.3: Exact islanding solutions for the IEEE 39-bus test system (Case Study 2)

No. of Islands (k)	*Cutset*	*Cut (MW)*	*Time (s)*
2	8-9, 3-4, 14-15	192.080	0.042
3	8-9, 3-4, 14-15, 1-39	319.994	0.051

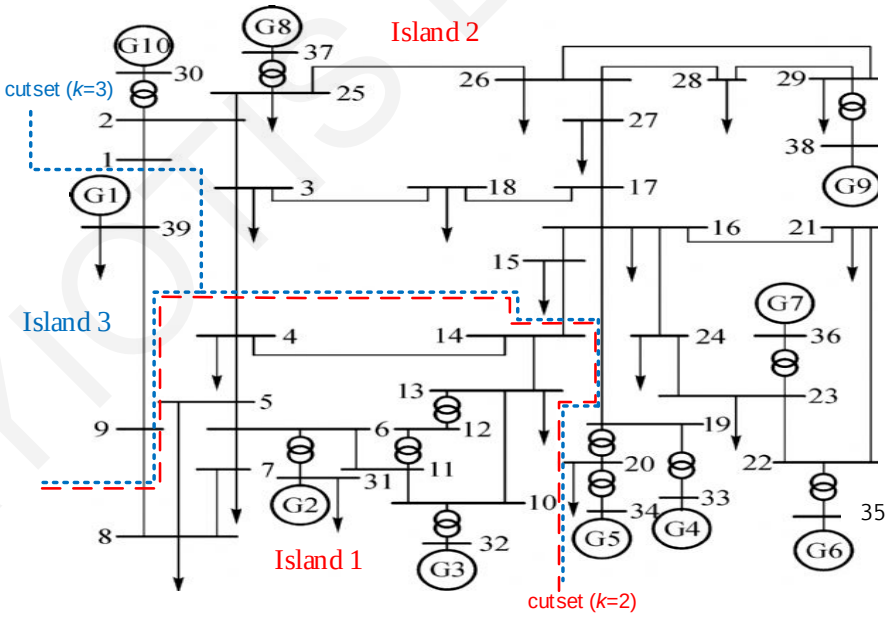

Figure 4.21: Case Study 2: Single-line diagram of IEEE 39-bus test system with optimal islanding solution for K=2 and K=3

to be at t = 2 s. For these cases, the trees found by the preprocessing procedure connecting the generators of each coherent group with the minimum number of nodes are shown in Figure 4.19 and Figure 4.20 respectively. At this point, it is important to mention that for the case of

three islands (K=3), an adjustment has been made by the algorithm in order to ensure that at least one load will be assigned to the island including only G39 (i.e., load 39). Hence, no isolated generator nodes are produced. Considering the power flow and actual topology of the system at t = 2 s, the islanding solutions determined by the execution of the exact ICI algorithm for both cases are marked in Figure 4.21 and summarized in Table 4.3.

B) IEEE 118-bus test system

The second test system used to demonstrate the efficiency of the proposed ICI algorithm was the IEEE 118-bus test system. The topology of the system is shown in Figure 4.22. This test system contains 19 synchronous generators, 177 transmission lines, 9 transformers and 91 constant power loads. The coherent generator groups of the IEEE 118-bus test system were obtained by using the coherency algorithm [78] for up to four groups (Table 4.4). Figure 4.23 to Figure 4.25 show the trees found by the preprocessing procedure for each case. As

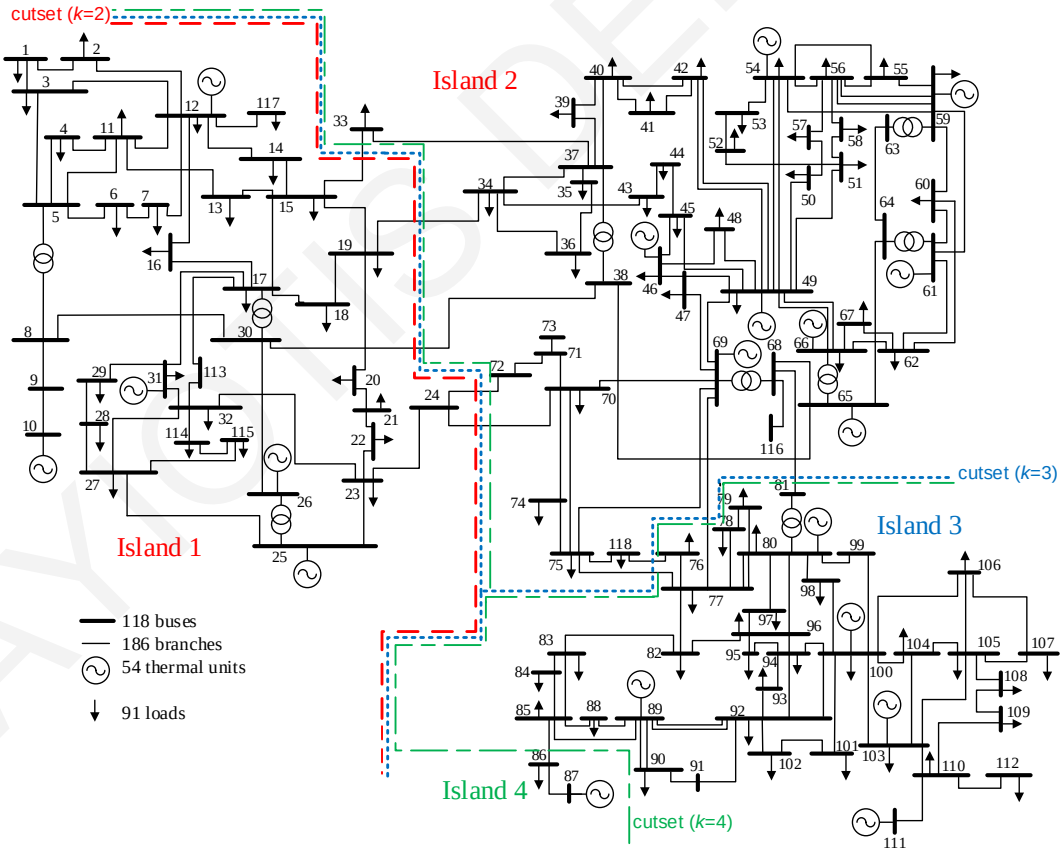

Figure 4.22: Single-line diagram of IEEE 118-bus test system with optimal islanding solution for K=2, K=3 and K=4

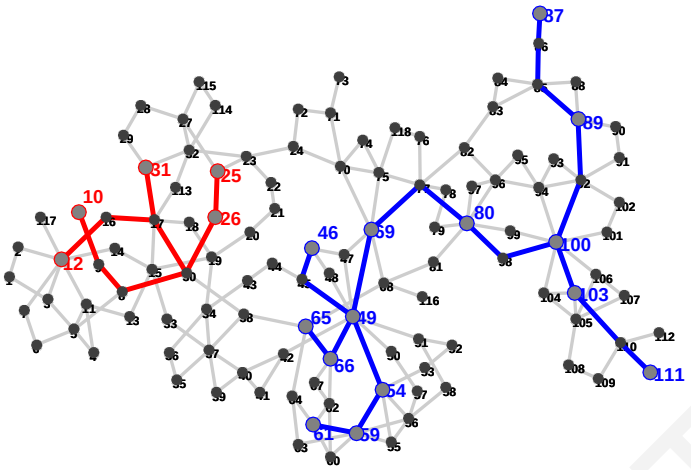

Figure 4.23: Preprocessing procedure on IEEE 118-bus test system for *K*=2

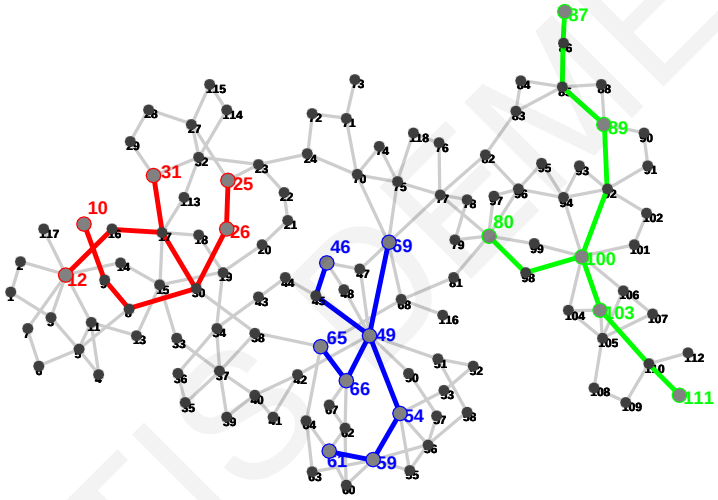

Figure 4.24: Preprocessing procedure on IEEE 118-bus test system for *K*=3

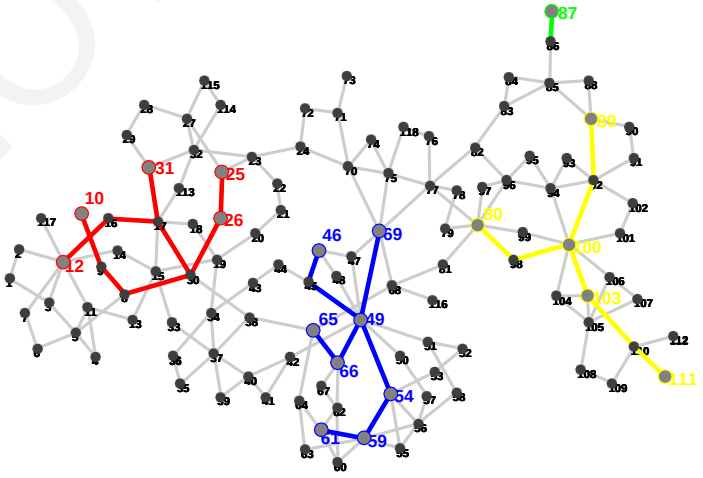

Figure 4.25: Preprocessing procedure on IEEE 118-bus test system for *K*=4

Table 4.4: Coherent generator groups for the IEEE 118-bus test

No. of Islands (k)	***Coherent Generator Groups***
2	{10, 12, 25, 26, 31}, {46, 49, 54, 61, 65, 66, 69, 80, 87, 89, 100, 103, 111}
3	{10, 12, 25, 26, 31}, {46, 49, 54, 59, 61, 65, 66, 69}, { 80, 87, 89, 100, 103, 111 }
4	{10, 12, 25, 26, 31}, {46, 49, 54, 59, 61, 65, 66, 69}, { 80, 89, 100, 103, 111 }, {87}

Table 4.5: Exact islanding solution for the IEEE 118-bus test system

No. of Islands (k)	***Cutset***	***Cut (MW)***	***Time (s)***
2	15-33, 19-34, 30-38, 24-70, 24-72	81.050	0.126
3	15-33, 19-34, 30-38, 24-70, 24-72, 76-118, 75-77, 69-77, 68-81	229.402	0.214
4	15-33, 19-34, 30-38, 24-70, 24-72, 76-118, 75-77, 69-77, 68-81, 85-86	246.574	0.319

mentioned above, the nodes of these trees will be served as an additional constraint to the MILP formulation which will contribute to the reduction of its search space. It is noted that for K=4 (Figure 4.25), the assignment of at least one load to the coherent group {87} (i.e., load 86) has been made (finding the minimum path between them) in order to avoid the collapse of the particular island. Figure 4.22 illustrates the islanding solutions determined by the execution of the exact ICI algorithm for all the possible number of coherent groups. The information about the splitting strategies found, the values of the cuts and the execution times are presented in Table 4.5.

4.6 ICI Algorithm Based on Linear Programming (LP) Formulation

This section proposes a novel ICI algorithm based on a Linear Programming (LP) formulation [16]. The proposed algorithm directly determines an optimal islanding solution with minimal power-flow disruption for large scale power systems, and for any given number of islands, in a timely manner. In addition, it ensures that each island contains only coherent generators, enables operators to constrain any transmission line to be excluded from the solution, allows the control of the size of islands and ensures their connectivity. The proposed algorithm is derived from the relaxation of the MILP formulation used in Section 4.5.

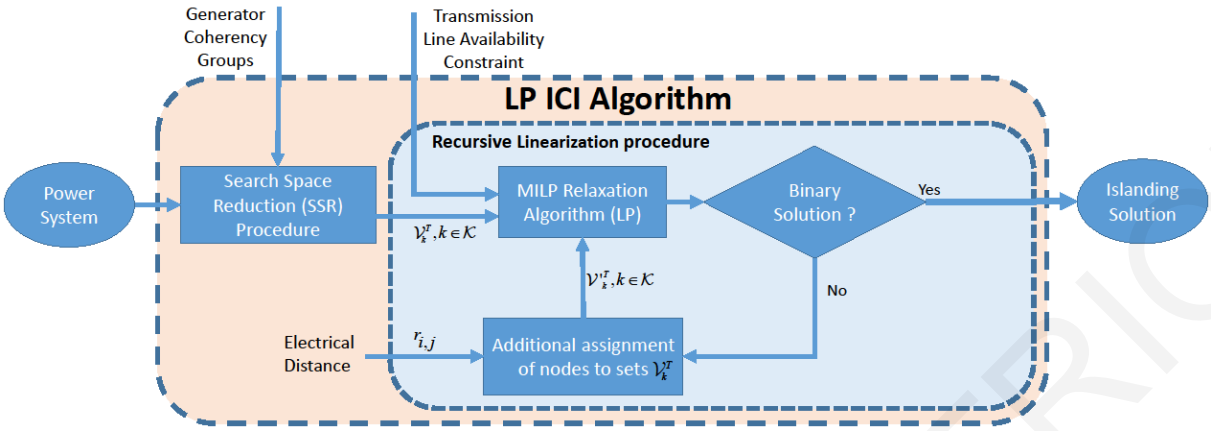

Figure 4.26: Proposed LP ICI Algorithm

Even though the MILP's execution time is improved by the additional constraints generated by the preprocessing procedure described in Section 4.5.3 (also called here Search Space Reduction (SSR) procedure), it does not negate the fact that the MILP formulation is of exponential complexity. Hence, the execution time cannot be guaranteed. On the other hand, the combination of all the additional constraints (i.e., SSR generated constraints and transmission line availability constraints) are, in most cases, enough for the relaxed MILP formulation (LP formulation) to generate binary solutions (solutions that satisfy the binary constraints of the MILP); hence, the optimality and viability of the results is confirmed. However, in case of non-binary solutions, a valid islanding solution is not attained.

To solve this problem, the LP formulation is executed as a part of a recursive linearization procedure which assigns additional nodes to each island through extra constraints. The additional nodes assigned to each island are those that are electrically closer to the preassigned groups (based on the electrical distance concept). After every addition of constraints, the solution search space is further reduced and the proposed LP formulation is re-executed. The linearization procedure is repeated until the LP formulation reaches a binary solution.

4.6.1 Recursive linearization procedure

The binary set of variables, $x_{i,h},\ i \in \mathcal{V},\ h \in \mathcal{K},$ is the output of the LP formulation and indicates whether or not, node i belongs to subgraph $\mathcal{G}_k$. The linearization of the binary variable is given by:

$$x_{i,h} \in [0, 1], \qquad i \in \mathcal{V},\ h \in \mathcal{K}, \tag{4.12}$$

To ensure that binary solutions are always generated, the proposed LP formulation is executed as a part of a recursive linearization procedure presented in Figure 4.27. At first, the LP formulation is executed using the additional constraints generated by the SSR procedure and transmission line availability constraints if any exist. If the generated islanding solution satisfies the binary constraints of the MILP formulation, then a valid ICI solution is achieved. On the other hand, if the solution is not binary (e.g., $x_{i,h}$ gets a value between 0 and 1) then additional nodes are assigned into individual islands based on the electrical distance concept. The electrical distance which corresponds to the Thevenin equivalent between the bus *i* and bus *j* is calculated as [79]:

$$r_{i,j} = \left|B\right|^{+}_{i,i} + \left|B\right|^{+}_{j,j} - \left|B\right|^{+}_{i,j} - \left|B\right|^{+}_{j,i} \quad i, j \in \mathcal{V} \tag{4.13}$$

where B is the system's susceptance matrix. Specifically, the nodes with electrical distance lower than a threshold $\overline{r}$ (if such nodes exist) are added to their closest group. The electrical distance metric is used to minimize the effect of the extra constraints to the islanding solution, as well as to ensure the electrical cohesiveness between the extra nodes and the nodes in the formed groups. The formation of islands with low electrical distance between their elements and high electrical distance between the elements of different islands indicates high electrical cohesiveness inside the islands, while there are evidence suggesting the reduction of loop flows (transaction leakages) between different islands [79]. The threshold is calculated as $\overline{r} = \frac{\sigma(R)}{K} \times I$, where R is a matrix including all the $r_{i,j}$, $i, j \in \mathcal{V}$ values, $\sigma(R)$ is the standard deviation of all elements in matrix R, K is the number of resulting islands and I is a counter indicating the number of times that the recursive procedure is executed. In other words, at each additional execution of the LP formulation the electrical distance threshold is broaden in order to preassign into the predetermined groups a larger number of nodes. This procedure is repeated until the LP ICI algorithm generates a valid solution. The extra time consumed by this recursive procedure is a small penalty that has to be paid, compared to the uncertainty of the execution time of the MILP. Note that multiple steps of the recursive procedure can be executed in parallel. Consequently, the recursive LP ICI algorithm is much faster than its

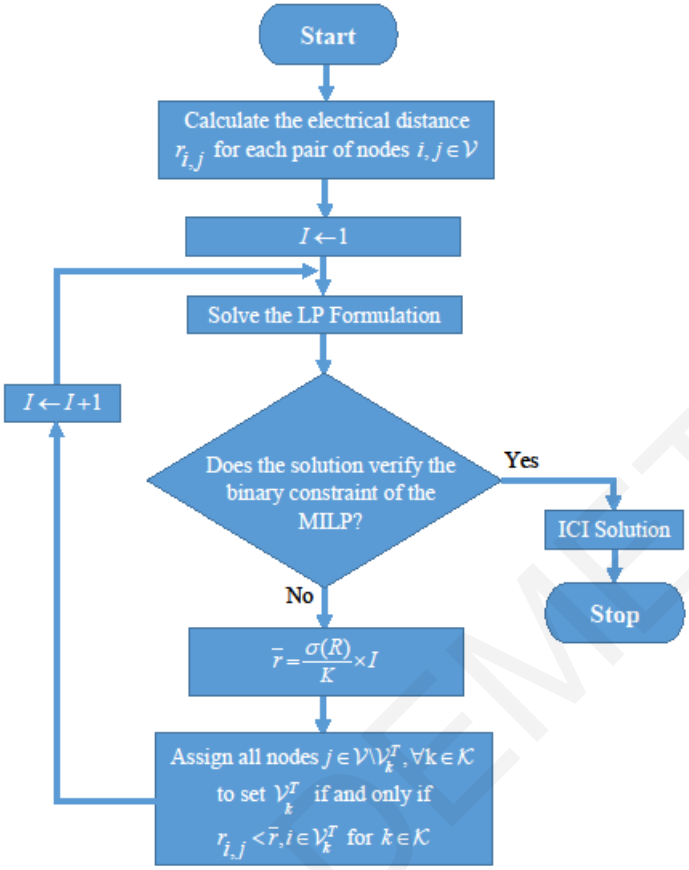

Figure 4.27: Flow chart of the recursive linearization procedure

MILP counterpart.

4.6.2 Simulation results

The proposed LP ICI algorithm was tested using the IEEE 118- and 300-bus test systems and was compared with the MILP ICI algorithm. The dynamic data of the generators and the details of the controllers (i.e., AVR and governors) can be found in [27]. The proposed LP ICI algorithm was also tested using a real large-scale power system that is more representative of modern system operations footprints, the Polish Network available in MatPower [69]. Note that both MILP ICI and LP ICI algorithms were aimed to be used following the determination of the necessity to split the power system. The two aforementioned algorithms were compared in terms of execution time and partitioning cost (given that both algorithms utilize the additional constraints generated from the SSR procedure presented in Section 4.5.3). It is important to mention that the LP ICI algorithm resulted in an optimal solution for the cases of splitting both test systems up to 4 islands. However, the recursive linearization procedure was

needed when splitting the IEEE 300-bus test system to 5 and 6 islands. For the case of the Polish Network, the recursive linearization procedure was needed when splitting this system to 4 islands.

A) IEEE 118-bus test system

Test case description: At time t = 0 s, a three phase to ground fault occurs near bus 25 at line 23−25 and is cleared after local relays open the faulty line at t = 0.18 s. The swing trajectories obtained are shown in Figure 4.28. It can be observed that within a short time after

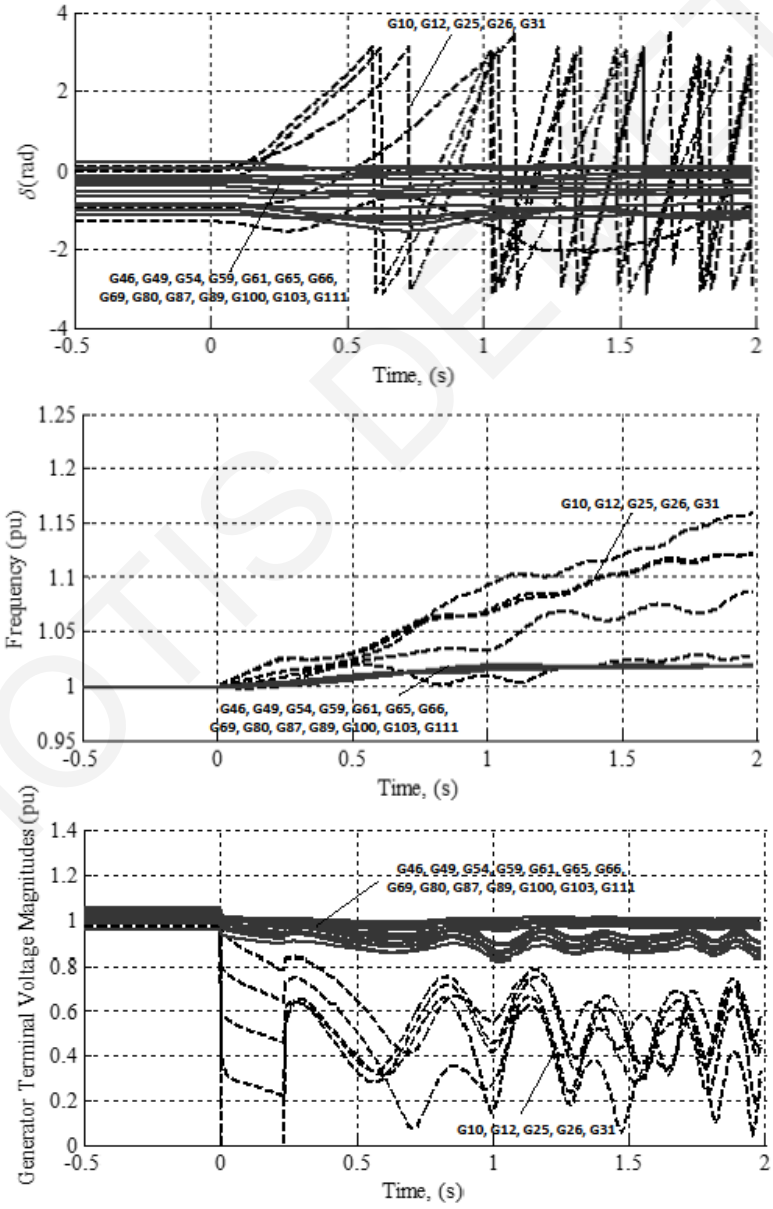

Figure 4.28: IEEE 118-bus test system - Electrical behavior without islanding

Table 4.6: Coherent generator groups for the IEEE 118-bus test system

No. of Islands (k)	***Coherent Generator Groups***
2	{10, 12, 25, 26, 31}, {46, 49, 54, 61, 65, 66, 69, 80, 87, 89, 100, 103, 111}
3	{10, 12, 25, 26, 31}, {46, 49, 54, 59, 61, 65, 66, 69}, { 80, 87, 89, 100, 103, 111 }
4	{10, 12, 25, 26, 31}, {46, 49, 54, 59, 61, 65, 66, 69}, { 80, 89, 100, 103, 111 }, {87}

Table 4.7: Islanding solutions for the IEEE 118-bus test system

No. of Islands (k)	***Cutset***	***Partitioning Cost (MW)***		***Execution Time (s)***		***% of time improvement***
		MILP ICI	LP ICI	MILP ICI	LP ICI	
2	24-70, 24-72, 38-65, 40-42, 41-42, 44-45	47.304	47.304	0.1534	0.1035	32%
3	24-70, 24-72, 38-65, 40-42, 41-42, 44-45, 69-77, 75-77, 76-118, 80-81	197.01	197.01	0.2296	0.1177	49%
4	24-70, 24-72, 38-65, 40-42, 41-42, 44-45, 69-77, 75-77, 76-118, 80-81 85-86	226.804	226.804	0.3021	0.1868	38%

the fault is cleared, the generators are divided into two groups: {G10, G12, G25, G26, G31} and {G46, G49, G54, G59, G61, G65, G66, G69, G80, G87, G89, G100, G103, G111}. Moreover, as it can be observed in Figure 4.28, if the system is not split into two islands, the frequency of the generators considerably increases and the terminal voltages of the generators significantly reduce. Hence, this disturbance will result to a blackout quickly after the fault is cleared. In this case, the necessity to split the system is considered to be at t = 0.28 s. Hence, considering the power flow and actual topology of the system at t = 0.28 s, the proposed LP ICI algorithm is used to find the optimal islanding solution. It is noted that, for demonstrated purposes, the proposed LP ICI algorithm is also used to split the system to up to four islands. Hence, the coherent generator groups for up to four groups are considered to be as presented in Table 4.6.

The trees found by the SSR procedure for each number of islands are presented in Figure 4.29 - Figure 4.31. The resulted trees span to each generator in each group. Specifically, the nodes $\mathcal{V}_k^T$ of each tree $\mathcal{T}_k$ will be directly assigned to the same resulting islands, ensuring the generator coherency. This assignment is achieved through additional constraints. Moreover, each tree $\mathcal{T}_k$ is enforced to include at least one load node in order to ensure the formation of more reliable and sustainable islands. Hence, no isolated generator nodes are produced. For

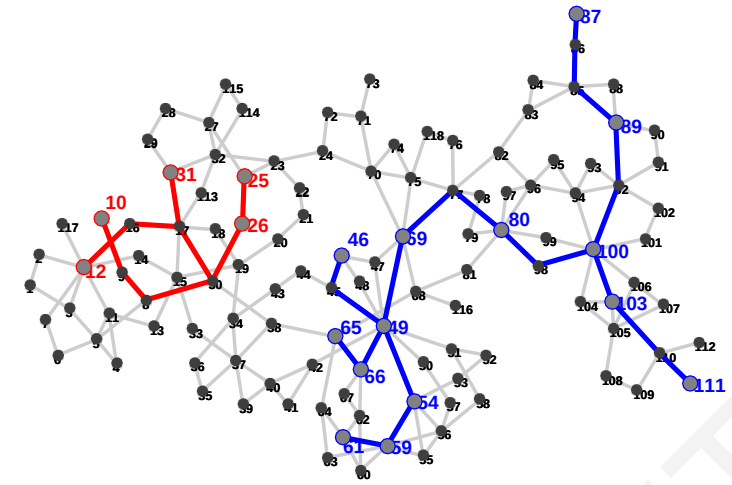

Figure 4.29: SSR procedure on IEEE 118-bus test system for *K*=2

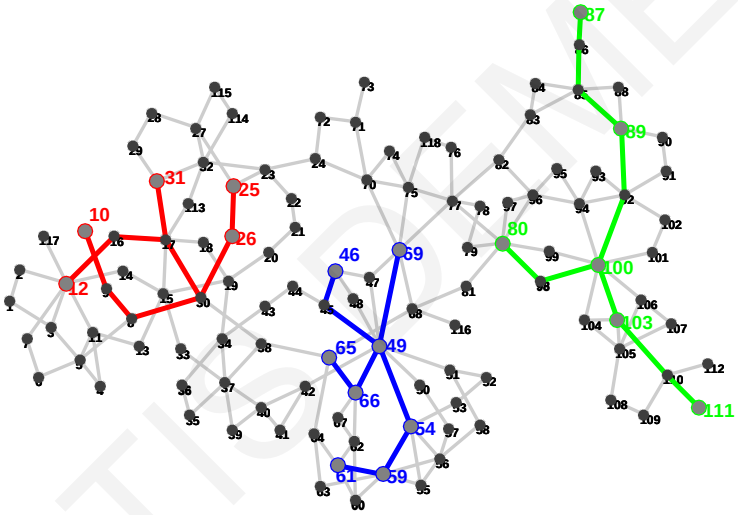

Figure 4.30: SSR procedure on IEEE 118-bus test system for *K*=3

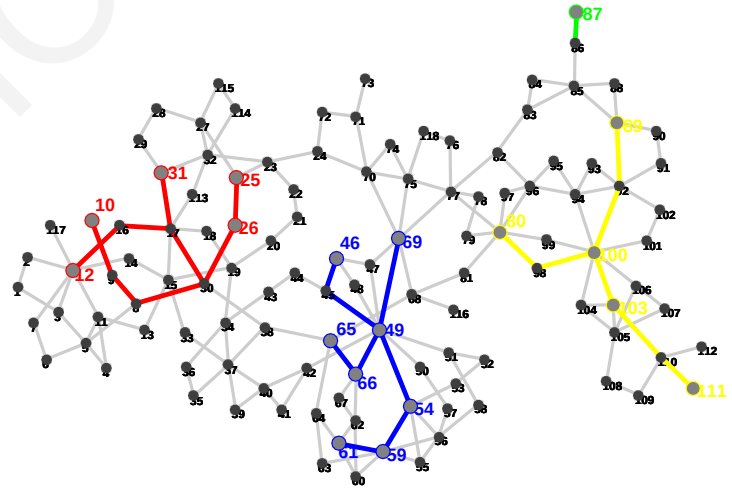

Figure 4.31: SSR procedure on IEEE 118-bus test system for *K*=4

instance, for $K = 4$, (Figure 4.31), the assignment of at least one load to the coherent group 87 (i.e., load 86) has been made (finding the minimum path between them) in order to avoid the collapse of the particular island. Following the additional constraint of the SSR and the transmission line availability constraints (if any exist), the islanding solutions for all the possible number of coherent generator groups as determined by both MILP ICI and the LP ICI algorithms are shown in Table 4.7. This table also summarizes the PC and the execution time of each islanding solution obtained. As can be seen, both approaches have resulted in identical solutions. However, as shown by the percentage of execution time improvement, the LP ICI is significantly faster than its MILP counterpart. In addition, it is important to mention that the final islanding solution for all the possible number of coherent groups was obtained in the first iteration of the recursive linearization procedure.

More specifically, for the case of two islands ($K = 2$), the islanding solution was found in approximately 0.1035 s. Hence, islanding was undertaken at $t = 0.3835$ s (0.1035 s after determining the necessity to island the system at $t = 0.28$ s). Considering that there are a few seconds for controlled islanding after system suffered a severe fault [77], it is obvious that the proposed LP ICI algorithm can meet the demand of real-time controlled islanding. Figure 4.32 shows the dynamic trajectories after implementing the solution. As noticed, two stable groups are created. Moreover, Figure 4.32 also shows the generator frequencies and the generator terminal voltages. As noticed, the frequencies of Island 1 and Island 2 are 0.9987 p.u. and 1.000 p.u., respectively. Voltages also reach values close to nominal values. Since the splitting strategy successfully retains the frequency of the islands within acceptable limits and the corresponding voltages within the thresholds, it can be concluded that the use of the proposed LP ICI algorithm to split the power system in a controlled manner can prevent the blackout. It is noted that, for $K = 3$ and $K = 4$, the behavior of the system without and with islanding is similar to the one presented in Figure 4.28 and Figure 4.32 for $K = 2$.

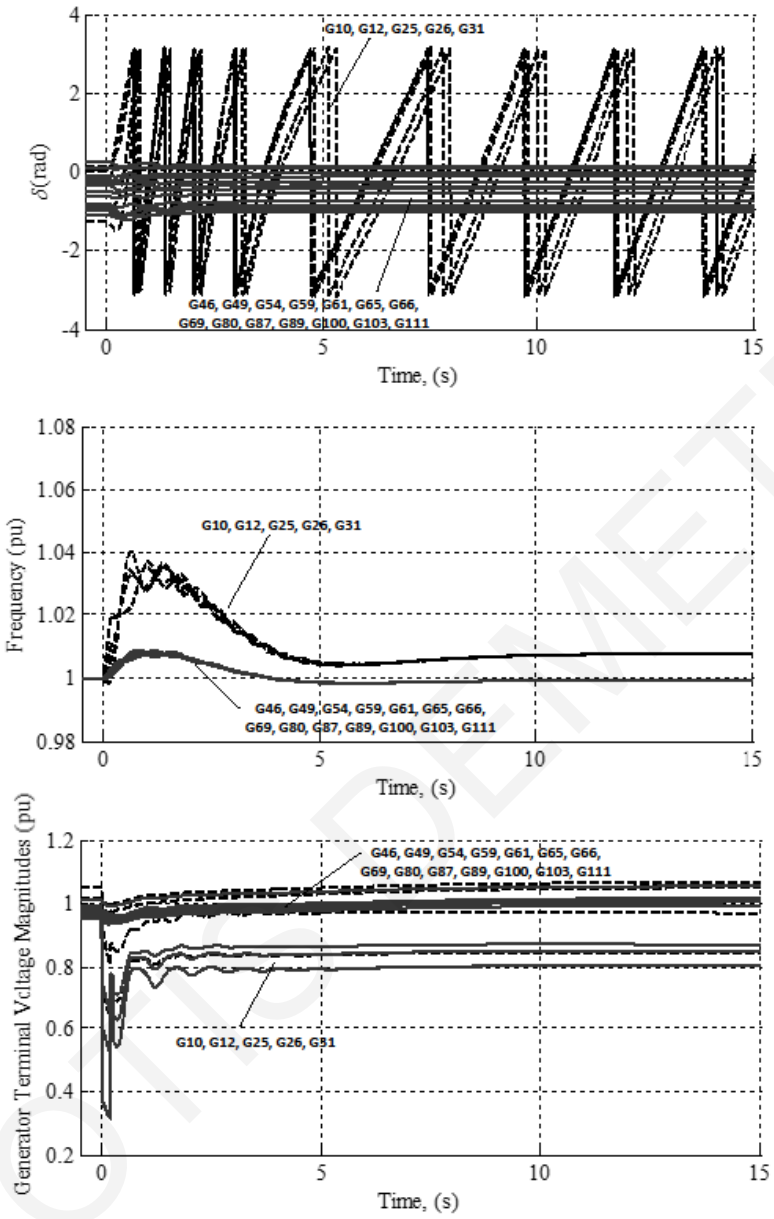

Figure 4.32: IEEE 118-bus test system - Electrical behavior with islanding

B) IEEE 300-bus test system

The IEEE 300-bus test system consists of 69 generators, 306 transmission lines, 174 transformers and 197 loads. All the generators are equipped with an IEEE type-1 exciter and a simple turbine governor. Taking into account that this test system consists of 3 individual systems, its coherent generator groups up to 6 groups were reasonably assumed and determined as presented in Table 4.8.

Table 4.8: Coherent generator groups for the IEEE 300-bus test system

No. of Islands (k)	***Coherent Generator Groups***
2	{301-310, 330-361, 365-369}, {311-329, 362-364}
3	{301-310, 346-361, 365-369}, {311-329, 362-364}, {330-345}
4	{301-310, 346-361, 365-369}, {311-329, 362-364}, {330, 331, 334-343}, {332, 333, 344, 345}
5	{301-310, 346-361, 365-369}, {311-314, 320-324, 327-329, 362, 364}, {315-319, 325, 326, 363}, {330, 331, 334-343}, {332, 333, 344, 345}
6	{301-303, 307-310, 346-353}, {304-306, 354-361, 365-369}, {311-314, 320-324, 327-329, 362, 364}, {315-319, 325, 326, 363}, {330, 331, 334-343}, {332, 333, 344, 345}

Table 4.9: Islanding solutions for the IEEE 300-bus test system

No. of Islands (k)	***Cutset***	***Partitioning Cost (MW)***		***Execution Time (s)***		***% of time improvement***
		MILP ICI	LP ICI	MILP ICI	LP ICI	
2	109-110, 122-123, 109-129	168.6	168.6	1.503	1.267	16%
3	109-110, 122-123, 109-129, 64-67, 66-57, 66-190, 68-173, 174-191, 174-198, 184-185, 185-187	311.6	311.6	1.227	0.727	41%
4	109-110, 122-123, 109-129, 64-67, 66-57, 66-190, 68-173, 174-191, 174-198, 184-185, 185-187, 195-196	330.5	330.5	1.628	0.893	45%
5	109-110, 122-123, 109-129, 64-67, 66-57, 66-190, 68-173, 174-191, 174-198, 184-185, 185-187, 195-196, 116-119	624.9	624.9	1.974	0.981*	50%
6	109-110, 122-123, 109-129, 64-67, 66-57, 66-190, 68-173, 174-191, 174-198, 184-185, 185-187, 195-196, 116-119, 15-31, 16-36, 31-74, 31-75, 42-87, 89-92	1087	1087	1.895	0.892*	53%

* Considers multiple iteration of the recursive linearization procedure (Section 4.6.1) which are executed in parallel.

The result of the SSR procedure for all the possible number of coherent groups are presented in Figure 4.33 - Figure 4.37. As can be observed, the SSR procedure managed to pre-assign a large number of nodes to the islands; hence, the complexity of the problem was significantly reduced. As a result, solutions for even 6 islands were able to be obtained close to 1 s as indicated in Table 4.9. A point worth mentioning is that the LP formulation was not able

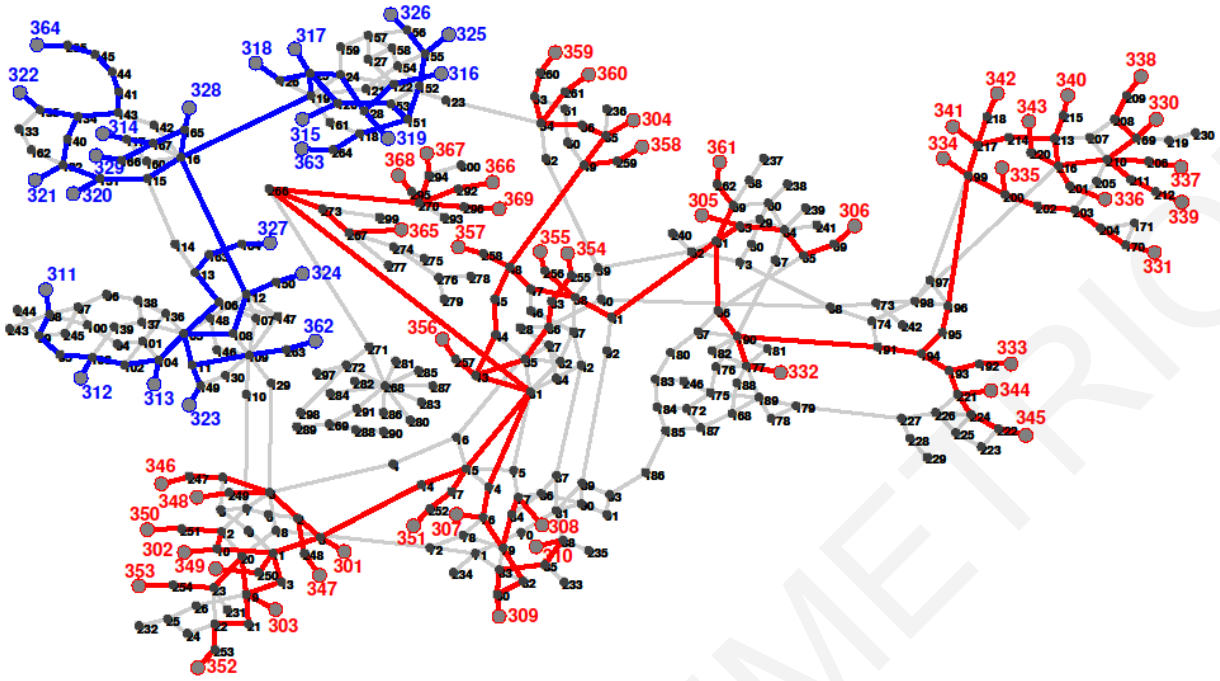

Figure 4.33: SSR procedure on IEEE 300-bus test system for $K = 2$

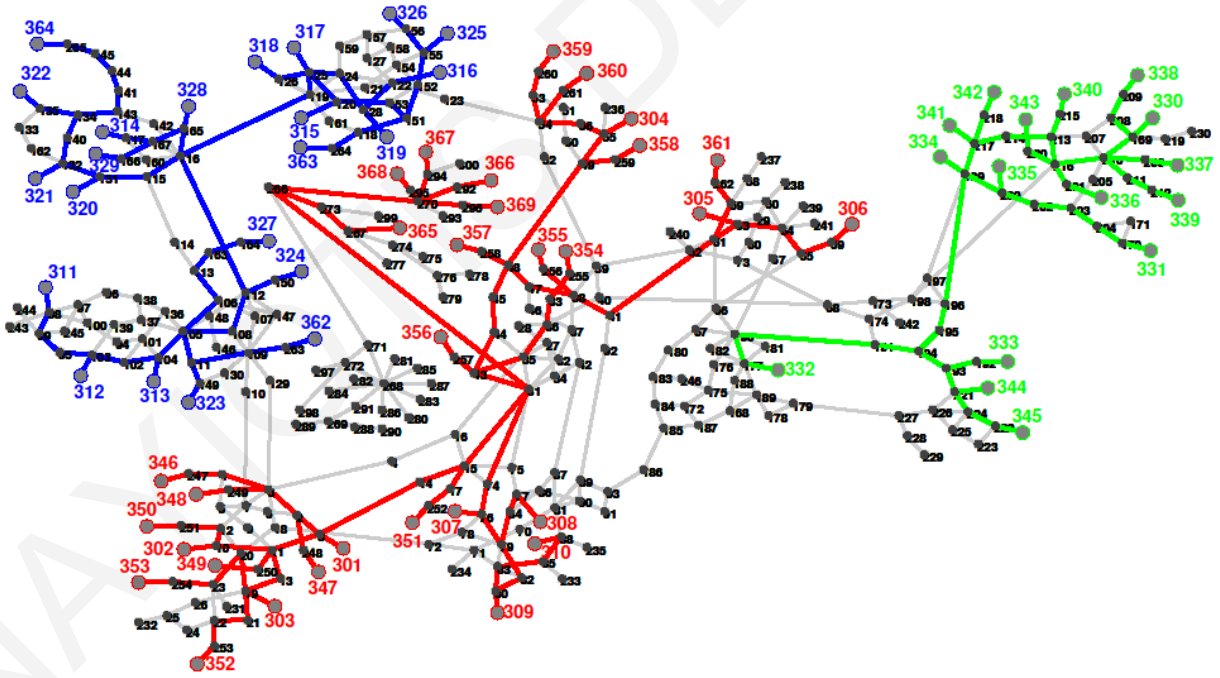

Figure 4.34: SSR procedure on IEEE 300-bus test system for $K = 3$

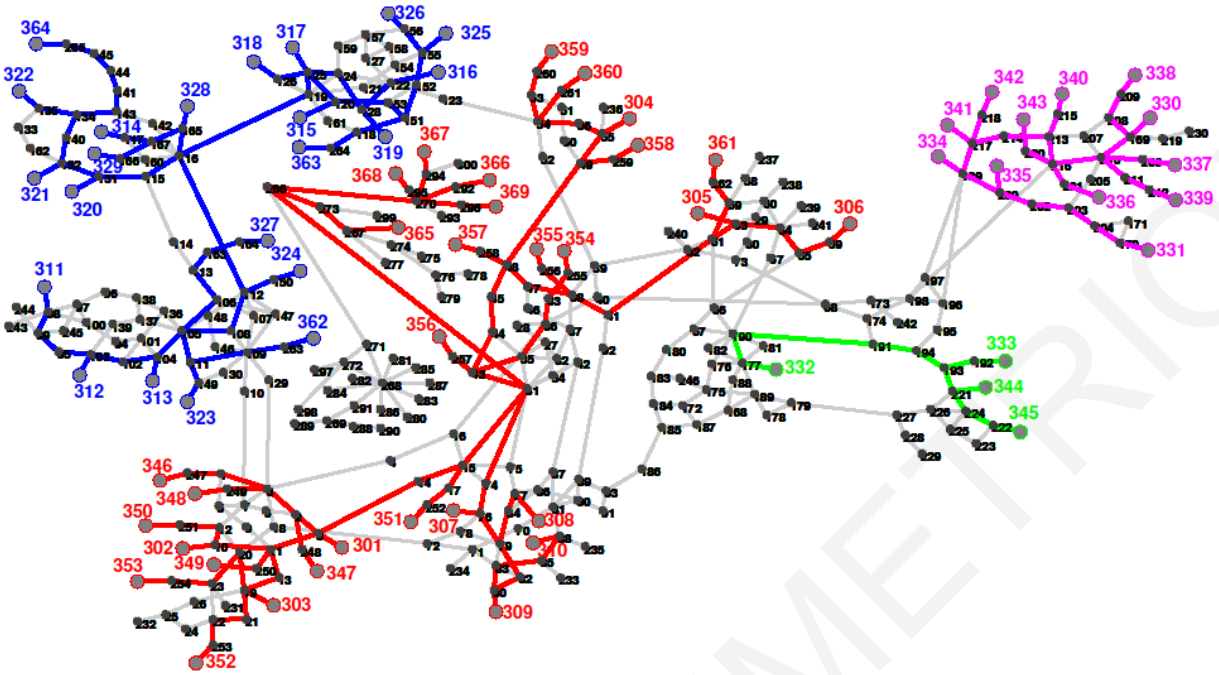

Figure 4.35: SSR procedure on IEEE 300-bus test system for $K = 4$

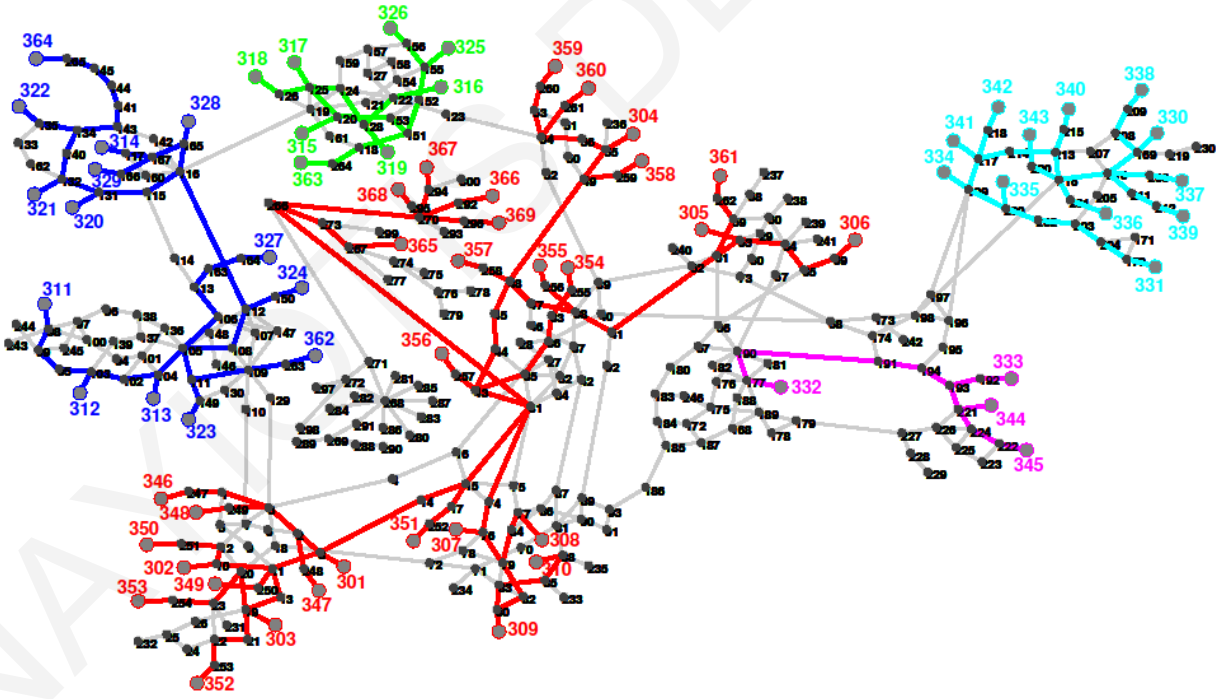

Figure 4.36: SSR procedure on IEEE 300-bus test system for $K = 5$

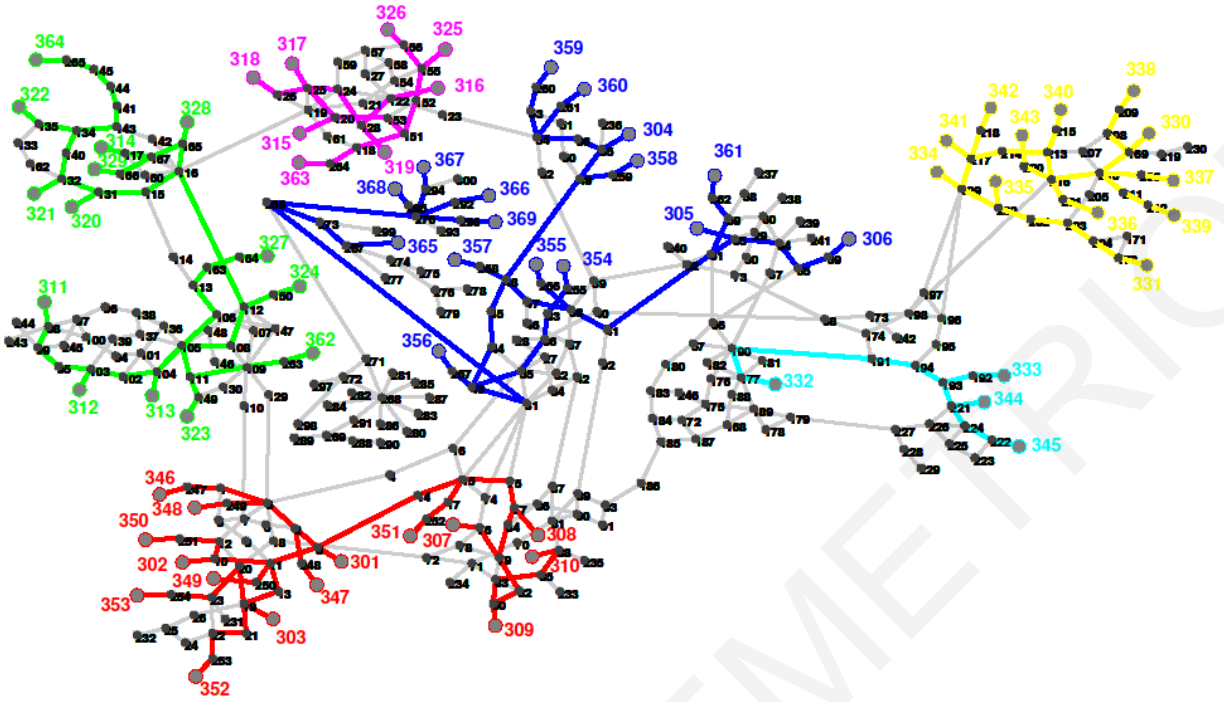

Figure 4.37: SSR procedure on IEEE 300-bus test system for $K = 6$

to provide a binary solution for $K = 5$ and $K = 6$ (indicated by the $*$ in their execution time in Table 4.9) in the first iteration of the recursive linearization procedure proposed in Section 4.6.1. However, an optimal solution was obtained for both cases in the second iteration of the procedure. Specifically, based on the electrical distance, 5 and 3 additional load nodes were assigned in specific islands for $K = 5$ and $K = 6$ respectively. Most importantly, since the extra iterations of the recursive procedure are executed in parallel, the execution time compared with the corresponding time of the MILP was improved by at least 50%. Consequently, it can be seen that the proposed ICI algorithm based on LP formulation can meet the requirements of real-time controlled islanding in case of large-scale power systems.

C) Polish Network (3375 buses)

The Polish Network available in MatPower [69] package of Matlab represents the Polish 400, 220 and 110 kV networks during winter 2007-08 evening peak conditions and includes some equivalents of the German, Czech and Slovak networks. Generator groups for up to four groups were generated based on the spatial network distribution. At this point, it is important to mention that for large-scale power systems (over 1000 nodes), the SSR procedure plays a crucial role on reducing as much as possible the search space of the optimization algorithm. The islanding solutions for all the possible numbers of coherent generator groups as

determined by both MILP ICI and the LP ICI algorithms appear in Table 4.10. As can be seen from the table, for $K = 2$ and $K = 3$, the additional constraints generated by the SSR procedure are enough to linearize the problem. Therefore, the solutions from the two algorithms are identical. However, the time needed to execute the LP algorithm is significantly less than its MILP counterpart. Specifically, the LP ICI shows over 85% and 73% improvement in execution times for $K = 2$ and $K = 3$, respectively. Nonetheless, for $K = 4$, it can be noticed

Table 4.10: Islanding solutions for the Polish Network

No. of Islands (k)	***Cutset***	***Partitioning Cost (MW)***		***Execution Time (s)***		***% of time improvement***
		MILP ICI	LP ICI	MILP ICI	LP ICI	
2	49-66, 49-83, 54-55, 60-68, 63-64, 63-3012, 100-114, 107-125, 132-140, 132-1859, 139-138, 141-140, 147-144, 151-123, 453-497, 758-960, 768-1001, 776-775, 818-1007, 834-838	1200.01	1200.01	84.974	12.090	85.77%
3	49-66, 49-83, 60-68, 132-140, 141-139, 141-140, 151-123, 758-960, 768-1001, 776-775, 1645-1646, 818-1007, 916-789 942-918, 966-1000, 1026-884 1079-1636 1635-1678, 1644-1460, 1050-879,90-145 2002-1232, 2017-1443, 2017-1625, 10201-3012, 54-55, 100-114 107-125, 134-135, 118-117, 453-497, 834-838, 839-863, 134-95, 70-117, 1031-1896, 1503-1915, 1641-1201, 150-95, 10059-10058, 10064-10058, 55-56, 10184-10209, 147-144, 71-76, 906-905, 106-94, 111-112, 132-1859, 124-1580,	1993.35	1993.35	183.126	49.327	73.06%
4	132-140, 141-139, 141-140, 2017-1625, 453-497, 758-960, 768-1001, 776-775, 818-1007, 834-838, 839-863, 906-905, 916-789, 942-918, 966-1000, 1026-884, 1031-1896, 1050-879, 1079-1636, 49-83 49-66, 1503-1915, 1635-1678,1644-1460 54-55, 1645-1646, 2002-1232,2017-1443 10184-10209, 151- 123, 107-125, 106-94 100-114, 1472-1942, **(10201-3012)**$_{MILP}$ **(3217-3225, 3218-3214, 3232-3213)**$_{LP}$ 135-94, 137-94, 1446-210, 1916-1226, 1917-1152, 2000-1402, 60-68, 132-1859, 147-144, 90-145, 1641-1201, 2057-2056, 10064-10058, 10184-10209, 92-3007, 1510-1920, 120-119, 111-112, 97-130, 124-1580, 150-102 1363-1362, 93-109 1364-2042, 1470-113, 1543-1331, 1943-1496, 1058-1057, 1220-1650, 1221-1205, 1397-1525, 1453-112,	1943	2071.73	677.158	54.46*	91.96%

* Considers multiple iteration of the recursive linearization procedure (Section 4.6.1) which are executed in parallel.

that the LP ICI algorithm provides a slightly worst solution, in terms of the PC (difference of 128.731 MW), than the MILP ICI algorithm. This deviation from the optimal solution provided by the MILP ICI relies on the added constraints that have been generated by the recursive linearization procedure. The difference in the two solutions is presented in Table 4.10. More specifically, the cutset for $K = 4$ includes the edge 10201 − 3012 for the MILP algorithm while for the LP includes the edges 3217 − 3225, 3218 − 3214, and 3232 – 3213 instead. For the linearization of the problem, 5 iterations were needed for the recursive linearization procedure, where at the last iteration which linearized the problem, 52 additional nodes were assigned to the groups. Note that, the iterations are executed in parallel. The execution time needed in order to get a binary result was 54.46 seconds.

From the results, it becomes evident that the proposed LP ICI algorithm can produce high quality results while its execution time is much lower than the execution time of the MILP algorithm. In particular, in two out of the three possible number of islands ($K = 2$ and $K = 3$), the LP ICI algorithm is able to provide the same optimal results as the MILP ICI algorithm, while for $K = 4$, its partitioning cost difference is lower than 7%. More importantly, the execution time of the MILP ICI algorithm for the Polish Network is unacceptable for ICI applications. On the other hand, the execution time of the LP ICI algorithm is within reasonable limits.

4.6.3 Discussion

The simulation results presented in this work indicate that the LP ICI algorithm is able to provide fast and high quality solutions, which in most presented cases is equal to the optimal solution given by the MILP ICI algorithm. In this Section a comparison of the proposed approach in terms of execution time with other existing MILP approaches is presented. Moreover, since the LP ICI algorithm is a combination of the SSR procedure and the LP optimization (which are interdependent), the interdependencies as well as some other unique characteristics of the proposed method are also discussed.

Firstly, it is important to highlight that no approach exists for a direct one to one comparison (an approach with the same objective function and the same number and type of constraints). Nevertheless, an execution time comparison with other existing MILP methods [80], [81] applied on the IEEE 118- and 300-bus test systems to solve the ICI problem is

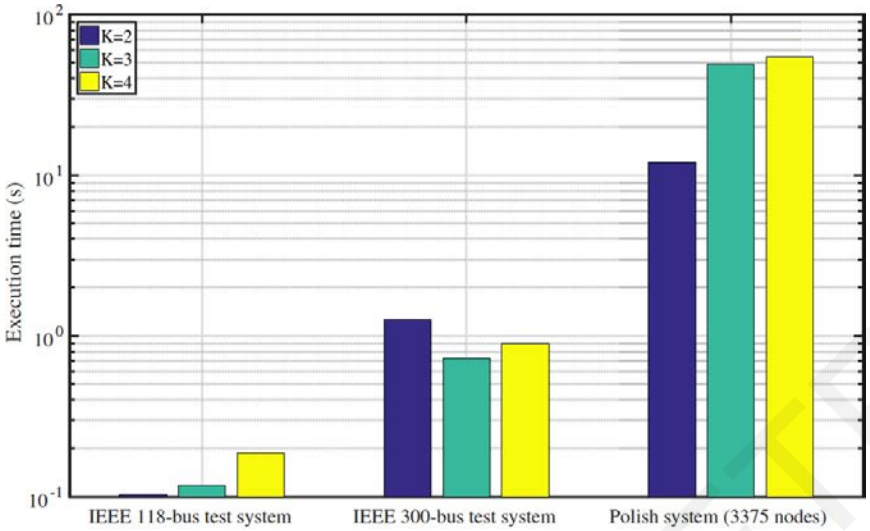

Figure 4.38: Execution times for the IEEE 118- and 300-bus test systems and the Polish Network for K = 2, 3, 4

Table 4.11: Execution time comparison

No. of Islands (k)	***Proposed LP ICI***	***Approach from*** [80]	***Approach from*** [81]
	IEEE 118-bus test system		
2	0.1035 s	-	$\approx 10^{*}$ s
3	0.1177 s	0.55 s	-
	IEEE 300-bus test system		
2	1.267 s	-	$\approx 30^{*}$ s
3	0.727	> 12 s	-

presented in Table 4.11. Note that no other approach exists based on a mathematical formulation that provides optimal results on the Polish Network. As can be seen from Table 4.11, the proposed approach is faster than the other two approaches, even if it satisfies a larger number of constraints. Note that while there are differences between the constraints used in the aforementioned approaches, additional constraints can easily be added to the proposed approach with minimal or no effect on its execution time.

The execution times reported are a combination of the SSR procedure and the optimization method used. Therefore, the reported times given in this work indicate the execution times of the whole ICI algorithm. It is important to mention that these execution times depend on multiple characteristics of the system (e.g., number of the coherent generator groups, number and location of the generators of each coherent group, number of resulting islands and system size). Nonetheless, a good estimation of the execution time increase with respect to the system size (e.g., 118, 300 and 3375 nodes) appears in Figure 4.38.

4.7 Conclusions

This Chapter has proposed several ICI methods for addressing the "*where to island*" problem, where each ICI method constitutes a different section in this Chapter. For completeness, the graph theory fundamentals applied in these methods were first provided.

An existing SCCI method [8] was further validated and improved using cases of real transmission networks of Cyprus and Poland. The application of this method on these networks highlighted some critical practical issues that have not been previously considered and that require to be addressed before implementing the method in real networks. In particular, the existing method is sensitive to outliers and does not constrain certain branches to be excluded from the splitting strategy. Therefore, Section 4.3 implemented a robust clustering algorithm, k-medoids, to solve the problem of outliers. As a consequence, a new Robust SCCI (RSCCI) method was developed. To constrain branches to be excluded from the islanding solution, the weight factors associated with the edges to be excluded are changed to the maximum weight value in the weighted adjacency matrix. Using this constraint, it is ensured that unavailable branches are not included in the splitting strategy. The existing SCCI and the proposed RSCCI methods were also tested on large-scale networks and its computation time was found to be expensive. The size of the network versus the computation time was studied and it was determined that the existing SCCI and the RSCCI are suitable for real-time applications, when the number of nodes is smaller than 300 nodes. Since current power systems contain several nodes, a reduced area i.e., reduced searching space, which concentrates potential splitting strategies, is proposed prior the application of the clustering technique. The determination of this reduced search space will improve the computation and the effectiveness of both methods, making these suitable for real-time applications.

Section 4.4 has proposed a novel ICI scheme based on the well-established cut-set matrix concept. The graph theoretic cut-set matrix is modeled as a combinatorial optimization problem with constraints. The objective function of this problem is the minimum power imbalance within islands, while the main constraints are the coherent generator groups and transmission line availability. The proposed ICI algorithm was tested using the IEEE 9-bus system and the real Cypriot system. Different case studies (i.e., faults) and demand levels were examined for illustrating the ICI algorithm using the Cypriot network, which demonstrated its adaptability and effectiveness in minimizing the impact of cascading outages leading to

blackouts under varying system conditions.

In Section 4.5 an exact ICI algorithm based on a MILP formulation that directly determines an islanding solution with minimal power-flow disruption for any given number of islands has been proposed. The constraints applied when satisfying this objective function deal with coherent generator groups and transmission line availability. Additionally, the algorithm allows the control of the size of islands and ensures the connectivity inside them. Since the MILP formulation allows the easy manipulation of its existing constraints, a preprocessing procedure is also developed for reducing the search space of the MILP. The objective of the preprocessing procedure is to find a tree for each island with minimum number of nodes, spanning to all generator nodes of its coherent group. The nodes that are included in these trees are directly assigned to their resulting island, ensuring the generator coherency. The effectiveness and the computational efficiency of the proposed ICI algorithm have been demonstrated under different system conditions.

Finally, in Section 4.6, an LP formulation for solving the ICI problem has been presented. The proposed LP ICI algorithm directly determines an islanding solution for large scale power systems with minimal power-flow disruption for any given number of islands in a timely manner. In addition, the algorithm ensures that only coherent generators are included in each island, enables operators to constrain any transmission line to be excluded from the solution, allows the control of the size of islands and ensures that each resulting island is connected. The proposed LP formulation is derived from the relaxation of the MILP formulation introduced in Section 4.5. This relaxation is achieved through the combination of all the additional constraints (i.e., Preprocessing/SSR generated constraints and transmission line availability constraints). The LP formulation is executed as a part of a recursive linearization procedure which ensures the generation of a binary solution; hence the validity of the resulting islanding solution is also ensured. The time improvement and effectiveness of the proposed ICI algorithm based on the LP formulation has been demonstrated using large-scale test systems such as the IEEE 118- and IEEE 300-bus test systems, as well as a real large-scale power system, the Polish Network available in MatPower.

CHAPTER 5
TIMING OF CONTROLLED ISLANDING – WHEN TO ISLAND

5.1 State-of-the-Art Overview

The question of when to island is critical for the success of the ICI scheme, since the possible issues of false alarm and false dismissal have to be handled. In the case of a false alarm, islanding is triggered too early, forcing a stable system to incorrectly be split into islands. In the case of false dismissal, islanding is triggered too late, allowing an unstable system to operate and to probably lead to an uncontrolled cascading blackout. Therefore, early recognition that could indicate if a disturbance will evolve into a blackout or not is important for mitigating the occurrence and cost of blackouts.

Despite being recognized that the timely implementation of the ICI scheme (i.e., to answer the question of when to island) is critical for its success, only a few works have attempted to solve the "when to island" problem [82], [83]. In [82], an adaptive controlled islanding as a component of an emergency power system control strategy is developed. It seeks to address the "when to island" aspect. A decision tree based tool is proposed to recognize conditions existing in the system that warrant controlled islanding. In [83], the authors have proposed a unified controlled separation scheme based on synchrophasors. The scheme partitioning the problem into sub-problems handled strategically in three time stages: the Offline Analysis stage, the Online Monitoring stage and the Real-time Control stage. The Real-time Control stage calculates a synchrophasor-based separation risk index for each island boundary to predict the time to perform separation. However, these approaches carry out offline estimations of the coherent groups of generators in advance. This practice, might lead to inadequate coherent groups given that different disturbances are likely to result in different groups of generators.

5.2 A Unified Methodology for Determining the Time of Islanding

A unified methodology to address the "*when to island*" problem has been proposed in [84]. The methodology initially uses synchronized system measurements of all generators in the system (i.e., generator speed, output power, voltage and current), provided by Phasor Measurement Units (PMUs), to estimate the generators rotor angles. The estimated rotor angles are then used to define the suitable number of coherent generator groups, and the generators within each coherent group. Once the coherent groups are identified, the proposed unified methodology adopts the concept of area-based Center of Inertia (COI)-referred rotor angle index [85], [86] , widely used in transient stability analysis for tracking the stability of interconnected areas, to determine the actual time for islanding. The time at which the system is defined to be unstable, and hence requires to be split, is defined as the moment at which one of the COI-angles deviates from the traditional threshold of ±180°. Defining the time of islanding allows the triggering of islanding schemes to split the interconnected power system and avoid large-area blackouts.

5.2.1 Area-based Center of Inertia (COI)-referred rotor angle index

Area-based COI [85], [86] is a common transformation used in transient stability analysis for tracking the stability of interconnected areas. The area-based COI-referred rotor angle index is associated with the rotor angle of each area of a power grid. It rests on an equivalent inertia that represents the total inertia of the generators in that area. Considering the fact that a large-scale power system is divided into several areas according to the coherency of generators in a particular area, it is reasonable to assume that an equivalent single large machine can represent all the generators in that area. This can be achieved by deriving the COI of that area. In order to do that, the area equivalent rotor angle needs to be defined first. Thus, for a particular area, with *N* number of generators, its equivalent rotor angle is the average rotor angle through all *N* measurements which is given by:

$$\bar{\delta}_j = \frac{1}{N}\sum_{i=1}^{N} \delta_i \,, \tag{5.1}$$

where $\overline{\delta}_j$ is the area equivalent rotor angle and δ_i the individual rotor angle in a particular area. Assuming a total number of *r* areas in a power system, the COI of the system can be defined as:

$$\bar{\delta}_{COI} = \frac{1}{H_T}\sum_{j=1}^{r} H_j \bar{\delta}_j \,, \tag{5.2}$$

in which

$$H_T = \sum_{j=1}^{r} H_j \,, \tag{5.3}$$

where H_T is the total inertia in the system and H_j the j^{th} inertia in an area. The area equivalent rotor angle is then expressed in the COI frame and is given by:

$$\delta_j^{COI} = \bar{\delta}_j - \bar{\delta}_{COI} \,. \tag{5.4}$$

The area-based COI-referred rotor angle as given in (5.4) can be used as a transient stability index (TSI) whose behavior is illustrated by plotting it against time. From the plot, it can be observed that, if the COI-referred rotor angle of any area (δ_j^{COI}) goes out of step after a fault is cleared (exceeds $\pm 180^0$), then the area is considered to be unstable. In contrast, if it remains in equilibrium (within $\pm 180^0$) then the area is considered to be stable [85], [86]. It is important to mention that the formulation of the area-based COI-referred rotor angle index is simple and straight forward, and thus suitable for applications in large-scale power systems. Moreover, the area-based COI-referred rotor angle index negates the need to assess all generator rotor angles in a power system, and, thus, fast stability assessments of the whole system after the occurrence of faults can be achieved. Crucially, this work utilizes the concept of area-based COI-referred rotor angle index to answer the question of when to island. It is not far from reality to assume that the moment where the COI-referred rotor angle of any area goes out of step after a fault is cleared (when it goes unstable), is also the most suitable moment where the unstable power system should be split into islands.

5.2.2 Suitable number of coherent generator groups (*k*) (extension of the two-step methodology for real-time identification of coherent generator groups)

The two-step methodology for real-time identification of coherent generator groups (presented in Section 3.2) can be completed by determining the suitable number of coherent generator groups (*k*). It is noted that for the ICI concept the parameter *k* corresponds also to the suitable number of islands to split the system since each of these dynamic groups of generators must be separated into different islands to assist the system's transient stability. The main steps for assessing the suitable number of coherent generator groups (*k*) are:

Step 1: Set the maximum number of coherent generator groups (k_{max}) according to system characteristics and topology.

Step 2: For the default case k=2, find the global minimum ICC (min_{global}) within both the created subgraphs and the next minimum (min_{next}) into its subgraph.

Step 3: If (($min_{next} - min_{global}$) x 100%) > a, $k = k + 1$, else stop. The parameter a may vary according to the inherent characteristics of each network. The exact value of this threshold can be set through sensitivity analyses.

Step 4: Find the next global minimum and the next minimum into its subgraph.

Step 5: Repeat steps 3 and 4 until $k = k_{max}$.

The extension of the two-step methodology for real-time identification of coherent generator groups is shown in Figure 5.1. As it can be seen, an online estimation of the generator rotor angles is firstly performed by solving the swing equation in the time domain using PMU measurements. The pairwise similarity coefficients are then calculated through an intraclass correlation analysis and are used as edge weights to a fully connected graph, where: a) the suitable number of coherent generator groups (k) is determined; and b) the coherent generator groups are formed by deriving its MST.

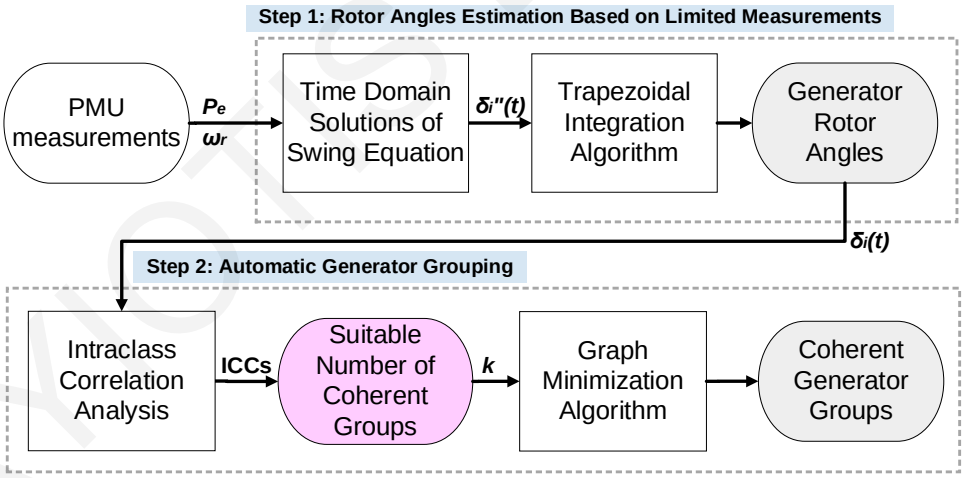

Figure 5.1: Extended two-step methodology for real-time identification of coherent generator groups

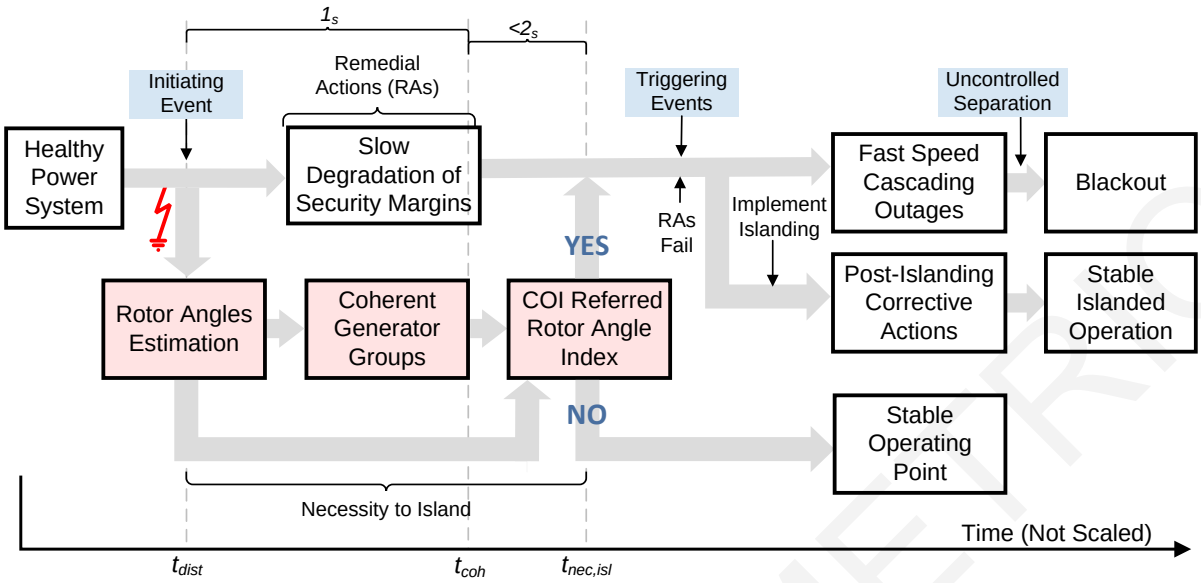

Figure 5.2: Time-line showing the implementation of the proposed methodology for determining the time of islanding

5.2.3 Proposed unified methodology for when to island

Figure 5.2 illustrates the general concept of the proposed unified methodology for triggering the ICI. A severe disturbance on a healthy power system (at $t = t_{dist}$) can cause the slow degradation of the grid [10]. Although Remedial Actions (RAs) may be applied to avoid this degradation, they may fail, either because they are not sufficient or they may not be implemented on time by operators. This typically leads to fast speed cascading outages, causing the uncontrolled separation of the system and resulting in blackouts.

To mitigate the impact of undesirable blackouts, ICI can be used. Now, in order to trigger promptly such a scheme, the time of defining the necessity to island the system, denoted in Figure 5.2 by $t_{nec,isl}$, needs to be determined. The main steps to assess this are:

Step i: Estimate the generator rotor angles (execution of Step 1 of the methodology for the real-time identification of coherent generator groups presented in Section 3.2.1) after the occurrence of a fault (for a $t < t_{dist} + 3$s).

Step ii: Determine both the suitable number of coherent generator groups (k) (as described in Section 5.2.2) and the coherent groups (execution of Step 2 of the methodology for the real-time identification of coherent generator groups presented in Section 3.2.2) exactly at $t = t_{dist} + 1$s, denoted by t_{coh}.

Step iii: Use the estimated rotor angles data collected in Step i to calculate the area-based

COI-referred rotor angle index of each coherent group (with a time step $\Delta t = 0.02$s), as described in Section 5.2.1 of this work. If the index of any coherent group exceeds $\pm 150^0$, send a warning signal for a possible islanding. If the index of any coherent group exceeds $\pm 180^0$, set this moment as the time of defining the necessity to island. If not, no islanding is needed.

The ICI algorithm can then be used to find the optimal points for islanding. Additional corrective measures (e.g., fast valving and load shedding) may be needed to ensure that each island will retain its security margins during the post-islanding stage [12], [16], [87], [13], and thus to obtain a stable islanded operation.

5.2.4 Simulation results

The proposed unified methodology was illustrated using the IEEE 39-bus test system (Figure 5.3). This system contains 10 synchronous generators, 34 transmission lines and 19 constant power loads. The dynamic data of the generators and the details of the controllers (i.e., exciters and governors) have been taken from [27].

A) Case Study 1

At time $t = 1$ s, a three-phase to ground fault occurs at bus 2 and is cleared at 1.25 s after local relays open both ends of transmission lines 2-3 and 2-25. Figure 5.4 highlights that this

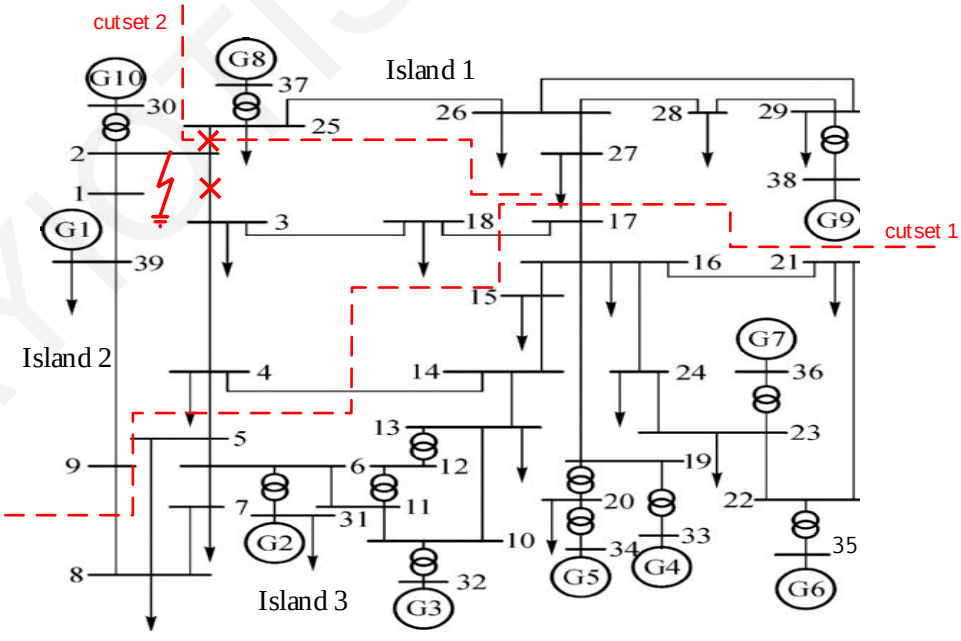

Figure 5.3: Case Study 1: IEEE 39-bus test system with optimal islanding solution

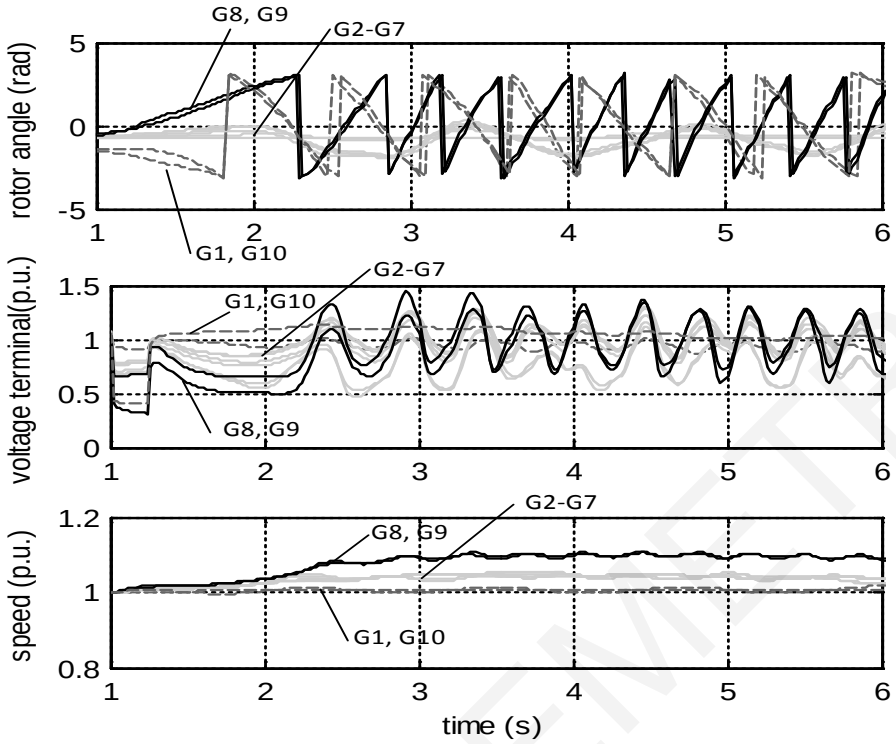

Figure 5.4: Case Study 1: IEEE 39-bus test system - Electrical behavior without islanding

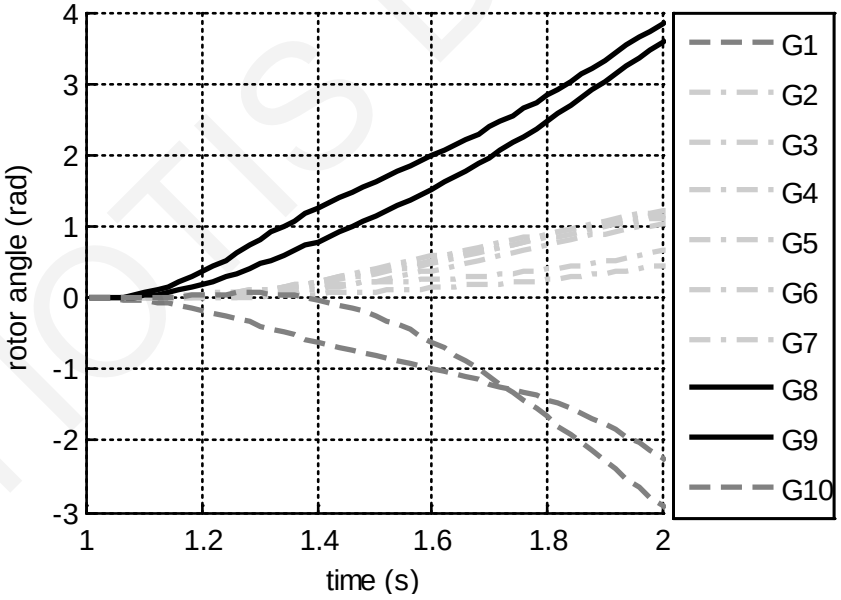

Figure 5.5: Case Study 1: Estimated generator swing curves of the IEEE 39-bus test system (for a 1 s time interval after the occurrence of the fault)

disturbance results to a blackout quickly after the fault is cleared. The generator rotor angles estimated (as described in Section 3.2.1) 1 s after the occurrence of the fault are shown in Figure 5.5 (assuming that 50 synchronized measurements of output power and generator speed per second are provided by a PMU installed at each generator terminal). As mentioned in

Section 5.2.3, exactly at this time ($t = t_{coh}$ =2 s), both the suitable number of coherent generator groups (k) and the generators within each coherent group are determined based on the extended automatic generator grouping analysis of Section 5.2.2.

Starting from the default case (k = 2), and examining the estimated rotor angle samples from 1 s to 2 s: i) the positive and negative swings are directly separated to two subgraphs; ii) the pairwise ICCs are calculated at each subgraph (Figure 5.6); iii) the suitable number of coherent generators is determined. It is noted that, after performing a sensitivity analysis, a value of 20% for parameter a was found suitable for this network. For this case study, the suitable number of coherent generator groups is found to be three and the coherent groups determined are {G1, G10}, {G8, G9} and {G2, G3, G4, G5, G6, G7} (Figure 5.7). Area 1 consists of coherent generators {G1, G10}, Area 2 consists of generators {G8, G9}, while {G2, G3, G4, G5, G6, G7} are the coherent generators belonging to Area 3. It is noted that the estimation procedure of the rotor angles continues for $t=t_{coh}$+2 s.

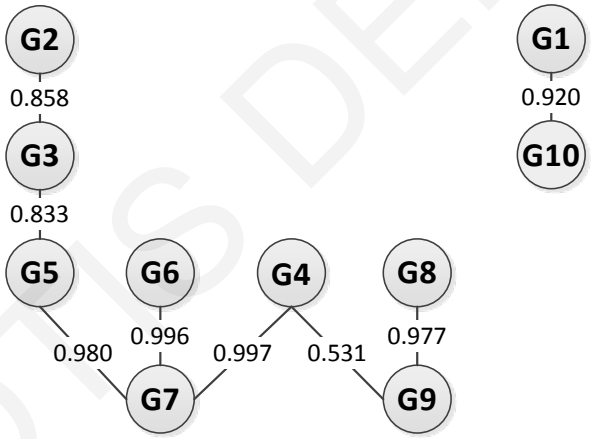

Figure 5.6: Case Study 1: Pairwise generator ICCs at each subgraph (default case k = 2)

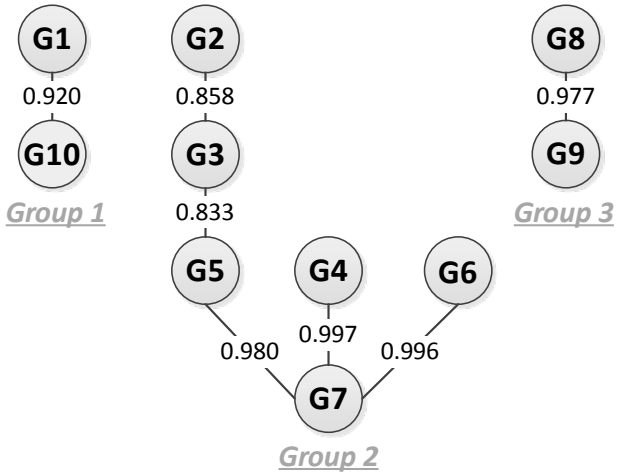

Figure 5.7: Case Study 1: Coherent generators of the IEEE 39-bus test system at $t=t_{coh}$

Having the knowledge of the generator coherency and using the estimated rotor angles data collected for $t<t_{coh}+2$s, the area based COI-referred rotor angle index of each coherent group is then calculated (with a time step Δt=0.02s). As mentioned in Section 5.2.1, the area-based COI-referred rotor angle indices are plotted to illustrate the severity of the disturbance (to recognize if the disturbance will evolve into a blackout or not). From Figure 5.8, it can be noticed that the Area 1 COI-referred rotor angle firstly intercepts the 180^0 line at t=2.0 s. This means that it is the weakest area in the system (first area to go out of step), and therefore, this is the most suitable time according to the proposed methodology where the unstable system should be split into islands.

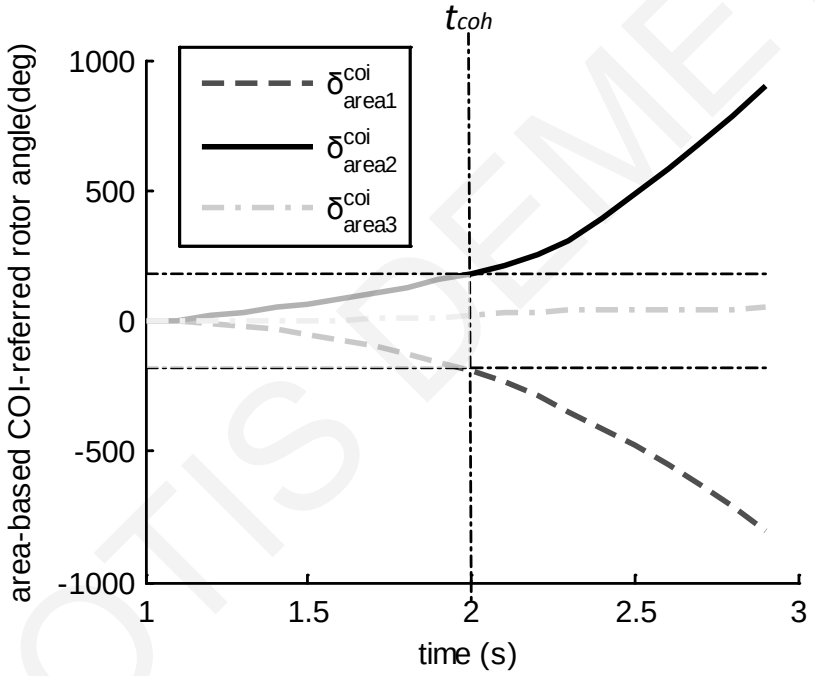

Figure 5.8: Case Study 1: Area-based COI-referred rotor angle indices (the calculation of the indices starts at $t=t_{coh}$ where the coherent generator groups are known)

To actually split the system, the ICI scheme proposed in [70] is adapted to determine an islanding solution that creates islands with minimum power imbalance, while ensuring that each island contains only coherent generators. The proposed ICI scheme enables the exclusion of critical branches (e.g., transformers) and explores the vast combinatorial space to find the optimal solution. Thus, considering the power flow and actual topology of the system at t = 2.0 s, the execution of the ICI algorithm determines two cutsets and creates three islands. The two cutsets produced (Cutset 1 and Cutset 2), separate Area 3 from Area 1 and 2, and then separate Area 1 from Area 2, respectively. The combination of these two cutsets forms the final islanding solution marked in Figure 5.3 (red dashed lines). This solution was found in

approximately 0.024 s. Hence, islanding was actually undertaken at t =2.024 s. Figure 5.9 shows the dynamic trajectories after implementing the optimal solution. Three stable groups are created. Moreover, the frequencies of Island 1, Island 2 and Island 3 are 1.01 p.u., 1.03 p.u. and 1.03 p.u. respectively. Voltages also reach values close to nominal values. Since the splitting strategy successfully retains the frequency of the islands within acceptable limits and the corresponding voltages within the thresholds, it can be concluded that the proposed unified methodology successfully defines the moment of when to island the system.

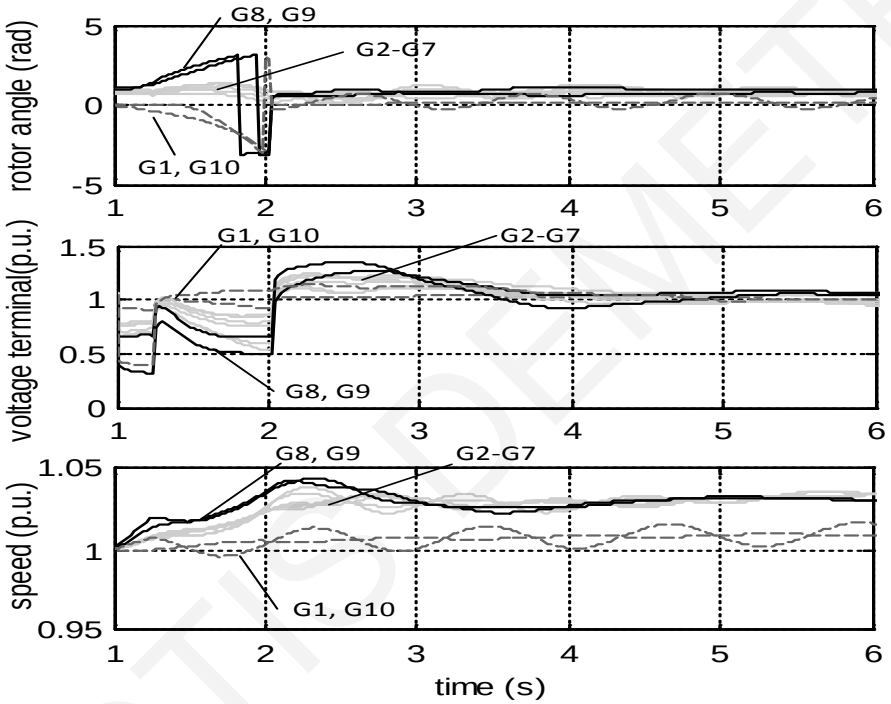

Figure 5.9: Case Study 1: IEEE 39-bus test system - Electrical behavior with islanding

B) Case Study 2

The same event as case study 1 is also examined here. However, in this case study the fault is cleared by the local relays much earlier, 0.10 s after the fault occurs and not after 0.25 s. Figure 5.10 shows the estimated generator rotor angles 2 s after the occurrence of the fault. Using the rotor angle data collected until $t=t_{coh}$, both the suitable number of coherent generator groups (k) and the actual groups are determined. For this case study, the suitable number of coherent generator groups is found to be 2 and the coherent groups determined are {G1, G10} (Area 1) and {G2, G3, G4, G5, G6, G7, G8, G9} (Area 2) (Figure 5.11). Then, the area-based COI-referred rotor angle indices of these particular areas are calculated and plotted to assess the severity of the disturbance. From Figure 5.12, it can be observed that no area-based COI-referred rotor angle violates the stability limit of the grid. Hence, the generators are considered

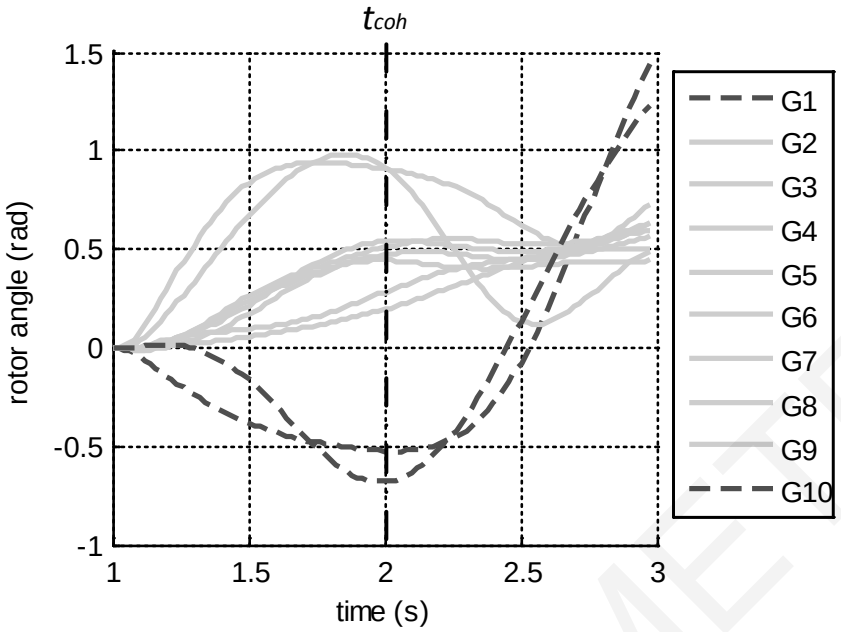

Figure 5.10: Case Study 2: Estimated generator swing curves of the IEEE 39-bus test system (for a 2 s time interval after the occurrence of the fault)

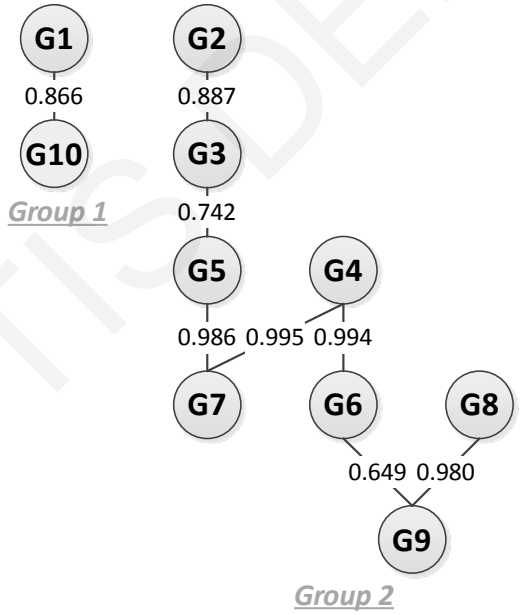

Figure 5.11: Case Study 2: Coherent generators of the IEEE 39-bus test system at $t=t_{coh}$

to remain synchronized to the system after the clearance of the fault, and therefore no controlled system separation is needed.

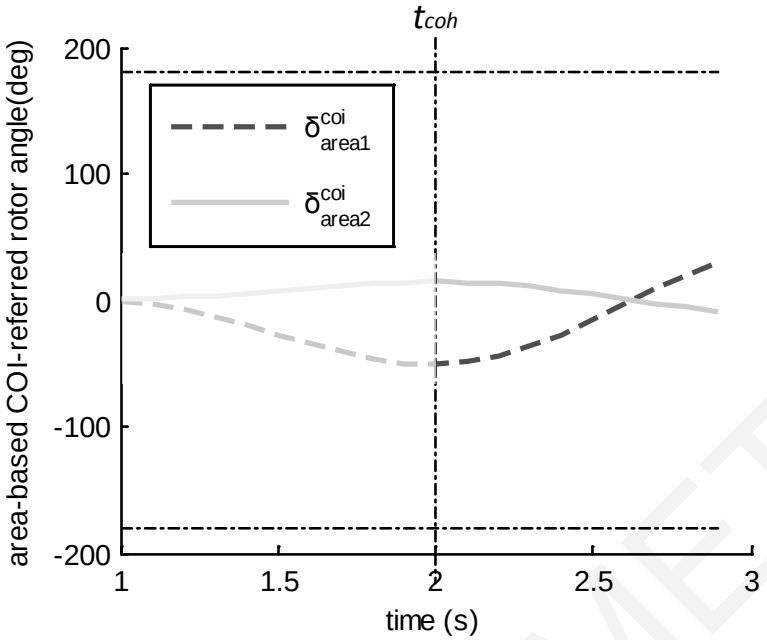

Figure 5.12: Case Study 2: Area-based COI-referred rotor angle indices (the calculation of the indices starts at $t=t_{coh}$ where the coherent generator groups are known)

C) Case Study 3

At time t = 1 s, a three-phase to ground fault occurs at bus 17 and is cleared after local relays open both ends of transmission lines 16-17, 17-18, and 17-27 at t = 1.20 s (0.20 s after the fault occurred). Figure 5.13 highlights the behavior of the system after the clearance of the

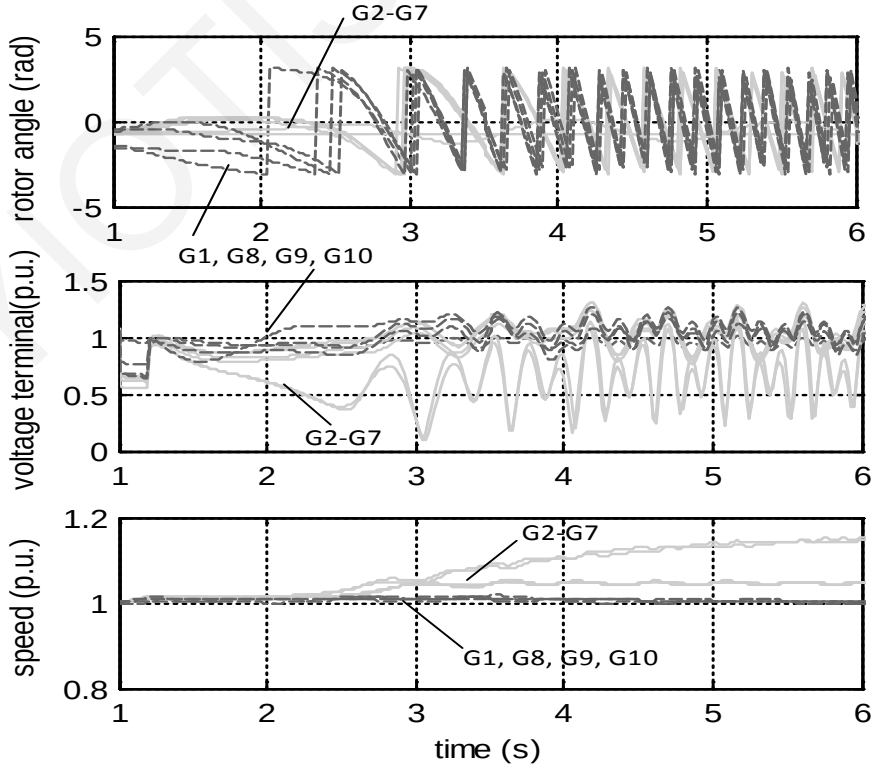

Figure 5.13: Case Study 3: IEEE 39-bus test system - Electrical behavior without islanding

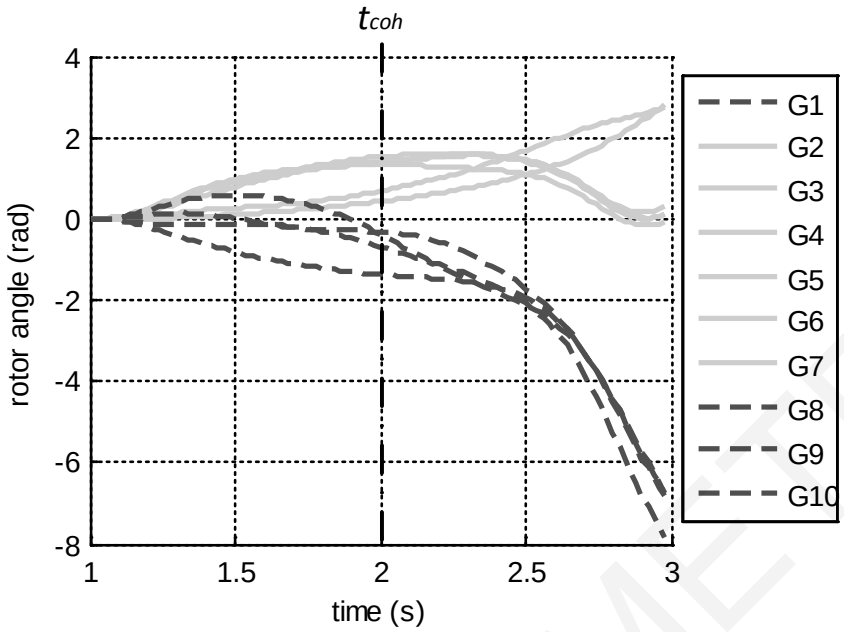

Figure 5.14: Case Study 3: Estimated generator swing curves of the IEEE 39-bus test system

fault. It is clear that the generators' speed increases and the generator terminal voltages become significantly lower. Thus, it can be concluded that the system needs to be split if the blackout is to be avoided. Using the estimated rotor angle data collected until $t=t_{coh}$ (as described in Section 5.2.3) (Figure 5.14), the suitable number of coherent generator groups (k) is found to be two (based on the extended automatic generator grouping analysis of Section5.2.2). The coherent groups determined are {G1, G8, G9, G10} (Area 1) and {G2, G3, G4, G5, G6, G7} (Area 2) (Figure 5.15). Using this information about the coherent groups along with the estimated rotor angles data collected for $t<t_{coh}+2$ s, the area-based COI-referred rotor angle indices are calculated and plotted to recognize if the disturbance will evolve into a blackout or not (Section 5.2.1). From Figure 5.16 it can be seen that the Area 1 COI-referred

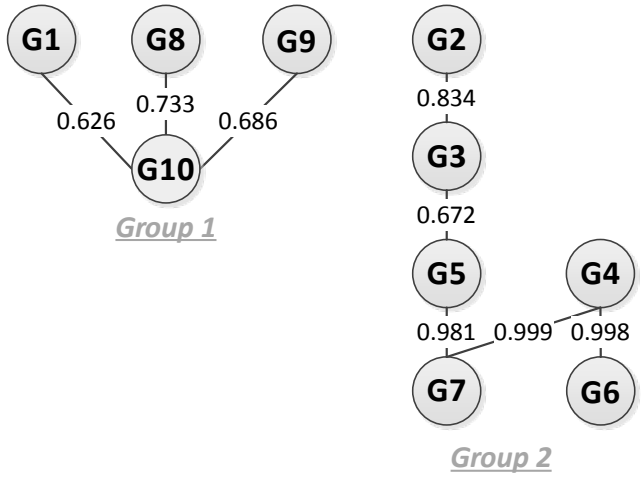

Figure 5.15: Case Study 3: Coherent generators of the IEEE 39-bus test system at $t=t_{coh}$

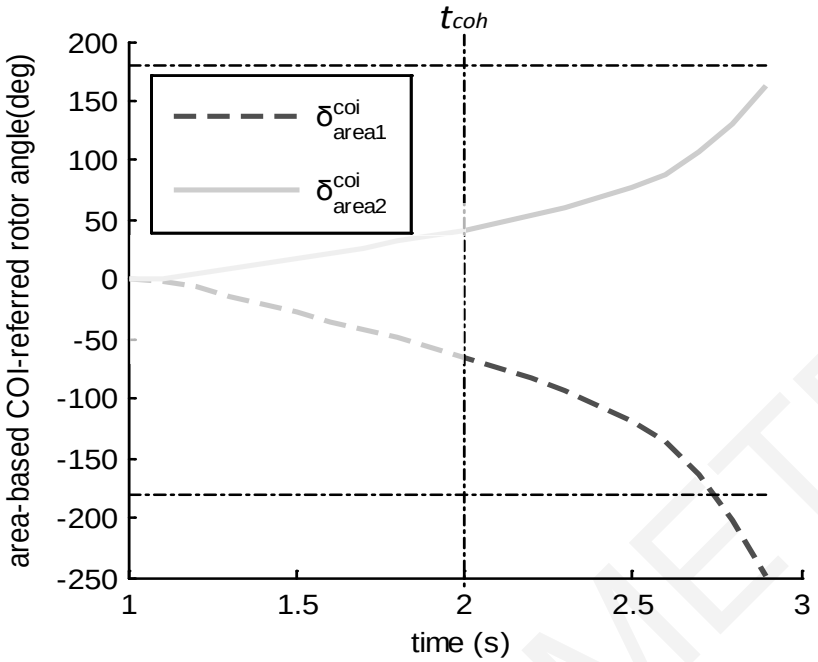

Figure 5.16: Case Study 3: Area-based COI-referred rotor angle indices (the calculation of the indices starts at $t=t_{coh}$ where the coherent generator groups are known)

rotor is the first to intercept the 180^0 line at t = 2.76 s. Therefore, this is the critical time for islanding the system. Considering the power flow and actual topology of the system at t = 2.76 s, the implementation of the ICI algorithm identifies the optimal solution (for minimum imbalance) across the lines 5-6, 6-7, 4-14, 17-18 and 17-27 (red dashed line in Figure 5.17). This solution was found in approximately 0.017 s; islanding was undertaken at t = 2.777 s.

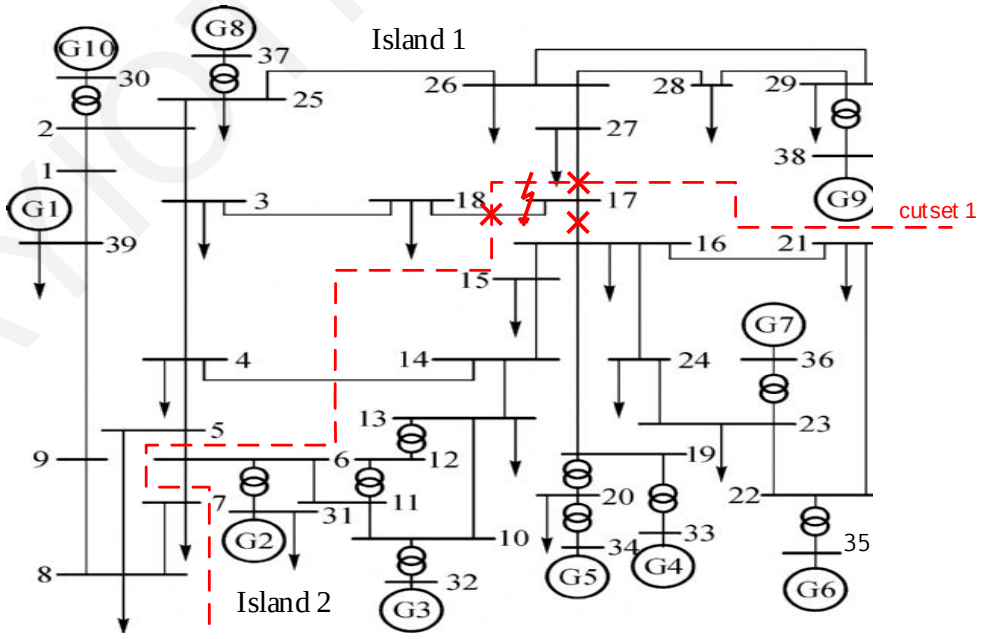

Figure 5.17: Case Study 3: IEEE 39-bus test system with optimal islanding solution

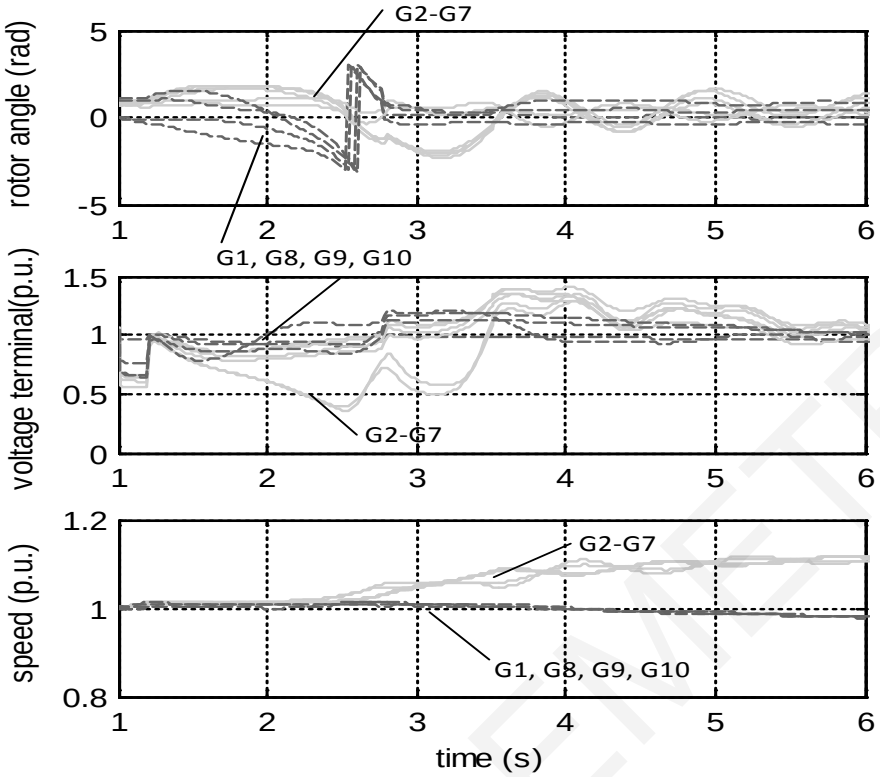

Figure 5.18: Case Study 3: IEEE 39-bus test system - Electrical behavior with islanding

The post-islanding behavior of the islands is shown in Figure 5.18. From the generator rotor angles in each island, it can be obtained that two stable groups are created. Figure 5.18 further shows that the generator speeds (0.981 p.u. and 1.107 p.u. respectively) are close to their nominal values, while the generator terminal voltages are successfully kept within the desirable limits (which are defined as ±10% deviation from the nominal value). Thus, it can be concluded that the decision when to island the system successfully prevents the total system blackout.

5.3 Conclusions

In this Chapter, the critical question of when to island, which has not been fully explored in the literature, has been investigated. The proposed methodolody utilizes the concept of the area-based COI-referred rotor angle index to illustrate the severity of the disturbance and thus to recognize if the disturbance will evolve into a blackout or not. It is not far from reality to assume that the moment at which a particular area is said to be unstable, is also the moment where the ICI scheme should be triggered to split the unstable system into islands. The calculation of the area-based COI-referred rotor angle index requires the knowledge of the

generator coherency and the rotor angles. Hence, the proposed methodology also identifies both the suitable number of coherent generator groups and the actual coherent groups based on an online visualization of the rotor angles. Different case studies were examined for illustrating the unified methodology using the IEEE 39-bus test system. The simulation results demonstrate its adaptability and effectiveness in triggering promptly the ICI scheme and thus in minimizing the impact and cost of large-area blackouts under varying system conditions.

CHAPTER 6

POWER SYSTEM RESTORATION – WHAT TO DO AFTER ISLANDING

6.1 State-of-the-Art Overview

Although the objective of controlled islanding schemes is to avoid a complete blackout, one or more islands might reach a local blackout after the splitting strategy is carried out. These undesirable events occur due to the lower stability margin in the created island compared to the one for the entire power system. When a local blackout occurs in an island, Parallel Power System Restoration (PPSR) should be carried out in order to restore the island, and therefore, restore the power system. It has been stated in [88] that the following constraints, regarding the PPSR, should be considered when applying controlled islanding strategies:

- Each island should have sufficient blackstart (BS) capability
- Each island should have enough cranking paths to crank non-blackstart units or pick-up loads
- Each island should have the ability to match generation and load within prescribed frequency limits
- Each island should have adequate voltage controls to maintain a suitable voltage profile
- All tie points for subsystems must be capable of synchronization with adjacent subsystems
- All islands should share information with other islands.

The integrity of the power system as a whole is recovered only when the system operators reconnect each island. The restoration of the power system is not an easy task given that it comprises several complex and time-consuming stages. Among these, synchronization of the islands to be connected is one major task. The synchronization requires the accurate knowledge of the operating condition of the islands to be connected (i.e., frequency of the islands, and voltage magnitude and angles of the boundary buses) [88]. At the circuit breaker (CB), where islands will be synchronized, the following three conditions should be respected:

- The voltage magnitudes on the two sides of the CB should be as close as possible to

one another. A rule of thumb would be to close the circuit breaker with no more than 2-5% voltage difference between the two islands.

- The frequencies of the two islands must be close to identical. Under abnormal conditions, a system may tolerate up to a 0.1 Hz frequency difference.
- The voltage phase angle between the two sides of the CB must be within allowable tolerance levels, as defined by the system engineers for the specific area where the synchronizing will occur (typically ± 20 degrees).

If the conditions are satisfied, there will be little or no transfer of energy between the two islands when the breaker is closed. The contemporary process by the electric utilities to restore the system is to equip with synchroscopes the candidate substations for reconnection. A synchroscope allows the operator to visually observe the voltage difference across a CB as well as to monitor the rate of frequency-slip, if a frequency-slip exists. The operator would then decide if and when to close the CB. The main disadvantage of the contemporary procedure for power system restoration is that only the substations that are equipped with synchroscopes can be employed for synchronization. However, it is difficult to pre-specify such substations that cover all possible scenarios of system restoration. In other words, the number of synchronizing locations is limited. Furthermore, the re-closure requires the presence of crew field in the candidate substations to monitor and operate the synchronization. This implies additional delay to the procedure of power system restoration since the substations have no control effect on the island's frequency and voltage.

As mentioned in Chapter 4, several methods are reported in the literature to determine possible splitting strategies. The main drawback of these methods is the lack of the PPSR planning stage. This disadvantage was attempted to be solved only by a few works. More specifically, an attempt to introduce PPSR constraints in a controlled islanding strategy has been made in [89]. The proposed methodology splits the power system across the weak areas of the network affected by a large disturbance, by opening the transmission lines with minimum power exchanges. In addition, it includes at least one blackstart unit within each island and ensures sufficient generation capability to match the load consumption within each island. However, data collection and information processing, essential for the assessment of the status of the formed islands (and thus for properly running the PPSR process), is not taken into account. This issue could be resolved by creating islands that are completely observable. On the other hand, the authors in [90] have developed a systematic algorithm for

sectionalizing a power system considering the PPSR constraints of blackstart capability, sufficient generation capacity and observability. However, the particular algorithm does not seek to find an islanding solution with minimal power flow disruption or minimal power imbalance that maintains the generator coherencies and other static and dynamic constraints. In other words, the algorithm sectionalizes the system focusing only on power system restoration and without solving the actual ICI problem. Hence, the stability of the formed islands is not guaranteed. On top of that, the concept of novel schemes that provide real-time solutions for both ICI and power system restoration is still an unexplored research area and a practical engineering challenge.

6.2 System Splitting Strategy Considering Power System Restoration

The exact MILP ICI algorithm proposed in Section 4.5 for solving effectively the ICI problem is extended here to consider power system restoration constraints. Assuming a completely observable power system at normal operating conditions, the extended ICI algorithm [87] creates islands that are also completely observable. Moreover, it includes at least one blackstart unit within each island and guarantees sufficient generation capacity to match the load consumption within each island. These new constraints can be viewed as a power system restoration planning stage.

6.2.1 Additional restoration constraints

In this Section, the concept of controlled islanding is combined with an approach of PPSR. This is achieved through the incorporation of the following additional restoration constraints to the MILP formulation of the aforementioned ICI algorithm:

A) Observability

Assuming that at normal operating conditions the system is completely observable by Phasor Measurement Units (PMUs), the additional observability constraint can be defined as,

$$\sum_{j \in \mathcal{V}} z_{i,j} r_j + r_i \geq 1, \quad i \in \mathcal{V}, \tag{6.1}$$

where r_i (i=1,…,n) are the elements of a binary vector defined as:

$$r_i = \begin{cases} 1, & \text{if there exists a PMU at bus } v_i \\ 0, & \text{otherwise.} \end{cases} \tag{6.2}$$

The above observability constraint ensures that each node bus v_i is observable either by at least one of its neighboring buses or by itself. This leads to the formation of islands that are also completely observable.

B) Blackstart (BS) availability

Assuming that sufficient BS units are available, this constraint includes at least one BS unit within each island. A BS unit is one that can start its own power without support from the grid in the event of a major system collapse or a system-wide blackout.

C) Sufficient generation capacity and unit commitment preservation

Consider the node sets $\mathcal{V}_k^{gen} = \{v_1, ..., v_{n_k^{gen}}\}$ and $\mathcal{V}_k^{load} = \{v_1, ..., v_{n_k^{load}}\}$ which denote the generator nodes and load nodes in each island $\mathcal{G}_k$ respectively, where n_k^{gen} denotes the number of generators and n_k^{load} the number of loads in island $\mathcal{G}_k$. Furthermore, consider a mapping function $F_{gen_k} : \{1, ..., n\} \to \{1, ..., n_k^{gen}\}$ for the generator nodes and its inverse function $F_{gen_k}^{-1} : \{1, ..., n_k^{gen}\} \to \{1, ..., n\}$ satisfying:

$$F_{gen_k}(i) = \left\{ j : v_j = v_i, i \in \{1, ..., n\},\ j \in \{1, ..., n_k^{gen}\} \right\}, \tag{6.3}$$

$$F_{gen_k}^{-1}(j) = \left\{ i : v_i = v_j, i \in \{1, ..., n\},\ j \in \{1, ..., n_k^{gen}\} \right\}. \tag{6.4}$$

Note that a similar mapping function is considered for the load nodes. The additional constraint of sufficient generation capacity and unit commitment preservation is as follows:

$$\sum_{i \in \{1, ..., n_k^{gen}\}} Pgen_{i,k}^{\max} \geq \sum_{i \in \{1, ..., n_k^{load}\}} Pload_{i,k}, \quad k \in \mathcal{K} \tag{6.5}$$

$$\sum_{i \in \{1, ..., n_k^{gen}\}} Pgen_{i,k}^{\min} \leq \sum_{i \in \{1, ..., n_k^{load}\}} Pload_{i,k}, \quad k \in \mathcal{K}, \tag{6.6}$$

where $Pgen_{i,k}$ and $Pload_{i,k}$ are the generation and load consumption in bus *i* of island *k* respectively. Assuming that the generators are able to operate at full rated power, (6.5) guarantees sufficient generation capacity to match the load consumption within each island. At the same time, (6.6) avoids the unnecessary shut down of generators just to achieve the load-generation balance. Hence, both the cost of disconnecting a generator from the system and the time delay of reconnecting it afterwards are negated.

6.2.2 Simulation results

To demonstrate the effectiveness of the extended MILP ICI algorithm, the IEEE 39- and 118-bus test systems were used. The dynamic data of the generators and the details of the controllers (i.e., AVR and governors) can be found in [27]. The algorithm was aimed to be used following the determination of the necessity to split the power system. Moreover, it was assumed that an optimal placement of Phasor Measurement Units (PMUs) has been previously performed for complete observability of these test systems at normal operating conditions. All times quoted are based upon simulations performed in Matlab (a PC with 3.10 GHz dual core CPU and 4 GB RAM).

A) IEEE 39-bus test system

The single-line diagram of the IEEE 39-bus test system along with the installed PMUs at the optimal locations is presented in Figure 6.1. The optimal PMU locations are also shown in Table 6.1 [91]. This study considers generators 30, 32, 34 and 39 as BS units.

Test case description: At time t = 1 s, the value of loads at buses 3, 4, 7, and 8 is increased by 10% (total step change of 157.78 MW). As a result, a transient instability is created into the

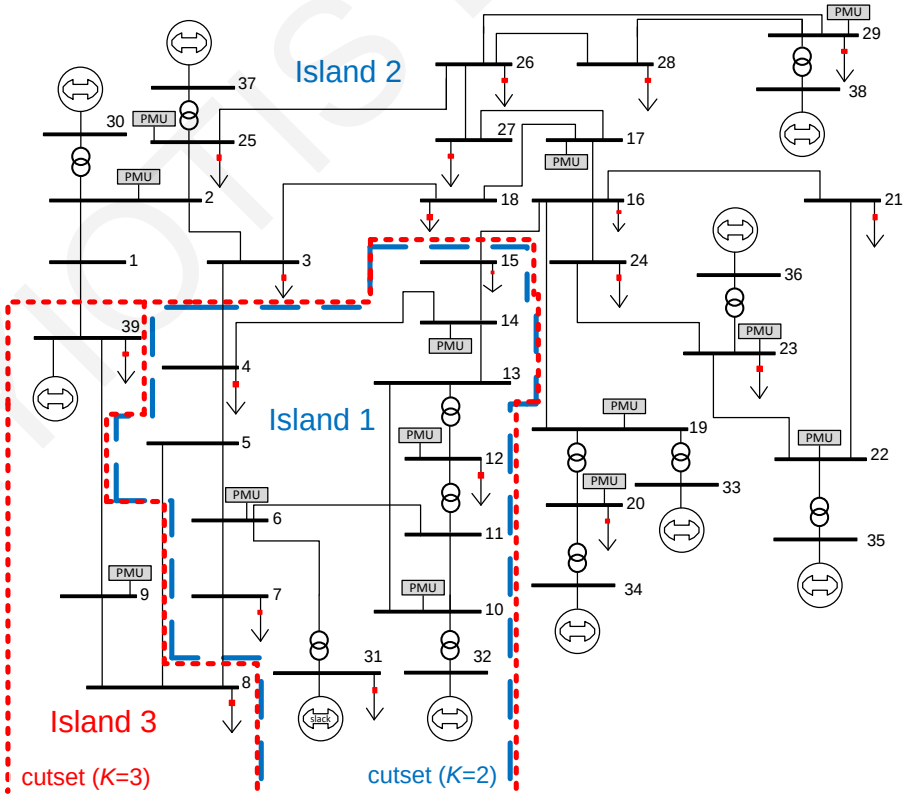

Figure 6.1: Single-line diagram of IEEE 39-bus test system with optimal islanding solution for K=2 and K=3

Table 6.1: Optimal PMU placement for the IEEE 39-bus test system

	Optimal PMU locations	***Optimal Number***
Normal operating conditions	2, 6, 9, 10, 12, 14, 17, 19, 20, 22, 23, 25, 29	13

Table 6.2: Exact islanding solutions for the IEEE 39-bus test system

No. of Islands (K)	***Cutset***	***Cut (MW)***	***Time (s)***
2	3-4, 5-8, 7-8, 15-16	998.55	0.047
3	3-4, 5-8, 7-8, 15-16, 1-39	1126.46	0.046

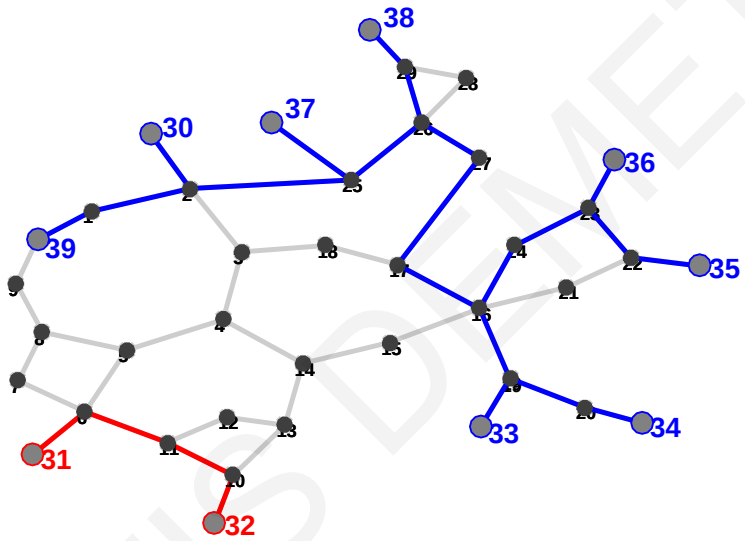

Figure 6.2: Preprossesing procedure on IEEE 39-bus test system for *K*=2

system. It is noted that this is the same event as in Case study 2 of Section 4.5.4. For this particular event, for the case of two islands (*K*=2), the coherent generator groups are {G31, G32} and {G30, G33, G34, G35, G36, G37, G38, G39} (based on a two-step methodology proposed in [47] for real-time identification of coherent generator groups). The necessity to split the system is considered to be at 2 s. Hence, considering the power flow and actual topology of the system at t = 2 s, the proposed extended ICI algorithm is used to find the optimal islanding solution. As mentioned in Section 4.5.3, the preprocessing procedure finds first the trees which connect all the generators of each coherent group with the minimum number of nodes (Figure 6.2). The nodes of these trees are then served as an additional constraint to the MILP formulation. The implementation of the proposed ICI algorithm identifies the optimal solution (minimal power-flow disruption) across the lines 3-4, 5-8, 7-8 and 15-16 (blue dashed line in Figure 6.1). The solution was found in approximately 0.047 s (Table 6.2). Hence, islanding was undertaken at t = 2.047 s. The load and generation in each

Table 6.3: Load and generation within each island for the IEEE 39-bus test system split into two islands (K=2)

Island number	*ΣPload (MW)*	*ΣPgen (MW)*	*Generation capacity (MW)*	*Available BS units*	*Observable?*
1	1143.9	1169.9	1670	32	YES
2	5111	4970	6676	30, 34, 39	YES

Table 6.4: Load and generation within each island for the IEEE 39-bus test system split into two islands (K=3)

Island number	*ΣPload (MW)*	*ΣPgen (MW)*	*Generation capacity (MW)*	*Available BS units*	*Observable?*
1	1143.9	1169.9	1670	32	YES
2	3432.8	3970	5676	30, 34	YES
3	1678.2	1000	1700	39	YES

island, as well as the generation capacity, BS availability and observability status of each island are presented in Table 6.3. As it can be noticed, at least one BS unit and sufficient generation capacity to match the load consumption are available in each island. Moreover, it is important to understand that the proposed ICI algorithm has ensured the creation of completely observable islands whose status can be assessed during the post-islanding stage.

For K=3, the coherent generator groups obtained are {G39}, {G31, G32} and {G30, G33, G34, G35, G36, G37, G38} [47]. Figure 6.3 shows the trees found by the preprocessing procedure. The islanding solution determined by the execution of the proposed extended ICI algorithm is marked in Figure 6.1 (red dotted line) and summarized in Table 6.2. This solution was obtained in approximately 0.046 s and thus the corresponding corrective control strategy was undertaken at t = 2.046 s. Table 6.4 presents the PPSR constraints included in the strategy. As it can be noticed, all the formed islands are completely observable and there is at least one BS unit and sufficient generation capacity in each of them.

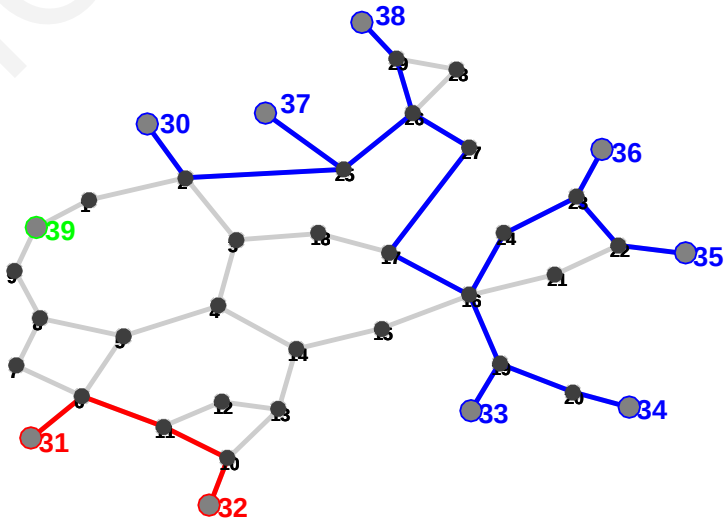

Figure 6.3: Preprossesing procedure on IEEE 39-bus test system for K=3

B) IEEE 118-bus test system

The second test system used to demonstrate the efficiency of the proposed extended ICI algorithm was the IEEE 118-bus test system. The topology of the system is shown in Figure 6.4. The optimal PMU locations for this test system are shown in Table 6.5 [92]. This study considered generators 25, 69, 87 and 89 as BS units.

The coherent groups of generators of the IEEE 118-bus test system were obtained by using the coherency algorithm [78] and by changing the number of coherent generator groups from two groups up to the number of available BS units (Table 6.6). The trees found by the preprocessing procedure for each case are the same as in Figure 4.23 - Figure 4.25 of Section 4.5.4. As mentioned above, the nodes of these trees will be served as an additional constraint to the MILP formulation which will contribute to the reduction of its search space. Figure 6.4 illustrates the islanding solutions determined by the execution of the proposed extended ICI algorithm for all the possible number of coherent groups. The information about the splitting strategies found, the values of the cuts and the execution times are presented in Table 6.7. Table 6.8 - Table 6.10 present the PPSR constraints included in the strategy for K=2,

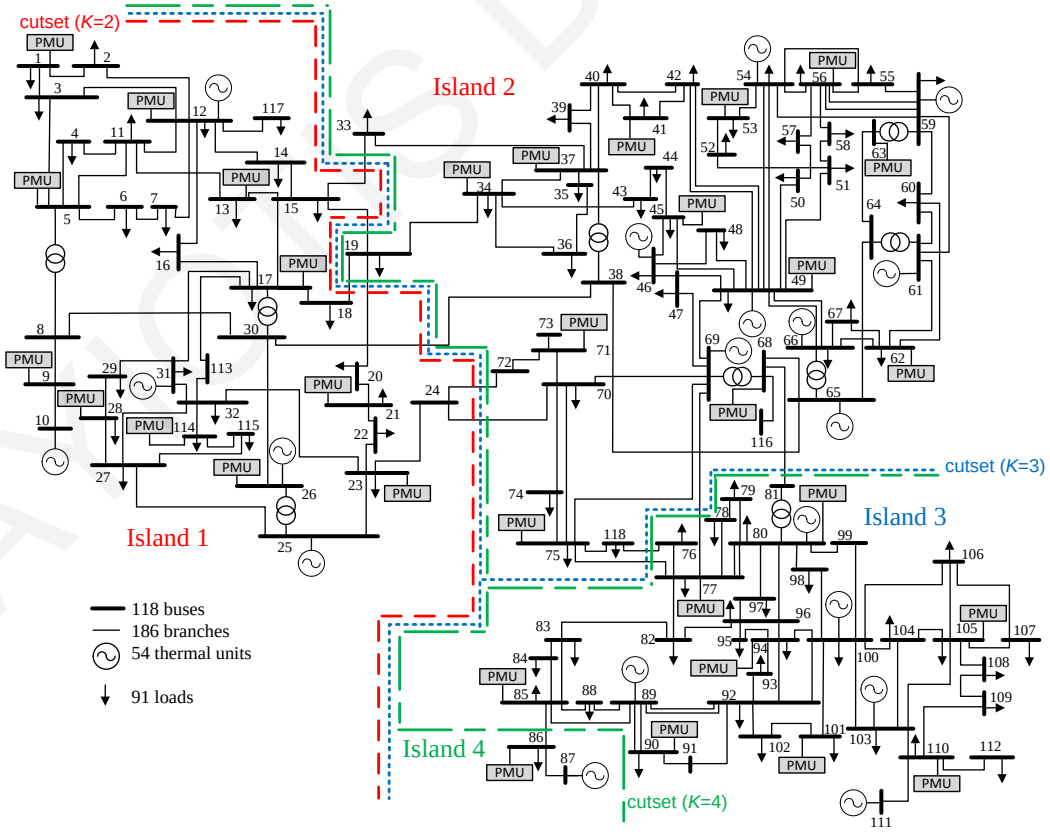

Figure 6.4: Single-line diagram of IEEE 118-bus test system with optimal islanding solution for K=2, K=3 and K=4

Table 6.5: Optimal PMU placement for the IEEE 118-bus test system

	Optimal PMU locations	***Optimal Number***
Normal operating conditions	1, 5, 9, 12, 13, 17, 21, 23, 26, 28, 34, 37, 41, 45, 49, 53, 56, 62, 63, 68, 71, 75, 77, 80, 85, 86, 90, 94, 101, 105, 110, 114	32

Table 6.6: Coherent generator groups for the IEEE 118-bus test

No. of Islands (k)	***Coherent Generator Groups***
2	{10, 12, 25, 26, 31}, {46, 49, 54, 61, 65, 66, 69, 80, 87, 89, 100, 103, 111}
3	{10, 12, 25, 26, 31}, {46, 49, 54, 59, 61, 65, 66, 69}, { 80, 87, 89, 100, 103, 111 }
4	{10, 12, 25, 26, 31}, {46, 49, 54, 59, 61, 65, 66, 69}, { 80, 89, 100, 103, 111 }, {87}

Table 6.7: Exact islanding solution for the IEEE 118-bus test system

No. of Islands (k)	***Cutset***	***Cut (MW)***	***Time (s)***
2	15-19, 15-33, 18-19, 19-20, 24-70, 24-72, 30-38	118.785	0.143
3	15-19, 15-33, 18-19, 19-20, 24-70, 24-72, 30-38, 68-81, 69-77, 75-77, 76-118	267.136	0.192
4	15-19, 15-33, 18-19, 19-20, 24-70, 24-72, 30-38, 68-81, 69-77, 75-77, 76-118, 85-86	284.310	0.235

K=3, and *K*=4 respectively. As it can be noticed, the proposed ICI algorithm has ensured the creation of completely observable islands for each case. In addition, at least one BS unit and sufficient generation capacity to match the load consumption are available in each island. As these constraints have been included in the proposed algorithm, PPSR is planned in case of a local blackout in any island.

Table 6.8: Load and generation within each island for the IEEE 118-bus test system split into two islands (*K*=2)

Island number	***ΣPload (MW)***	***ΣPgen (MW)***	***Generation capacity (MW)***	***Available BS units***	***Observable?***
1	1076	931	1530	25	YES
2	3300.1	3311	4615	69, 87, 89	YES

Table 6.9: Load and generation within each island for the IEEE 118-bus test system split into two islands (*K*=3)

Island number	***ΣPload (MW)***	***ΣPgen (MW)***	***Generation capacity (MW)***	***Available BS units***	***Observable?***
1	931	1076	1530	25	YES
2	1947	1884.1	2585	69	YES
3	1364	1416	2030	87, 89	YES

Table 6.10: Load and generation within each island for the IEEE 118-bus test system split into two islands (K=4)

Island number	*ΣPload (MW)*	*ΣPgen (MW)*	*Generation capacity (MW)*	*Available BS units*	*Observable?*
1	931	1076	1530	25	YES
2	1947	1884.1	2585	69	YES
3	1343	1412	1955	89	YES
4	21	4	75	87	YES

6.3 A Real-Time Controlled Islanding & Restoration Scheme Based on Estimated States

The advent of the Synchronized Measurement Technology offers great flexibility to power system operators in several control and monitoring applications. The process of the PMU measurements (i.e., synchronized voltage and current phasors, frequency, and rate of change of frequency) can provide to the power system operators a real-time wide area visualization of the system operating condition. For instance, the installation of PMUs in an optimal way for rendering the power system fully observable by PMUs makes feasible the operation of a real-time state estimator that is based only on PMU measurements. Such a state estimator can estimate in real time (as the PMU measurements arrive to the control center) the states of the system (i.e., voltage magnitude and angle of the buses) and can track effectively power system transients [93]. Although the complete observability of the system by only PMUs is not a realistic case today, the trend of the electric utilities to install PMUs shows that such a case will be realistic in the near future. For instance, a recent report by the US DOE indicates that the PMUs in North America have increased from 166 in 2009 to 1700 in 2015 [94].

Crucially, in this Section a real-time state estimator serves as the connection point between the controlled islanding and the power system restoration. In particular, this Section presents a real-time ICI and restoration scheme that consists of a sophisticated intentional controlled islanding algorithm, i.e., the extended MILP ICI algorithm of Section 6.2, a real-time state estimator, and a power system restoration process [95]. The main assumption in the work is that the power system is observable by PMUs before the system splitting. In this sense, during the pre-islanding and the post-islanding stage, the state estimator provides the power system operating condition to the operators. This requires that all the formed islands are still observable by PMUs in the post-islanding stage; such condition is ensured by the ICI algorithm that is used in this work. This allows the reconnection of the islands in quasi real time, as soon as their synchronizing conditions are met, without the presence of any

synchroscopes and crew in the substations. The proposed ICI and restoration scheme is tested and evaluated using the dynamic models of the IEEE 39- and 118-bus test systems.

6.3.1 Real-time state estimator

The state estimator constitutes the cornerstone of the power system control center since it provides the operating condition of the system in consecutive time intervals. The states of the system (i.e. voltage magnitude and angle of the buses) are estimated by processing redundant measurements of the system. The contemporary state estimation scheme uses conventional measurements (i.e., real/reactive power flows and injections, and voltage magnitudes) and is intended for providing the steady state operating condition. This is because the reporting rate of the conventional measurements is slow (i.e., 5 to 30 s) and the measurements are reported in an asynchronous way. In this sense, the conventional state estimator cannot be used for tracking the transients of the system in case of a disturbance.

With the advent of the Synchronized Measurement Technology and the installation of PMUs in the power system measurement layer, the concept of a real-time state estimator is feasible. The execution of a real-time state estimator implies a PMU observable system; therefore, the real-time state estimator is solely based on PMU measurements and is able to track the transients in case of fault [93]. The linear state estimator in this work is formulated in a Weighted Least Squares (WLS) framework and processes the real and imaginary parts of the current and voltage phasor measurements provided by the PMU. Therefore, the measurement model is formulated as,

$$\mathbf{z} = \mathbf{H}\mathbf{x} + \mathbf{e} = \begin{bmatrix} \mathbf{V}_r^{meas} \\ \mathbf{V}_i^{meas} \\ \mathbf{I}_r^{meas} \\ \mathbf{I}_i^{meas} \end{bmatrix} = \begin{bmatrix} \partial\mathbf{V}_r/\partial\mathbf{V}_r & \partial\mathbf{V}_r/\partial\mathbf{V}_i \\ \partial\mathbf{V}_i/\partial\mathbf{V}_r & \partial\mathbf{V}_i/\partial\mathbf{V}_i \\ \partial\mathbf{I}_r/\partial\mathbf{V}_r & \partial\mathbf{I}_r/\partial\mathbf{V}_i \\ \partial\mathbf{I}_i/\partial\mathbf{V}_r & \partial\mathbf{I}_i/\partial\mathbf{V}_i \end{bmatrix} \begin{bmatrix} \mathbf{V}_r \\ \mathbf{V}_i \end{bmatrix} + \mathbf{e}, \tag{6.7}$$

where **z** is the measurement vector, **H** is Jacobian that relates the measurements to the system states, **x** is the state vector containing the power system states, **e** is the Gaussian noise in the measurements, and $\mathbf{V_r}$, $\mathbf{V_i}$, $\mathbf{I_r}$, $\mathbf{I_i}$ are the real and imaginary parts of the bus voltage phasors and the line current phasors, respectively, when they are expressed in rectangular form.

It should be noted that the real and imaginary parts of the current phasor measurements are expressed in relation to the states of the system. Therefore, assuming a line represented by a pi model that connects bus *i* and bus *j*, the real and imaginary parts of the current phasor

measurements are expressed as,

$$I_{real}^{meas} = V_i \cos\theta_i (g_{si} + g_{ij}) - V_i \sin\theta_i (b_{si} + b_{ij}) + b_{ij} V_j \sin\theta_j - g_{ij} V_j \cos\theta_j \quad (6.8)$$

$$I_{imag}^{meas} = V_i \cos\theta_i (b_{si} + b_{ij}) + V_i \sin\theta_i (g_{si} + g_{ij}) - b_{ij} V_j \cos\theta_j - g_{ij} V_j \sin\theta_j \ , \quad (6.9)$$

where V_i, V_j, θ_i, and θ_j are the voltage magnitudes and angles of bus i and bus j respectively, and $g_{ij} + jb_{ij}$, $g_{si} + jb_{si}$ are the series and shunt admittances respectively of the transmission line connecting buses i and j.

Based on the WLS formulation the state vector **x** can be obtained by minimizing the function $J(\mathbf{x})$,

$$Min\ J(\mathbf{x}) = [\mathbf{z} - \mathbf{H}\mathbf{x}]^T \mathbf{R}^{-1} [\mathbf{z} - \mathbf{H}\mathbf{x}], \quad (6.10)$$

where **R** is the measurement error covariance matrix and its elements are used as weights of the measurements. By minimizing the objective function in (6.10) the state vector **x** can be estimated as,

$$\hat{\mathbf{x}} = (\mathbf{H}^T \mathbf{R}^{-1} \mathbf{H})^{-1} \mathbf{H}^T \mathbf{R}^{-1} \mathbf{z} . \quad (6.11)$$

It is worth mentioning that based on (6.11) no iteration procedure is needed for estimating the states of the system and therefore the linear state estimator can be executed as new PMU measurements arrive to the control center.

6.3.2 Proposed ICI – restoration scheme

Figure 6.5 illustrates the general concept of the proposed ICI and restoration scheme based on estimated states. In general, the main steps for executing the scheme are:

Step 1: Following the determination of the necessity to split the power system, use the extended MILP ICI algorithm (of Section 6.2) to find the optimal islanding solution.

Step 2: After system splitting, perform a linear state estimation at the control center.

Step 3: Use the estimated states to assess the status of the islands' boundary buses and their synchronization.

Step 4: If there are any islands that are in synchronism, reclose the CBs of their boundaries to reconnect them. Otherwise, apply additional corrective measures while assessing the boundary status through state estimation until the synchronizing conditions of some islands are met.

Step 5: Reconnect the synchronized islands.

Step 6: Repeat Steps 4-5 until all the islands are reconnected and the system is restored.

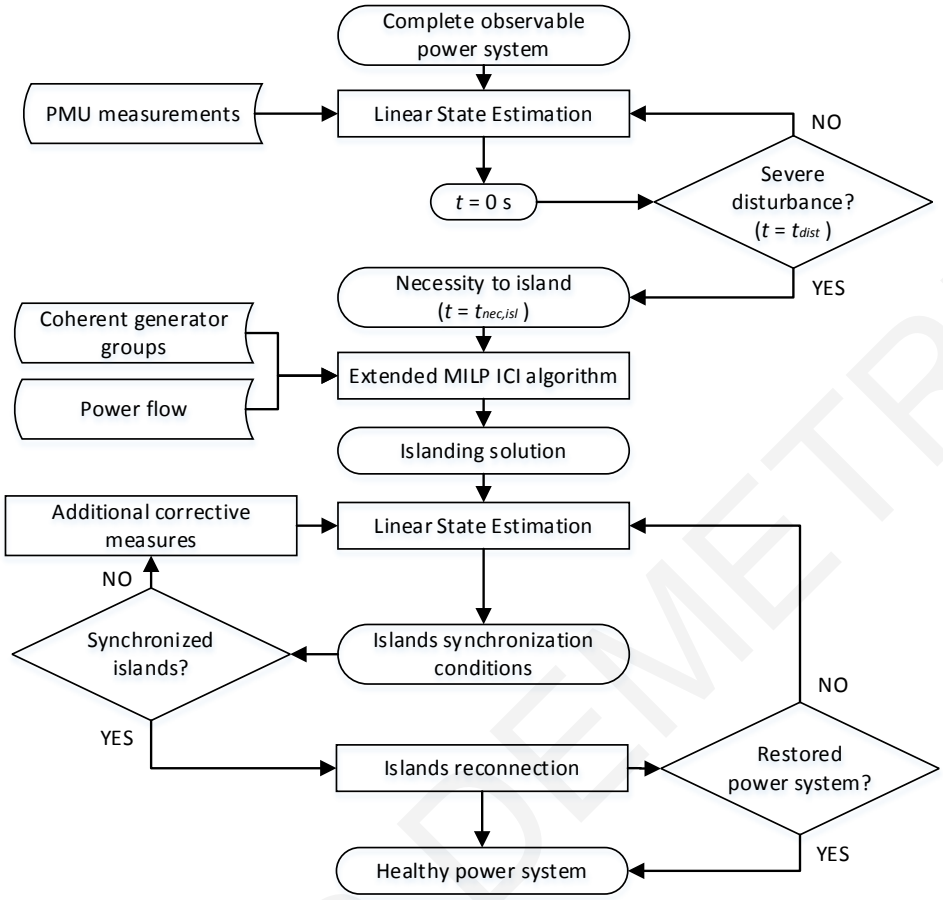

Figure 6.5: Flowchart diagram of the proposed real-time controlled islanding and restoration scheme based on estimated states

6.3.3 Simulation results

The proposed real-time controlled islanding and restoration scheme was tested using the IEEE 39- and 118-bus test systems. The dynamic data of the generators and the details of the controllers (i.e., AVR and governors) can be found in [27]. Moreover, it was assumed that an optimal placement of Phasor Measurement Units (PMUs) has been previously performed for complete observability of these test systems at steady state conditions. This allows the execution of a linear state estimation directly from the control center. All times quoted are based upon simulations performed in Matlab (a PC with 3.10 GHz dual core CPU and 4 GB RAM).

A) IEEE 39-bus test system

The single-line diagram of the IEEE 39-bus test system along with the installed PMUs at the optimal locations are presented in Figure 6.6. The optimal PMU locations are also shown in Table 6.11 [91]. This study considers generators 30, 32, 34 and 39 as BS units.

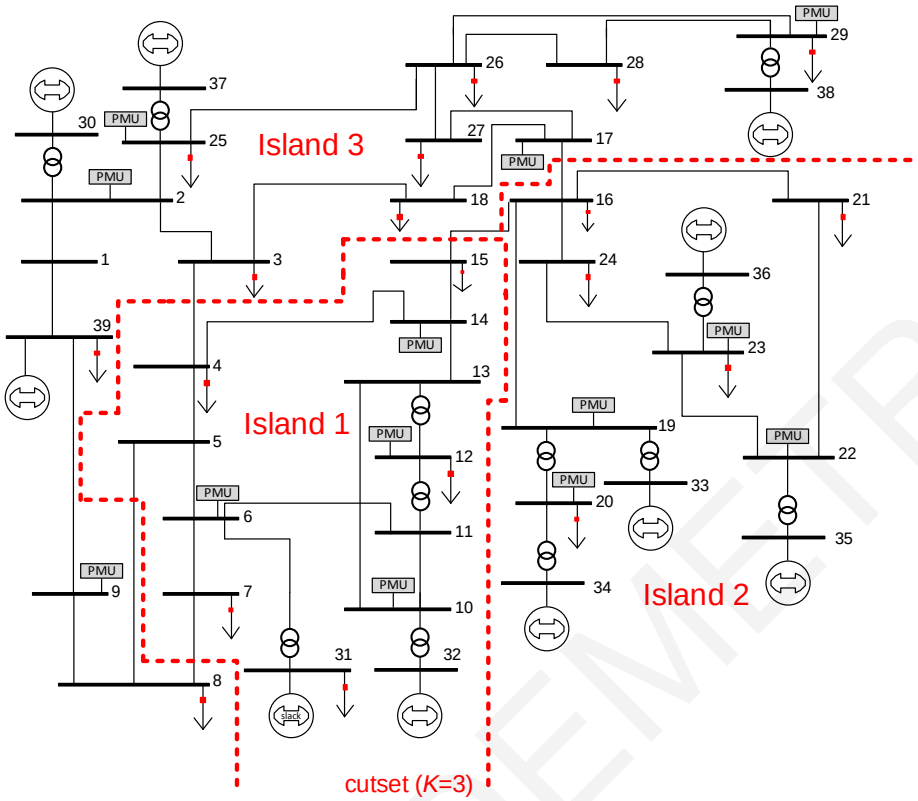

Figure 6.6: Single-line diagram of IEEE 39-bus test system with optimal islanding solution

Test case description: At time t = 1 s, a three phase to ground fault occurs at bus 2 and is cleared 0.65 s later, at t = 1.65 s. The swing trajectories obtained are shown in Figure 6.7. It can be observed that within a short time after the fault is cleared, the generators are divided into three groups: {G31, G32}, {G33, G34, G35, G36}, and {G30, G37, G38, G39}. Although these groups can be created through visualization of the generator rotor angle trends, algorithms to automatically identify coherent groups of generators (e.g., [43], [47]) must be adopted in large-scale systems to ensure adequate generator grouping, and to further improve the islanding-restoration scheme proposed here. Moreover, as it can be observed in Figure 6.7, if the system is not split into three islands, the frequency of the generators considerably increases and the terminal voltages of the generators significantly reduce. Thus, this disturbance will result to a blackout quickly after the fault is cleared. In this case, the necessity to split the system is considered to be at 1.7 s. Hence, considering the power flow and actual topology of the system at t = 1.7 s, the proposed ICI and restoration scheme is used to find the optimal islanding solution.

The scheme identifies the optimal solution (for minimal power-flow disruption) to open the lines 3-4, 5-8, 7-8, 15-16 and 16-17 (red dotted line in Fig. 2). The solution was found in

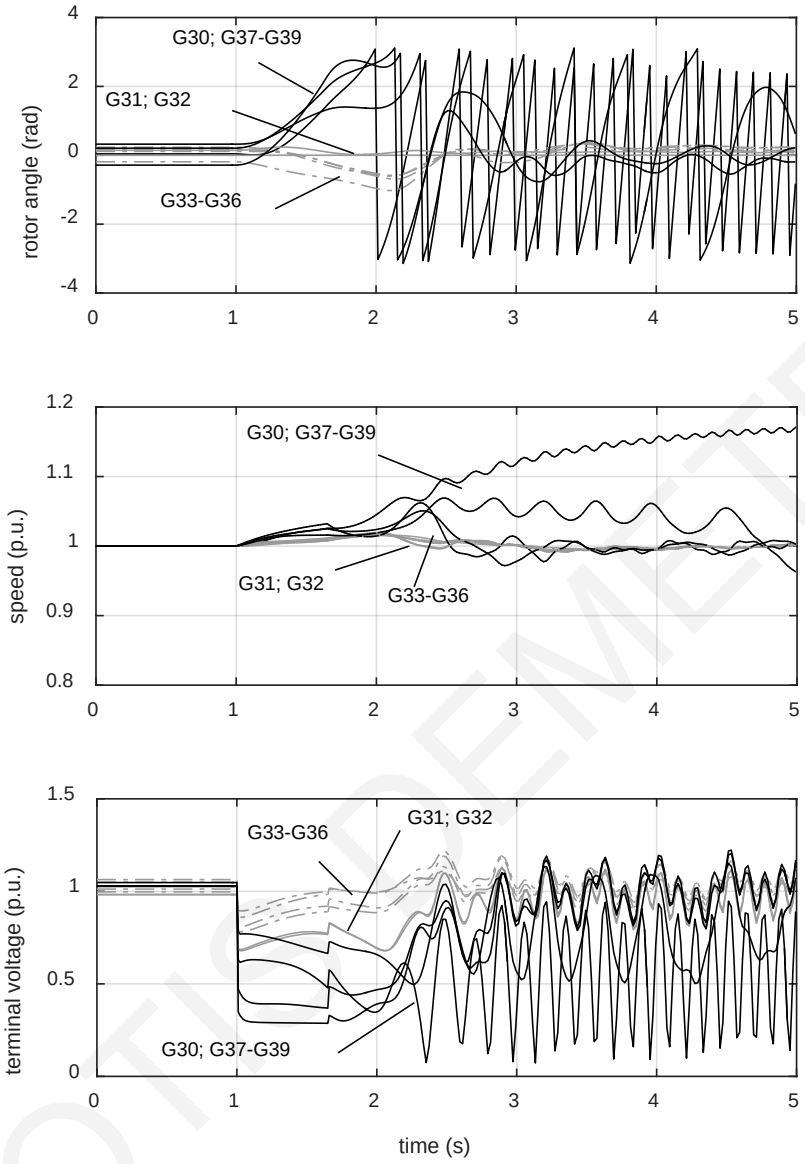

Figure 6.7: IEEE 39-bus test system - Electrical behavior without islanding

Table 6.11: Optimal PMU placement for the IEEE 39-bus test system

	Optimal PMU locations	***Optimal Number***
Normal operating conditions	2, 6, 9, 10, 12, 14, 17, 19, 20, 22, 23, 25, 29	13

Table 6.12: Exact islanding solutions for the IEEE 39-bus test system

No. of Islands (K)	***Cutset***	***Cut (MW)***	***Time (s)***
3	3-4, 5-8, 7-8, 15-16, 16-17	1027.21	0.021

approximately 0.021 s (Table 6.12). Hence, islanding was undertaken at t = 1.721 s. Figure 6.8 shows the dynamic trajectories after implementing the solution. As noticed, three stable

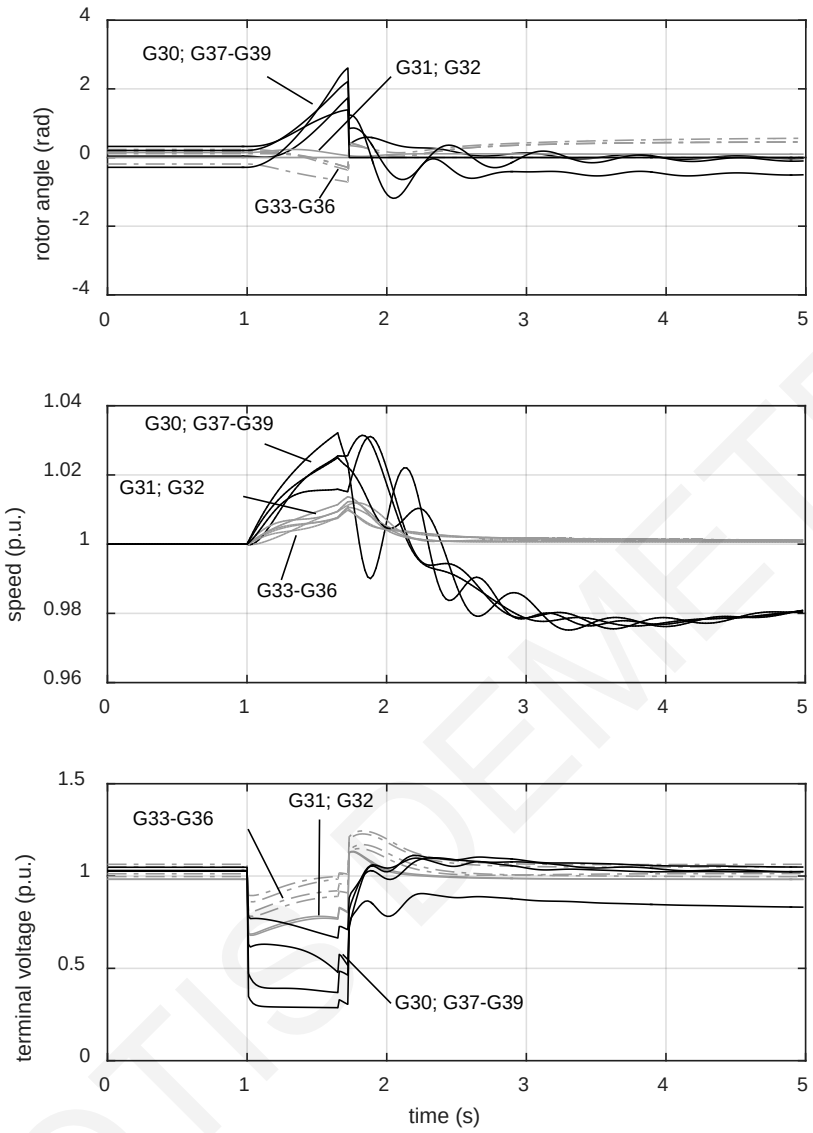

Figure 6.8: IEEE 39-bus test system - Electrical behavior with islanding

groups are created. Moreover, the frequencies of Island 1, Island 2, and Island 3 are 1.001 p.u., 1.001 p.u., and 0.981 p.u. respectively (Figure 6.8). Voltages also reach values close to nominal values (Figure 6.8). Since the splitting strategy successfully retains the frequency of the islands within acceptable limits and the corresponding voltages within the thresholds, it can be concluded that the use of the proposed ICI and restoration scheme to split the power system in a controlled manner can prevent the blackout.

The load and generation in each island, as well as the generation capacity, BS availability and observability status of each island (i.e., the PPSR constraints included in the splitting strategy) are presented in Table 6.13. As it can be noticed, at least one BS unit and sufficient generation capacity to match the load consumption are available in each island. In addition, it is important to understand that the proposed ICI scheme has ensured the creation of

Table 6.13: Load and generation within each island for the IEEE 39-bus test system split into two islands (K=3)

Island number	***ΣPload (MW)***	***ΣPgen (MW)***	***Generation capacity (MW)***	***Available BS units***	***Observable?***
1	1143.88	1169.9	1670	32	YES
2	1787.1	2350	3340	34	YES
3	3323.9	2620	4036	30, 39	YES

Table 6.14: Corrective measures for island synchronization of the IEEE 39-bus test system

Time (s)	***Corrective measure***
11	Reclose CB of transmission line 16-17
40	30% load shedding of load 8
40	30% load shedding of load 39
97	Reclose CB of transmission line 5-8
97	Reclose CB of transmission line 7-8
115	Change tap position of transformer 25-37 from 1 to -4
115	Change tap position of transformer 2-30 from 1 to -4
130	Reclose CB of transmission line 3-4
150	Change tap position of transformer 10-32 from 2 to 5
150	Change tap position of transformer 23-36 from 0 to -5
170	Reclose CB of transmission line 15-16

completely observable islands, and therefore, the continuous execution of the linear state estimation at the control center. In other words, the scheme has enabled the system operator to assess both the status of the islands' boundary buses during the post-islanding stage and their resynchronization using estimated system states.

In this sense, the voltage magnitude and angle difference of boundary buses based on the estimated states available at the control center are shown in Figure 6.9. Figure 6.10 further illustrates the frequency difference of the islands. It is noted that the frequency of each island is available by the PMUs exist in each island. Based on Figure 6.9 - Figure 6.10, few seconds after the system separation, none of the boundaries satisfies all three conditions for island synchronization. Therefore, additional corrective measures (e.g., generation rescheduling, load shedding and transformer tap change) are needed to achieve island synchronization and thus to complete system restoration. In this case, the corrective measures required to resynchronize the islands are summarized in Table 6.14. The synchronizing status of the islands' boundary buses during the application of these corrective measures is shown in Figure 6.9 - Figure 6.10. As it can be noticed, Island 2 and Island 3 are synchronized approximately 9 seconds after the

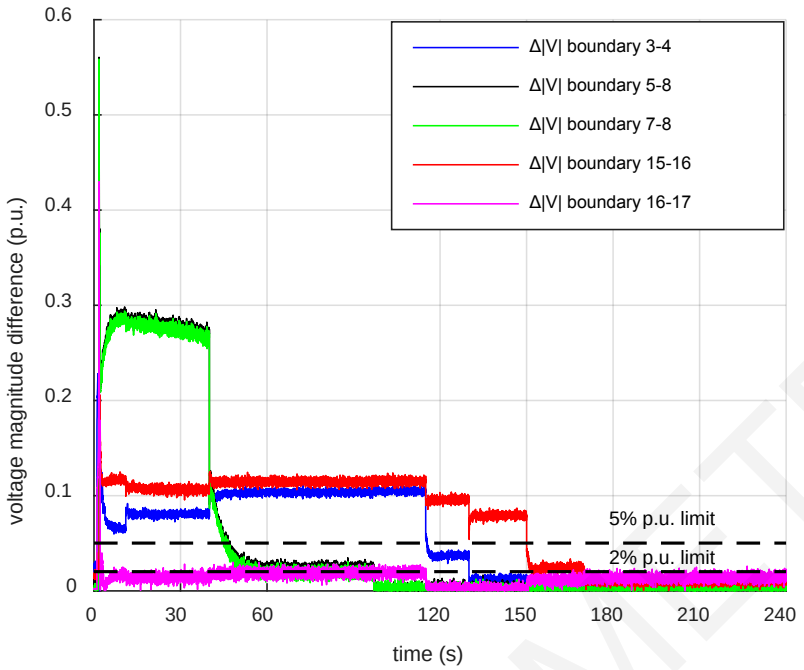

(a)

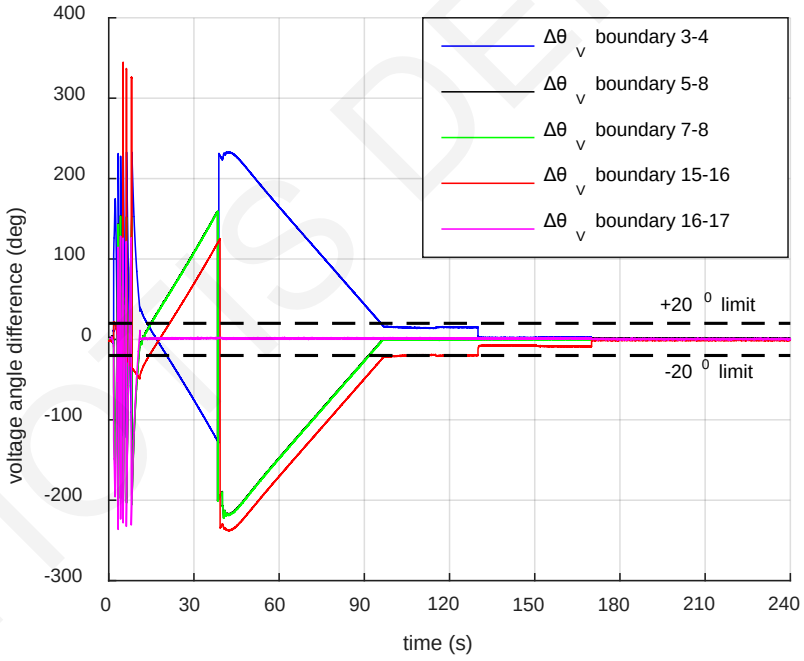

(b)

Figure 6.9: IEEE 39-bus test system: (a) Voltage magnitude and (b) Angle difference of islands boundary buses during their resynchronization

splitting strategy is carried out and are reconnected at time t = 11 s by reclosing the CB of transmission line 16-17. The restoration of the whole power system is completed at time t = 170 s. Note that the loads that were shed (Table 6.14) can be reconnected hereafter. At this point, it is important to clarify that the corrective measures applied may vary based on the experience and knowledge of the system operator.

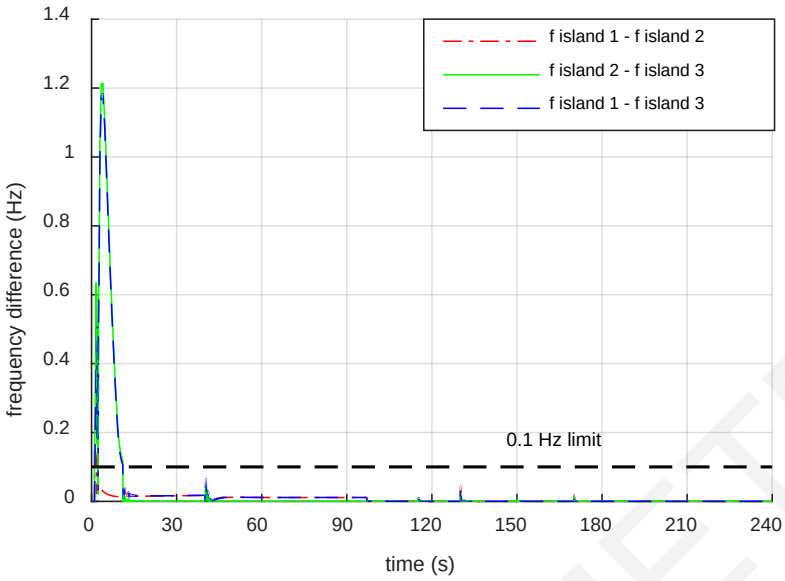

Figure 6.10: IEEE 39-bus test system: Islands frequency difference during their resynchronization

B) IEEE 118-bus test system

The topology of the IEEE 118-bus test system is shown in Figure 6.11. The optimal PMU locations for this system are also shown in Figure 6.11 and summarized in Table 6.15 [92].

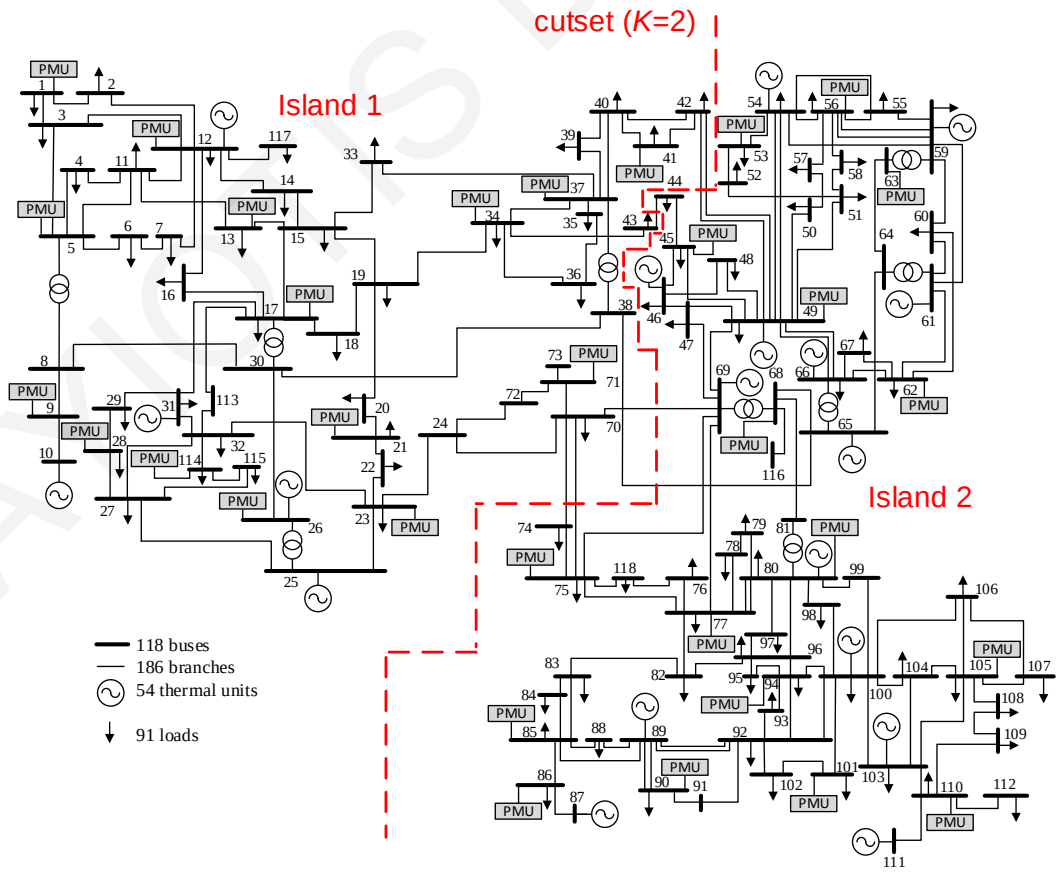

Figure 6.11: Single-line diagram of IEEE 118-bus test system with optimal islanding solution

Table 6.15: Optimal PMU placement for the IEEE 118-bus test system

	Optimal PMU locations	***Optimal Number***
Normal operating conditions	1, 5, 9, 12, 13, 17, 21, 23, 26, 28, 34, 37, 41, 45, 49, 53, 56, 62, 63, 68, 71, 75, 77, 80, 85, 86, 90, 94, 101, 105, 110, 114	32

Table 6.16: Exact islanding solution for the IEEE 118-bus test system

No. of Islands (k)	***Cutset***	***Cut (MW)***	***Time (s)***
2	38-65, 42-49, 43-44, 69-70, 70-74, 70-75	511.675	0.09

Table 6.17: Load and generation within each island for the IEEE 118-bus test system split into two islands (K=2)

Island number	***ΣPload (MW)***	***ΣPgen (MW)***	***Generation capacity (MW)***	***Available BS units***	***Observable?***
1	1450	1076	1530	25	YES
2	2792	3300.1	4615	69, 87, 89	YES

Table 6.18: Corrective measures for island synchronization of the IEEE 118-bus test system

Time (s)	***Corrective measure***
30	Shed loads 13, 14, and 15
33	Shed loads 16, and 18
35	Shed load 19
38	Reclose CB of transmission line 43-44
38	Reclose CB of transmission line 70-74
38	Reclose CB of transmission line 70-75
50	Change step of shunt controller from 1 to 5
55	Change tap position of transformer 37-38 from 1 to -1
70	Reclose CB of transmission line 38-65
90	Shed load 70
100	Reclose CB of transmission line 69-70
125	Shed loads 41, and 42
135	Reclose CB of transmission line 42-49

This study considers generators 25, 69, 87 and 89 as BS units.

Test case description: At t = 1 s, a three phase to ground fault occurs at bus 30 and is cleared 1 s later, at t = 2 s. The generator rotor angles without islanding are shown in Figure 6.12. Shortly after the fault, a group of 5 generators swing together and the rest ones swing apart. Two groups are created: {G10, G12, G25, G26, G31} and {G46, G49, G54, G59, G61, G65, G66, G69, G80, G87, G89, G100, G103, G111}. In terms of the generators' speed,

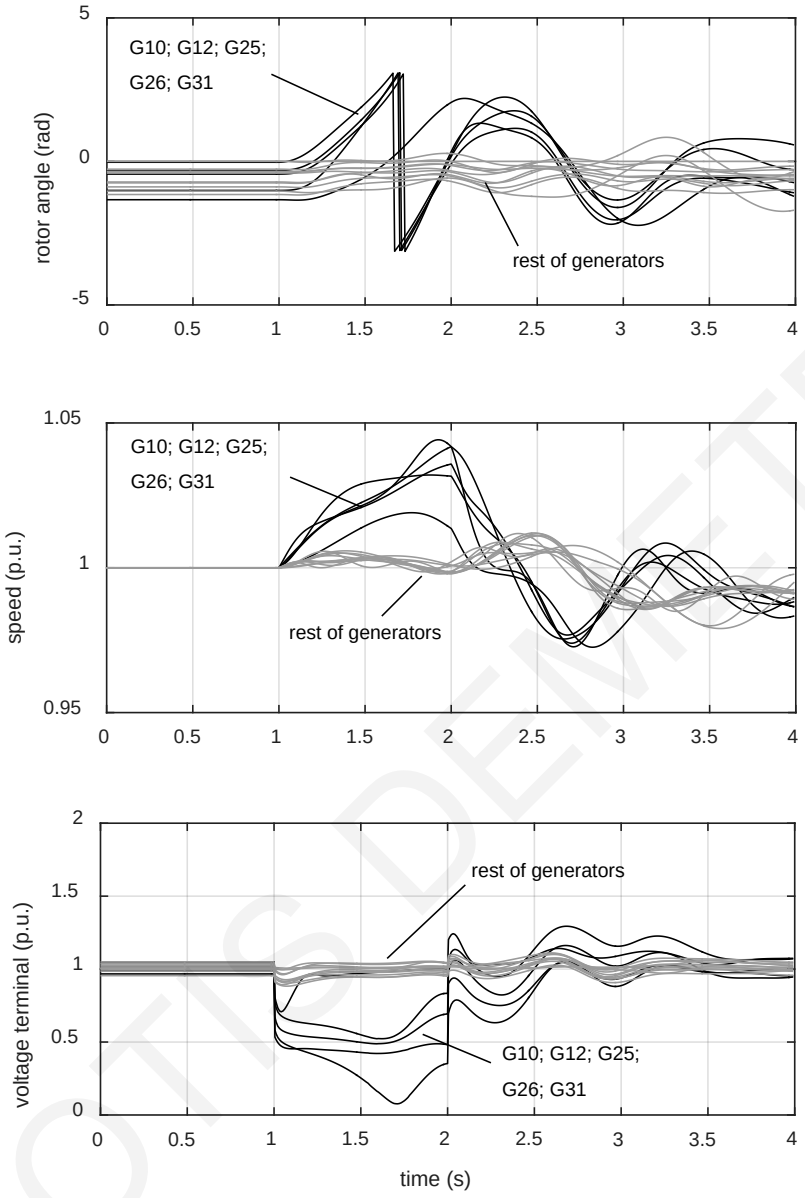

Figure 6.12: IEEE 118-bus test system - Electrical behavior without islanding

Figure 6.12 shows that they increase. Figure 6.12 finally highlights that the generator terminal voltages are significantly low. Thus, it can be concluded that the system needs to be split, if the blackout is to be avoided. Here, the necessity to split the system is considered to 2.1 s. Hence, considering the power flow and actual topology of the system at t = 2.1 s, the proposed ICI and restoration scheme is used to find the optimal islanding solution (Figure 6.11). The information about the splitting strategy found, the value of the cut and the execution time are presented in Table 6.16. The post-islanding behavior of the islands is shown in Figure 6.13. As it can be obtained, two stable groups are created. Figure 6.13 further shows that the generator speeds (0.965 p.u. and 1.002 p.u. respectively) are within the limits and the generator terminal

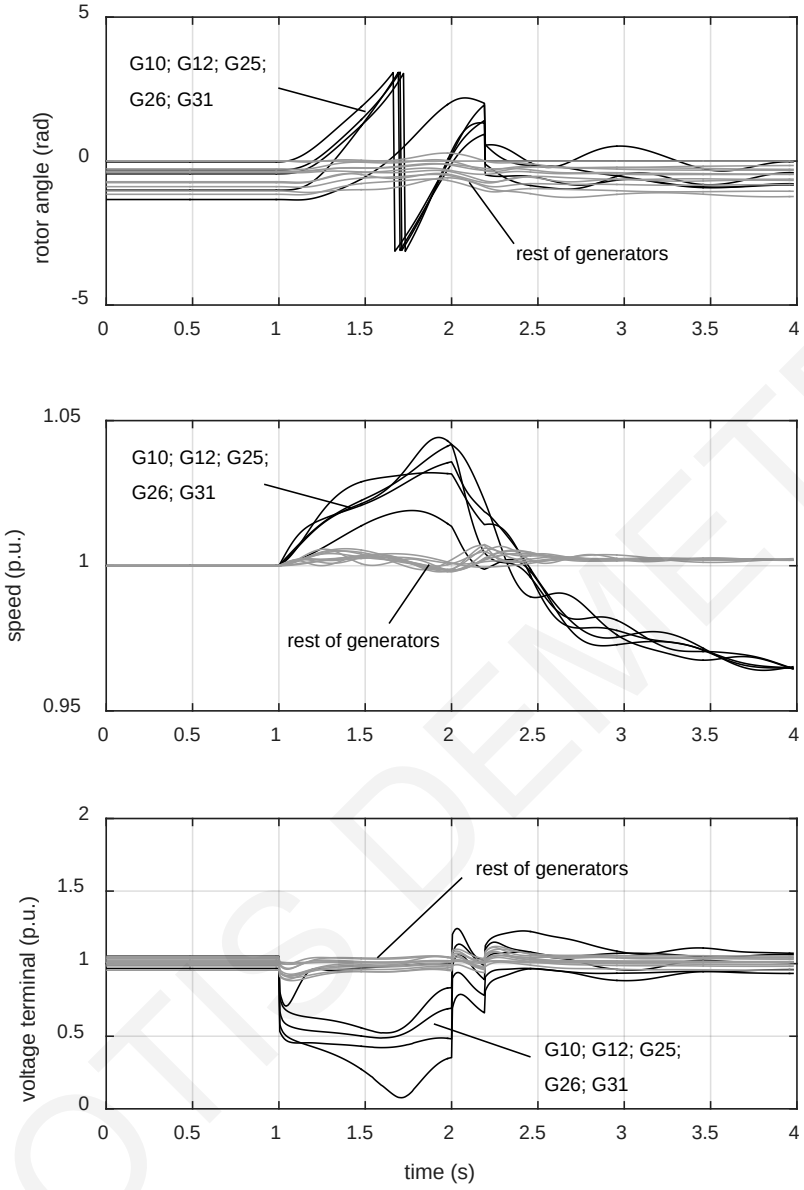

Figure 6.13: IEEE 118-bus test system - Electrical behavior with islanding

voltages are successfully kept within the desirable thresholds. Consequently, it can be concluded that the proposed ICI and restoration scheme successfully prevents the power system blackout. Table 6.17 presents the PPSR constraints included in the strategy. As it can be seen, the ICI scheme has ensured the creation of completely observable islands. In addition, at least one BS unit and sufficient generation capacity to match the load consumption are available in each island. Since these constraints have been included in the strategy, a PPSR is planned in case of any eventuality which can be carried out at the control center with the use of the linear state estimator. In this sense, the corrective measures applied to synchronize the islands in this test system are summarized in Table 6.18, while the synchronizing status of

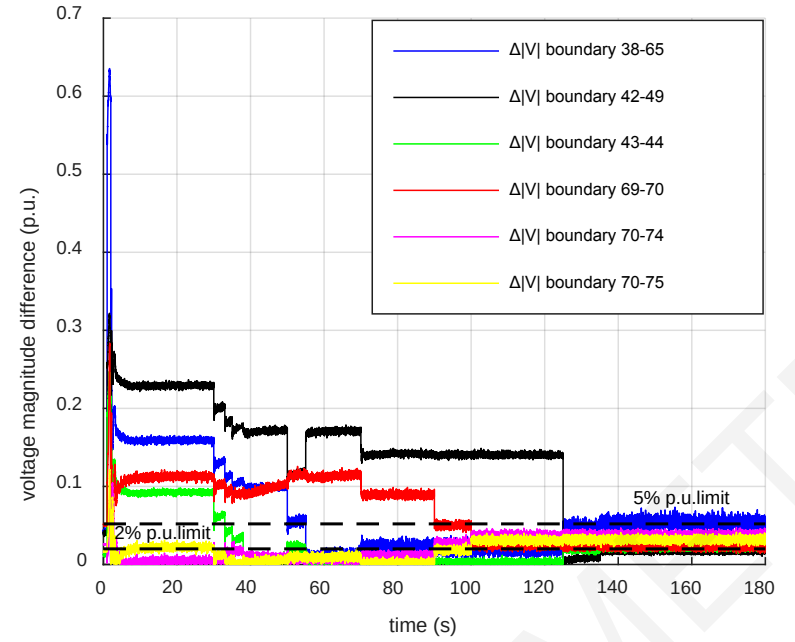

(a)

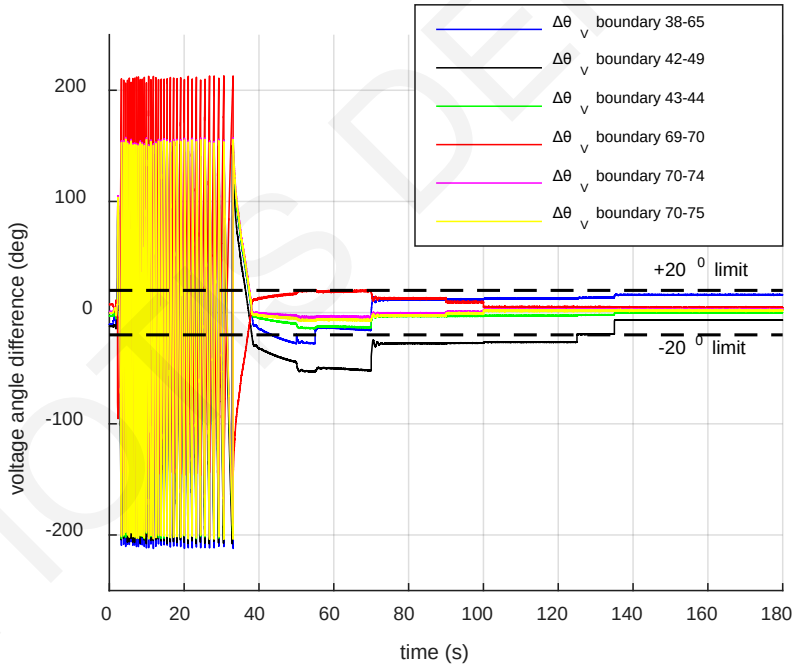

(b)

Figure 6.14: IEEE 118-bus test system: (a) Voltage magnitude and (b) Angle difference of islands boundary buses during their resynchronization

their boundaries is illustrated in Figure 6.14 - Figure 6.15. At this point, it is important to mention that, after the islanding, the frequencies of the two islands were not close. According to NERC [88], if the frequency of the two islands are different, the frequency of the smaller island should be adjusted to match the frequency of the larger island. Hence, the first

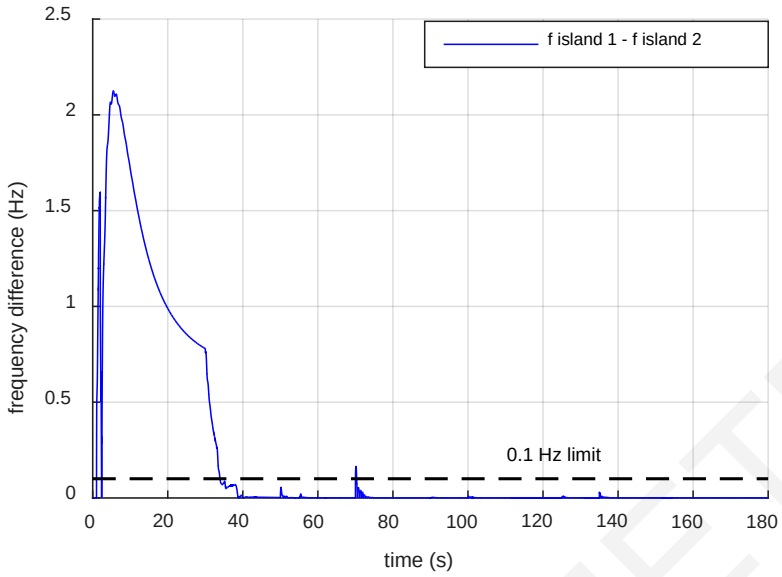

Figure 6.15: IEEE 118-bus test system: Islands frequency difference during their resynchronization

corrective measure was to shed some loads in the smaller island (Island 1) in order to increase its frequency and match it with the frequency of the larger island (Island 2). As noticed from Table 6.18, this led to the re-closure of 3 boundary lines. The last boundary line was able to reconnect at t = 135 s, where the restoration is completed. More importantly, the restoration was completed without the presence of synchroscopes and field crew at the substations; thus, without any additional delays.

6.4 Conclusions

In this Chapter, the exact ICI algorithm based on a MILP formulation (Section 4.5) that directly determines an islanding solution with minimal power-flow disruption for any given number of islands has been extended to consider power system restoration constraints. The new constraints deal with sufficient generation capacity, blackstart availability and observability within each created island. The proposed extended ICI algorithm was tested using dynamic models of the IEEE 39- and 118-bus test systems. Multiple case studies were developed to demonstrate the effectiveness of the algorithm to different system conditions. It is important to note that there are a few seconds for controlled islanding after the system suffers a severe fault [77]. Based on the simulation results, it can be seen that the proposed extended ICI algorithm can meet the requirement of real-time controlled islanding while planning a parallel power system restoration in case of any eventuality.

Next, a novel real-time ICI and restoration scheme has been proposed. The proposed scheme consists of a sophisticated ICI algorithm (i.e., the aforementioned extended MILP ICI algorithm), a real-time linear state estimator and a restoration process. Following the necessity to split the system, the extended MILP ICI algorithm firstly determines an exact islanding solution with minimal power-flow disruption while ensuring that each resulting island contains only coherent generators. At the same time, it creates islands that are also completely observable, includes at least one BS unit within each island and guarantees sufficient generation capacity to match the load consumption within each island. Since system observability is guaranteed, the real-time state estimator can continuously provide to the system operator the operating conditions of the power system before and after its splitting. This gives the operator the flexibility to monitor the islands during the post-islanding stage. Hence, the reconnection of the islands can be achieved in quasi real time, as soon as their synchronizing conditions are met. This leads to the restoration of the whole power system.

CHAPTER 7
CONTROLLED ISLANDING & RISK ASSESSMENT

7.1 State-of-the-Art Overview

Although the several methods reported in the literature can find a solution to the ICI problem, the potential sources of misoperation of the schemes and the impact of these undesirable events on the system reliability have not yet been assessed, as it has been done for other ones, e.g., generation rejection schemes [96], [97], [98]. These studies are capable of conducting highly accurate reliability modeling of wide-area protection schemes, both at a component and at a scheme level. In addition, different techniques for boosting their reliability have been evaluated, e.g., adding redundancy and voting schemes. As discussed in these previous works, a misoperation of wide-area protection schemes can have a significant impact on the network reliability. Thus, the reliable and timely implementation of ICI schemes, and in general of System Integrity Protection Schemes (SIPS), is critical for boosting the reliability of electrical power systems.

7.2 A Unified Framework for Assessing the Risk of ICI Schemes

A unified framework to assess the risk of ICI schemes on the electricity system has been proposed in [70]. First, the ICI algorithm described in Section 4.4 (based on graph theoretic cut-set matrix) is used to determine an islanding solution that creates islands with minimum power imbalance, while ensuring that each island contains only coherent generators. Then, a risk assessment methodology for estimating the risk introduced by the ICI failure modes is proposed. The main failure modes of ICI schemes considered here are (i) the failure to operate when needed and (ii) the spurious operation when the network is stable and no system splitting is required. The ICI and the risk assessment proposals result in a unified framework that provides insights on the benefits and risks of implementing ICI schemes, considering different sources of uncertainties and concerns related to their reliability.

7.2.1 Risk assessment methodology

Figure 7.1 shows the framework for assessing the risk introduced by the ICI failure modes. It can be seen that it is composed of three steps: reliability, impact and risk assessment. These steps are thoroughly presented and discuss below.

A) Reliability assessment

As shown in the left side of Figure 7.1, the main steps for assessing the reliability of ICI an scheme are the following:

Step 1: Develop the logic design of the ICI scheme. This would provide the components required for realizing the scheme. Figure 7.2 shows a generic ICI logic design, where the key components of an ICI scheme can be seen, e.g., field measuring devices and actuators, communication links, and Programable Logic Controllers (PLCs). The main steps of the ICI scheme operation are the following (Figure 7.2):

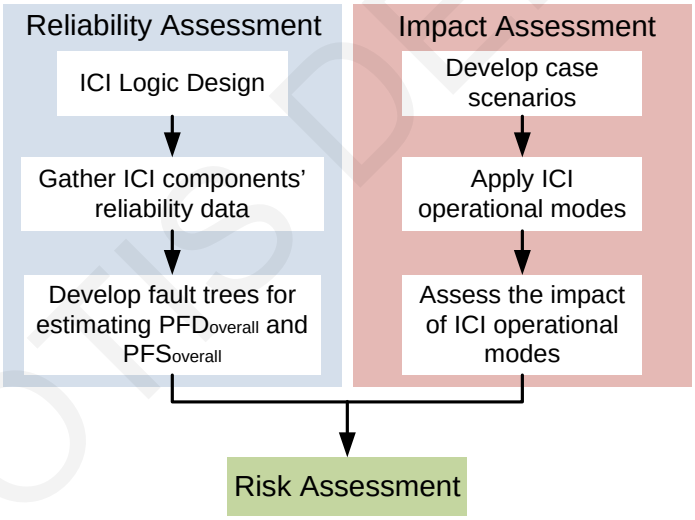

Figure 7.1: Framework for assessing the risk of ICI failure modes

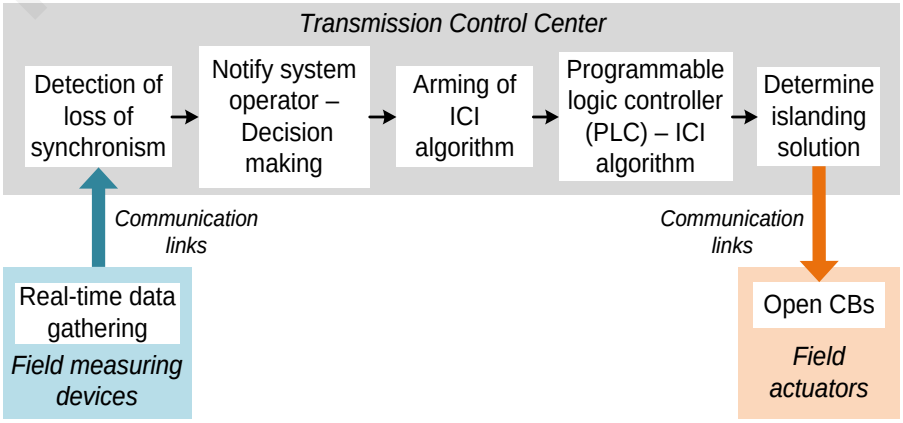

Figure 7.2: Generic ICI logic design

i) Detection of loss of synchronism using real-time data.

ii) Alarm/notification to the Transmission System Operator (TSO) by the information/alarm processing system to manually arm in service the ICI algorithm.

iii) Logic operation of ICI algorithm (presented in Section 4.4) by the PLC to decide when and where to split the network.

iv) Automatic implementation/activation of the ICI scheme to send the inter-trip signals and open the appropriate circuit breakers (CBs) in order to split the network to stable islands.

Step 2: Gather the individual ICI components' reliability data. As mentioned at the beginning, the main failure modes of ICI schemes considered here are (i) the failure to operate when needed and (ii) the spurious operation when the network is stable and no system splitting is required. Therefore, the components' reliability data required for assessing ICI reliability are the Mean Time To Failure (*MTTF*), and Mean Time To Fail Spurious (*MTTFS*).

Step 3: Estimate the probabilities of the ICI components' failure modes. These can be expressed using the probability of failure on demand (*PFD*) and probability to fail spurious (*PFS*, also known as probability to fail safe), respectively. Considering an exponential distribution for the failure rates of the components and that they are constant over their operating life, the ICI components' *PFD* and *PFS*, defined as the probability of failure to operate in a specified test interval (*TI*) and the probability of a spurious trip of the components in a given time period (*TP*) respectively, can be calculated as follows:

$$PFD = \lambda \frac{TI}{2} \qquad \left(\lambda = \frac{1}{MTTF} \right) \tag{7.1}$$

$$PFS = \lambda_s \times TP \qquad \left(\lambda_s = \frac{1}{MTTFS} \right) \tag{7.2}$$

where λ and λ_s are the failure and spurious rates of the components, and *TP* refers to the time period that λ_s is expressed (e.g., per week, month, year, etc.). It is considered that during the testing of the individual ICI components, the sources of failure to operate of the components are identified and removed**,** while a spurious operation is repaired once it occurs within the *TP* considered in the analysis.

Step 4: Estimate the probabilities of the ICI failure modes. To estimate the overall *PFD* ($PFD_{overall}$) and *PFS* ($PFS_{overall}$) of the scheme, fault tree analysis (FTA) is used [99]. FTA is a top-down deductive failure analysis that uses Boolean logic for determining the lower-level events or combination of events that lead to the occurrence of the top event. This technique

has been effectively used for assessing the reliability of SIPS [97], [98]. The individual components' *PFD* and *PFS* calculated at Step 3 are inserted to the fault trees. Then, by using the logic operations of the fault trees, the $PFD_{overall}$ and $PFS_{overall}$ can be accurately estimated. These will be used for estimating the risk introduced to the system by the undesirable operations of the ICI scheme.

B) Impact assessment

The right side of Figure 7.1 shows the main steps proposed in this work for assessing the impact of ICI operational modes:

Step 1: Develop case scenarios for different operating conditions, for which the ICI would be needed. As the ICI scheme is to be used only during severe disturbances, these case scenarios should ideally reflect electrical events that typically result in a partial or complete blackout. Since the possible number of scenarios that could occur in a real power system is large, the focus of the development of these case scenarios will be on the "*worst-case scenarios*", similarly to the approach followed in previous works, such as [9], [15], [59].

Step 2: Apply the ICI operational modes to the case scenarios. Based on feedback from the TSO and worldwide practices [96], [100], three operational modes are considered here:

i) the failure of the scheme to operate when the loss of synchronism occurs;
ii) the incorrect operation of the ICI scheme before the system stability is compromised; and
iii) the success operation of the ICI scheme, as the ICI schemes' aim is not to eliminate the amount of customer interruptions but to mitigate it as much as possible. It would therefore result in an amount of load shedding for balancing the formed islands.

Step 3: Estimate the impact of ICI operational modes. The amount of load shedding (MW) is used in this work for this quantification as it is the main concern when blackout events take place. However, any other index can be used if desired.

C) Risk assessment

Following the reliability and impact assessment of the ICI operational modes (including both successful and failure modes), the risk with the ICI in operation is assessed, which is given by the product of the probability of the ICI operational mode and its impact. To determine if the ICI scheme benefits the reliability of the network, this risk is then compared to the risk of the electrical event without the ICI scheme.

The risk of the electrical event without the ICI scheme in operation is calculated as follows:

$$Risk = P(E) \times Im(E) \tag{7.3}$$

where *P(E)* and *Im(E)* are the probability of occurrence per year and impact of the electrical event (*E*), respectively.

In order to assign an economic value to the impact assessment, the Value of Lost Load (*VoLL*, €/MWh) is used. The impact is thus expressed as follows (measured in €/h):

$$Im(E) = L_{shed} \times VoLL \tag{7.4}$$

where L_{shed} is the amount of load shedding (MW) after (*E*).

The risk with the ICI scheme in operation is [100]:

$$Risk_{ICI} = Risk(Success) + Risk(Failure) + Risk(Spurious) \tag{7.5}$$

$$Risk(Success) = P(E) \times (1 - PFD_{overall}) \times Im(Success) \tag{7.6}$$

$$Risk(Failure) = P(E) \times PFD_{overall} \times Im(Failure) \tag{7.7}$$

$$Risk(Spurious) = P(\overline{E}) \times PFS_{overall} \times Im(Spurious) \tag{7.8}$$

The risk in (7,3) and (7.5)-(7.8) would thus be expressed in €/h. $PFD_{overall}$ and $PFS_{overall}$ are provided by the reliability assessment of the scheme and *Im(Success)*, *Im(Failure)* and *Im(Spurious)* are given by the impact assessment of the ICI operational modes (in terms of load shedding) for the different scenarios developed, which are quantified using (7.4). The risk of failure to operate is estimated upon the occurrence of the electrical event, and the risk of spurious operation is assessed in the absence of the event ($\bar{E}$) requiring the ICI operation. The latter is derived by the definition of a spurious operation per se, which means undesirable/unnecessary operation of a function in the absence of the triggering event.

7.2.2 Simulation results

The proposed unified framework was applied on the actual power system of Cyprus in order to give an indication of the network risk to large-area blackouts with and without the ICI scheme in operation. For this purpose, two case studies were developed (i.e., two different faults leading to blackout), the description of which can be found in Section 4.4.3. Note that the information about the splitting strategy found by the ICI scheme for each case study can also be found in Section 4.4.3.

Following discussions with the Cypriot TSO, three operational modes of the ICI scheme

Table 7.1: Reliability data of ICI components

ICI Component	*MTTF/MTTFS (years)*	*PFD ($x10^{-3}$)*	*PFS ($x10^{-3}$)*
Data gathering	400	6.25	2.5
Detection of Loss of Synchronism	300	8.33	3.33
UFLS relays	500	5	2
UVLS relays	500	5	2
Communication links	500	5	2
Circuit breakers	1700	1.47	0.58
PLC	300	8.33	3.33
Operator error	1000	2.5	1

(and its components) were considered (as done for other SIPS): success, failure to operate and spurious operation. While the impact may vary from one case to another, it was the intention of this work to produce a framework that will help TSOs in assessing the impact of ICI schemes on their networks. Based on the logic design shown in Figure 7.2, Table 7.1 presents the main ICI components and their reliability data (extracted from the literature and used for illustrating the risk assessment framework).

The test interval of the components was set to 5 years, based on feedback from the main component manufacturer and provider of the Cypriot network. Due to lack of reliability data, the same *MTTF* and *MTTFS* were assumed for each component, which resulted in equal *PFD* and *PFS*. If the historical database of the electrical utility was available, more accurate *MTTF* and *MTTFS* could be used. It can also be seen that the operator was considered as an individual component of the ICI scheme, i.e., operator error. Table 7.1 also shows the *PFD* and *PFS* of each ICI component as estimated using (7.1) and (7.2), using a simulation period (*TP*) of one year.

A) Fault trees design for the Cypriot network

Figure 7.3 and Figure 7.4 present the fault trees for evaluating the $PFD_{overall}$ and $PFS_{overall}$, respectively. They indicate the events and/or combination of events that may lead to a failure of the ICI scheme to operate or to a spurious operation.

As it can be seen in Figure 7.3, a failure of the ICI scheme to operate as designed can occur due to: (i) a failure in the field data gathering devices; (ii) failure in the software applications for detecting the loss of synchronism or carrying out the logic operation of the scheme (i.e., PLC); (iii) the operator's failure to detect the alarm by the information/alarm processing system or failure to manually arm in service the ICI algorithm in a timely manner; (iv) a communication failure between field – control center and vice-versa; (v) a failure in the CBs

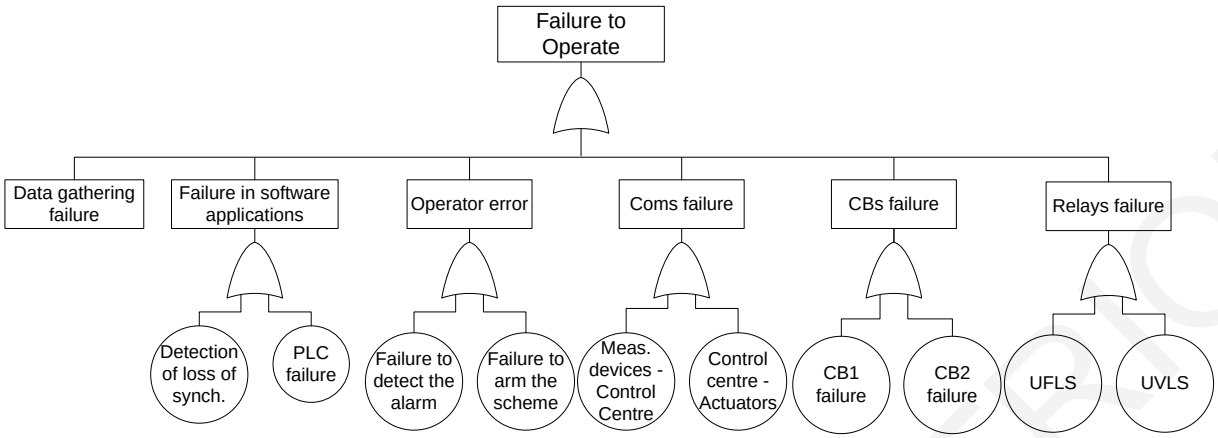

Figure 7.3: Fault tree for estimating the probability of failure on demand ($PFD_{overall}$)

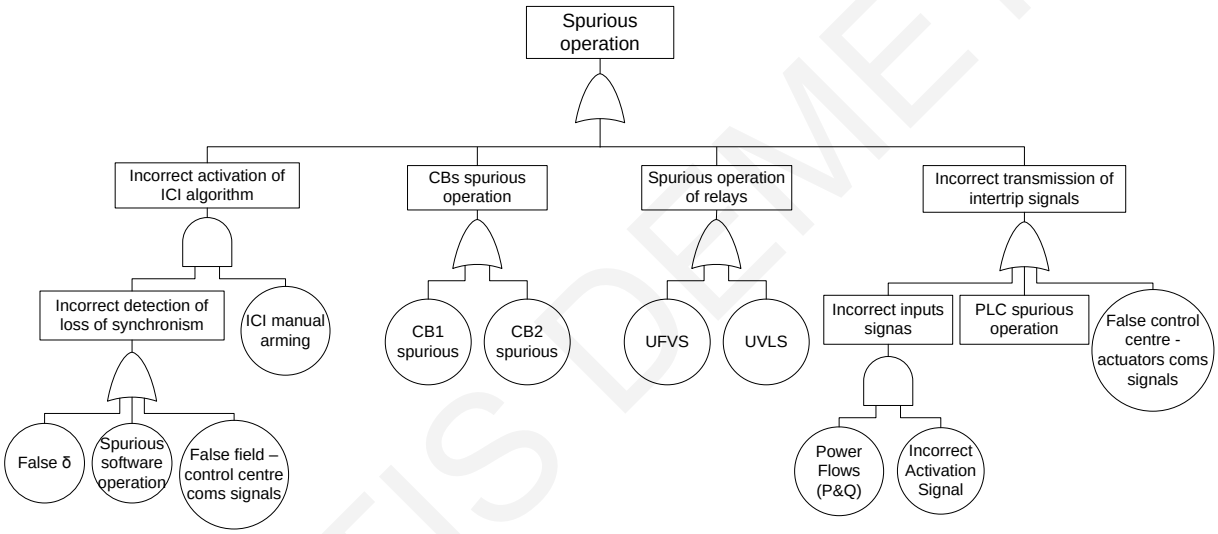

Figure 7.4: Fault tree for estimating the probability of spurious operation ($PFS_{overall}$)

to open the lines determined by the ICI solution, which will consequently result in the failure of the scheme to split the network into stable islands; and vi) a failure in the under-frequency or under-voltage load shedding relays (UFLS and UVLS respectively) to shed load for balancing the formed islands. In this work, and like the risk assessments available in the literature, it was considered that the failure to operate as designed of one single ICI component leads to the complete failure of the overall ICI scheme – this may vary among TSOs.

Figure 7.4 further shows that a spurious operation of the ICI scheme may occur due to: (i) an incorrect activation of the ICI solution which will occur in case of an incorrect detection of loss of synchronism and manual arming by the operator; (ii) an incorrect transmission of intertrip signals; (iii) a spurious operation of CBs, and/or iv) a spurious operation of the UFLS and UVLS relays, i.e., shed load when not required. As above, and like other risk assessments, it was considered that the spurious operation of one single ICI component leads to the

complete spurious operation of the overall ICI scheme – and again this may vary among TSOs.

The fault trees shown in Figure 7.3 and Figure 7.4 are generic (as the logic in Figure 7.2) and can be applied to any ICI scheme. Indeed, if the detailed architecture of the ICI scheme becomes available, then these fault trees can be extended to cater for any other IC component. The events considered were selected as they have been taken into account in past reliability studies of other protection schemes, such as generation rejection [96], [100]. Finally, the fault trees were designed based on feedback from the Cypriot TSO, and can be easily adapted if further needs are required.

B) Risk assessment in the Cypriot network

The *PFD* and *PFS* of the individual component of Table 7.1 were inserted in the fault trees of Figure 7.3 and Figure 7.4 for quantifying $PFD_{overall}$ and $PFS_{overall}$. The risk assessment was carried out only for the two case studies discussed in Section 4.4.3, as they were of interest in this work. Table 7.2 and Table 7.3 show the probabilities of the ICI operational modes, the load shedding occurring due to each ICI operational mode, and the overall risk without and with the ICI in operation for the two case studies and demand levels (i.e., winter and summer peak demands). The *VoLL* for the Cypriot system was considered equal to 6,500€/MWh, based on a typical value reported in [101], and the probability of the electrical event per year, *P(E)*, equal to $1x10^{-2}$, based on feedback from the TSO.

To define the risk without ICI in operation, the case studies presented in Section 4.4.3 that resulted in the complete blackout of the Cypriot system were considered. The impact *Im(E)* (i.e., using the load shedding) for the winter and summer peak demands was equal to 848.71 MW and 1187 MW, respectively. Thus, the risk without ICI could be calculated using (7.3) and (7.4).

The risk with ICI in operation was estimated using (7.5) - (7.8). It should be noted here that the impact of an ICI failure to operate was equal to the impact without the ICI in operation. The risk assessment results are shown in Table 7.2 and Table 7.3 for case studies 1 and 2, respectively. In these tables, the probabilities of the ICI operational modes and the resulting load shedding and risk per hour of the interruption duration are given.

C) Analysis of the risk in the Cypriot network

For case study 1 (Table 7.2), in the winter peak demand study and for a successful ICI

Table 7.2: Risk assessment results for case study 1

	Probability of Event/ICI Operation		***Load shedding (MW)***		***Risk (x10³ €/h)***	
			Winter	***Summer***	***Winter***	***Summer***
W/o ICI	$P(E)$	0.01	848.71	1187	55.16	77.15
With ICI	$P(E)\times(1\text{-}PFD_{overall})$	9.53×10^{-3}	99.57	208.11	6.17	12.89
	$P(E)\times PFD_{overall}$	4.7×10^{-4}	848.71	1187	2.59	3.62
	$P(\bar{E}) \times PFS_{overall}$	1.05×10^{-2}	42.78	260.8	2.89	17.62
	Total Risk with ICI (x10³ €/h)				11.65	34.13
	Risk decrease (%)				78.88	55.76

Table 7.3: Risk assessment results for case study 2

	Probability of Event/ICI Operation		***Load shedding (MW)***		***Risk (x10³ €/h)***	
			Winter	***Summer***	***Winter***	***Summer***
W/o ICI	$P(E)$	0.01	848.71	1187	55.16	77.15
With ICI	$P(E)\times(1\text{-}PFD_{overall})$	9.53×10^{-3}	0.00	0.00	0	0
	$P(E)\times PFD_{overall}$	4.7×10^{-4}	848.71	1187	2.59	3.62
	$P(\bar{E}) \times PFS_{overall}$	1.05×10^{-2}	39.79	249.66	2.69	16.87
	Total Risk with ICI (x10³ €/h)				5.28	20.49
	Risk decrease (%)				90.43	73.44

operation, the risk was reduced from 55.16 to 6.17 ($\times10^3$ €/h). This difference was also high for the summer peak demand, i.e., from 77.15 to 12.89 ($\times10^3$ €/h). Despite the analyzed peak demand, a successful operation of the ICI scheme in case study 2 (Table 7.3) leaded to no load shedding, i.e., no risk was introduced by the successful operation of the ICI scheme. Finally, it must be noted that a high risk was introduced by a spurious operation during summer, i.e., 17.62 and 16.87 ($\times10^3$ €/h) for the two case studies. An incorrect scheme operation during highly stressed conditions resulted in a high amount of load shedding for creating two stable islands.

Comparing the total risk without and with ICI, a significant decrease in the risk was observed for both case studies, with the risk decrease being significantly higher for the winter peak demand than for the summer peak demand. This shows the effectiveness of the proposed ICI algorithm and its contribution as an emergency control action to mitigating the risk of the disturbance, even during peak demand conditions. These results also show that even when the uncertainty associated with its reliability was considered, the risk with the ICI in operation is significantly lower. This is due to the fact that the probability of an ICI undesirable operation is low and, additionally, the amount of load shedding required for stabilizing the islands is much lower than the load shedding following a complete blackout, as shown in Table 7.2 and Table 7.3. This altogether lead to a much lower risk with the ICI scheme in operation.

Table 7.4: Risk decrease by adding full redundancy to the ICI scheme

Case Study	*Risk Decrease (%)*	
	Winter	*Summer*
1	77.67	36.68
2	90.12	56.14

D) Effects of adding redundancy to the ICI scheme

The effects of adding full redundancy to the ICI scheme on the risk evaluation was also evaluated, which affected the reliability analysis as follows (details can be found in [98]):

- A failure of both the primary and secondary (redundant) component needs to occur for a function to fail to be executed when required (i.e., $PFD_{overall}$ wa decreased).
- A spurious operation of either the primary or the secondary component is capable of incorrectly activating a function and triggering the scheme (i.e., $PFS_{overall}$ increases).

Therefore, on the one hand, an improvement in the risk by a failure of the ICI scheme to operate can be observed; however, on the other hand, adding redundancy results in an increase in the risk introduced by a spurious operation of the ICI scheme.

Table 7.4 summarizes the results of this analysis. By adding full redundancy, the risk decrease with the ICI in operation for the winter peak demand study remained approximately the same for case studies 1 and 2, i.e., 77.67 and 90.12% respectively (compared to 78.88 and 90.43% without redundancy). This means that the improvement in the risk by reducing $PFD_{overall}$ compensates for the increase in the risk due to a higher $PFS_{overall}$. On the other hand, for the summer peak demand study, the risk decrease reduced to 36.68 and 56.14% for the case studies 1 and 2 from 55.76 and 73.44% respectively.

This is because a higher load shedding occurred for the summer peak demand from a spurious operation of the ICI scheme, i.e., 260.8 and 249.66 MW for case studies 1 and 2 respectively (compared to 42.78 and 39.79 MW respectively for the winter peak demand), which in combination with the increase in $PFS_{overall}$ due to the full redundancy added to the scheme, resulted in high risk by a spurious operation.

E) Sensitivity analysis

In order to tackle the uncertainty associated with the reliability data used, sensitivity studies were performed. In particular, based on (7.1)-(7.2) the test interval and the *MTTF* of the components were varied to evaluate their impact on the estimated risk with the ICI in operation.

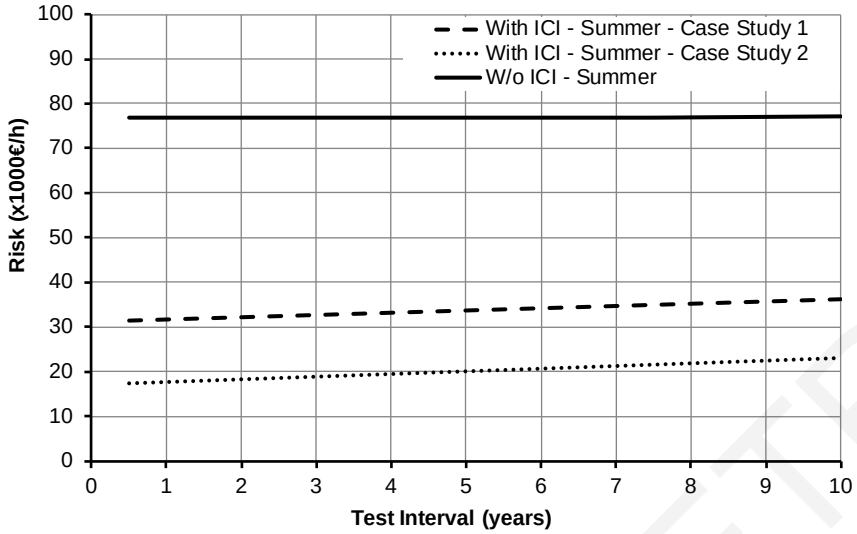

Figure 7.5: Effect of ICI scheme's test interval (*TI*) on overall system risk for the summer peak demand

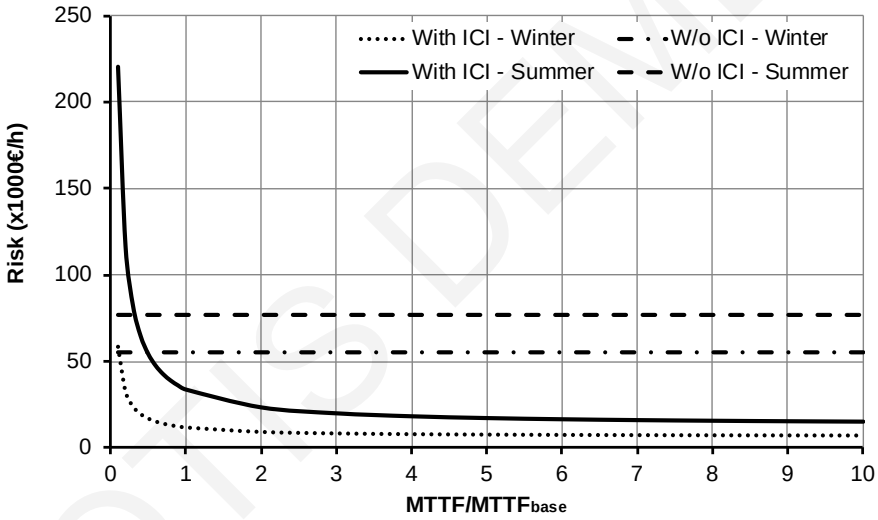

Figure 7.6: Effect of components' *MTTF* on overall system risk for the winter and summer peak demand, case study 1

1) Varying components' test interval (TI)

The test interval of the ICI scheme has been varied in the range of [0.5, 10] years with a step of 0.5 years. Figure 7.5 shows the results of this analysis only for the summer peak demand studies (it had a higher risk than the winter peak demand, see Table 7.2 and Table 7.3). The increase in the *TI* results in an increase in the risk introduced by the ICI. However, the slope of the risk curves with ICI in operation is smooth, and as a result they do not cross the risk curve without (w/o) ICI, even for the highest *TI* used here, i.e., 10 years. It is not expected that such a scheme of vital importance for the stability of a network will not be tested and maintained with a frequency lower than 10 years (this may vary among TSOs). It can

therefore be concluded that the *TI* is not a determining factor that can result in higher risks by having the proposed ICI scheme in operation.

2) Varying components' MTTF

The ICI components' *MTTF* (and *MTTFS*) has been varied in the range of [0.1x$MTTF_{base}$, 10x$MTTF_{base}$], where $MTTF_{base}$ refers to the components' *MTTF* and *MTTFS* presented in Table 7.1. Figure 7.6 shows the results of this analysis for case study 1, for the winter and summer peak demands. Similar results were obtained for case study 2.

As can be seen in Figure 7.6, the risk w/o ICI in operation becomes lower than the risk with ICI for much lower values of *MTTF* compared to the ones of Table 7.1 (approximately $0.1\times MTTF_{base}$ and $0.3\times MTTF_{base}$ for the winter and summer peak demand case studies respectively). In fact, based on experience and on published reliability data of the components of Table 7.1, it is quite easy and possible to achieve higher *MTTF* than these values; hence it is rather impossible to obtain higher risks with the proposed ICI in operation using the available components by the manufacturers for realizing the scheme. It can also be observed that as the *MTTF* of the ICI components increases, the decline in the risk becomes smoother, which will ultimately converge to values close to the risk by a successful ICI operation (but not equal, because even though the risk of failure and spurious operations will be very low, it will still be higher than zero).

7.3 Conclusions

This Chapter has presented a unified framework that first introduces an effective ICI scheme and then assesses the risk of the system with the ICI scheme in operation to tackle the uncertainty and concerns related to the reliability of such schemes. Considering the increasing complexity and vulnerability of power systems to electrical disturbances, such a systematic and comprehensive analysis becomes critical and contributes significantly to the decision-making on the most appropriate reliability enhancement and investment strategies.

The proposed ICI scheme is based on the well-established cut-set matrix concept, which is modeled as a combinatorial optimization problem with constraints. The objective function of this problem is the minimum power imbalance within islands, while the main constraints are the coherent generator groups and transmission line availability. Different case studies (i.e.,

faults) and demand levels were examined for illustrating the ICI algorithm using the Cypriot network, which demonstrated its adaptability and effectiveness in minimizing the impact of cascading outages leading to blackouts under varying system conditions.

Further, the application of the fault tree-based risk assessment methodology using the ICI scheme applied on the Cypriot network showed that the overall system risk is significantly reduced when the ICI scheme is in operation. This indicates that the system robustness to sudden electrical contingencies is enhanced with the proposed ICI scheme, even when the probability of the scheme's failure modes is considered.

Simulation results of adding redundancy and considering sensitivity analysis were carried out to provide useful insights on the aspects affecting the reliability of the proposed ICI scheme, and thus the risk introduced by their undesirable operations. The unified framework presented in this work can provide an effective solution in mitigating the effect of large disturbances, as well as estimating the risk associated with an undesirable operation of the ICI scheme. If the relevant data is available, then the proposed unified framework can be applied to any power system, which would provide insights on the benefits and risks of applying the ICI scheme.

CHAPTER 8
CONCLUSIONS

8.1 Conclusions and Impact

Despite the efforts for boosting the immunity of power systems to large-scale blackouts, recent electrical disturbances show that they are still vulnerable to such events. This calls for more effective and drastic measures for improving their reliability and mitigating the impact of widespread blackouts. Intentional Controlled Islanding (ICI) has been proposed by a number of task forces and advisory groups as an effective corrective measure of last resort to split the power system into several sustainable islands and prevent cascading outages.

For the success of an ICI scheme, three critical problems must be addressed: "*where to island*", "*when to island*" and "*what to do after islanding*". One of the main objectives of this thesis was the development of computationally efficient ICI methods for addressing the first problem. For this purpose, several novel ICI schemes for determining optimal splitting strategies in strong connected networks (including small systems and very large-scale power systems) have been proposed and presented in Chapter 4. The proposed schemes aim to split the system with minimal power-flow disruption or minimal power imbalance within islands, for any given number of islands, while maintaining generator coherencies and other static and dynamic constraints (e.g., transmission line availability, connectivity). The adaptability and effectiveness of the proposed ICI schemes in minimizing the impact of cascading outages leading to blackouts under varying system conditions have been tested and demonstrated using different IEEE test systems and real power systems. Moreover, the simulation results have highlighted that the proposed ICI schemes are suitable for real-time applications.

Further, the development of a two-step approach for defining coherent generators in disturbed power systems based on the similarity among their inter-area oscillations and swing curves was also achieved (see Section 3.2). This methodology can be a useful tool for the system operators to find and apply suitable islanding solutions in real-time, knowing that the generator coherency constraint is vital for the success of the controlled separation. Therefore, it might be a new WAMPAC application.

Another important objective of this thesis was the implementation of a methodology to address the "*when to island*" problem. Crucially, in Section 5.2, a unified methodology based on the area-based Center of Inertia (COI)-referred rotor angle index has been introduced to determine the most suitable time for splitting the system. Different case studies have demonstrated the adaptability and effectiveness of the proposed methodology in triggering promptly the ICI scheme and thus in minimizing the impact and cost of large-scale blackouts. At this point, it is important to mention that this timely definition of the time for islanding can easily be combined with approaches to determine the points where to island the system.

In addition, this thesis aimed to investigate the concept of controlled islanding strategies combined with an approach of Parallel Power System Restoration (PPSR), as well as to develop a novel scheme that provides real-time solutions for both ICI and power system restoration. The concept of such schemes is still an unexplored research area and a practical engineering challenge. For this purpose, the proposed ICI algorithm of Section 4.5 was extended to consider power system restoration constraints (e.g., complete observability, sufficient blackstart (BS) capability and sufficient generation capacity to match the load consumption within each island). The extended ICI algorithm (see Section 6.2) was tested and it was found that it can meet the requirement of real-time controlled islanding while planning a parallel power system restoration in case of any eventuality. Next, the aforementioned ICI algorithm was introduced as a part of a proposed real-time ICI and restoration scheme. The particular scheme (see Section 6.3), which further consists of a real-time state estimator and a power system restoration process, gives the operator the flexibility to monitor the islands during the post-islanding stage and reconnect them in quasi real time (without the presence of any synchroscopes and crew in the substations), as soon as their synchronizing conditions are met.

Table 8.1 summarizes the advantages of the aforementioned proposed ICI methods and schemes over the existing ICI methods in the literature, considering the requirements for a successful real-time islanding solution. These requirements include the determination of an optimal islanding solution, for any given number of islands, while considering dynamic (i.e., generator coherency) and static (i.e., transmission line availability) constraints. Furthermore, an ICI scheme should consider PPSR constraints, or even to be able to provide the actual PPSR solution while being computationally efficient for both small-scale and large-scale power systems. As it can be observed from the table, most of the existing ICI methods

Table 8.1: Comparison between existing ICI methods in the literature and the proposed ICI methods

Proposed ICI method	*Optimal islanding solution*	*Any given number of islands*	*Dynamic constraints (e.g. generator coherency)*	*Static constraints (e.g. line availability)*	*PPSR constraints*	*PPSR solution*	*Comput. efficient for small-scale power systems*	*Comput. efficient for large-scale power systems*
Ref. [57], [58] (OBDD, DFS/BFS)	✓	×	✓	✓	×	×	×	×
Ref. [9], [15], [59] (Slow coherency)	×	✓	✓	×	×	×	✓	✓
Ref. [60] (Spectral Clustering (SC))	×	×	×	×	×	×	✓	×
Ref. [8] (Spectral Clustering (SC))	×	×	✓	×	×	×	✓	×
Ref [63], [64] (Efficient SC)	×	✓	✓	✓	×	×	✓	✓
Ref [89] (Weak areas)	×	✓	✓	✓	✓	×	✓	✓
Ref [80] (MILP)	✓	✓	✓	×	×	×	✓	×
RSCCI method	×	×	✓	✓	×	×	✓	×
ICI algorithm (Cut-Set Matrix)	×	✓	✓	✓	×	×	✓	×
MILP ICI algorithm	✓	✓	✓	✓	×	×	✓	✓
LP ICI algorithm	✓*	✓	✓	✓	×	×	✓	✓+
Extended MILP ICI algorithm	✓	✓	✓	✓	✓	×	✓	✓
ICI & Restoration Scheme	✓	✓	✓	✓	✓	✓	✓	✓

*optimal solution as MILP ICI algorithm (without multiple iteration of recursive linearization procedure) +faster than MILP ICI algorithm

approximate the optimal islanding solution in order to be computationally efficient [8], [9], [15], [59], [60], [63], [64], [89]. In addition, most of them consider only the dynamic constraint of generator coherency and not static constraints [8], [9], [15], [59], [80]. A main drawback of the existing ICI methods is the lack of the PPSR planning stage. This disadvantage was attempted to be solved only by a few works [89]. In the case of the ICI methods proposed in this thesis, most of them determine an optimal islanding solution, for any given number of islands, while being computationally efficient [16], [75], [87], [95]. Moreover, the proposed ICI methods consider both dynamic and static constraints. A few of them also consider PPSR constraints [87], [95]. Finally, the proposed ICI and restoration scheme of Section 6.3 provides real-time solutions for both the ICI and power system restoration [95].

The last part of this thesis has presented a unified framework, which first introduces an effective ICI scheme and then assesses the risk of the system with the ICI scheme in operation, in order to tackle the uncertainty and concerns related to the reliability of such schemes (see Section 7.2). Considering the increasing complexity and vulnerability of power systems to electrical disturbances, such a systematic and comprehensive analysis becomes critical and contributes significantly to the decision-making on the most appropriate reliability enhancement and investment strategies.

Finally, for the completion of this research, the thesis has also proposed dynamic test bed systems suitable for transient analysis studies. The proposed dynamic models allow

researchers to test their methodologies on common test systems in order to compare results and performance. The dynamic test systems complement the existing steady state systems. The transient analysis results from the testing of the proposed test systems have demonstrated that the dynamic models with the proposed typical parameters are reliable since the dynamic response of the IEEE modified test systems follows the expected behavior of actual systems under contingencies. Consequently, these dynamic test systems were also used throughout the thesis for the validation of the proposed methodologies.

8.2 Future Work

The research described in this thesis addresses the key aspects crucial for the success of ICI: "*where to island*", "*when to island*" and "*what to do after islanding*". These key aspects are investigated separately, and several computationally efficient methodologies and schemes are developed which are suitable for real-time applications. Therefore, they might be new WAMPAC applications and/or useful tools at the control centers of power system operators.

Next, the above key aspects are also investigated together under the same framework in order to accomplish the development of a complete controlled islanding scheme. Such an ICI scheme could be used, usually after severe disturbances and when conventional control systems have failed to keep the system within stability margins, to determine sequentially and in real-time the suitable number of coherent groups, the generators within each coherent group, the most suitable time for splitting the system, the optimal splitting solution, and the PPSR planning stage. However, significant further research may be needed before the complete ICI scheme can be implemented in the real power system.

A typical wide-area measurement system consists of strategically located PMUs that provide synchronized system measurements. As highlighted in the thesis, the proposed ICI methods and schemes use Wide Area Monitoring Systems (WAMS) to gather these synchronized real-time measurements (with a sampling rate between 30 to 60 samples per second). However, the utilization and analysis of such huge amounts of data requires the presence of a real time wide area control system. The main operational issue of such a control system is the inevitable time delay of the wide area signal transmission. The time delay of the data transmission can vary from tens to hundreds of milliseconds. It depends on the communication distance, protocols and time consumed by numerical calculations. Therefore, a

main future aspect of this work is to consider the negative effect introduced by time delays. More specifically, to investigate if these time delays could affect the computational execution time of the proposed ICI schemes.

Moreover, another task for future work is to consider voltage stability constraints in the proposed ICI methods and schemes. Although, in most cases, the islanding solutions found using the proposed ICI methods retain voltages within the statutory thresholds, it is expected that the incorporation of voltage constraints in the optimization problem (for solving the ICI problem) will further improve the transient stability of the formed islands.

In addition, as mentioned in Chapter 1 of this thesis, the increasing integration of renewable energy sources into the grid based on power electronics converters interfaces is affecting the power systems dynamics. Since power system coherency refers to the property of generators having similar time-domain responses during a system transient, a critical challenge is to investigate how the coherency of the synchronous generators is affected by the use of high power electronic converters. Based on the result of this investigation, a second challenge is how to represent the time-domain responses of the integrated RES in order to be considered in the generator grouping.

REFERENCES

[1] REN21, "Renewables 2007 Global Status Report," 2008. [Online]. http://www.worldwatch.org/files/pdf/renewables2007.pdf

[2] C. Hor, J. Finn, G. Thumm, and S. Mortimer, "Introducing series compensation in the UK transmission network," *9th IET International Conference on AC and DC Power Transmission*, Mar. 2010.

[3] CIGRE. Task Force 38.02.19, "System protection schemes in power networks," 2001.

[4] V. Terzija and *et al*., "Wide-area monitoring, protection and control of future electric power networks," Jan. 2011.

[5] Y. Hu, V. Madani, R. M. Moraes, and D. Novosel, "Requirements of large-scale wide area monitoring, protection and control systems," *10th Annual Conference, Fault and Disturbance Analysis*, Georgia Tech, Apr. 2007.

[6] P. Kundur, C. Taylor, and P. Pourbeik, "Blackout experiences and lessons, best practices for system dynamic performance, and the role of new technologies," IEEE Task Force Report, 2007.

[7] G. Andersson *et al*., "Causes of the 2003 major grid blackouts in North America and Europe, and recommended means to improve system dynamic performance," *IEEE Transactions on Power Systems*, vol. 20, no. 4, pp. 1922-1928, Nov. 2005.

[8] L. Ding, F.M. Gonzalez-Longatt, P. Wall, and V. Terzija, "Two-step spectral clustering controlled islanding algorithm," *IEEE Transactions on Power Systems*, vol. 28, no. 1, pp. 75-84, Feb. 2013.

[9] G. Xu and V. Vittal, "Slow coherency based cutset determination algorithm for large power systems," *IEEE Transactions on Power Systems*, vol. 25, no. 2, pp. 877-884, May 2010.

[10] P. Pourbeik, P. Kundur, and C.W. Taylor, "The anatomy of a power grid blackout - Root causes and dynamics of recent major blackouts," *IEEE Power & Energy Magazine*, vol. 4, no. 5, pp. 22-29, Sept.-Oct. 2006.

[11] P. Kundur and C. W. Taylor, "Blackout experiences and lessons, best practices for system dynamic performance, and the role of new technologies," IEEE Task Force

Report 2007.

[12] P. Kundur, *Power system stability and control*. New York: McGraw-Hill, 1994.

[13] R. Sánchez-García and *et al*., "Hierarchical clustering of power grids," *IEEE Transactions on Power Systems*, vol. 29, no. 5, pp. 2229-2237, Sept. 2014.

[14] K. Sun, D.Z. Zheng, and Q. Lu, "Splitting strategies for islanding operation of large-scale power systems using OBDD-based methods," *IEEE Transactions on Power Systems*, vol. 18, no. 2, pp. 912-923, May 2003.

[15] H. You, V. Vittal, and X. Wang, "Slow coherency-based islanding," *IEEE Transactions on Power Systems*, vol. 19, no. 1, pp. 483-491, Feb. 2004.

[16] A. Kyriacou, P. Demetriou, E. Kyriakides, and C. Panayiotou, "Controlled islanding solutions for large-scale power systems," *IEEE Transactions on Power Systems*, vol. PP, no. 99, pp. 1-11, Aug. 2017.

[17] N. Senroy, G. T. Heydt, and V. Vittal, "Closure to discussion of 'Decision tree assisted controlled islanding'," *IEEE Transactions on Power Systems*, vol. 22, no. 4, pp. 2293–2293, Nov. 2007.

[18] B. Yang, V. Vittal, G.T. Heydt, and A. Sen, "A novel slow coherency based graph theoretic islanding strategy," *Presented at Power Engineering Society General Meeting*, Florida, Jun. 2007.

[19] U.G. Knight, *Power System in Emergencies*. London, 2001.

[20] ESB and National Grid, "Report on Investigation into System Disturbance of August 5th 2005," Dec. 2005.

[21] R. Christie, "Power system test archive," Aug. 1999. [Online]. http://www.ee.washington.edu/research/pstca

[22] R. Shad, N. Mithulananthan, and T. Saha, "Development of a comprehensive Power System Simulation Laboratory (PSS-L) at the University of Queensland," Test System Report, pp. 1-28, Apr. 2011. [Online]. http://www.itee.uq.edu.au/pssl/drupal7_with_innTheme/?q=node/374

[23] Illinois Center for a Smarter Electric grid (ICSEG), "Power Cases". [Online]. http://icseg.iti.illinois.edu/power-cases/

[24] IEEE Committee Report, "Transient stability test systems for direct stability methods,"

IEEE Transactions on Power Systems, vol. 7, no. 1, pp. 37-44, Feb. 1992.

[25] Institute of Electrical Engineers of Japan (IEEJ), "Bulk power system models". [Online]. http://www2.iee.or.jp/ver2/pes/23-st_model/english/index020.html

[26] G. Rogers, *Power Systems Oscillations*. Norwell, MA: Kluwer, 2000.

[27] P. Demetriou, M. Asprou, J. Q. Tortos, and E. Kyriakides, "Dynamic IEEE test systems for transient analysis," *IEEE Systems Journal*, vol. PP, pp. 1-10, Jul. 2015.

[28] P. M Anderson and A. A Fouad, *Power system stability and control.*: Wiley India Pvt., 2008.

[29] *PowerWorld Corporation*. [Online]. http://powerworld.com

[30] *DIgSILENT PowerFactory*. [Online]. http://www/digsilent.de

[31] PowerWorld Simulator 18 Block Diagrams,. [Online]. http://www.powerworld.com/files/Block-Diagrams-18.pdf

[32] *IEEE Recommended Practice for Excitation System Models for Power System Stability Studies.*, IEEE Standard 421.5, 2005.

[33] N. Senroy, G. T. Heydt, and V. Vittal, "Closure to discussion of 'Decision tree assisted controlled islanding'," *IEEE Transactions on Power Systems*, vol. 22, no. 4, pp. 2293–2293, Nov. 2007.

[34] X. Lei, D. Povh, and O. Ruhle, "Industrial approaches for dynamic equivalents of large power systems," *IEEE Power Engineering Society Winter Meeting*, Jan. 2002.

[35] R. Podmore, "Identification of coherent generators for dynamic equivalents," *IEEE Transactions on Power Apparatus and Systems*, vol. PAS-97, no. 4, pp. 1344–1354, Jul. 1978.

[36] S. Yusof, G. Rogers, and R. Alden, "Slow coherency based network partitioning including load buses," *IEEE Transactions on Power Systems*, vol. 8, no. 3, pp. 1375–1382, Aug. 1993.

[37] J. Chow, "Slow coherency and aggregation," in *Power System Coherency and Model Reduction*. New York, USA: Springer, 2013, pp. 39–72.

[38] I. Kamwa and R. Grondin, "PMU configuration for system dynamic performance measurement in large multi-area power systems," *IEEE Transactions on Power Systems*, vol. 17, no. 2, pp. 385–394, May 2002.

[39] E. Ghahremani and I. Kamwa, "Online state estimation of a synchronous generator using unscented Kalman filter from phasormeasurements units," *IEEE Transactions on Energy Conversion*, vol. 26, no. 4, pp. 1099–1108, Dec. 2011.

[40] P. Zhang, J. Chen, and M. Shao, "Considerations about synchrophasors measurement in dynamic system conditions," Dept. Transmiss. Distrib., Elect. Power Res. Inst., Marco Island, FL, USA, Rep. 1015511, Oct. 2007.

[41] *MRC Approvals 5/30/13: PMU Costs, CFTC Order, UTC.*, Jun. 2013. [Online]. http://www.rtoinsider.com/mrc-approvals-53013-pmu-costs-cftc-order-utc-credit/

[42] M.-E.-A. Abd-EI-Rehim, I. Helal, and M. Omar, "Multi-machine power system dynamic equivalents using artificial intelligence (ANN)," in *Proc. 2006 11th Int. Middle East Power System Conference*, 2006, pp. 197–207.

[43] M. Jonsson, M. Begovic, and J. Daalder, "A new method suitable for real-time generator coherency determination," *IEEE Transactions on Power Systems*, vol. 19, no. 3, pp. 1473–1482, Aug. 2004.

[44] T. Nababhushana, K. Veeramanju, and Shivanna, "Coherency identification using growing self organizing feature maps [power system stability]," in *Proc. 1998 International Conference on Energy Management and Power Delivery*, 1998, pp. 113–116.

[45] K. Anaparthi, B. Chaudhuri, N. Thornhill, and B. Pal, "Coherency identification in power systems through principal component analysis," *IEEE Transactions on Power Systems*, vol. 20, no. 3, pp. 1658–1660, Aug. 2005.

[46] N. Senroy, "Generator coherency using the Hilbert-Huang transform," *IEEE Transactions on Power Systems*, vol. 23, no. 4, pp. 1701–1708, Nov. 2008.

[47] P. Demetriou, L. Hadjidemetriou, A. Kyriacou, E. Kyriakides, and C. Panayiotou, "Real-time identification of coherent generator groups," in *Proc 2015 IEEE Eindhoven PowerTech*, pp. 1-6, Eindhoven, Jul. 2015.

[48] P. E. Shrout and J. L. Freiss, "Intraclass correlations: uses in assessing rater reliability," *Psychol Bull 86*, pp. 486-504, 1979.

[49] P. W. Sauer and M. A. Pai, *Power System Dynamics and Stability*.: Prentice Hall, 1998.

[50] H. W. Dommel and N. Sato, "Fast transient stability solutions," *IEEE Transaction on*

Power Apparatus and Systems, vol. PAS-91, pp. 1643-1650, 1972.

[51] C. Spatz, *Basic Statistics: Tales of Distributions*, 10th ed.: Wadsworth, 2011.

[52] M. A. Pai, *Energy function analysis for power system stability*. Boston/Dordrecht/London: Klumer, 1989.

[53] IEEE PES PSDPC SCS. Task force on benchmark systems for stability controls, "Power system test cases". [Online]. http://www.sel.eesc.usp.br/ieee/index.htm

[54] IEEE PES PSDPC SCS. Task force on benchmark systems for stability controls, "IEEE 10 generator 39 bus system," Mar. 2014. [Online]. http://www.sel.eesc.usp.br/ieee/IEEE39/main.htm

[55] J.A. Bondy and U.S.R. Murty, *Graph Theory*. 2nd Ed:Springer, 2008.

[56] W. K. Chen, *Graph theory and its engineering applications vol. 5.*, Singapore: World Scientific Publishing, 1997.

[57] Q. Zhao, K. Sun, D.Z. Zheng, J. Ma, and Q Lu, "A study of system splitting strategies for island operation of power system: A two-phase method based on OBDDs," *IEEE Transactions on Power Systems*, vol. 18, no. 4, pp. 1556-1565, Nov. 2003.

[58] X. Wang, "Slow coherency grouping based islanding using minimal cutsets and generator coherency index tracing using the continuation method," Ph.D., Iowa State University, Ames, 2005.

[59] G. Xu, V. Vittal, A. Meklin, and J.E. Thalman, "Controlled Islanding Demonstrations on the WECC System," *IEEE Transactions on Power Systems*, vol. 26, no. 1, pp. 334-343, Feb. 2011.

[60] L. Hao, G.W. Rosenwald, J. Jung, and C.C. Liu, "Strategic power infrastructure defense," *Proceedings of the IEEE*, vol. 93, no. 5, pp. 918-933, May 2005.

[61] X. Wang, B. Qian, and I. Davidson, "On constrained spectral clustering and its applications," *Data Mining and Knowledge Discovery*, pp. 1-29, Sep. 2012.

[62] A.Y. Ng, M.I. Jordan, and Y. Weiss, "On spectral clustering: Analysis and an algorithm," *Advances in Neural Information Processing Systems*, vol. 2, pp. 849-856, 2002.

[63] A. Peiravi and R. Ildarabadi, "A fast algorithm for intentional islanding of power systems using the multilevel kernel k-means approach," *Journal of Applied Sciences*,

vol. 9, no. 12, pp. 2247-2255, 2009.

[64] J. Quiros-Tortos, R. Sánchez-García, J. Brodzki, J. Bialek, and J. Terzija, "Constrained spectral clustering based methodology for intentional controlled islanding of large-scale power systems," *IET Generation, Transmission & Distribution*, vol. 9, no. 1, pp. 31-42, Jan. 2015.

[65] S. Theodoridis and K. Koutroumba, *Pattern Recognition*., 4th Ed:American Press, 2008.

[66] T. D. Bie, J. Suykens, and B. D. Moor, "Learning from general label constraints," *IAPR International Workshop on Statistical Pattern Recognition*, Lisbon, Portugal, 2004.

[67] D. Cao and B. Yang, "An improved k-medoids clustering algorithm," *2nd International Conference on Computer and Automation Engineering*, Feb. 2010.

[68] V.G. Koutsoloukas, "Modelling of Cypriot power system on PSS/SinCal, study of disturbances, and influence of wind penetration," Dissertation, National Technical University, 2007 (in Greek).

[69] R.D. Zimmerman, C.E. Murillo-Sanchez, and R.J. Thomas, "MATPOWER: Steady-state operations, planning, and analysis tools for power systems research and education," *IEEE Transactions on Power Systems*, vol. 26, no. 1, pp. 12-19, Feb. 2011.

[70] J. Quiros-Tortos, P. Demetriou, M. Panteli, E. Kyriakides, and V. Terzija, "Intentional controlled islanding and risk assessment: A unified framework," *IEEE Systems Journal*, pp. 1-10, Feb. 2017 (submitted).

[71] C. Moler, *Numerical Computing with MATLAB: Society for Industrial and Applied Mathematics*., 2004.

[72] J. Quiros-Tortos, M. Panteli, P. Wall, and V. Terzija, "A sectionalising methodology for parallel system restoration based on graph theory," *IET Generation, Transmission & Distribution*, vol. 9, no. 11, pp. 1216-1225, Aug. 2015.

[73] *Electricity Authority of Cyprus*. [Online]. https://www.eac.com.cy/EN/CustomerService/Pages/default.aspx.

[74] A. Kyriacou, S. Timotheou, M. Michaelides, C. Panayiotou, and M. Polycarpou, "Multi-constraint building partitioning formulation for effective contaminant detection and isolation," *IEEE World Congress on Computational Intelligence*, Jul. 2016, in press.

[75] P. Demetriou, A. Kyriacou, E. Kyriakides, and C. Panayiotou, "Applying exact MILP

formulation for controlled islanding of power systems," in *Proc 51st International Universities Power Engineering Conference*, Coimbra, Portugal, Jul. 2016, pp. 1-6.

[76] V.E. Henner, "A network separation scheme for emergency control," *International Journal of Electrical Power & Energy Systems*, vol. 2, no. 2, pp. 109-114, 1980.

[77] M. M. Adibi, R. J. Kafka, S. Maram, and L. M. Mili, "On power system controlled separation," *IEEE Transactions on Power Systems*, vol. 21, no. 4, pp. 1894-1902, Nov. 2006.

[78] J. H. Chow, "Time-scale modeling of dynamic networks with applications to power systems," Lecture Notes on Control and Information Sciences, Springer-Verlag, New York, 1982.

[79] E. Cotilla-Sanchez, P. D. H. Hines, C. Barrows, S. Blumsack, and M. Patel, "Multi-attribute partitioning of power networks based on electrical distance," *IEEE Transactions on Power Systems*, vol. 28, no. 4, pp. 4979-4987, Nov. 2013.

[80] T. Ding, K. Sun, C. Huang, Z. Bie, and F. Li, "Mixed–integer linear programming–based splitting strategies for power system islanding operation considering network connectivity," *IEEE System Journal*, vol. PP, no. 99, pp. 1-10, Nov. 2015.

[81] P. A. Trodden, W. A. Bukhsh, A. Grothey, and K. I. McKinnon, "Optimization–based islanding of power networks using piecewise linear AC power flow," *IEEE Transactions on Power Systems*, vol. 29, no. 3, pp. 1212-1220, Dec. 2013.

[82] N. Senroy, G T. Heydt, and V Vittal, "Decision tree assisted controlled," *IEEE Transactions on Power Systems*, vol. 21, no. 4, pp. 1790-1797, Nov. 2006.

[83] K. Sun, K. Hur, and P. Zhang, "A new unified scheme for controlled power system separation using synchronized phasor measurements," *IEEE Transactions on Power Systems*, vol. 26, no. 3, Aug. 2011.

[84] P. Demetriou, J.Q. Tortos, and E. Kyriakides, "When to island for blackout prevention," *IET Generation, Transmission & Distribution*, pp. 1-8, Feb. 2017 (submitted).

[85] P. Kundur, "Introduction to the Power System Stability Problem – Basic Concept and Definitions, Mid-term and Long-Term Stability," in *Power System Stability and Control*.: McGraw-Hill, 1994, pp. 33-34.

[86] J. Machowski, J. W. Bialek, and J. R. Bumby, *Power System Dynamics Stability and*

Control.: John Wiley & Sons, 2008.

[87] P. Demetriou, A. Kyriacou, E. Kyriakides, and C. Panayiotou, "System splitting strategy considering power system restoration," *2017 IEEE PowerTech*, pp. 1-6, Jul. 2017.

[88] *North American Electric Reliability Corporation*. [Online]. http://www.nerc.com

[89] J. Q. Tortós and V. Terzija, "Controlled islanding strategy considering power system restoration constraints," *2012 IEEE Power and Energy Society General Meeting*, pp. 1-8, San Diego, CA, 2012.

[90] S. A. Nezam Sarmadi, A. S. Dobakhshari, S. Azizi, and A. M. Ranjbar, "A sectionalizing method in power system restoration based on WAMS," *IEEE Transactions on Smart Grid*, vol. 2, no. 1, pp. 190-197, Mar. 2011.

[91] S. Chakrabarti and E. Kyriakides, "Optimal placement of phasor measurement units for power system observability," *IEEE Transactions on Power Systems*, vol. 23, no. 3, pp. 1433-1440, Aug. 2008.

[92] B. K. S. Roy, A. K. Sinha, and A. K. Pradhan, "An optimal PMU placement technique for power system observability," *International Journal of Electrical Power & Energy Systems*, vol. 42, no. 1, pp. 71-77, Nov. 2012.

[93] M. Asprou, S. Chakrabarti, and E. Kyriakides, "The use of a PMU-based state estimator for tracking power system dynamics," *IEEE Power and Energy Society General Meeting 2014*, Washington DC, Jul. 2014.

[94] U. S. Department of Energy, "Advancement of Synchrophasor Technology," Mar. 2016.

[95] P. Demetriou, M. Asprou, and E. Kyriakides, "A real-time controlled islanding and restoration scheme based on estimated states," *IEEE Transactions on Smart Grid*, pp. 1-8, Oct. 2017 (submitted).

[96] W. Fu, S. Zhao, J. D. McCalley, V. Vittal, and N. Abi-Samra, "Risk assessment for special protection schemes," *IEEE Transactions on Power systems*, vol. 17, no. 1, pp. 63-72, Feb. 2002.

[97] M. Esmaili, A. Akbar Hajnoroozi, and H. Ali Sha-yanfar, "Risk evaluation of online special protection systems," *International Journal of Electrical Power & Energy Systems*, vol. 41, no. 1, pp. 137-144, Oct. 2012.

[98] M. Panteli, P. Crossley, and J. Fitch, "Quantifying the reliability level of system

integrity protection schemes," *IET Generation, Transmission and Distribution*, vol. 8, no. 4, pp. 753-764, Apr. 2014.

[99] U.S. Nuclear Regularoty Commission, "Fault Tree Handbook," 1981.

[100] T. Y. Hsiao and C. N. Lu, "Risk informed design refinement of a power system protection scheme," *IEEE Transactions on Reliability*, vol. 57, no. 2, pp. 311-321, Jun. 2008.

[101] T. Zachariadis and A. Poullikkas, "The costs of power outages: A case study from Cyprus," *Energy Policy*, vol. 51, pp. 630-641, Sept. 2012.

[102] M. M. Adibi and *et al.*, "Power system restoration - A task force report," *IEEE Transactions on Power Systems*, vol. 2, no. 2, pp. 271-277, May 1987.

LIST OF PUBLICATIONS

[1] **P. Demetriou**, M. Asprou, and E. Kyriakides, "A real-time controlled islanding and restoration scheme based on estimated states," *IEEE Transactions on Smart Grid*, pp. 1-8, Oct. 2017 (submitted).

[2] **P. Demetriou**, J.Q. Tortos, and E. Kyriakides, "When to island for blackout prevention," *IET Generation, Transmission & Distribution*, pp. 1-8, Feb. 2017 (submitted).

[3] J. Quiros-Tortos, **P. Demetriou**, M. Panteli, E. Kyriakides, and V. Terzija, "Intentional controlled islanding and risk assessment: A unified framework," *IEEE Systems Journal*, pp. 1-10, Feb. 2017 (accepted).

[4] A. Kyriacou, **P. Demetriou**, E. Kyriakides, and C. Panayiotou, "Controlled islanding solutions for large-scale power systems," *IEEE Transactions on Power Systems*, vol. PP, no. 99, pp. 1-11, Aug. 2017

[5] **P. Demetriou**, A. Kyriacou, E. Kyriakides, and C. Panayiotou, "System splitting strategy considering power system restoration," in *Proc 2017 IEEE Manchester PowerTech*, pp. 1-6, Manchester, UK, Jul. 2016.

[6] **P. Demetriou**, A. Kyriacou, E. Kyriakides, and C. Panayiotou, "Applying exact MILP formulation for controlled islanding of power systems," in *Proc 51st International Universities Power Engineering Conference*, pp. 1-6, Coimbra, Portugal, Jul. 2016.

[7] L. Hadjidemetriou, A. Charalambous, **P. Demetriou** and E. Kyriakides, "Dynamic Modeling of IEEE Test Systems Including Renewable Energy Sources," *18th Mediterranean Electrotechnical Conference (MELECON 2016)*, Limassol, Cyprus, Apr. 2016.

[8] **P. Demetriou**, M. Asprou, and J. Kyriakides, E. Quiros-Tortos, "Dynamic IEEE test systems for transient analysis," *IEEE Systems Journal*, vol. PP, no. 99, pp. 1-10, Jul. 2015.

[9] **P. Demetriou**, L. Hadjidemetriou, A. Kyriacou, E. Kyriakides, and C. Panayiotou, "Real-time identification of coherent generator groups," in *Proc 2015 IEEE Eindhoven PowerTech*, pp. 1-6, Eindhoven, Netherlands, Jul. 2015.

[10] L. Hadjidemetriou, **P. Demetriou**, and E. Kyriakides, "Investigation of different

Fault Ride Through strategies for renewable energy sources," in *Proc 2015 IEEE Eindhoven PowerTech*, pp. 1-6, Eindhoven, Netherlands, Jul. 2015

[11] L. Hadjidemetriou, M. Asprou, **P. Demetriou**, and E. Kyriakides, "Enhancing power system voltage stability through a centralized control of renewable energy sources," in *Proc 2015 IEEE PowerTech*, pp. 1-6, Eindhoven, Netherlands, Jul. 2015.

[12] **P. Demetriou**, J. Quirós-Tortós, E. Kyriakides, and V. Terzija, "On implementing a spectral clustering controlled islanding algorithm in real power systems," in *Proc 2013 IEEE Grenoble Conference*, pp. 1-6, Grenoble, France, Jun. 2013.

APPENDICES

Appendix A

Table A.1: Nomenclature

Rated MVA	Machine-rated MVA; base MVA for impedances
Rated kV	Machine-rated terminal voltage in kV; base kV for impedances
H	Inertia constant in s
D	Machine load damping coefficient
r_a	Armature resistance in p.u.
x_d	Unsaturated *d* axis synchronous reactance in p.u.
x_q	Unsaturated *q* axis synchronous reactance in p.u.
x'_d	Unsaturated *d* axis transient reactance in p.u.
x'_q	Unsaturated *q* axis transient reactance in p.u.
x''_d	Unsaturated *d* axis subtransient reactance in p.u.
x''_q	Unsaturated *q* axis subtransient reactance in p.u.
$x_l \; or \; x_p$	Leakage or Potier reactance in p.u.
T'_{d0}	*d* axis transient open circuit time constant in s
T'_{q0}	*q* axis transient open circuit time constant in s
T''_{d0}	*d* axis subtransient open circuit time constant in s
T''_{q0}	*q* axis subtransient open circuit time constant in s
$S(1.0)$	Machine saturation at 1.0 p.u. voltage in p.u.
$S(1.2)$	Machine saturation at 1.2 p.u. voltage in p.u.
T_r	Regulator input filter time constant in s
K_a	Regulator gain (continuous acting regulator) in p.u.
T_a	Regulator time constant in s
V_{Rmax}	Maximum regulator output, starting at full load field voltage in p.u.
V_{Rmin}	Minimum regulator output, starting at full load field voltage in p.u.
K_e	Exciter self-excitation at full load field voltage in p.u.
T_e	Exciter time constant in s
K_f	Regulator stabilizing circuit gain in p.u.
T_f	Regulator stabilizing circuit time constant in s
E_1	Field voltage value,1 in p.u.
$SE(E_1)$	Saturation factor at E_1
E_2	Field voltage value,2 in p.u.
$SE(E_2)$	Saturation factor at E_2

P_{max}	Maximum turbine output in p.u.
R	Turbine steady-state regulation setting or droop in p.u.
T_1	Control time constant (governor delay) in s
T_2	Hydro reset time constant in s
T_3	Servo time constant in s
T_4	Steam valve bowl time constant in s
T_5	Steam reheat time constant in s
F	Shaft output ahead of reheater in p.u.

IEEE 30-bus modified test system

Table A.2: IEEE 30-bus modified test system machine data

Type	GENROU	GENROU	GENROU	GENROU
Operation	Sync. Gen.	Sync. Gen.	Condenser	Condenser
Default Unit no. (New Unit no.)	1(31)	2(32)	5(33), 8(34)	11(35), 13(36)
Rated power (MVA)	270	51.2	40	25
Rated voltage (kV)	18	13.8	13.8	13.8
Rated pf	0.85	0.8	0.0	0.0
H (s)	4.130	5.078	1.520	1.200
D	2.000	2.000	0.000	0.000
r_a (p.u)	0.0016	0.000	0.000	0.0025
x_d (p.u)	1.700	1.270	2.373	1.769
x_q (p.u)	1.620	1.240	1.172	0.855
x'_d (p.u)	0.256	0.209	0.343	0.304
x'_q (p.u)	0.245	0.850	1.172	0.5795
x''_d (p.u)	0.185	0.116	0.231	0.2035
x''_q (p.u)	0.185	0.116	0.231	0.2035
x_l or x_p (p.u)	0.155	0.108	0.132	0.1045
T'_{d0} (s)	4.800	6.600	11.600	8.000
T'_{q0} (s)	0.004	0.004	0.159	0.008
T''_{d0} (s)	0.004	0.004	0.058	0.0525
T''_{q0} (s)	0.004	0.004	0.201	0.0151
$S(1.0)$	0.125	0.2067	0.295	0.304
$S(1.2)$	0.450	0.724	0.776	0.667

Table A.3: IEEE 30-bus modified test system exciter data

Type	IEEET1	IEEET1	IEEET1	IEEET1
Default Unit no. (New Unit no.)	1(31)	2(32)	5(33), 8(34)	11(35), 13(36)
Rated power (MVA)	270	51.2	40	25
Rated voltage (kV)	18	13.8	13.8	13.8
T_r (s)	0.000	0.000	0.000	0.000
K_a (p.u)	30	400	400	400
T_a (s)	0.400	0.050	0.050	0.050
V_{Rmax} (p.u)	4.590	0.613	6.630	4.407
V_{Rmin} (p.u)	-4.590	-0.613	-6.630	-4.407
K_e (p.u)	-0.02	-0.0769	-0.170	-0.170
T_e (s)	0.560	1.370	0.950	0.950
K_f (p.u)	0.050	0.040	0.040	0.040
T_f	1.300	1.000	1.000	1.000
E_1	2.5875	3.0975	6.375	4.2375
$SE(E_1)$	0.7298	0.1117	0.2174	0.2174
E_2	3.450	4.130	8.500	5.650
$SE(E_2)$	1.3496	0.2248	0.9388	0.9386

Table A.4: IEEE 30-bus modified test system governor data

Type	BPA_GG	BPA_GG
Default Unit no. (New Unit no.)	1(31)	2(32)
Rated power (MVA)	270	51.2
Rated voltage (kV)	18	13.8
P_{max} (p.u)	0.8518	1.035
R (p.u)	0.0185	0.1523
T_1 (s)	0.100	0.200
T_2 (s)	0.000	0.000
T_3 (s)	0.259	0.300
T_4 (s)	0.100	0.090
T_5 (s)	10.000	0.000
F	0.272	1.000

IEEE 39-bus modified test system

Table A.5: IEEE 39-bus modified test system machine data

Type	GENROU	GENROU	GENROU
Operation	Sync. Gen.	Sync. Gen.	Sync. Gen.
Default Unit no. (New Unit no.)	30(40)	31(41), 32(42), 33(43) 34(44), 35(45), 36(46) 37(47)	38(48) 39(49)
Rated power (MVA)	590	835	911
Rated voltage (kV)	22	20	26
Rated pf	0.95	0.9	0.9
H (s)	2.3186	2.6419	2.4862
D	2.00	2.00	2.00
r_a (p.u)	0.0046	0.0019	0.0010
x_d (p.u)	2.110	2.183	2.040
x_q (p.u)	2.020	2.157	1.960
x'_d (p.u)	0.280	0.413	0.266
x'_q (p.u)	0.490	1.285	0.262
x''_d (p.u)	0.215	0.339	0.193
x''_q (p.u)	0.215	0.339	0.193
$x_l \; or \; x_p$ (p.u)	0.155	0.246	0.154
T'_{d0} (s)	4.200	5.690	6.000
T'_{q0} (s)	0.565	1.500	0.900
T''_{d0} (s)	0.032	0.041	0.004
T''_{q0} (s)	0.062	0.144	0.004
$S(1.0)$	0.079	0.134	0.340
$S(1.2)$	0.349	0.617	1.120

Table A.6: IEEE 39-bus modified test system exciter data

Type	IEEET1	IEEET1	IEEET1
Default Unit no. (New Unit no.)	30(40)	31(41), 32(42), 33(43) 34(44), 35(45), 36(46) 37(47)	38(48)
Rated power (MVA)	590	835	911
Rated voltage (kV)	22	20	26

T_r (s)	0.000	0.000	0.000
K_a (p.u)	200	400	50
T_a (s)	0.3575	0.020	0.060
V_{Rmax} (p.u)	5.730	18.300	1.000
V_{Rmin} (p.u)	-5.730	-18.300	-1.00
K_e (p.u)	1.000	1.000	-0.0393
T_e (s)	0.004	0.942	0.440
K_f (p.u)	0.0529	0.030	0.070
T_f	1.000	1.000	1.000
E_1	4.2975	3.765	3.375
$SE(E_1)$	0.000	0.8147	0.0644
E_2	5.730	5.020	4.5
$SE(E_2)$	0.000	2.6756	0.2363

Table A.7: IEEE 39-bus modified test system governor data

Type	BPA_GG	BPA_GG	BPA_GG
Default Unit no. (New Unit no.)	30(40)	31(41), 32(42), 33(43) 34(44), 35(45), 36(46) 37(47)	38(48)
Rated power (MVA)	590	835	911
Rated voltage (kV)	22	20	26
P_{max} (p.u)	0.9373	0.9177	0.9001
R (p.u)	0.0085	0.006	0.00548
T_1 (s)	0.080	0.180	0.100
T_2 (s)	0.000	0.030	0.000
T_3 (s)	0.150	0.200	0.200
T_4 (s)	0.050	0.000	0.100
T_5 (s)	10.000	8.000	8.720
F	0.280	0.300	0.300

IEEE 57-bus modified test system

Table A.8: IEEE 57-bus modified test system machine data

Type	GENROU	GENROU	GENROU
Operation	Sync. Gen.	Sync. Gen.	Condenser
Default Unit no. (New Unit no.)	1(60), 8(59), 12(61)	3(58)	2(62), 6(63), 9(64)
Rated power (MVA)	512	51.2	25
Rated voltage (kV)	24	13.8	13.8
Rated pf	0.9	0.8	0.0
H (s)	2.6309	5.078	1.200
D	2.000	2.000	0.000
r_a (p.u)	0.004	0.000	0.0025
x_d (p.u)	1.700	1.270	1.769
x_q (p.u)	1.650	1.240	0.855
x'_d (p.u)	0.270	0.209	0.304
x'_q (p.u)	0.470	0.850	0.5795
x''_d (p.u)	0.200	0.116	0.2035
x''_q (p.u)	0.200	0.116	0.2035
x_l or x_p (p.u)	0.160	0.108	0.1045
T'_{d0} (s)	3.800	6.600	8.000
T'_{q0} (s)	0.480	0.004	0.008
T''_{d0} (s)	0.004	0.004	0.0525
T''_{q0} (s)	0.004	0.004	0.0151
$S(1.0)$	0.090	0.2067	0.304
$S(1.2)$	0.400	0.724	0.666

Table A.9: IEEE 57-bus modified test system exciter data

Type	IEEET1	IEEET1	IEEET1
Default Unit no. (New Unit no.)	1(60), 8(59), 12(61)	3(58)	2(62), 6(63), 9(64)
Rated power (MVA)	512	51.2	25
Rated voltage (kV)	24	13.8	13.8
T_r (s)	0.000	0.000	0.000
K_a (p.u)	200	400	400
T_a (s)	0.395	0.050	0.050
V_{Rmax} (p.u)	3.840	0.613	4.407

V_{Rmin} (p.u)	-3.840	-0.613	-4.407
K_e (p.u)	1.000	-0.0769	-0.170
T_e (s)	0.002	1.370	0.950
K_f (p.u)	0.0635	0.040	0.040
T_f	1.000	1.000	1.000
E_1	2.880	3.0975	4.2375
$SE(E_1)$	0.000	0.1117	0.2174
E_2	3.840	4.130	5.650
$SE(E_2)$	0.000	0.2248	0.9386

Table A.10: IEEE 57-bus modified test system governor data

Type	BPA_GG	BPA_GG
Default Unit no. (New Unit no.)	1(60), 8(59), 12(61)	3(58)
Rated power (MVA)	512	51.2
Rated voltage (kV)	24	13.8
P_{max} (p.u)	0.8984	1.035
R (p.u)	0.0098	0.1523
T_1 (s)	0.150	0.200
T_2 (s)	0.050	0.000
T_3 (s)	0.300	0.300
T_4 (s)	0.260	0.090
T_5 (s)	8.000	0.000
F	0.270	1.000

IEEE 118-bus modified test system

Table A.11 (a): IEEE 118-bus modified test system generator data

Type	GENROU	GENROU	GENROU	GENROU	GENROU
Operation	Sync. Gen.	Sync. Gen.	Sync. Gen.	Sync. Gen.	Sync. Gen.
Default Unit no. (New Unit no.)	10(119) 69(131) 80(132)	12(120)	25(121) 49(125) 100(135)	26(122)	31(123) 46(124) 87(133)
Rated power (MVA)	590	125	330	410	75
Rated voltage (kV)	22	15.5	20	24	13.8
Rated pf	0.95	0.85	0.9	0.9	0.8
H (s)	2.319	4.768	3.006	3.704	6.187
D	2.000	2	2.000	2.000	2.000
r_a (p.u)	0.0046	0.004	0.000	0.0019	0.0031
x_d (p.u)	2.110	1.220	1.950	1.7668	1.050
x_q (p.u)	2.020	1.160	1.920	1.7469	0.980
x'_d (p.u)	0.280	0.174	0.317	0.2738	0.185
x'_q (p.u)	0.490	0.250	1.120	1.0104	0.360
x''_d (p.u)	0.215	0.134	0.200	0.2284	0.130
x''_q (p.u)	0.215	0.134	0.200	0.2284	0.130
x_l or x_p (p.u)	0.155	0.0078	0.199	0.1834	0.070
T'_{d0} (s)	0.5573	8.970	0.9754	0.8418	1.0748
T'_{q0} (s)	0.1371	0.500	0.875	0.8676	0.1102
T''_{d0} (s)	0.0246	0.033	0.0473	0.035	0.0267
T''_{q0} (s)	0.0272	0.070	0.0134	0.035	0.0358
$S(1.0)$	0.079	0.1026	0.082	0.2632	0.100
$S(1.2)$	0.349	0.432	0.290	0.5351	0.3928

Table A.12 (b): IEEE 118-bus modified test system generator data

Type	GENROU	GENROU	GENROU	GENROU
Operation	Sync. Gen.	Sync. Gen.	Sync. Gen.	Sync. Gen.
Default Unit no. (New Unit no.)	54(126) 103(136) 111(137)	59(127) 61(128)	65(129) 66(130)	89(134)
Rated power (MVA)	100	233	512	835
Rated voltage (kV)	13.8	20	24	20

Rated pf	0.8	0.85	0.9	0.9
H (s)	4.985	4.122	2.631	2.6419
D	2.000	2.000	2.000	2.00
r_a (p.u)	0.0035	0.0016	0.004	0.0019
x_d (p.u)	1.180	1.569	1.700	2.183
x_q (p.u)	1.050	1.548	1.650	2.157
x'_d (p.u)	0.220	0.324	0.270	0.413
x'_q (p.u)	0.380	0.918	0.470	1.285
x''_d (p.u)	0.145	0.249	0.200	0.339
x''_q (p.u)	0.145	0.249	0.200	0.339
x_l or x_p (p.u)	0.075	0.204	0.160	0.246
T'_{d0} (s)	1.100	1.0614	0.6035	5.690
T'_{q0} (s)	0.1086	0.8895	0.1367	1.500
T''_{d0} (s)	0.0277	0.0336	0.0556	0.041
T''_{q0} (s)	0.0351	0.0381	0.0319	0.144
$S(1.0)$	0.0933	0.0987	0.090	0.134
$S(1.2)$	0.4044	0.303	0.400	0.617

Table A.13 (a): IEEE 118-bus modified test system condensers and motors data

Type	GENROU	GENROU	GENROU	GENROU
Operation	Condenser	Condenser	Motor	Motor
Default Unit no. (New Unit no.)	1(138), 6(139), 15(140), 19(142) 32(143), 34(144), 36(145), 55(146) 56(147), 62(148), 74(150), 76(151) 77(152), 85(153), 92(154) 104(155), 105(156), 110(157)	18(141) 70(149)	4(158) 24(160) 27(161) 72(164) 73(165)	8(159) 91(167) 107(169)
Rated power (MVA)	25	40	25	35.29
Rated voltage (kV)	13.8	13.8	13.8	13.8
Rated pf	0.0	0.0	0.8	0.85
H (s)	1.200	1.520	5.016	4.4893
D	0.000	0.000	2.000	2.000
r_a (p.u)	0.0025	0.000	0.0014	0.000
x_d (p.u)	1.769	2.373	1.250	1.400
x_q (p.u)	0.855	1.172	1.220	1.372
x'_d (p.u)	0.304	0.343	0.232	0.231

x'_q (p.u)	0.5795	1.172	0.715	0.060
x''_d (p.u)	0.2035	0.231	0.120	0.050
x''_q (p.u)	0.2035	0.231	0.120	0.050
x_l or x_p (p.u)	0.1045	0.132	0.114	0.000
T'_{d0} (s)	8.000	11.600	4.750	5.500
T'_{q0} (s)	0.008	0.159	1.500	0.008
T''_{d0} (s)	0.0525	0.058	0.0035	0.008
T''_{q0} (s)	0.0151	0.201	0.210	0.008
$S(1.0)$	0.304	0.295	0.279	0.210
$S(1.2)$	0.666	0.776	0.886	0.805

Table A.14 (b): IEEE 118-bus modified test system condensers and motors data

Type	GENROU	GENROU	GENROU	GENROU
Operation	Motor	Motor	Motor	Motor
Default Unit no. (New Unit no.)	40(162) 113(171)	42(163) 99(168)	90(166) 112(170)	116(172)
Rated power (MVA)	51.2	75	100	384
Rated voltage (kV)	13.8	13.8	13.8	24
Rated pf	0.8	0.8	0.8	0.85
H (s)	5.078	6.186	4.985	2.621
D	2.000	2.000	2.000	2.000
r_a (p.u)	0.000	0.000	0.000	0.000
x_d (p.u)	1.270	1.050	1.180	1.798
x_q (p.u)	1.240	0.980	1.050	1.778
x'_d (p.u)	0.209	0.185	0.220	0.324
x'_q (p.u)	0.850	0.360	0.380	1.051
x''_d (p.u)	0.105	0.130	0.145	0.260
x''_q (p.u)	0.105	0.130	0.145	0.260
x_l or x_p (p.u)	0.104	0.070	0.075	0.193
T'_{d0} (s)	6.600	6.100	5.900	5.210
T'_{q0} (s)	0.008	0.300	0.300	1.500
T''_{d0} (s)	0.008	0.038	0.038	0.042
T''_{q0} (s)	0.008	0.099	0.092	0.042
$S(1.0)$	0.2067	0.100	0.0933	0.162
$S(1.2)$	0.724	0.3928	0.4044	0.508

Table A.15 (a): IEEE 118-bus modified test system exciter data for generators

Type	IEEET1	IEEET1	IEEET1	IEEET1	IEEET1
Default Unit no. (New Unit no.)	10(119) 69(131) 80(132)	12(120)	25(121) 49(125) 100(135)	26(122)	31(123) 46(124) 87(133)
Rated power (MVA)	590	125	330	410	75
Rated voltage (kV)	22	15.5	20	24	13.8
T_r (s)	0.000	0.060	0.000	0.000	0.000
K_a (p.u)	200	25	400	400	0.050
T_a (s)	0.3575	0.200	0.050	0.020	20.000
V_{Rmax} (p.u)	5.730	1.000	3.810	5.270	4.380
V_{Rmin} (p.u)	-5.730	-1.000	-3.810	-5.270	0.000
K_e (p.u)	1.000	-0.0601	-0.170	1.000	1.000
T_e (s)	0.011	0.6758	0.950	0.920	1.980
K_f (p.u)	0.0529	0.108	0.040	0.030	0.000
T_f	1.000	0.350	1.000	1.000	0.100
E_1	4.2975	2.4975	3.6675	2.4675	2.385
$SE(E_1)$	0.000	0.0949	0.0111	0.4351	0.0951
E_2	5.730	3.330	4.890	3.290	3.180
$SE(E_2)$	0.000	0.37026	0.0178	0.6001	0.3712

Table A.16 (b): IEEE 118-bus modified test system exciter data for generators

Type	IEEET1	IEEET1	IEEET1	IEEET1
Default Unit no. (New Unit no.)	54(126) 103(136) 111(137)	59(127) 61(128)	65(129) 66(130)	89(134)
Rated power (MVA)	100	233	512	835
Rated voltage (kV)	13.8	20	24	20
T_r (s)	0.060	0.000	0.000	0.000
K_a (p.u)	25	250	200	400
T_a (s)	0.200	0.060	0.395	0.020
V_{Rmax} (p.u)	1.000	4.420	3.840	18.300
V_{Rmin} (p.u)	-1.000	-4.420	-3.840	-18.300
K_e (p.u)	-0.0582	1.000	1.000	1.000
T_e (s)	0.6544	0.613	0.008	0.942

K_f (p.u)	0.105	0.053	0.0635	0.030
T_f	0.350	0.330	1.000	1.000
E_1	2.5785	2.610	2.880	3.765
$SE(E_1)$	0.0889	0.000	0.000	0.8147
E_2	3.438	3.480	3.840	5.020
$SE(E_2)$	0.3468	0.000	0.000	2.6756

Table A.17 (a): IEEE 118-bus modified test system exciter data for condensers and motors

Type	IEEET1	IEEET1	IEEET1	IEEET1
Default Unit no. (New Unit no.)	1(138), 6(139) 15(140), 19(142) 32(143), 34(144) 36(145), 55(146) 56(147), 62(148) 74(150), 76(151) 77(152), 85(153) 92(154), 104(155) 105(156),110(157)	18(141) 70(149)	4(158), 24(160) 27(161), 72(164) 73(165)	8(159) 91(167) 107(169)
Rated power (MVA)	25	40	25	35.29
Rated voltage (kV)	13.8	13.8	13.8	13.8
T_r (s)	0.000	0.000	0.000	0.000
K_a (p.u)	400	400	0.050	57.140
T_a (s)	0.050	0.050	20.000	0.050
V_{Rmax} (p.u)	4.407	6.630	6.812	1.000
V_{Rmin} (p.u)	-4.407	-6.630	1.395	-1.000
K_e (p.u)	-0.170	-0.170	1.000	-0.0445
T_e (s)	0.950	0.950	0.700	0.500
K_f (p.u)	0.040	0.040	0.000	0.080
T_f	1.000	1.000	0.008	1.000
E_1	4.2375	6.375	2.6753	3.375
$SE(E_1)$	0.2174	0.2174	0.4135	0.0711
E_2	5.650	8.500	3.567	4.500
$SE(E_2)$	0.9386	0.9388	0.907	0.2774

Table A.18 (b): IEEE 118-bus modified test system exciter data for condensers and motors

Type	IEEET1	IEEET1	IEEET1	IEEET1
Default Unit no. (New Unit no.)	40(162) 113(171)	42(163) 99(168)	90(166) 112(170)	116(172)
Rated power (MVA)	51.2	75	100	384
Rated voltage (kV)	13.8	13.8	13.8	24
T_r (s)	0.000	0.000	0.060	0.000
K_a (p.u)	400	0.050	25	400
T_a (s)	0.050	20.000	0.200	0.020
V_{Rmax} (p.u)	0.613	4.380	1.000	8.130
V_{Rmin} (p.u)	-0.613	0.000	-1.000	-8.130
K_e (p.u)	-0.0769	1.000	-0.0582	1.000
T_e (s)	1.370	1.980	0.6544	0.812
K_f (p.u)	0.040	0.000	0.105	0.060
T_f	1.000	0.008	0.350	1.000
E_1	3.0975	2.385	2.5785	3.6825
$SE(E_1)$	0.1117	0.0951	0.0889	0.4589
E_2	4.130	3.180	3.438	4.910
$SE(E_2)$	0.2248	0.3712	0.3468	0.6558

Table A.19 (a): IEEE 118-bus modified test system governor data for generators

Type	BPA_GG	BPA_GG	BPA_GG	BPA_GG	BPA_GG
Default Unit no. (New Unit no.)	10(119) 69(131) 80(132)	12(120)	25(121) 49(125) 100(135)	26(122)	31(123) 46(124) 87(133)
Rated power (MVA)	590	125	330	410	75
Rated voltage (kV)	22	15.5	20	24	13.8
P_{max} (p.u)	0.9372	1.056	1.050	0.8951	1.000
R (p.u)	0.0085	0.040	0.0152	0.0122	0.066
T_1 (s)	0.080	0.083	0.100	0.180	0.090
T_2 (s)	0.000	0.000	0.000	0.000	0.000
T_3 (s)	0.150	0.200	0.400	0.040	0.200
T_4 (s)	0.050	0.050	0.050	0.250	0.300
T_5 (s)	10.000	5.000	8.000	8.000	0.000
F	0.280	0.280	0.250	0.267	1.000

Table A.20 (b): IEEE 118-bus modified test system governor data for generators

Type	BPA_GG	BPA_GG	BPA_GG	BPA_GG
Default Unit no. (New Unit no.)	54(126) 103(136) 111(137)	59(127) 61(128)	65(129) 66(130)	89(134)
Rated power (MVA)	100	233	512	835
Rated voltage (kV)	13.8	20	24	20
P_{max} (p.u)	1.050	0.901	0.898	0.9177
R (p.u)	0.050	0.0214	0.0098	0.006
T_1 (s)	0.090	0.150	0.150	0.180
T_2 (s)	0.000	0.000	0.050	0.030
T_3 (s)	0.200	0.100	0.300	0.200
T_4 (s)	0.300	0.300	0.260	0.000
T_5 (s)	0.000	10.000	8.000	8.000
F	1.000	0.237	0.270	0.300